Interactions between organic matter and minerals for soil carbon sequestration

By

Zongtang Yang

A thesis submitted to fulfil requirements for the degree of
Doctor of Philosophy

2026

School of Life and Environmental Sciences

Faculty of Science

The University of Sydney

New South Wales, Australia

Statement of originality

This is to certify that the content of this thesis is my own work. This thesis has not been submitted for any other degree or purpose.

I certify that the intellectual content of this thesis is the product of my own work. Chapters that include published or submitted to journals are clearly indicated. All assistance received in preparing this thesis and all sources of information have been acknowledged.

Zongtang Yang

20 January 2026

Authorship attribution statement

Chapter 3 of this thesis has been published on *Organic Geochemistry* as Yang, Z., Mohanty, B., Dijkstra, F.A., Guggenberger, G., Singh, B. (2025). Insights into the complex nature of dissolved organic matter from plant residues using multiple spectroscopic techniques. *Organic Geochemistry* 210, 105095.

I designed the study with co-authors, conducted the experiments, analysed the data, wrote the original drafts of the manuscript.

Chapter 4 of this thesis has been submitted to *Geoderma* as Yang, Z., Thomsen, L., Dijkstra, F.A., Guggenberger, G., Singh, B. (2025). Dissolved organic matter composition and mineral surface chemistry modulate carbon sequestration in soils. *Geoderma*. Under review.

I designed the study with co-authors, conducted the experiments, analysed the data, wrote the original drafts of the manuscript.

Chapter 6 of this thesis has been published on *Environmental Science & Technology* as Yang, Z., Ohno, T., Singh, B. (2024). Effect of land use change on molecular composition and concentration of organic matter in an Oxisol. *Environmental Science & Technology*. 58(23), 10095-10107.

I designed the study with co-authors, conducted the experiments, analysed the data, wrote the original drafts of the manuscript.

In addition to the authorship attribution statements above, in cases where I am not the corresponding author of a published item, permission to include the published material has been granted by the corresponding author.

Zongtang Yang

20 January 2026

As supervisor for the candidature upon which this thesis is based, I can confirm that the authorship attribution statements above are correct.

Balwant Singh

20 January 2026

Artificial intelligence statement

During the preparation of the thesis, the author used ChatGPT (GPT-5.2, OpenAI) for the purposes of language editing. The use of this generative AI tool includes spelling, grammar and sentence structures. The author confirms that any text modified by generative AI was subsequently reviewed by the author to identify and correct potential errors, inaccuracies, and bias. The author takes full responsibility for the submitted thesis, ensures the work is their own and has used generative AI within the parameters of use in accordance with guideline and policies in the University of Sydney.

Scholarship support

This PhD research reported in this thesis was supported by the Postgraduate Research Scholarship in Unlocking the Anchors of Soil Organic Carbon to Manage Climate Change (SC4187) from the Australian Research Council Discovery Project (DP220103026), and by the Francis Henry Loxton Supplementary Scholarship (Agriculture) (SC2297) from the University of Sydney.

Acknowledgements

Completing this dissertation would not have been possible without the support, guidance, and encouragement of many. I am deeply grateful to everyone who contributed to my PhD journey.

First and foremost, my deeply gratitude goes to my supervisor Prof. Balwant Singh, for his patient guidance, enthusiastic encouragement and insight feedback throughout this journey. His expertise and mentorship shaped every stage of this thesis and inspired my growth as a researcher. I would like to express my gratitude to my co-supervisors, Prof. Feike A. Dijkstra and Prof. Georg Guggenberger. Their generosity with their time, expertise, and guidance profoundly influenced the development and completion of this work.

I extend my sincere thanks to my co-authors, Prof. Tsutomu Ohno, Dr. Biswaranjan Mohanty, and Dr. Lars Thomsen, for their time, effort and feedback in preparing the manuscripts that underpin this thesis. Special thanks to technical scientists who provide their invaluable support and assistance: Michelle Wood for FTIR and OPTIR, Nicholas Proschogo for FT-ICR-MS, Lars Thomsen for NEXAFS, Biswaranjan Mohanty for NMR, Bin Gong for XPS analysis. My appreciation also goes to Iona Gyorgy, Michael Turner, and Hero Tahaei in C81 Biomedical building for their technical support in the laboratory. Shoutout to my lovely colleagues and friends in C81 Biomedical building, especially Yuxin, Bright, Jay, Yijia, Anna, Rachel, Sandra, Mingming, Peipei, Lloyd, Marliana, Oscar and Christy for their camaraderie and support during both breakthroughs and setbacks.

My last tribute is to those who know I am not perfect but still love and support me. To my family, my grandparents, my parents, my sister and my little nephew, for their unwavering and endless love, patience and belief in me. To my partner, Evelyn, for her constant love, kindness, and steadfast faith in me. Her listen, encouragement, and care made this work possible and filled my PhD journey with warmth and joy.

欲买桂花同载酒，终不负，少年游

Table of contents

List of figures

List of tables

Abstract

The processes and mechanisms that govern soil organic carbon (SOC) sequestration are a central focus of environmental research because their critical influence in soil function and climate regulation. Soil mineral mediated retention and stabilisation of mineral associated organic matter (MAOM) represents the major pathway for the long-term carbon storage. However, the investigation of mineral-organic interactions is constrained by the inherent complexity of both organic fractions such as dissolved organic matter (DOM) and mineral phases (i.e., phyllosilicates and metal oxides), the influence of external conditions related to land use, and the limitations in available analytical techniques. This thesis investigates the heterogeneity and chemical convergence of DOM derived from common Australian plant residues using multiple analytical techniques coupled with multivariate analysis. This thesis synthesises prototype MAOM by systemically interacting DOM with a range of mineral phases to reveal the sequential and selectivity of organic compounds on mineral surfaces with contrasting properties. This thesis also evaluates the utility of optical photothermal infrared (OPTIR) spectroscopy for revealing key functional group information at mineral-organic interfaces in both synthetic and natural MAOM at submicron spatial resolution. This thesis examines the effect of land use conversion from native vegetation to cropping on the concentration and molecular composition of OM associated with different mineral phases in a Ferrasol. Overall, this thesis establishes a mechanistic and analytical framework that links DOM composition, mineral surface chemistry, and land use conversation to the formation and persistence of MAOM, and it provides a robust foundation for improving long-term SOC storage to support soil function and climate regulation.

Chapter 1 General introduction

1.1 Background

Soil plays an essential role in the global carbon cycling, and soil organic matter (SOM) is the largest terrestrial organic carbon (OC) reservoir, storing carbon across different OM fractions with turnover time ranging from centuries to millennia (Lal, 2004). Pedogenic minerals are recognised as key drivers of SOM sequestration and turnover (Hemingway et al., 2019), yet the mechanism that govern their interactions with SOM and the stability of mineral associated carbon remain unclear and debated. The pathways of SOM stabilisation are commonly considered to be (i) inherently recalcitrance of specific OM compounds that aggregated as particulate organic matter (POM); (ii) physical protection through occlusion within sol aggregates; and (iii) mineral-organic interactions on mineral surfaces that preserved carbon as mineral associated organic matter (MAOM) (Sollins et al., 1996; Lützow et al., 2006; Kleber et al., 2015). A large proportion of SOM is stored in association with minerals, and the OM preserved as MAOM can minimise degradation by limiting enzyme and microbial attack. Therefore, the formation of MAOM is recognised to play as a key route for carbon sequestration in soil (Kleber et al., 2021; Cotrufo and Lavallee, 2022).

MAOM fractions largely result from the interactions of labile dissolve organic matter, that directly derived from plant decomposition or microbial progressing, with soil minerals including phyllosilicates, metal oxides, and poorly crystalline materials (Basile-Doelsch et al., 2020; Angst et al., 2021). However, mineral-organic interactions are complex and depend strongly on the properties of both minerals and DOM fractions involved. Variation in mineral surface chemistry, such as type, abundance, and charge of reactive surface sites, as well as the size, shape, and specific surface area of mineral particles, contributes to differences in preservation capacity and in the reaction mechanism that occur at mineral surfaces (Chorover and Amistadi, 2001; Mikutta et al., 2007; Barré et al., 2014). The quantity and quality of organic inputs, microbial activity, and soil and climate conditions, together shape the composition and functions of DOM fractions, including element composition, molecular size, functional groups, molecular structure, hydrophobicity or hydrophilicity and redox potential (Kalbitz et al., 2000; Neff and Asner, 2001; Chantigny, 2003; Cleveland et al., 2004). Depending on the organic characteristics of DOM, the pathway by which it stabilises with minerals will also differ. However, the contribution and relationship between mineral types and DOM fractions in the formation of MAOM remains ambiguous and poorly understand. Preferential preservation or molecular fractionation can occur at the mineral-organic interfaces, where mineral surfaces selectively retain specific DOM compounds according to the surface properties and binding mechanisms (Kalbitz et al., 2000; Neff and Asner, 2001; Chantigny, 2003; Cleveland et al., 2004). In addition, not all organic groups within MAOM persist consistently over long-term timescales in soil, since some loosely bond or exchangeable compound can be decomposed through microbial process, such as priming induced by plant exudates (Schmidt et al., 2011; Keiluweit et al., 2015; Basile-Doelsch et al., 2020). As a result, MAOM composition is expected to vary across soil types and land use systems (Leinemann et al., 2018; Mikutta et al., 2019). It is necessary to quantify the contribution of different MAOM fractions to SOM storage under contrasting land uses and soil types, and to identify the most stable fractions, including their organic composition and associated mineral phases. These insights will provide an effective and feasible land management strategy to enhance soil carbon sequestration by targeting specific fractions.

1.2 Aims and scopes of the thesis

The formation of persistent MAOM fractions is not a universal process but is critically dependent on the molecular composition of DOM inputs, the surface chemistry of minerals, the activity and diversity of microbial communities, as well as the soil and environmental conditions. This thesis established synthesised prototype MAOM by systematically investigating the interplay between DOM composition and soil mineralogy to advance understanding of binding mechanisms in mineral-organic interactions. Meanwhile, this thesis focused on the application of different advanced analytical techniques in the MAOM formation studies, and characterised the diversity of MAOM fractions isolated from natural environment under different land use systems. The investigation of SOM stabilisation pathways medicated by DOM and soil minerals in this thesis included laboratory experimental synthesis to mimic and monitor the formation of MAOM fractions, and scaled these mechanistic insights to the field level to characterise and determine the importance of MAOM in soil environments.

In summary, this thesis includes 7 chapters. **Chapter 1** introduced the general background, aims, and structure of the thesis. **Chapter 2** provided a concise and systematic review of current knowledge and gaps on the formation of MAOM, including OM sources, reaction mechanisms, land use effects, and available analytical techniques. **Chapter 3** integrated traditional and advanced spectroscopic techniques to comprehensively characterise DOM fractions from key plant residues, and established a foundation knowledge for chemical convergence in DOM formation; **Chapter 4** investigated reaction behaviours and sequences at mineral-organic interfaces by pairing well-characterised DOM fractions with pure minerals of define surface chemistry to clarify the affinity of different minerals and the relationship between DOM and minerals in MAOM formations; **Chapter 5** applied and compared a novel microspectroscopic imaging technique with a commonly used characterisation method to determine the composition of synthesised mineral-organic complexes and field isolated soil OM fractions; **Chapter 6** evaluated the effect of land use change on the concentration and molecular composition of OM fractions associated with specific mineral phases in a soil; **Chapter 7** highlighted the main outcomes of mineral-organic interactions from laboratory and field investigation and outlined the future research directions for SOM sequestration and preservation. The objective of this thesis is to build a mechanistic and analytical framework that can link DOM features to mineral affinity, enabling robustly predicting the stabilisation of SOM, which is essential for the development of targeted land management strategies to enhance terrestrial carbon sequestration in long-term.

In detail, the main research aims and topics are:

- Determine the complex nature of DOM from contrasting plant residues (i.e., pine, eucalypts, pasture and wheat) using multiple spectroscopic techniques, including Fourier transform infrared spectroscopy (FTIR), X-ray photoelectron spectroscopy (XPS), nuclear magnetic resonance (NMR), near edge X-ray absorption fine structure (NEXAFS), and Fourier-transform ion cyclotron resonance mass spectrometry (FT-ICR-MS) techniques, and integrate the resulting information with multivariate analysis to comprehensively characterise DOM fractions.
- Elucidate the specific reaction processes and preferential adsorption at mineral-organic interfaces by paring DOM fractions with pure minerals (i.e., kaolinite, montmorillonite, goethite, birnessite, ferrihydrite, allophane) using attenuated total reflectance (ATR) FTIR coupled with two dimensional correlation spectroscopy (2D-COS) analysis and NEXAFS spectroscopy, and quantify the contribution of DOM composition and mineral surface chemistry in MAOM formation.
- Compare the analytical capacities of submicron-scale optical photothermal infrared (OPTIR) spectroscopy with ATR-FTIR spectroscopy to characterise the composition of synthesised mineral-organic complexes from model chemical compounds and mineral mixtures, and the nature of POM and MAOM fractions isolated from contrasting mineral soils (i.e., a Ferrasol and a Vertisol).
- Determine the effect of conversion from native vegetation to cropping on the concentration and composition of DOM fraction, organo-metal complex fraction, and OM fractions associated with poorly crystalline and well crystalline mineral phases isolated from a Ferrasol (or Oxisol) using FT-ICR-MS technique, and examine the role of mineral phases in stabilising SOM across land use and depth.

References

Angst, G., Mueller, K.E., Nierop, K.G.J.,Simpson, M.J., 2021. Plant- or microbial-derived? A review on the molecular composition of stabilized soil organic matter. *Soil Biology and Biochemistry 156*, 108189.

Barré, P., Fernandez-Ugalde, O., Virto, I., Velde, B.,Chenu, C., 2014. Impact of phyllosilicate mineralogy on organic carbon stabilization in soils: incomplete knowledge and exciting prospects. *Geoderma 235-236*, 382-395.

Basile-Doelsch, I., Balesdent, J.,Pellerin, S., 2020. Reviews and syntheses: the mechanisms underlying carbon storage in soil. *Biogeosciences 17*(21), 5223-5242.

Chantigny, M.H., 2003. Dissolved and water-extractable organic matter in soils: a review on the influence of land use and management practices. *Geoderma 113*(3), 357-380.

Chorover, J.,Amistadi, M.K., 2001. Reaction of forest floor organic matter at goethite, birnessite and smectite surfaces. *Geochimica et Cosmochimica Acta 65*(1), 95-109.

Cleveland, C.C., Neff, J.C., Townsend, A.R.,Hood, E., 2004. Composition, dynamics, and fate of leached dissolved organic matter in terrestrial ecosystems: results from a decomposition experiment. *Ecosystems 7*(3), 175-285.

Cotrufo, M.F.,Lavallee, J.M., 2022. Chapter one - Soil organic matter formation, persistence, and functioning: a synthesis of current understanding to inform its conservation and regeneration. In: D. L. Sparks (Ed.), *Advances in Agronomy.* Academic Press, pp. 1-66.

Hemingway, J.D., Rothman, D.H., Grant, K.E., Rosengard, S.Z., Eglinton, T.I., Derry, L.A.,Galy, V.V., 2019. Mineral protection regulates long-term global preservation of natural organic carbon. *Nature 570*(7760), 228-231.

Kalbitz, K., Solinger, S., Park, J.H., Michalzik, B.,Matzner, E., 2000. Controls on the dynamics of dissolved organic matter in soils: a review. *Soil Science 165*(4).

Keiluweit, M., Nico, P., Harmon, M.E., Mao, J., Pett-Ridge, J.,Kleber, M., 2015. Long-term litter decomposition controlled by manganese redox cycling. *Proceedings of the National Academy of Sciences 112*(38), E5253-E5260.

Kleber, M., Bourg, I.C., Coward, E.K., Hansel, C.M., Myneni, S.C.B.,Nunan, N., 2021. Dynamic interactions at the mineral–organic matter interface. *Nature Reviews Earth & Environment 2*(6), 402-421.

Kleber, M., Eusterhues, K., Keiluweit, M., Mikutta, C., Mikutta, R.,Nico, P.S., 2015. Chapter one - Mineral–organic associations: formation, properties, and relevance in soil environments. In: D. L. Sparks (Ed.), *Advances in Agronomy.* Academic Press, pp. 1-140.

Lal, R., 2004. Soil carbon sequestration impacts on global climate change and food security. *Science 304*(5677), 1623-1627.

Leinemann, T., Preusser, S., Mikutta, R., Kalbitz, K., Cerli, C., Höschen, C., Mueller, C.W., Kandeler, E.,Guggenberger, G., 2018. Multiple exchange processes on mineral surfaces control the transport of dissolved organic matter through soil profiles. *Soil Biology and Biochemistry 118*, 79-90.

Lützow, M.v., Kögel-Knabner, I., Ekschmitt, K., Matzner, E., Guggenberger, G., Marschner, B.,Flessa, H., 2006. Stabilization of organic matter in temperate soils: mechanisms and their relevance under different soil conditions – a review. *European Journal of Soil*

Science 57(4), 426-445.

Mikutta, R., Mikutta, C., Kalbitz, K., Scheel, T., Kaiser, K.,Jahn, R., 2007. Biodegradation of forest floor organic matter bound to minerals via different binding mechanisms. *Geochimica et Cosmochimica Acta 71*(10), 2569-2590.

Mikutta, R., Turner, S., Schippers, A., Gentsch, N., Meyer-Stüve, S., Condron, L.M., Peltzer, D.A., Richardson, S.J., Eger, A., Hempel, G., Kaiser, K., Klotzbücher, T.,Guggenberger, G., 2019. Microbial and abiotic controls on mineral-associated organic matter in soil profiles along an ecosystem gradient. *Scientific Reports 9*(1), 10294.

Neff, J.C.,Asner, G.P., 2001. Dissolved organic carbon in terrestrial ecosystems: synthesis and a model. *Ecosystems 4*(1), 29-48.

Schmidt, M.W.I., Torn, M.S., Abiven, S., Dittmar, T., Guggenberger, G., Janssens, I.A., Kleber, M., Kögel-Knabner, I., Lehmann, J., Manning, D.A.C., Nannipieri, P., Rasse, D.P., Weiner, S.,Trumbore, S.E., 2011. Persistence of soil organic matter as an ecosystem property. *Nature 478*(7367), 49-56.

Sollins, P., Homann, P.,Caldwell, B.A., 1996. Stabilization and destabilization of soil organic matter: mechanisms and controls. *Geoderma 74*(1), 65-105.

Chapter 2 The dynamics of soil organic matter fractions and mineral-organic interactions in carbon sequestration: A review

2.1 Introduction

Soil organic matter (SOM) is the largest terrestrial organic carbon (OC) pool that containing approximately 2400-3400 Pg of OC within the top 1 m depth, which is more than twice the amount of OC stored in terrestrial vegetations and in the atmosphere (Lal, 2004; Friedlingstein et al., 2025). Changes in SOM pool from mineralisation, leaching, erosion as well as from anthropogenic activities, particularly deforestation and agricultural activities, can significantly increasing CO_2 emissions from soil to atmosphere (Jenkinson et al., 1991). In recent decades, there is growing research interests in the sequestration and preservation of SOM into more stable OC pools for its long-term stabilisation and mitigate climate change (Lal et al., 2015). However, the stabilisation of SOM involves diverse interactions among OM, minerals and microbes, which are affected by many biotic and abiotic factors in soil systems. These mechanisms and processes remain poorly understood.

The stabilisation of SOM is known to occur via (i) molecular recalcitrance of specific OM compounds; (ii) physical protection through occlusion of OM within sol aggregates; and (iii) mineral-organic interactions (Lützow et al., 2006; Kleber et al., 2015). Among these pathways, interactions with minerals have been considered to be critical and important for the long-term preservation of OM. A large portion of SOM (~ 60%) is reported to be intimately associated with minerals, particularly in deeper soil layer (Georgiou et al., 2022). However, SOM is a heterogenous pool that has been partitioned among different fractions. Many recent studies have conceptualised SOM into three fractions based on their size and density: dissolved organic matter (DOM), particulate organic matter (POM) and mineral associated organic matter (MAOM) (Lavallee et al., 2020; Cotrufo and Lavallee, 2022). While researchers debate and focus on the differences between POM and MAOM fractions, in terms of formation pathways, chemical and physical constructs, and stabilisation mechanisms, the importance of the most mobile, reactive and diverse OM pool, i.e., DOM fraction, has largely been neglected (Gmach et al., 2020; Tian et al., 2025). The DOM fraction is also diverse in its composition, being influenced by plant, microbes, minerals, and soil environmental conditions (Kögel-Knabner, 2002). This diversity in the DOM fraction contributes to substantial variability in the SOM stabilisation. Regardless the diverse sources of DOM fraction, once DOM is released in the soil, it can interact and be selectively stabilised by minerals through different chemical mechanisms (Bolan et al., 2011). As a major precursor source of the stabilised OM pools, understanding the dynamics of DOM in soils, including its sources, functions, and transformations is critical for SOM preservation.

Soil minerals exhibit distinct surface characteristics that govern the chemical interactions occurring between DOM and mineral phases (Kleber et al., 2015). Selective adsorption of DOM with minerals, and resulting stability of OM in MAOM may vary substantially, depending upon the binding mechanisms and mineral characteristics (Eusterhues et al., 2011; Avneri-Katz et al., 2017). However, our understanding of these complex mineral-organic interactions is still inadequate. In addition, the composition and stability of OM present in MAOM may differ across soil types and land use systems in combination with the environmental conditions (Bailey et al., 2019; Mayer et al., 2023). In particular, unstable soil conditions resulting from land use change and different agricultural management practices makes it difficult to predict SOM stabilisation (Fu et al., 2024; Ruiz et al., 2024). There is increased focus on increasing MAOM formation, considering it a promising strategy to enhance the sequestration and long-term preservation of SOM. However, the sources, decomposition, transformation, and preservation of SOM are complex and involve various stabilisation and degradation mechanisms. Understanding the pathway of SOM stabilisation with mineral requires a fully characterisation of both DOM and mineral phases. It is also vital to identify limitations for the mineral-organic interactions in specific soil types and land use contexts, which would be essential for designing strategies to enhance SOM storage for climate change mitigation.

To predict the fate of SOM and its stability in soil environments, it is necessary to consider the composition of each participating phase from input through stabilisation, and to evaluate the contribution of each of the reaction mechanisms. This requires advanced analytical techniques to resolve the characteristics and behaviour of OM fractions at molecular scale. With recent advances in novel and sensitive methods, techniques such as ultrahigh-resolution mass spectrometry, synchrotron-based spectroscopy coupled with microscopy, and microscopic imaging, can now probe SOM fractions at nano- to micro-scale and characterise their compositions in natural states or with minimal pre-treatments (Lv et al., 2022). However, different techniques rely on different underlying principles, and each technique provides a specific information reflecting a partial view of SOM. Therefore, investigations of SOM and minerals should employ and integrate multiple techniques to obtain a comprehensive and complete information.

Our understanding of SOM stabilisation remains limited. We can experimentally examine how specific organic compounds or functional groups are stabilised in soil or particular minerals. However, the soil environment is complex and remains a "black box", which shaped by various interacting biotic and abiotic factors. The more deeply we investigate, the more robust and reliable mechanistic models can be built to predict the fate of SOM and to design management strategies increase carbon sequestration in soils. This review focuses on the influence of DOM, minerals, and land use on the mechanisms of mineral-organic interactions and SOM stabilisation pathways. The relevant analytical techniques employed to investigate SOM composition and stability are also discussed. With systematically integrating current knowledge on the interactions between OM and minerals in soil carbon sequestration, the key gaps have been identified. This review proposes a targeted research agenda for examining the role of soil mineral and DOM in SOM stabilising, which will be directly used to design effective land management strategies for climate change mitigation.

2.2 The sources, functions and transformations of dissolved organic matter

Dissolved organic matter is the water-soluble fraction of organic matter that can pass a 0.45 μm filter, which is a complex mixture of low molecular weight compounds and humic-like substances (Herbert and Bertsch, 1995; Haynes, 2005). It participates in physical (leaching and eluviation), chemical (adsorption, complexation, and photodegradation) and biological (decomposition and biotransformation) processes that control the accumulation and stabilisation of SOM in terrestrial ecosystems (Guggenberger and Kaiser, 2003; Marschner and Kalbitz, 2003; Dalzell et al., 2009; Scott and Rothstein, 2014). Understanding the sources, functions and transformations of DOM is crucial for quantifying OM inputs from different origins and their contribution to carbon sequestrations in soils. DOM originates from above-ground inputs and below-ground inputs, including plant residues, root exudates, and microbial metabolites (Kögel-Knabner, 2002), which are influenced by climate conditions, the quantity and quality of organic inputs, microbial activity, soil texture, mineral adsorption and leaching (Kalbitz et al., 2000; Neff and Asner, 2001; Chantigny, 2003; Cleveland et al., 2004).

Plant-derived DOM originates from above-ground plant litter leachate and the below-ground plant root exudates and tissues. It contains cellulose, hemicellulose, lignin, tannin, lipids, cutin and suberin (Kögel-Knabner, 2002). In contrast, microbial-derived DOM is enriched in extracellular enzymes, metabolites and cell-wall derived compounds, including polysaccharides, lipids, proteins, amino sugars, nucleic acids, and chin (Dilly et al., 2004; Kögel-Knabner et al., 2008). Therefore, different sources may impact organic characteristics and functions in DOM, and their fates in soil environment would be expected to be different. Large, hydrophobic plant-derived fragments with polymeric or aromatic structures and low ratio of carboxyl functional groups are preferentially retained on mineral surface in soils, with decreasing proportion through profile (Qualls et al., 1991; Guggenberger et al., 1994; Yan et al., 2018). In contrast, lower molecular weights, more aliphatic, carboxyl- and N-rich microbial derived compounds are more hydrophilic and tend to increase with depths (Veldkamp et al., 2003; Miltner et al., 2009; Kallenbach et al., 2016). The concentration and fluxes of DOM generally decline with soil depth due to the loss of soluble fraction via leaching and runoff into groundwater, as well as microbial respiration and mineralisation (Qualls and Haines, 1992; Sollins et al., 1996). However, some studies have reported that below-ground inputs can exceed above-ground inputs in contributing to recalcitrant OM, especially through plant root exudates and microbial residues and products (Rasse et al., 2005; Kätterer et al., 2011; Sokol and Bradford, 2019). Large uncertainties in the physical, chemical, and biological controls on DOM transformation and decomposition blur the boundaries between above- and below-ground inputs, and also between plant- and microbial-derived contributions (Angst et al., 2018; Angst et al., 2021).

There is an ongoing debate about the mechanisms that govern the fate of DOM through soil profile, including the humification model, progressive decomposition model, selective preservation model and soil continuum model (Sollins et al., 1996; Burdon, 2001; Lehmann and Kleber, 2015; Li et al., 2023b). Regardless their controversial descriptions of the composition and decomposition processes of DOM, there is a basic consensus about the OC preservation after DOM enters soil, which occurs through physical, chemical or biochemical interactions with soil minerals restricting microbial access and decomposition of SOM (Kaiser and Guggenberger, 2000; Kalbitz et al., 2005; Chen et al., 2014). Although some recalcitrant, lightweight plant fragments with partial microbial process can aggregate as particulate organic matter (POM) inhibiting microbial accesses, their stability can be easily altered by any change of environmental conditions (Lavallee et al., 2020; Angst et al., 2023). In contrast, MAOM is widely regarded as the primary stable anchor for preserving OC in soils over centuries to millennia (Sokol et al., 2019). Globally, between 66 and 70% of total SOC is associated with soil mineral, but this represents only about half of their potential capacity to retain SOC and there is still a large deficit for restoring or enhancing storage of MAOM (Georgiou et al., 2022). Therefore, expanding the storage of OC in MAOM is a sound strategy for long-term preservation of SOC, especially in subsoils that contain large volume of mineral fractions with deficit OC saturation, and low DOM concentration and fluxes (Rumpel and Kögel-Knabner, 2011; Kaiser and Kalbitz, 2012; Angst et al., 2018). Understanding the interactions between DOM and minerals is therefore essential for designing management strategies to maximise SOC sequestration under specific land use and soil conditions.

2.3 Mineral-organic interactions and stabilisation pathways

Minerals that participate in the mineral-organic interactions in soil environments may include phyllosilicates (e.g., 1:1 and 2:1 phyllosilicates), metal oxides (the term used to include metal oxides, hydroxides, oxyhydroxides) and poorly crystalline aluminosilicates, all of these exhibit distinct surface characteristics, as well as the size, shape, and specific surface area (Kleber et al., 2015). Depending on the DOM molecular characteristics, such as charges and the abundance of reactive functional groups in relation to mineral surface chemistry, mineral-organic interactions can involve adsorption, complexation, coprecipitation, intercalation within interlayers, and redox reactions (Gu et al., 1994; Kaiser and Guggenberger, 2000; Eusterhues et al., 2011; Chen et al., 2014; Zhang et al., 2019; Hong et al., 2020; Liu et al., 2023). These processes alter the composition of DOM left in solution and selectively fractionate certain OM compounds according to the dominant mechanisms (Eusterhues et al., 2011; Avneri-Katz et al., 2017; Coward et al., 2018; Ding et al., 2019). The adsorption of DOM to minerals is a crucial process in the formation of MAOM in soils, which commonly reflects a combination of mechanisms that include ligand exchange, cation-bridging, electrostatic attraction, H-bond formation, van der Waals interactions, and hydrophobic interactions (Amrhein and Suarez, 1988; Kubicki et al., 1999; Arnarson and Keil, 2000). The prevalence of any of these mechanisms depends on mineral surface chemistry, which governs ligand types, coordination state and spatial organisations (Johnston, 1996; Koretsky et al., 1998).

Mineral surfaces can be grouped based on their charge characteristics variably charged metal oxides, permanently negatively charged phyllosilicates and non-charged phyllosilicates, each favouring different interaction pathways. In variable charged metal oxides, surface hydroxyl groups can be protonated and deprotonated depending on the soil solution pH (Oren and Chefetz, 2012; Mikutta et al., 2014). Under acidic conditions, positively charged surfaces of Fe/Al oxides can attract anionic functional groups (e.g., carboxyl and phenolic groups) in DOM and promote inner-sphere complexes through ligand exchange (Gu et al., 1994; Norén et al., 2008), while at alkaline condition, surface sites become less positive or negative, which increases electrostatic repulsion to inhibit non-specific adsorption (Kleber et al., 2015). However, DOM adsorption can still proceed through cation bridging involving polyvalent ions (such as Ca^{2+}, Mg^{2+}, Fe^{3+} and Al^{3+}) and H-bonding with anionic or polar functional groups (e.g., amino, carboxyl, and hydroxyl groups) in DOM (Johnson et al., 2004; Norén and Persson, 2007). Permanent charged phyllosilicates, such as smectites, isomorphous substitution (e.g., Mg^{2+}, for Al^{3+}, Al^{3+} for Si^{3+} substitution) in the structure promotes the absorption of DOM compounds on negatively charged surfaces, mainly through cation bridging and H-bonding, forming inner- and outer-sphere complexes (Arnarson and Keil, 2000; Chefetz et al., 2011; Chen et al., 2017). In the expandable 2:1 clay minerals, suitable DOM molecules can also penetrate in their interlayer region, but it is limited by the DOM size, shape and charges (Hong et al., 2020; Liu et al., 2023). For variable charge phyllosilicates, such as kaolinite, the entropy-derived hydrophobic attraction with van der Waals forces and H-bonding can be the primary adsorption pathways for nonpolar DOM molecules (Ghosh et al., 2009; Chen et al., 2017; Kasprzhitskii et al., 2022). In addition, variably charged hydroxyl groups present at the edge of minerals, particularly octahedral sheets, can behave similar to Fe/Al oxide surfaces by forming inner- and outer-sphere complexes with DOM (Jaynes and Boyd, 1991; Feng et al., 2005; Chen et al., 2017).

In addition, coprecipitation between DOM and multivalent metal specisies provides another pathway for stablising OM in soil envrionments (Kleber et al., 2015; Chen et al., 2016; Hamada et al., 2025). During the hydrolysis of multivalent metals (e.g., Fe^{3+} and Al^{3+}) toward nucleation, crystal growth, and subsequent aggregation to larger oxide particles, monomeric or polymeric Fe/Al species can coprecipitate with different size of organic ligands, forming two types of coprecipitates: organic moelcules occluded within metal clusters or metal oxides embedded in organic matrixs (Mikutta et al., 2011; Mikutta et al., 2014; Kleber et al., 2015; Possinger et al., 2021). Compared with adsorption complexes, these more uniformly mixed coprecipitates often retain more organic carbon, and their formartions depends largely on the initial metal to organic ratio (Chen et al., 2014; Sodano et al., 2017; Wen et al., 2021; Lenhardt et al., 2022). Microbial activities on mineral surfaces also has major effects on the mineral-organic interactions.

Microbes can interact with soil minerals by ultilising organic fractions stablsied by minerals to release CO_2, by mediating mineral formation and dissolution, as well as by inducing electron transfer between organic carbon and minerals to organic transfromation (Kleber et al., 2015; Pronk et al., 2017; Zhang et al., 2021). Their residues, such as extracellular polymeric substances (EPS), enzymes and organic acids, are another major sources of mineral associated organic matter, and have been reproted to account for at least half of stablised OM fractions in soils (Six et al., 2006; Paul, 2016; Angst et al., 2021). However, the detailed mechanisms by which microbial activities mediate mineral-organic interactions and drive the formation and stabilisation of mineral associated organic matter remain poorly understood.

Mineral-organic interaction is dynamic in nature. Diffusion, competition and exchange reactions occur concurrently at mineral-organic interface (Kleber et al., 2021). The stability of adsorbed OM depends on the bonding mechanisms and strength of resulting complexes (Oren and Chefetz, 2012; Azimzadeh and Martínez, 2024). In addition, competition between organic compounds and ongoing biotic or abiotic degradation of adsorbed OM continually reshape carbon cycling in soils, through leaching desorbed OM to deeper layers or through mineralisation to release CO_2 to the atmosphere (Violante and Pigna, 2002; Mikutta et al., 2007). To enhance the formation of MAOM toward mineral saturation and increase SOC sequestration, management should focus on maintaining favourable soil pH and electrolyte regimes, increasing reactive mineral surfaces and supply of high quality DOM with functional groups matching with the soil minerals (Angst et al., 2023; Angst et al., 2025). Therefore, a clear understanding of adsorption and transformation pathway across minerals and DOM sources is necessary and would provide the basis for predicting SOC sequestration potential across land uses and soil types. However, in soil environments, heterogenous DOM input and diverse soil mineralogy complicate the attribution of specific mechanism and the organic composition retained on mineral fractions. A systematic study that pairs well characterised DOM fractions with minerals of defined surface chemistry is needed to investigate the mechanism, behaviour and consequences of mineral-organic interactions.

2.4 Effect of land use and management

The content of SOM is sensitive to the changes in land use and management. Such changes can alter the quantity and quality of organic inputs, abundance and activity of microbial communities, and soil properties including aggregation, temperature, aeration, and water retention, reflecting a combination of effects and complex interactions in soil environment (Hoffland et al., 2020). For example, the conversion of land use from native forest to agricultural cropland or grassland can result in SOC losses of 15 to 25 % (Beillouin et al., 2023). However, with appropriate management, such as manure application, no-till farming, cover cropping and agroforestry, the loss of SOC stock in agricultural systems can be restored, yet the recovery of SOC is still slower and the level lower than the original SOC contents (Dignac et al., 2017). DOM equilibrates between labile aqueous pools and immobile solid pools in the territorial environment, contributing to the amount of SOC, which is always associated to the amount of DOC (Marschner and Kalbitz, 2003; Eder et al., 2022). Therefore, the change of land use (e.g., deforestation and forestation) and the cover of landscape (e.g., agricultural activities and managements) will also affect the quantity and quality of DOM (Graeber et al., 2012; Humbert et al., 2020). However, the relationship between SOC and DOC is not always consistent. Many studies have indicated that the concentration of DOC is not solely correlated to the concentration of SOC alone, but is also influenced by other factors, such as the weather conditions, topography and soil texture, particularly in the context of land conversion from native to cultivated land (Giling et al., 2014; Chen et al., 2021; Tong et al., 2021).

Different DOM fractions respond differently to changes in land use or management. Labile DOM and less protected POM fractions are particularly sensitive to land use and vegetation cover because they are dynamic and transient, with short residence time (i.e., decades) controlled by plant litter inputs and microbial activity (Haynes, 2005; Kögel-Knabner et al., 2008; Derrien et al., 2023). In contrast, MAOM fractions is less responsive to altered soil conditions resulting from land use change, due to physical and chemical protection by mineral fractions (Kögel-Knabner et al., 2008; Jilling et al., 2025). However, changes in organic inputs and microbial processing also influence OC cycling within MAOM. Agricultural managements can alter disturbance regimes, external inputs, plant diversity, and soil environments including temperature and moisture, which would influence mineral-organic interactions (Bailey et al., 2019; Mayer et al., 2023). For example, tillage can disrupt soil aggregates, changing the physical contact between OM and minerals and increasing microbial accessibility (Fu et al., 2024). Irrigation or rainfall can modify redox conditions and solution chemistry, which would shift dynamic of adsorption, desorption and exchange reactions at mineral-organic interfaces and ultimately influences the stability of MAOM (Ruiz et al., 2024). Some studies have reported that recalcitrant and resistant OM fractions may be less stable than traditionally assumed - that labile OM fractions deplete first, followed by recalcitrant pools (Dalal et al., 2021; Hondroudakis et al., 2024). Instead, all OM fractions may be altered and decomposed simultaneously by different microbial processes (Thevenot et al., 2010). This increases uncertainty to predict the stability of SOM due to the complex of input, decomposition, transformation and preservation of OM fractions (Li et al., 2023b). To experimentally characterise the stabilisation mechanisms in context of land use change, targeted studies should focus on specific OM fraction in soil or on the effects of specific mineral phases on OM stabilisation.

2.5 Analytical spectroscopic, spectrometric and microscopic approaches at molecular level

Analytical techniques for OM characterisation can be broadly grouped into spectroscopic, spectrometric, and microscopic methods, which rely on their different fundamental principles to target different aspects of organic characteristics. Spectroscopic techniques use various radiation sources, including X-ray, UV, visible, infrared, as well as radio wave or magnetic field, to probe the molecular bonds, functional groups, structures in organic particles or solutions (Minor et al., 2014; Lv et al., 2022). They include, but are not limited to, ultraviolet-visible (UV-vis) spectroscopy, Fourier transform infrared (FTIR) spectroscopy, X-ray photoelectron spectroscopy (XPS), Nuclear magnetic resonance (NMR) spectroscopy and Near edge X-ray absorption fine structure (NEXAFS) spectroscopy. Ultrahigh spectrometric techniques, such as Fourier transform ion cyclotron resonance mass spectrometry (FT-ICR-MS), are increasingly used to decipher the molecular characteristics of SOM (Bahureksa et al., 2021). These can detect and resolve individual molecular compositions in complex SOM fractions with ultrahigh mass accuracy by ionising molecules via electrospray or at atmospheric pressure (Kim et al., 2022). However, each molecular formula detected by FT-ICR-MS may correspond to many isomers, with limited ability to provide structural information (Nebbioso and Piccolo, 2013; Minor et al., 2014). In such cases, FT-ICR-MS is typically used in conjunction with other techniques, such as NMR. Recent developments in microimaging techniques have enabled *in situ* analysis of elemental, isotopic, molecular visualisation at very fine-scale in mineral-organic complexes and aggregates without destructive extraction (Lv et al., 2022). Synchrotron-based spectroscopy, such as NEXAFS, can be coupled with scanning transmission X-ray microscopy (STXM) to provide spatially resolved elemental speciation of SOM fractions within 30 nm resolution (Lehmann et al., 2005). Synchrotron-based FTIR (SR-FTIR) microscopy also offers high spatial resolution (~10 μm) and sensitivity for mapping the distribution of OM components according to their chemical bond or functional groups (Xiao et al., 2018). Nanoscale secondary ion mass spectrometry (NanoSIMS) is another powerful technique that linking microscopy with isotopic analysis to generate nanoscale (~50 nm) spatial information of elemental isotopes in organic materials (Remusat et al., 2012). However, limited access and high cost for synchrotron techniques, and the cumbersome sample preparation required for NanoSIMS and sensitivity in some cases (Lehmann and Solomon, 2010; Li et al., 2023a), there is still a need for an analytical technique that is easily accessible, requires minimal preparation, non-destructive and can balance sensitivity, chemical specificity, spatial resolution and sample throughput. Recently, optical photothermal infrared (OPTIR) microscopy has been developed to map the molecular distributions of OM components using optical thermal sources. It achieves spatial resolution within 500 nm and requires only minimal sample preparation, and this has been recently applied for the organic characterisation of mineral-organic complexes in soils (Olson et al., 2020; Jubb et al., 2023; Liu et al., 2024; Jamoteau et al., 2025).

However, no single analytical technique can fully elucidate the complexity of SOM. Due to the inherent limitation of different techniques in their sample preparation and sensitivity, only partial or contrasting information can be obtained by using only one or limited number of techniques. Therefore, to capture the complementary aspects of their composition and reactivity, and to generate reliable and accurate results, it is essential to integrate several techniques, which enables cross-checking of obtained information and provides a more complete picture of SOM fractions at the molecular level.

2.6 Conclusion

This review has briefly synthesised the complex interplay among DOM, soil mineral, and land use as primary drivers of SOM stabilisation. The long-term sequestration of OC in soils is not a passive but dynamic process. The progress from fresh plant and microbial debris to the stable MAOM pool and is fundamentally governed by the transformation of DOM and its subsequent interactions with minerals at the molecular level. Therefore, rigorous characterisation of DOM fractions prior to any model experimental studies is not merely an analytical exercise but a critical prerequisite for understanding SOM sequestration. The heterogeneous nature of DOM, whether plant or microbial derived, dictates its fate, mobility and reactivity at mineral surfaces. Predicting the complex chemical mechanisms at mineral-organic interfaces is difficult due to these intricate processes, which are profoundly sensitive to chemical characteristics of both DOM and mineral phases, as well as external environmental factors. Different land use and management practises exert a profound influence on this delicate system. Land use change affects not only the quantity and quality of SOM input but also disrupts mineral-organic interactions and the stability of SOM fractions. However, there is still a large uncertainty about the role of mineral phases in protecting stabilised OM fractions after the land use change. Identifying the most stable OM fractions and facilitating their stabilisation would be an effective land management strategy to enhance the carbon sequestration in soil. In addition, advanced analytical techniques are indispensable for observing and predicting mineral-organic interactions at molecular level. However, no single method can unravel the inherent complexity of OM fractions. It is therefore necessary to integrate multiple complementary techniques to fully resolve the composition, spatial distribution and bonding mechanisms of MAOM from the nano- to micro-scale.

Therefore, closing the current knowledge gaps requires a targeted research agenda that includes (i) conducting systemic experiments paring well-characterised DOM with soil minerals of defined surface chemistry to isolate and quantify mineral-organic interactions; (ii) identifying the stable OM fractions associated with specific mineral phases across different land use; (iii) developing integrated analytical frameworks that integrate data from multiple techniques; and (iv) promoting and examining new high-resolution techniques to probe mineral-organic interactions and heterogeneity of mineral-organic complexes in their natural state. By deepening our understanding of the nexus between DOM, minerals, and land use, we can advance beyond generic carbon input strategies to effectively engineer the formation of stable OM fractions, thereby maximise the terrestrial carbon sink for climate change mitigation.

References

Amrhein, C.,Suarez, D.L., 1988. The use of a surface complexation model to describe the kinetics of ligand-promoted dissolution of anorthite. *Geochimica et Cosmochimica Acta 52*(12), 2785-2793.

Angst, G., Messinger, J., Greiner, M., Häusler, W., Hertel, D., Kirfel, K., Kögel-Knabner, I., Leuschner, C., Rethemeyer, J.,Mueller, C.W., 2018. Soil organic carbon stocks in topsoil and subsoil controlled by parent material, carbon input in the rhizosphere, and microbial-derived compounds. *Soil Biology and Biochemistry 122*, 19-30.

Angst, G., Mueller, K.E., Castellano, M.J., Vogel, C., Wiesmeier, M.,Mueller, C.W., 2023. Unlocking complex soil systems as carbon sinks: multi-pool management as the key. *Nature Communications 14*(1), 2967.

Angst, G., Mueller, K.E., Nierop, K.G.J.,Simpson, M.J., 2021. Plant- or microbial-derived? A review on the molecular composition of stabilized soil organic matter. *Soil Biology and Biochemistry 156*, 108189.

Angst, Š., Angst, G., Mueller, K.E., Lange, M.,Eisenhauer, N., 2025. Un(der)explored links between plant diversity and particulate and mineral-associated organic matter in soil. *Nature Communications 16*(1), 5548.

Arnarson, T.S.,Keil, R.G., 2000. Mechanisms of pore water organic matter adsorption to montmorillonite. *Marine Chemistry 71*(3), 309-320.

Avneri-Katz, S., Young, R.B., McKenna, A.M., Chen, H., Corilo, Y.E., Polubesova, T., Borch, T.,Chefetz, B., 2017. Adsorptive fractionation of dissolved organic matter (DOM) by mineral soil: macroscale approach and molecular insight. *Organic Geochemistry 103*, 113-124.

Azimzadeh, B.,Martínez, C.E., 2024. Unraveling the role of polysaccharide-goethite associations on glyphosate' adsorption–desorption dynamics and binding mechanisms. *Journal of Colloid and Interface Science 653*, 1283-1292.

Bahureksa, W., Tfaily, M.M., Boiteau, R.M., Young, R.B., Logan, M.N., McKenna, A.M.,Borch, T., 2021. Soil organic matter characterization by Fourier transform ion cyclotron resonance mass spectrometry (FTICR MS): a critical review of sample preparation, analysis, and data interpretation. *Environmental Science & Technology 55*(14), 9637-9656.

Bailey, V.L., Pries, C.H.,Lajtha, K., 2019. What do we know about soil carbon destabilization? *Environmental Research Letters 14*(8), 083004.

Beillouin, D., Corbeels, M., Demenois, J., Berre, D., Boyer, A., Fallot, A., Feder, F.,Cardinael, R., 2023. A global meta-analysis of soil organic carbon in the Anthropocene. *Nature Communications 14*(1), 3700.

Bolan, N.S., Adriano, D.C., Kunhikrishnan, A., James, T., McDowell, R.,Senesi, N., 2011. Chapter one - Dissolved organic matter: biogeochemistry, dynamics, and environmental significance in soils. In: D. L. Sparks (Ed.), *Advances in Agronomy.* Academic Press, pp. 1-75.

Burdon, J., 2001. Are the traditional concepts of the structures of humic substances realistic? *Soil Science 166*(11), 752-769.

Chantigny, M.H., 2003. Dissolved and water-extractable organic matter in soils: a review on the influence of land use and management practices. *Geoderma 113*(3), 357-380.

Chefetz, B., Eldad, S.,Polubesova, T., 2011. Interactions of aromatic acids with montmorillonite: Ca2+- and Fe3+-saturated clays versus Fe3+–Ca2+-clay system. *Geoderma 160*(3), 608-613.

Chen, C., Dynes, J.J., Wang, J.,Sparks, D.L., 2014. Properties of Fe-organic matter associations via coprecipitation versus adsorption. *Environmental Science & Technology 48*(23), 13751-13759.

Chen, H., Koopal, L.K., Xiong, J., Avena, M.,Tan, W., 2017. Mechanisms of soil humic acid adsorption onto montmorillonite and kaolinite. *Journal of Colloid and Interface Science 504*, 457-467.

Chen, K.-Y., Chen, T.-Y., Chan, Y.-T., Cheng, C.-Y., Tzou, Y.-M., Liu, Y.-T.,Teah, H.-Y., 2016. Stabilization of natural organic matter by short-range-order iron hydroxides. *Environmental Science & Technology 50*(23), 12612-12620.

Chen, S., Du, Y., Das, P., Lamore, A.F., Dimova, N.T., Elliott, M., Broadbent, E.N., Roebuck, J.A., Jaffé, R.,Lu, Y., 2021. Agricultural land use changes stream dissolved organic matter via altering soil inputs to streams. *Science of The Total Environment 796*, 148968.

Cleveland, C.C., Neff, J.C., Townsend, A.R.,Hood, E., 2004. Composition, dynamics, and fate of leached dissolved organic matter in terrestrial ecosystems: results from a decomposition experiment. *Ecosystems 7*(3), 175-285.

Cotrufo, M.F.,Lavallee, J.M., 2022. Chapter one - Soil organic matter formation, persistence, and functioning: a synthesis of current understanding to inform its conservation and regeneration. In: D. L. Sparks (Ed.), *Advances in Agronomy.* Academic Press, pp. 1-66.

Coward, E.K., Ohno, T.,Plante, A.F., 2018. Adsorption and molecular fractionation of dissolved organic matter on iron-bearing mineral matrices of varying crystallinity. *Environmental Science & Technology 52*(3), 1036-1044.

Dalal, R.C., Thornton, C.M., Allen, D.E., Owens, J.S.,Kopittke, P.M., 2021. Long-term land use change in Australia from native forest decreases all fractions of soil organic carbon, including resistant organic carbon, for cropping but not sown pasture. *Agriculture, Ecosystems & Environment 311*, 107326.

Dalzell, B.J., Minor, E.C.,Mopper, K.M., 2009. Photodegradation of estuarine dissolved organic matter: a multi-method assessment of DOM transformation. *Organic Geochemistry 40*(2), 243-257.

Derrien, D., Barré, P., Basile-Doelsch, I., Cécillon, L., Chabbi, A., Crème, A., Fontaine, S., Henneron, L., Janot, N., Lashermes, G., Quénéa, K., Rees, F.,Dignac, M.-F., 2023. Current controversies on mechanisms controlling soil carbon storage: implications for interactions with practitioners and policy-makers. A review. *Agronomy for Sustainable Development 43*(1), 21.

Dignac, M.-F., Derrien, D., Barré, P., Barot, S., Cécillon, L., Chenu, C., Chevallier, T., Freschet, G.T., Garnier, P., Guenet, B., Hedde, M., Klumpp, K., Lashermes, G., Maron, P.-A., Nunan, N., Roumet, C.,Basile-Doelsch, I., 2017. Increasing soil carbon storage: mechanisms, effects of agricultural practices and proxies. A review. *Agronomy for Sustainable Development 37*(2), 14.

Dilly, O., Bloem, J., Vos, A.,Munch Jean, C., 2004. Bacterial diversity in agricultural soils during litter decomposition. *Applied and Environmental Microbiology 70*(1), 468-474.

Ding, Y., Lu, Y., Liao, P., Peng, S., Liang, Y., Lin, Z., Dang, Z.,Shi, Z., 2019. Molecular fractionation and sub-nanoscale distribution of dissolved organic matter on allophane. *Environmental Science: Nano 6*(7), 2037-2048.

Eder, A., Weigelhofer, G., Pucher, M., Tiefenbacher, A., Strauss, P., Brandl, M.,Blöschl, G., 2022. Pathways and composition of dissolved organic carbon in a small agricultural catchment during base flow conditions. *Ecohydrology & Hydrobiology 22*(1), 96-112.

Eusterhues, K., Rennert, T., Knicker, H., Kögel-Knabner, I., Totsche, K.U.,Schwertmann, U., 2011. Fractionation of organic matter due to reaction with ferrihydrite: coprecipitation versus adsorption. *Environmental Science & Technology 45*(2), 527-533.

Feng, X., Simpson, A.J.,Simpson, M.J., 2005. Chemical and mineralogical controls on humic acid sorption to clay mineral surfaces. *Organic Geochemistry 36*(11), 1553-1566.

Friedlingstein, P., O'Sullivan, M., Jones, M.W., Andrew, R.M., Hauck, J., Landschützer, P., Le Quéré, C., Li, H., Luijkx, I.T., Olsen, A., Peters, G.P., Peters, W., Pongratz, J., Schwingshackl, C., Sitch, S., Canadell, J.G., Ciais, P., Jackson, R.B., Alin, S.R., Arneth, A., Arora, V., Bates, N.R., Becker, M., Bellouin, N., Berghoff, C.F., Bittig, H.C., Bopp, L., Cadule, P., Campbell, K., Chamberlain, M.A., Chandra, N., Chevallier, F., Chini, L.P., Colligan, T., Decayeux, J., Djeutchouang, L.M., Dou, X., Duran Rojas, C., Enyo, K., Evans, W., Fay, A.R., Feely, R.A., Ford, D.J., Foster, A., Gasser, T., Gehlen, M., Gkritzalis, T., Grassi, G., Gregor, L., Gruber, N., Gürses, Ö., Harris, I., Hefner, M., Heinke, J., Hurtt, G.C., Iida, Y., Ilyina, T., Jacobson, A.R., Jain, A.K., Jarníková, T., Jersild, A., Jiang, F., Jin, Z., Kato, E., Keeling, R.F., Klein Goldewijk, K., Knauer, J., Korsbakken, J.I., Lan, X., Lauvset, S.K., Lefèvre, N., Liu, Z., Liu, J., Ma, L., Maksyutov, S., Marland, G., Mayot, N., McGuire, P.C., Metzl, N., Monacci, N.M., Morgan, E.J., Nakaoka, S.I., Neill, C., Niwa, Y., Nützel, T., Olivier, L., Ono, T., Palmer, P.I., Pierrot, D., Qin, Z., Resplandy, L., Roobaert, A., Rosan, T.M., Rödenbeck, C., Schwinger, J., Smallman, T.L., Smith, S.M., Sospedra-Alfonso, R., Steinhoff, T., Sun, Q., Sutton, A.J., Séférian, R., Takao, S., Tatebe, H., Tian, H., Tilbrook, B., Torres, O., Tourigny, E., Tsujino, H., Tubiello, F., van der Werf, G., Wanninkhof, R., Wang, X., Yang, D., Yang, X., Yu, Z., Yuan, W., Yue, X., Zaehle, S., Zeng, N.,Zeng, J., 2025. Global carbon budget 2024. *Earth Syst. Sci. Data 17*(3), 965-1039.

Fu, Z., Hu, W., Beare, M.,Baird, D., 2024. Soil macroaggregate-occluded mineral-associated organic carbon drives the response of soil organic carbon to land use change. *Soil and Tillage Research 244*, 106271.

Georgiou, K., Jackson, R.B., Vindušková, O., Abramoff, R.Z., Ahlström, A., Feng, W., Harden, J.W., Pellegrini, A.F.A., Polley, H.W., Soong, J.L., Riley, W.J.,Torn, M.S., 2022. Global stocks and capacity of mineral-associated soil organic carbon. *Nature Communications 13*(1), 3797.

Ghosh, S., Wang, Z.-Y., Kang, S., Bhowmik, P.C.,Xing, B.S., 2009. Sorption and fractionation of a peat derived humic acid by kaolinite, montmorillonite, and goethite. *Pedosphere 19*(1), 21-30.

Giling, D.P., Grace, M.R., Thomson, J.R., Mac Nally, R.,Thompson, R.M., 2014. Effect of native vegetation loss on stream ecosystem processes: dissolved organic matter composition and export in agricultural landscapes. *Ecosystems 17*(1), 82-95.

Gmach, M.R., Cherubin, M.R., Kaiser, K.,Cerri, C.E.P., 2020. Processes that influence dissolved organic matter in the soil: a review. *Scientia Agricola 77*.

Graeber, D., Gelbrecht, J., Pusch, M.T., Anlanger, C.,von Schiller, D., 2012. Agriculture has changed the amount and composition of dissolved organic matter in Central European headwater streams. *Science of The Total Environment 438*, 435-446.

Gu, B., Schmitt, J., Chen, Z., Liang, L.,McCarthy, J.F., 1994. Adsorption and desorption of natural organic matter on iron oxide: mechanisms and models. *Environmental Science & Technology 28*(1), 38-46.

Guggenberger, G.,Kaiser, K., 2003. Dissolved organic matter in soil: challenging the paradigm of sorptive preservation. *Geoderma 113*(3), 293-310.

Guggenberger, G., Zech, W.,Schulten, H.-R., 1994. Formation and mobilization pathways of dissolved organic matter: evidence from chemical structural studies of organic matter fractions in acid forest floor solutions. *Organic Geochemistry 21*(1), 51-66.

Hamada, K., Yimatsa, N., Ohtsuka, T., Fujitake, N., Miyajima, T., Yokoyama, Y., Miyairi, Y.,Kida, M., 2025. Organo-metal coprecipitation contributes to stable organic carbon fraction in mangrove soil. *CATENA 256*, 109075.

Haynes, R.J., 2005. Labile organic matter fractions as central components of the quality of agricultural soils: an overview. In: *Advances in Agronomy.* Academic Press, pp. 221-268.

Herbert, B.E.,Bertsch, P.M., 1995. Characterization of dissolved and colloidal organic matter in soil solution: a review. In: *Carbon Forms and Functions in Forest Soils.* pp. 63-88.

Hoffland, E., Kuyper, T.W., Comans, R.N.J.,Creamer, R.E., 2020. Eco-functionality of organic matter in soils. *Plant and Soil 455*(1), 1-22.

Hondroudakis, L., Kopittke, P.M., Dalal, R.C., Barnard, M.,Weng, Z.H., 2024. The influence of land use and management on the behaviour and persistence of soil organic carbon in a subtropical Ferralsol. *SOIL 10*(2), 451-465.

Hong, H., Fang, Q., Churchman, G.J., Zhao, L., Ji, K., Jin, X., Yin, K., Wang, C.,Liu, C., 2020. Study of organic-matter intercalated vermiculitic phases in the hydromorphic red earth sediments. *Applied Clay Science 196*, 105744.

Humbert, G., Parr, T.B., Jeanneau, L., Dupas, R., Petitjean, P., Akkal-Corfini, N., Viaud, V., Pierson-Wickmann, A.-C., Denis, M., Inamdar, S., Gruau, G., Durand, P.,Jaffrézic, A., 2020. Agricultural practices and hydrologic conditions shape the temporal pattern of soil and stream water dissolved organic matter. *Ecosystems 23*(7), 1325-1343.

Jamoteau, F., Kansiz, M., Unger, M.,Keiluweit, M., 2025. Probing mineral-organic interfaces in soils and sediments using optical photothermal infrared microscopy. *Environmental Science & Technology 59*(1), 501-512.

Jaynes, W.F.,Boyd, S.A., 1991. Hydrophobicity of siloxane surfaces in smectites as revealed by aromatic hydrocarbon adsorption from water. *Clays and Clay Minerals 39*(4), 428-436.

Jenkinson, D.S., Adams, D.E.,Wild, A., 1991. Model estimates of CO2 emissions from soil in response to global warming. *Nature 351*(6324), 304-306.

Jilling, A., Grandy, A.S., Daly, A.B., Hestrin, R., Possinger, A., Abramoff, R., Annis, M., Cates, A.M., Dynarski, K., Georgiou, K., Heckman, K., Keiluweit, M., Lang, A.K., Phillips, R.P., Rocci, K., Shabtai, I.A., Sokol, N.W.,Whalen, E.D., 2025. Evidence for the existence and ecological relevance of fast-cycling mineral-associated organic matter. *Communications Earth & Environment 6*(1), 690.

Johnson, S.B., Yoon, T.H., Kocar, B.D.,Brown, G.E., 2004. Adsorption of organic matter at mineral/water interfaces. 2. outer-sphere adsorption of maleate and implications for dissolution processes. *Langmuir 20*(12), 4996-5006.

Johnston, C.T., 1996. Sorption of organic compounds on clay minerals: a surface functional group approach. In: J. W. Blackburn, F. Cadena, E. Cazares, S. Chattopadhyay, R. W. Gullick, D. Gray, C. T. Johnston, B. L. Sawhney, S. Traina, W. Weber, and B. L. Sawhney (Eds.), *Organic Pollutants in the Environment.* Clay Minerals Society, pp. 0.

Jubb, A.M., Rebecca Stokes, M., McAleer, R.J., Hackley, P.C., Dillon, E.,Qu, J., 2023. Mapping ancient sedimentary organic matter molecular structure at nanoscales using optical photothermal infrared spectroscopy. *Organic Geochemistry 177*, 104569.

Kaiser, K.,Guggenberger, G., 2000. The role of DOM sorption to mineral surfaces in the preservation of organic matter in soils. *Organic Geochemistry 31*(7), 711-725.

Kaiser, K.,Kalbitz, K., 2012. Cycling downwards – dissolved organic matter in soils. *Soil Biology and Biochemistry 52*, 29-32.

Kalbitz, K., Schwesig, D., Rethemeyer, J.,Matzner, E., 2005. Stabilization of dissolved organic matter by sorption to the mineral soil. *Soil Biology and Biochemistry 37*(7), 1319-1331.

Kalbitz, K., Solinger, S., Park, J.H., Michalzik, B.,Matzner, E., 2000. Controls on the dynamics of dissolved organic matter in soils: a review. *Soil Science 165*(4).

Kallenbach, C.M., Frey, S.D.,Grandy, A.S., 2016. Direct evidence for microbial-derived soil organic matter formation and its ecophysiological controls. *Nature Communications 7*(1), 13630.

Kasprzhitskii, A., Lazorenko, G., Kharytonau, D.S., Osipenko, M.A., Kasach, A.A.,Kurilo, I.I., 2022. Adsorption mechanism of aliphatic amino acids on kaolinite surfaces. *Applied Clay Science 226*, 106566.

Kätterer, T., Bolinder, M.A., Andrén, O., Kirchmann, H.,Menichetti, L., 2011. Roots contribute more to refractory soil organic matter than above-ground crop residues, as revealed by a long-term field experiment. *Agriculture, Ecosystems & Environment 141*(1), 184-192.

Kim, S., Kim, D., Jung, M.-J.,Kim, S., 2022. Analysis of environmental organic matters by ultrahigh-resolution mass spectrometry—a review on the development of analytical methods. *Mass Spectrometry Reviews 41*(2), 352-369.

Kleber, M., Bourg, I.C., Coward, E.K., Hansel, C.M., Myneni, S.C.B.,Nunan, N., 2021. Dynamic interactions at the mineral–organic matter interface. *Nature Reviews Earth & Environment 2*(6), 402-421.

Kleber, M., Eusterhues, K., Keiluweit, M., Mikutta, C., Mikutta, R.,Nico, P.S., 2015. Chapter one - Mineral–organic associations: formation, properties, and relevance in soil environments. In: D. L. Sparks (Ed.), *Advances in Agronomy.* Academic Press, pp. 1-140.

Kögel-Knabner, I., 2002. The macromolecular organic composition of plant and microbial residues as inputs to soil organic matter. *Soil Biology and Biochemistry 34*(2), 139-162.

Kögel-Knabner, I., Guggenberger, G., Kleber, M., Kandeler, E., Kalbitz, K., Scheu, S., Eusterhues, K.,Leinweber, P., 2008. Organo-mineral associations in temperate soils: integrating biology, mineralogy, and organic matter chemistry. *Journal of Plant Nutrition and Soil Science 171*(1), 61-82.

Koretsky, C.M., Sverjensky, D.A.,Sahai, N., 1998. A model of surface site types on oxide and silicate minerals based on crystal chemistry: implications for site types and densities, multi-site adsorption, surface infrared spectroscopy, and dissolution kinetics. *American Journal of Science 298*(5), 349-438.

Kubicki, J.D., Schroeter, L.M., Itoh, M.J., Nguyen, B.N.,Apitz, S.E., 1999. Attenuated total reflectance Fourier-transform infrared spectroscopy of carboxylic acids adsorbed onto mineral surfaces. *Geochimica et Cosmochimica Acta 63*(18), 2709-2725.

Lal, R., 2004. Soil carbon sequestration impacts on global climate change and food security. *Science 304*(5677), 1623-1627.

Lal, R., Negassa, W.,Lorenz, K., 2015. Carbon sequestration in soil. *Current Opinion in Environmental Sustainability 15*, 79-86.

Lavallee, J.M., Soong, J.L.,Cotrufo, M.F., 2020. Conceptualizing soil organic matter into particulate and mineral-associated forms to address global change in the 21st century. *Global Change Biology 26*(1), 261-273.

Lehmann, J.,Kleber, M., 2015. The contentious nature of soil organic matter. *Nature 528*(7580), 60-68.

Lehmann, J., Liang, B., Solomon, D., Lerotic, M., Luizão, F., Kinyangi, J., Schäfer, T., Wirick, S.,Jacobsen, C., 2005. Near-edge X-ray absorption fine structure (NEXAFS) spectroscopy for mapping nano-scale distribution of organic carbon forms in soil: application to black carbon particles. *Global Biogeochemical Cycles 19*(1).

Lehmann, J.,Solomon, D., 2010. Chapter 10 - Organic carbon chemistry in soils observed by synchrotron-based spectroscopy. In: B. Singh and M. Gräfe (Eds.), *Developments in Soil Science.* Elsevier, pp. 289-312.

Lenhardt, K.R., Breitzke, H., Buntkowsky, G., Mikutta, C.,Rennert, T., 2022. Interactions of dissolved organic matter with short-range ordered aluminosilicates by adsorption and co-precipitation. *Geoderma 423*, 115960.

Li, Q., Chang, J., Li, L., Lin, X.,Li, Y., 2023a. Research progress of nano-scale secondary ion mass spectrometry (NanoSIMS) in soil science: evolution, applications, and challenges. *Science of The Total Environment 905*, 167257.

Li, Q., Wang, L., Fu, Y., Lin, D., Hou, M., Li, X., Hu, D.,Wang, Z., 2023b. Transformation of soil organic matter subjected to environmental disturbance and preservation of organic matter bound to soil minerals: a review. *Journal of Soils and Sediments 23*(3), 1485-1500.

Liu, D., Li, M., Yu, R., Li, H., Shen, Y., Tian, Q., Bu, H., Huang, C.,Tan, W., 2023. Interlayer organic matter within hydroxy-interlayered clay minerals enhances soil organic carbon stability under long-term organic fertilization. *Applied Clay Science 239*, 106963.

Liu, X., Barres, O., Pironon, J., Unger, M., Beck, P., Fan, J.,Ostadhassan, M., 2024. Molecular fractionation of ancient organic compounds in deeply buried Halite crystals. *Analytical Chemistry 96*(42), 16493-16498.

Lützow, M.v., Kögel-Knabner, I., Ekschmitt, K., Matzner, E., Guggenberger, G., Marschner, B.,Flessa, H., 2006. Stabilization of organic matter in temperate soils: mechanisms and their relevance under different soil conditions – a review. *European Journal of Soil Science 57*(4), 426-445.

Lv, J., Huang, Z., Luo, L., Zhang, S.,Wang, Y., 2022. Advances in molecular and microscale characterization of soil organic matter: current limitations and future prospects. *Environmental Science & Technology 56*(18), 12793-12810.

Marschner, B.,Kalbitz, K., 2003. Controls of bioavailability and biodegradability of dissolved organic matter in soils. *Geoderma 113*(3), 211-235.

Mayer, M., Leifeld, J., Szidat, S., Mäder, P., Krause, H.-M.,Steffens, M., 2023. Dynamic stability of mineral-associated organic matter: enhanced stability and turnover through organic fertilization in a temperate agricultural topsoil. *Soil Biology and Biochemistry 184*, 109095.

Mikutta, R., Lorenz, D., Guggenberger, G., Haumaier, L.,Freund, A., 2014. Properties and reactivity of Fe-organic matter associations formed by coprecipitation versus adsorption: clues from arsenate batch adsorption. *Geochimica et Cosmochimica Acta 144*, 258-276.

Mikutta, R., Mikutta, C., Kalbitz, K., Scheel, T., Kaiser, K.,Jahn, R., 2007. Biodegradation of forest floor organic matter bound to minerals via different binding mechanisms. *Geochimica et Cosmochimica Acta 71*(10), 2569-2590.

Mikutta, R., Zang, U., Chorover, J., Haumaier, L.,Kalbitz, K., 2011. Stabilization of extracellular polymeric substances (Bacillus subtilis) by adsorption to and coprecipitation with Al forms. *Geochimica et Cosmochimica Acta 75*(11), 3135-3154.

Miltner, A., Kindler, R., Knicker, H., Richnow, H.-H.,Kästner, M., 2009. Fate of microbial biomass-derived amino acids in soil and their contribution to soil organic matter. *Organic Geochemistry 40*(9), 978-985.

Minor, E.C., Swenson, M.M., Mattson, B.M.,Oyler, A.R., 2014. Structural characterization of dissolved organic matter: a review of current techniques for isolation and analysis. *Environmental Science: Processes & Impacts 16*(9), 2064-2079.

Nebbioso, A.,Piccolo, A., 2013. Molecular characterization of dissolved organic matter (DOM): a critical review. *Analytical and Bioanalytical Chemistry 405*(1), 109-124.

Neff, J.C.,Asner, G.P., 2001. Dissolved organic carbon in terrestrial ecosystems: synthesis and a model. *Ecosystems 4*(1), 29-48.

Norén, K., Loring, J.S.,Persson, P., 2008. Adsorption of alpha amino acids at the water/goethite interface. *Journal of Colloid and Interface Science 319*(2), 416-428.

Norén, K.,Persson, P., 2007. Adsorption of monocarboxylates at the water/goethite interface: the importance of hydrogen bonding. *Geochimica et Cosmochimica Acta 71*(23), 5717-5730.

Olson, N.E., Xiao, Y., Lei, Z.,Ault, A.P., 2020. Simultaneous optical photothermal infrared (O-PTIR) and raman spectroscopy of submicrometer atmospheric particles. *Analytical Chemistry 92*(14), 9932-9939.

Oren, A.,Chefetz, B., 2012. Sorptive and desorptive fractionation of dissolved organic matter by mineral soil matrices. *Journal of Environmental Quality 41*(2), 526-533.

Paul, E.A., 2016. The nature and dynamics of soil organic matter: plant inputs, microbial transformations, and organic matter stabilization. *Soil Biology and Biochemistry 98*, 109-126.

Possinger, A.R., Zachman, M.J., Dynes, J.J., Regier, T.Z., Kourkoutis, L.F.,Lehmann, J., 2021. Co-precipitation induces changes to iron and carbon chemistry and spatial distribution at the nanometer scale. *Geochimica et Cosmochimica Acta 314*, 1-15.

Pronk, G.J., Heister, K., Vogel, C., Babin, D., Bachmann, J., Ding, G.-C., Ditterich, F., Gerzabek, M.H., Giebler, J., Hemkemeyer, M., Kandeler, E., Kunhi Mouvenchery, Y., Miltner, A., Poll, C., Schaumann, G.E., Smalla, K., Steinbach, A., Tanuwidjaja, I., Tebbe, C.C., Wick, L.Y., Woche, S.K., Totsche, K.U., Schloter, M.,Kögel-Knabner, I., 2017. Interaction of minerals, organic matter, and microorganisms during biogeochemical interface formation as shown by a series of artificial soil experiments. *Biology and Fertility of Soils 53*(1), 9-22.

Qualls, R.G.,Haines, B.L., 1992. Biodegradability of dissolved organic matter in forest throughfall, soil solution, and stream water. *Soil Science Society of America Journal 56*(2), 578-586.

Qualls, R.G., Haines, B.L.,Swank, W.T., 1991. Fluxes of dissolved organic nutrients and humic substances in a deciduous forest. *Ecology 72*(1), 254-266.

Rasse, D.P., Rumpel, C.,Dignac, M.-F., 2005. Is soil carbon mostly root carbon? Mechanisms for a specific stabilisation. *Plant and Soil 269*(1), 341-356.

Remusat, L., Hatton, P.-J., Nico, P.S., Zeller, B., Kleber, M.,Derrien, D., 2012. NanoSIMS study of organic matter associated with soil aggregates: advantages, limitations, and combination with STXM. *Environmental Science & Technology 46*(7), 3943-3949.

Ruiz, F., Bernardino, A.F., Queiroz, H.M., Otero, X.L., Rumpel, C.,Ferreira, T.O., 2024. Iron's role in soil organic carbon (de)stabilization in mangroves under land use change. *Nature Communications 15*(1), 10433.

Rumpel, C.,Kögel-Knabner, I., 2011. Deep soil organic matter-a key but poorly understood component of terrestrial C cycle. *Plant and Soil 338*(1), 143-158.

Scott, E.E.,Rothstein, D.E., 2014. The dynamic exchange of dissolved organic matter percolating through six diverse soils. *Soil Biology and Biochemistry 69*, 83-92.

Six, J., Frey, S.D., Thiet, R.K.,Batten, K.M., 2006. Bacterial and fungal contributions to carbon sequestration in agroecosystems. *Soil Science Society of America Journal 70*(2), 555-569.

Sodano, M., Lerda, C., Nisticò, R., Martin, M., Magnacca, G., Celi, L.,Said-Pullicino, D., 2017. Dissolved organic carbon retention by coprecipitation during the oxidation of ferrous iron. *Geoderma 307*, 19-29.

Sokol, N.W.,Bradford, M.A., 2019. Microbial formation of stable soil carbon is more efficient from belowground than aboveground input. *Nature Geoscience 12*(1), 46-53.

Sokol, N.W., Sanderman, J.,Bradford, M.A., 2019. Pathways of mineral-associated soil organic matter formation: integrating the role of plant carbon source, chemistry, and point of entry. *Global Change Biology 25*(1), 12-24.

Sollins, P., Homann, P.,Caldwell, B.A., 1996. Stabilization and destabilization of soil organic matter: mechanisms and controls. *Geoderma 74*(1), 65-105.

Thevenot, M., Dignac, M.-F.,Rumpel, C., 2010. Fate of lignins in soils: a review. *Soil Biology and Biochemistry 42*(8), 1200-1211.

Tian, S., Yao, S., Zhu, S., Li, P., Zhang, T., Su, X., Huang, R., Yin, Y., Lv, J., Jiang, T.,Wang, D., 2025. Evaluating soil dissolved organic matter as a proxy for soil organic matter properties across diverse ecosystems. *Soil Biology and Biochemistry 204*, 109752.

Tong, H., Simpson, A.J., Paul, E.A.,Simpson, M.J., 2021. Land-use change and environmental properties alter the quantity and molecular composition of soil-derived dissolved organic matter. *ACS Earth and Space Chemistry 5*(6), 1395-1406.

Veldkamp, E., Becker, A., Schwendenmann, L., Clark, D.A.,Schulte-Bisping, H., 2003. Substantial labile carbon stocks and microbial activity in deeply weathered soils below a tropical wet forest. *Global Change Biology 9*(8), 1171-1184.

Violante, A.,Pigna, M., 2002. Competitive sorption of arsenate and phosphate on different clay minerals and soils. *Soil Science Society of America Journal 66*(6), 1788-1796.

Wen, Y.-L., Guo, X.-Y., Cheng, L., Yu, G.-H., Xiao, J., He, X.-H.,Goodman, B.A., 2021. Organic amendments stimulate co-precipitation of ferrihydrite and dissolved organic matter in soils. *Geoderma 402*, 115352.

Xiao, J., Wen, Y., Yu, G.,Dou, S., 2018. Strategy for microscale characterization of soil mineral-organic associations by synchrotron-radiation-based FTIR technology. *Soil Science Society of America Journal 82*(6), 1583-1591.

Yan, J., Wang, L., Hu, Y., Tsang, Y.F., Zhang, Y., Wu, J., Fu, X.,Sun, Y., 2018. Plant litter composition selects different soil microbial structures and in turn drives different litter decomposition pattern and soil carbon sequestration capability. *Geoderma 319*, 194-203.

Zhang, H., Rasamani, K.D., Zhong, S., Taujale, S., Baratta, L.R.,Yang, Z., 2019. Dissolution, adsorption, and redox reaction in ternary mixtures of goethite, aluminum oxides, and hydroquinone. *The Journal of Physical Chemistry C 123*(7), 4371-4379.

Zhang, L., Gadd, G.M.,Li, Z., 2021. Chapter four - Microbial biomodification of clay minerals. In: G. M. Gadd and S. Sariaslani (Eds.), *Advances in Applied Microbiology.* Academic Press, pp. 111-139.

Chapter 3 Insights into the complex nature of dissolved organic matter from plant residues using multiple spectroscopic techniques

This chapter has been published on *Organic Geochemistry*:

Yang, Z., Mohanty, B., Dijkstra, F.A., Guggenberger, G., Singh, B. (2025). Insights into the complex nature of dissolved organic matter from plant residues using multiple spectroscopic techniques. *Organic Geochemistry* 210, 105095.

Highlights

- DOM composition from different plant residues was broadly similar.
- Multiple spectroscopic techniques identified DOM similarities and differences.
- Multivariate analysis reconciled results and clarified DOM composition.

Abstract

Dissolved organic matter (DOM) is the most active and labile organic fraction in soils, participating in numerous biogeochemical processes. Comprehensive understanding of DOM composition at the molecular level remains a challenge due to limited or contrasting analytical data based on a single technique or limited analysis, which may be addressed using multiple complementary techniques. In this study, we utilized five prevalent and novel spectroscopic and spectrometric techniques, i.e., XPS, FTIR, NEXAFS, NMR, and FT-ICR-MS, coupled with multivariate analysis to decipher the complexity of DOM. We extracted DOM from four decomposed plant residues - pine, eucalyptus, pasture, and wheat. The organic carbon concentration in the DOM samples followed the order: pine > eucalyptus > wheat > pasture. Eucalyptus and pasture DOM exhibited similarities in aromatic compounds but differed in saturation and O-containing groups. Pine DOM was enriched in aromatic and carboxylic compounds, whereas wheat DOM contained more lipid and aliphatic compounds. The differences in the abundance of functional groups and compound families were attributed to the influence of both the original plant residues and microbial degradation. Chemical convergence of the four DOM samples, reflected by their broadly similar spectral composition was possibly due to similar biodegradation processes but in different stages. Multivariate analysis of multiple spectroscopic data comprehensively captured the DOM composition.

Keywords

Dissolved organic matter, Plant residues, XPS, FTIR, NEXAFS, NMR, FT-ICR-MS, Multivariate analysis

3.1 Introduction

Being the most mobile and actively cycled fraction of soil organic matter (SOM), dissolved organic matter (DOM) is widely recognized as a key environmental fraction that is involved in numerous biogeochemical processes (Kaiser and Kalbitz, 2012). Although it represents only a small fraction of SOM, DOM plays an important role in carbon (C) cycling and distribution in soils (Lehmann et al., 2020). Therefore, an understanding of the molecular composition and structure of DOM is fundamental to assessing the effects of environmental changes on soil C preservation and stabilization (Schmidt et al., 2011). However, due to the complex and heterogeneous composition of DOM, characterization of its molecular structure and composition remains a challenge (Nebbioso and Piccolo, 2013; Chen and Yu, 2021; Lv et al., 2022).

The diversity in the chemical composition and properties of DOM in soils is affected by several environmental factors and processes, including climatic conditions, the quantity and quality of organic inputs, microbial activity, soil texture, adsorption reaction with minerals, and leaching (Guggenberger and Kaiser, 2003; Kaiser and Kalbitz, 2012; Roth et al., 2019). DOM is a mixture of truly dissolved and very fine colloidal suspension that can pass through the 0.45 µm filter pore and exhibits more diverse organic structures than other OC pools (Haynes, 2005). It contains a mixture of biochemical compounds (e.g., amino acids, fatty acids and carbohydrates), complex biopolymers (e.g., proteins, polysaccharides, lignin), and more complex recalcitrant compounds (e.g., phenolic and condensed aromatic structures) (Haynes, 2005; Kalembasa and Kalembasa, 2016; Angst et al., 2021; Allain et al., 2023). The origin of DOM, derived either directly from plant residues and roots or degradation produced from biotic (microbial metabolism) or abiotic (photodegradation or Fenton degradation) processes, plays a crucial role in its composition and bioavailability in soil (Craig et al., 2022). At the soil surface, DOM is primarily plant-derived, originating from the decomposition of plant residues or the exudation of substances by roots (Kögel-Knabner, 2002; Lange et al., 2021). As DOM moves within the soil profile, it is increasingly utilized and transformed by soil microbes, and undergoes interactions with soil minerals (e.g., adsorption and coprecipitation), which may alter its composition (Guggenberger and Kaiser, 2003; Whalen et al., 2022).

The greatest challenge in DOM characterization lies in the complexity and heterogeneity of DOM molecules, which have been investigated using traditional and advanced spectroscopic techniques (Nebbioso and Piccolo, 2013; Minor et al., 2014; Chen and Yu, 2021; Lv et al., 2022). Common spectroscopic techniques used for DOM characterization include, but not limited to, ultraviolet-visible (UV-vis) spectroscopy, Fourier transform infrared (FTIR) spectroscopy, nuclear magnetic resonance (NMR) spectroscopy, X-ray photoelectron spectroscopy (XPS), near edge X-ray absorption fine structure (NEXAFS) spectroscopy, and Fourier transform ion cyclotron resonance mass spectrometry (FT-ICR-MS). Each technique is based on a distinct theoretical principle and detects specific aspects of DOM composition. For example, FTIR spectroscopy characterizes DOM functional groups by measuring the absorption of infrared light at specific wavelengths corresponding to different molecular bond vibrations (Solomon et al., 2005). NEXAFS selects a specific atomic species (e.g., C and N) through their K-edges where K-shell electrons of the atom are excited and probe their intramolecular bonds and, to a lesser extent extra-molecular neighbouring atoms. It has the ability to detect bonds that can be correlated with specific C bonds in molecules (Solomon et al., 2005; Lehmann and Solomon, 2010). NMR spectroscopy utilizes the magnetic spin properties of certain atomic nuclei (e.g., 1H, 13C, 15N and 31P etc.), with resonance occurring at specific radio frequencies that enables structural analysis by distinguishing signals from different atomic environments (Hertkorn et al., 2013). It can characterize the full-range of organic compounds in DOM by using high resolution one- and/or two-dimensional heteronuclear and homonuclear correlation spectral analyses (Minor et al., 2014; Soucémarianadin et al., 2017). FT-ICR-MS can ionize DOM molecules into the gas phases and analyse their mass-to-charge ratio and intensity with ultra-high mass accuracy and resolution, which enables the identification of thousands of individual molecular formulae (Bahureksa et al., 2021; Qi et al., 2022). The use of multiple techniques in DOM characterization is necessary, because all these techniques have their strengths, limitations, and biases. If only one or two analytical techniques are used to characterize DOM molecules, information on the DOM composition may be biased by the choice of methods. Hence, it is important to integrate and combine multiple techniques to obtain a more comprehensive understanding of the DOM composition at a molecular level.

In this study, we investigated the molecular composition of DOM from four plant residues, i.e., pine, eucalyptus, pasture, and wheat, which are common sources of OM in soils in Australia. We used multivariate statistics (i.e., principal coordinate analysis) to integrate the data obtained from FTIR, XPS, solution-state NMR, NEXAFS, and FT-ICR-MS. The specific aims of the study were to: 1) obtain a comprehensive understanding of the DOM composition at molecular level, 2) compare compositional differences among DOM derived from different plant materials, and 3) evaluate the integrated data from different techniques for DOM analysis. We hypothesized that the composition of DOM extracted from different plant residues vary in specific organic compounds or structures, reflecting their origin and decomposition processes. We further expected that a comprehensive chemical understanding at the molecular level of DOM can only be achieved by utilizing multiple analytical techniques, as an individual technique can provide only methodologically specific information about DOM characteristics.

3.2 Materials and methods

3.2.1 Extraction of dissolved organic matter

The sampling fields at Lansdowne Farm for the University of Sydney, Australia (34.023353 °S, 150.663983 °E), represented four common land use systems in Australia. The vegetations were characterized by pine (*Pinus radiata*), eucalyptus (*Eucalyptus tereticornis*), managed pasture (mixture species with *Bothriochloa macra*, *Poa labillardierei* and *Trifolium subterraneum* as the dominant species), and wheat (*Triticum aestivum L.*). The composition of plant samples varied slightly with pine residues included needles, cones, twigs and minor bark fragments; eucalyptus residues consisted of leaves and twigs; pasture residues comprised grass leaves and stems; and wheat residues include wheat straw and husks that had been decomposed in the field after harvest. The plant residues were deposited on the surface field for natural decomposition over a decade with no interaction with soil minerals and minimal human disturbance, but were subject to regular natural disturbances such as bushfires (Wang et al., 2022). Plant residues were collected from the ground surface (above soil organic horizon). No identifiable animal residues were found in any of the plant residues.

DOM was extracted by mixing 20 g homogenized plant residues with 200 mL of Milli-Q water at a 1:10 w/v ratio, and the mixture was shaken (300 rpm for 3 h) on a horizontal shaker at room temperature (Jones and Willett, 2006). The mixture was then centrifuged (3000 × g for 30 min) and filtered through a 0.45 μm glass fibre filter. The DOM solutions were preserved in the dark at -20 °C and lyophilized for further analysis. The concentration of total organic carbon (TOC) and total dissolved nitrogen (TDN) in DOM solution was analysed on a TOC-L Analyzer (SHIMADZU, Japan). Basic DOM properties are provided in Supplementary Table

S1. The ultraviolet-visible (UV-vis) spectroscopy was first used to analyse the basic characteristics of DOM using a 1 cm pathlength quartz cell with an Agilent Cary 300 UV-visible spectrophotometer (Agilent Technologies, Australia). DOM solution was pre-diluted to approximately 10 mg C L^{-1}, and Mili-Q water was used to as a reference to calibrate the instrument. The following parameters were measured: $SUVA_{254}$, $SUVA_{260}$ (L mg^{-1} m^{-1}) (absorbance at 254 and 260 normalized by the pathlength and organic carbon concentration), E_2:E_3 (absorbance ratio at 254 to 365 nm), and the spectra slope between 300 and 375 nm. The UV-vis parameters obtained from DOM samples are shown in Table S 3.2.

3.2.2 X-ray photoelectron spectroscopy (XPS)

X-ray photoelectron spectroscopy (XPS) analysis was conducted using an ESCALAB250Xi (Thermo Scientific, United Kingdom) spectrometer with a monochromatic Al Kα source (1486.68 eV) at 160 W and 0.5 mm spot size. Freeze-dried, finely ground DOM samples were analysed in the analytical chamber under a vacuum of $< 2 \times 10^{-9}$ mbar. Survey scans were collected using a pass energy of 100 eV, with 20 eV used for region scans. To determine the C, N, and O groups in the DOM samples, the C 1s, N 1s, and O 1s spectra were collected and deconvoluted using the Gaussian-Lorentzian function via Avantage software after subtraction of a Shriley baseline. The relative abundance of each group was calculated based on its peak area and normalized by the number of the groups (Table S 3.3). The C 1s spectra were deconvoluted into four peaks representing aliphatic and aromatic C-C/C-H (284.8 eV), aromatic C-O (286.3 eV), ketone C=O (287.9 eV), and carboxylic O-C=O (288.8 eV) (Singh et al., 2014). Additional C peaks were recognized in O 1s spectra (C=O at 531.4 eV and C-O-H at 532.7 eV) and N 1s spectra (C=N at 399.9 eV and C-N at 401.6 eV) (Abe and Watanabe, 2004).

3.2.3 Fourier-transform infrared (FTIR) spectroscopy

The freeze-dried DOM samples were diluted with KBr (mixed and finely ground with spectroscopic-grade KBr in a ratio of 1:100) and diffuse reflectance infrared Fourier transform (DRIFT) spectra were collected using a Vertex 80V spectrometer (Bruker, Germany). The spectra were recorded in the frequency region from 4000 to 600 cm^{-1} with the co-addition of 256 scans at a spectral resolution of 4 cm^{-1}. The sample chamber was evacuated prior to spectral acquisition to minimize atmospheric contributions from CO_2 and moisture. To quantify the relative abundance of functional group bands, the FTIR spectra were fitted with Gaussian-Lorentzian function in OPUS 8.7.31, with a fitting error of less than 3%, after atmospheric compensation, scattering baseline correction, and normalisation. The identification of peaks of different functional groups is shown in Table S 3.4.

3.2.4 Near edge X-ray absorption fine structure (NEXAFS) spectroscopy

Carbon-1s NEXAFS spectra were obtained at the soft X-ray spectroscopy beamline of the Australian Synchrotron, Melbourne. The beam operated in top-up mode with the storage ring beam current of 200 mA. Ground samples were mounted onto a sample loading ruler using a double-sided copper tape and placed inside a high throughput NEXAFS vacuum chamber (with a base pressure of 1×10^{-7} mbar) for analysis. The nominal beam size on the sample under the operating conditions was 1 × 1 mm. The NEXAFS spectra were collected in both total electron yield (TEY) and partial electron yield (PEY) modes at an angle of 55° to the beam. The settings for C scanning signals of PEY were 200 eV on channeltron front detector (CHF) and 100 eV on hemispherical analyzer (HA), with the flood gun off and I_0 In. C-1s K-edge spectra were collected in the 270-340 eV energy range using a step size of 0.1 eV and dwell time of 0.8 s. The drain current from TEY were selected because of their high quality, and were double normalized with I_0 and photodiode background spectra, and corrected with C reference spectra on the Quick AS NEXAFS Tool (QANT) v1.13 (Gann et al., 2016). To evaluate variations in the functional groups of DOM samples, we performed a semi-quantitative analysis of normalized C-1s NEXAFS spectra through peak deconvolution. All peaks were fitted to the Gaussian-Lorentzian function with an expected error of 1-3 % (Singh et al., 2014). The photon energy positions, and their associated functional groups are shown in Table S 3.5.

3.2.5 Solution-state nuclear magnetic resonance (NMR) spectroscopy

To ensure high-quality results, the extracted DOM solutions were first concentrated using solid phase extraction (SPE) procedure with an Agilent Bond Elut-PPL cartridge (200 mg, 3 ml) (carbon loading efficiency ~60 %) (Dittmar et al., 2008). While the SPE procedure can concentrate the organic carbon (OC) concentration, it may result in the loss of dissolved nitrogen-containing compounds (Jerusalén-Lleó et al., 2023). DOM solution was loaded through cartridge and eluted with 3 ml of d_4-methanol to achieve a final OC concentration of ~3 mg mL^{-1}. For pasture and eucalyptus DOM, signals in the 1D ^1H NMR quality control (QC) experiments were found lower than in pine and wheat samples. Therefore, d_4-methanol in these DOM samples was evaporated under reduced pressure in a desiccator overnight and re-dissolved in 600 µL of d_4-methanol for the further acquisition and analysis (Hertkorn et al., 2013).

The 1D ^{1}H (Bruker pulsesequence: zgesgppe), 2D [^{1}H, ^{1}H]- total correlation spectroscopy (TOCSY) (Bruker pulsesequence: dipsi2esgpph) and [^{13}C, ^{1}H]- heteronuclear single quantum coherence (HSQC) (Bruker pulsesequence: hsqcedetgpsp.3) spectra were acquired at 298 K on a Bruker Avance III 800 MHz spectrometer equipped with a CryoProbe. ^{1}H 90° hard pulses were manually calibrated for each sample before acquisition. In the 2D HSQC spectrum, the ^{13}C chemical shifts appear along F1 (the indirect dimension), while the ^{1}H signals were recorded along F2 (the direct dimension), thus, we have used the nomenclature of [^{13}C(F1),^{1}H(F2)]-HSQC as [^{13}C,^{1}H]-HSQC. Cross-peak intensities in the 2D [^{13}C, ^{1}H]-HSQC NMR spectra were used to analyse the DOM composition. The HSQC spectra were divided into three regions based on the δ_C/δ_H chemical shifts (Soucémarianadin et al., 2017): alkyl C (10-50/0.5-3.0 ppm), O-alkyl C (50-110/2.5-5.5 ppm), and aromatic C (105-140/6.0-8.5 ppm).

In order to obtain a more detailed understanding of the complex molecular structure of DOM, 2D [^{13}C, ^{1}H] NMR spectra of DOM samples were compared with a synthetic spectrum based on the chemical shifts of different organic moieties in δ_C and δ_H axes, as provided in Soucémarianadin et al. (2017). By overlapping peak positions in the DOM spectra with known database chemical shifts, the structure of organic moieties in the DOM samples was identified. More information about the 1D and 2D NMR data acquisition, processing and analysis are reported in section 3.5.5 in Appendix.

3.2.6 Fourier transform ion cyclotron resonance mass spectrometry (FT-ICR-MS)

The extracted DOM solutions were desalinated and concentrated by SPE with an Agilent Bond Elut-PPL cartridge following the procedure described by Dittmar et al. (2008). After SPE, DOM solutions were diluted to obtain the final concentration of methanol: water (50:50 v/v) and characterized by a 7 T Bruker SolariX 2xR FT-ICR-MS instrument with both positive and negative ion mode electrospray ionization (ESI). The instrument was externally calibrated with ESI-L low concentration Tuning Mix, with mass error < 1 ppm. DOM extracts were introduced by a syringe pump with an infusion rate of 120 µL h^{-1}, and mass spectra were collected over a range of 150 to 3000 m/z, using 4 MWord Size domains with 300 scans co-added. Collision cell accumulation time was set 0.05 s. Detailed instrument parameters and settings are shown in Table S 3.9. Both negative and positive mode spectra of DOM samples were internal calibrated using the MATLAB script from Fu et al. (2022), within error ≤ 5 ppm for negative and 10 ppm for positive. Only peaks falling within the 150-850 m/z range with signal-to-noise (S/N) ratios ≥10 were considered for formulae assignment. We used a MATLAB-based toolbox

- TEnvR - to assign formulae for both negative and positive ion spectra (Goranov et al., 2023). Spectra of a methanol: water (50: 50, v/v) solution were also analysed and removed as blanks from the DOM spectra. In addition, peaks identified as salts, doubly charged species, or isotopologues were removed. Elemental assignments conditions were: $C_{5-\infty}$, H_{5-100}, O_{1-50}, N_{0-5}, S_{0-4}, P_{0-2}, with a mass error tolerance of ± 1 ppm. Each DOM extract was analysed in triplicate. Only formulae detected in all three replicates were retained for further analysis.

The nine categories of organic compound groups of assigned formulae based on their H/C, O/C and N content were: aliphatic-like ($1.5 < H/C \leq 2.2$, $0.3 < O/C \leq 0.67$, N=0), lipid-like ($1.5 < H/C \leq 2.0$, $O/C \leq 0.30$), peptide-like ($1.5 < H/C \leq 2.2$, $0.3 < O/C \leq 0.67$, $N > 0$), unsaturated hydrocarbon-like ($0.7 < H/C \leq 1.5$, $O/C \leq 0.1$), carbohydrate-like ($1.5 < H/C \leq 2.5$, $0.67 < O/C \leq 1.2$), condensed aromatic-like ($0.2 < H/C \leq 0.67$, $O/C \leq 0.67$), lignin-like ($0.67 < H/C \leq 1.5$, $0.1 < O/C \leq 0.67$), tannin-like ($0.67 < H/C \leq 1.5$, $0.67 < O/C \leq 1.2$), and other (any remaining unassigned formulae) (Hockaday et al., 2009; Ohno and Ohno, 2013). It should be noted that the compound groups used in our study are referred to "-like" compounds, rather than specific individual organic compound. These groups represent mixtures of organic compounds categorized under a family name based on their most representative compounds or structures, as identified by spectroscopic techniques.

3.2.7 Multivariate statistics

To analyse relationships in organic functional groups and compound families obtained from different analytical techniques, multivariate analysis of principal coordinate analysis (PCoA) was employed to visualize the variability within the four DOM datasets using the Bray-Curtis dissimilarity matrix (Ramette, 2007; Seidel et al., 2022). The spatial arrangement and perpendicular projections of DOM points onto vector arrows in PCoA plot visualized sample similarities and depicted maximum correlations with the relative abundance. In addition, Spearman rank correlation coefficient was computed and visualized by a heatmap to highlight the relationships. The relative abundances of different functional groups and compound families from different techniques were normalized before conducting PCOA and correlation matrix analysis. The multivariate analysis was performed in R version 4.4.1 with *vegdist*, function provided in the *vegan* package.

3.3 Results and discussions

3.3.1 *General characteristics of DOM*

Dissolved organic carbon (DOC) concentration in the DOM extracts followed the order: pine (351.6 mg L^{-1}) > eucalyptus (162.9 mg L^{-1})> wheat (81.2 mg L^{-1}) > pasture (69.4 mg L^{-1}) (Table S 3.1). Many studies have shown that the amount of DOC released from plant residues differed among plant species (Smolander and Kitunen, 2002; Augusto et al., 2015; Ho et al., 2023). For example, deciduous plant residues tend to have higher release efficiencies of DOC compared to coniferous residues (Smolander and Kitunen, 2002; Ho et al., 2023). Smolander and Kitunen (2002) extracted approximately twice the concentration of DOC from birch soils compared to pine soils. Similarly, Ho et al. (2023) collected 12 types of plant litter and found greater DOC released from deciduous leaf litter than coniferous leaf litter. However, we found a higher concentration of DOC in the coniferous residues (i.e., pine) than in the deciduous residues (i.e., eucalyptus) in this study. Even though the original C concentration of eucalyptus residues (272 mg C g^{-1}) was higher than that of pine residues (255 mg C g^{-1}) (Table S 3.1). This finding indicates that the decomposition of plant residues is not always reflected by the DOC concentration, as the release of DOM is determined by both production and consumption processes by microbes (Smolander and Kitunen, 2002; Augusto et al., 2015). The decomposition of plant residues was also reflected in the C to N (C:N) ratios of both original residues and extracted DOM (Nicolardot et al., 2001; Ho et al., 2023). In our study, similar C:N ratios were observed in pine, eucalyptus, and pasture residues (24.2 to 24.6), whereas wheat residues exhibited a distinctly lower C:N ratio (15.5) (Table S 3.1), suggesting a greater degree of humification or decomposition (Nicolardot et al., 2001). The C:N ratio in extracted DOM was also used to indicate the degree of microbial utilization or contribution on the plant residues to release DOM. Among the DOM samples, eucalyptus DOM exhibited the highest C:N ratio (16.0), which may suggest lower microbial processing compared to other DOM. This could be attributed to the lower microbial colonization of the original eucalyptus residues or a greater abundance of recalcitrant compounds that resist microbial degradation and limit DOM release (Ho et al., 2023).

$SUVA_{254}$ and $SUVA_{260}$ values have been used to characterize the aromaticity and hydrophobicity of DOM composition (Traversa et al., 2014). The $SUVA_{254}$ and $SUVA_{260}$ values were high in pine, eucalyptus and pasture DOM samples, indicating a relatively high abundance of aromatic hydrocarbons and double bond or hydroxyl conjugate systems of organic compounds. The wheat DOM exhibited the lowest $SUVA_{254}$ and $SUVA_{260}$ values, suggesting lower aromaticity of organic compounds in the sample (Table S 3.2). The E_2:E_3 ratio indicated larger molecule sizes and more complex structure in pasture DOM (0.1) compared to pine, eucalyptus and wheat DOM, all having E_2:E_3 of 0.4. Similar values of UV-vis spectral slopes (300-375 nm) were observed for all DOM samples, implying the presence and distribution of similar aromatic moieties and conjugated systems across these samples, despite differences in their structural complexity.

3.3.2 Chemical element and OC functional group composition of DOM by XPS analysis

The high resolution XPS spectra of the extracted DOM from pine, eucalyptus, pasture and wheat for the C-1s, O-1s, and N-1s regions are shown in the Figure S 3.2 to Figure S 3.4. After XPS peak fitting, four C peaks were identified and assigned as C-C/C-H aliphatic C and aromatic C (284.8 eV), C-O aromatic C (286.3 eV), C=O ketone C (287.9 eV), and COO carboxylic C (288.8 eV). Two K peaks were also observed at 292.9 eV and 295.7 eV in the C-1s region across all DOM samples. The relative abundance of assigned C groups is shown in Table S 3.3. Among the assigned OC groups, pasture and wheat DOM exhibited a greater abundance of aliphatic C (46.9 % and 56.6 %), and a smaller abundance of aromatic C compared to pine and eucalyptus DOM. A greater abundance of ketone C was observed in the pine and pasture DOM (13.1 % and 13.5 %), and a much lower abundance in the wheat DOM (7.4 %). Eucalyptus DOM exhibited the highest relative abundance of carboxylic C (10.2 %), whereas pasture DOM showed the lowest (3.3 %). Two O peaks were identified in the O-1s region at 531.4 eV for C=O and at 532.7 eV for C-OH in the O-1s region. Among the assigned O groups, eucalyptus DOM exhibited a relatively smaller abundance of C=O (27.4 %) which contrasted with its highest COO and high C=O abundances observed in C-1s region. The abundance of the C-OH groups was relatively small in the pasture DOM (58.4 %) to the other DOM samples. We observed two to three N peaks in the N-1s spectra (Abe and Watanabe, 2004), where 399.9 eV was assigned to C=N (peptide), 401.8 eV to C-N (amine), and 406.9 eV to NO_2. The NO_2 peak was only observed in pine and wheat DOM. Compared to the other samples, eucalyptus DOM showed a smaller abundance of C=N and C-N functional groups, and pine displayed a smaller abundance of C-N. The variability in the composition of C, O and N functional groups in the DOM samples was likely due to the biochemical composition of plant residues, selective preservation of recalcitrant compounds, and microbial transformation of labile OC fractions (Kögel-Knabner, 2002).

3.3.3 OC functional group composition of DOM by FTIR spectroscopy

The FTIR spectra (Figure 3.1a) and relative abundance of assigned functional groups (Table S 3.4) of the four DOM highlight compositional differences linked to their biochemical origins. The broad O-H stretching band (3700-3100 cm^{-1}) with shoulders at 3694 cm^{-1} and 3623 cm^{-1}, was attributed to the O-H bonds of carboxylic acids, alcohols and phenols (Johnston and Aochi, 1996). However, overlapping O-H from water and amine (N-H) stretching vibrations complicate interpretation (Keiluweit et al., 2010). Eucalyptus DOM exhibited the smallest O-H abundance (36.7 %) with lower polarity, whereas other DOM samples contained more hydrophilic moieties. Aliphatic C-H stretching bands (2950 cm^{-1} and 2877 cm^{-1}) were observed in the pine, eucalyptus and pasture DOM samples, while in the wheat DOM spectrum, a shift occurred and only one band was observed at 3014 cm^{-1}. The abundance of C-H bonds from alkyl groups (i.e., CH, CH_2, and CH_3) varied among the DOM samples, with the highest abundance observed in the eucalyptus DOM (8.4 %). We observed two small bands at around 2350 cm^{-1} in the wheat spectrum which possibly resulted from the CO_2 effects from atmosphere (Michael, 1968). The greater abundance of C=O bands (1764 cm^{-1} and 1720 cm^{-1}) in pine and eucalyptus DOM indicated the presence of carboxylic acids, ketones, aldehydes and esters (Pedersen et al., 2011). Conjugated C=O/C=C vibrations observed at 1606 cm^{-1} were present in woody residues (pine and eucalyptus) and pasture residues, indicating the extended or conjugated aromatic π structures. The band shifted to 1630 cm^{-1} in the wheat DOM, which may be attributed to the electron delocalization where the aromatic ring is attached to a nitrogen atom (i.e., C=N) (Kaczmarczyk, 2013). The highest abundance of C=C/C=O bands in the pasture DOM (16.4 %) could be attributed to peptide-associated carboxylates and amides, as well as lignin-derived unsaturated aromatic structures, while the wheat DOM showed the smallest relative abundance (10.5 %), reflecting its cellulose-dominated origin and reduced aromaticity (Johnston and Aochi, 1996; Solomon et al., 2005). A broader and weaker band at 1400 cm^{-1} in pine and eucalyptus DOM, and a sharper and stronger band at 1385 cm^{-1} in pasture and wheat DOM, were attributed to the deformation of C-H in aliphatic methyl groups and phenolic structures, along with C-O stretching in carboxylic and phenolic groups (Parfitt et al., 1977; Kaiser et al., 1997). The C-H band at 1343 cm^{-1} was observed only in the DOM extracted from pasture and wheat residues, constituting 1.7 % and 3.5 % of the total fitted area, respectively. The highest abundance of phenolic C-O (1266 cm^{-1}) was observed in the eucalyptus DOM (12.7 %), underscoring the persistence of lignin, compared to the smallest abundance in the wheat DOM (4.1 %) (Solomon et al., 2005). The C-O-C stretching band at

1118 cm^{-1} and the C-O bond at 1039 cm^{-1} were observed in similar abundance in all DOM samples, and these bands were attributed to carbohydrates and polysaccharides in cellulose and hemicellulose (Bellamy, 1975). The bands at 914 cm^{-1} (O-H bending) and 823 cm^{-1} (C-H bending), corresponding to carbohydrates and aromatic structures, respectively, were observed in greater abundance in the pasture and wheat DOM samples (Keiluweit et al., 2010).

The disparities in functional groups of DOM between woody residues and herbaceous residues likely arise from differences in the biochemistry and decomposition pathway of plant residues (Yan et al., 2018). DOM derived from pine residues contained higher abundances of C-O stretching (from phenolic-OH) and O-H bending (from carboxylic groups), indicative of a greater presence of lignin-derived compounds. Eucalyptus DOM exhibited elevated abundances of C-H stretching (from alkyl groups) and C=O stretching (from carboxylic groups), indicative of a greater amount of hydrophobic aliphatic compounds in the sample. The quantity of eucalyptus residues may have exceeded the capacity of microbes to metabolize them, contributing to a greater input of metabolizable organic compounds into the DOM that caused an enrichment of aliphatic structures (Traversa et al., 2014). In contrast, pasture DOM displayed a greater abundance of C=O stretching (from carboxylates/amides) and C=C stretching (from unsaturated aromatic structures), alongside C-O stretching (from carbohydrates and polysaccharides), indicating more contributions of complex degradation products of plant biomass such as peptides, tannins and non-cellulosic polysaccharides (Kögel-Knabner, 2002; Angst et al., 2021). Wheat DOM, however, was characterized by prominent abundances of O-H stretching (from carboxylic acids) and C-H bending (from aliphatic methyl groups), reflecting aliphatic-rich and cellulose-dominated compounds with less aromaticity.

(a) DRIFTS

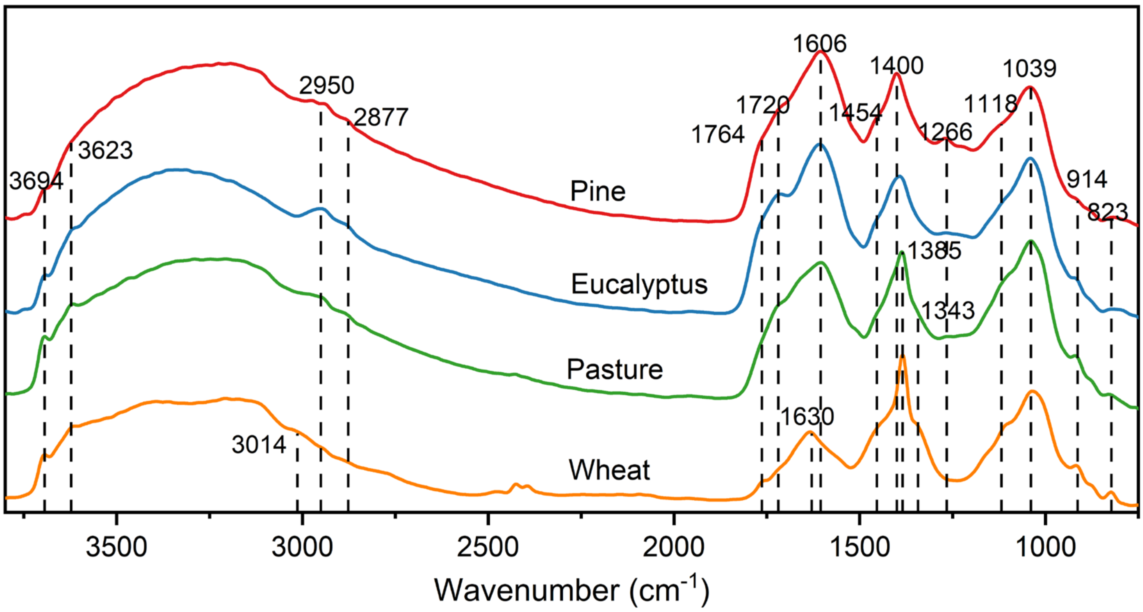

(b) C-1s NEXAFS

(c) Relative Abundance

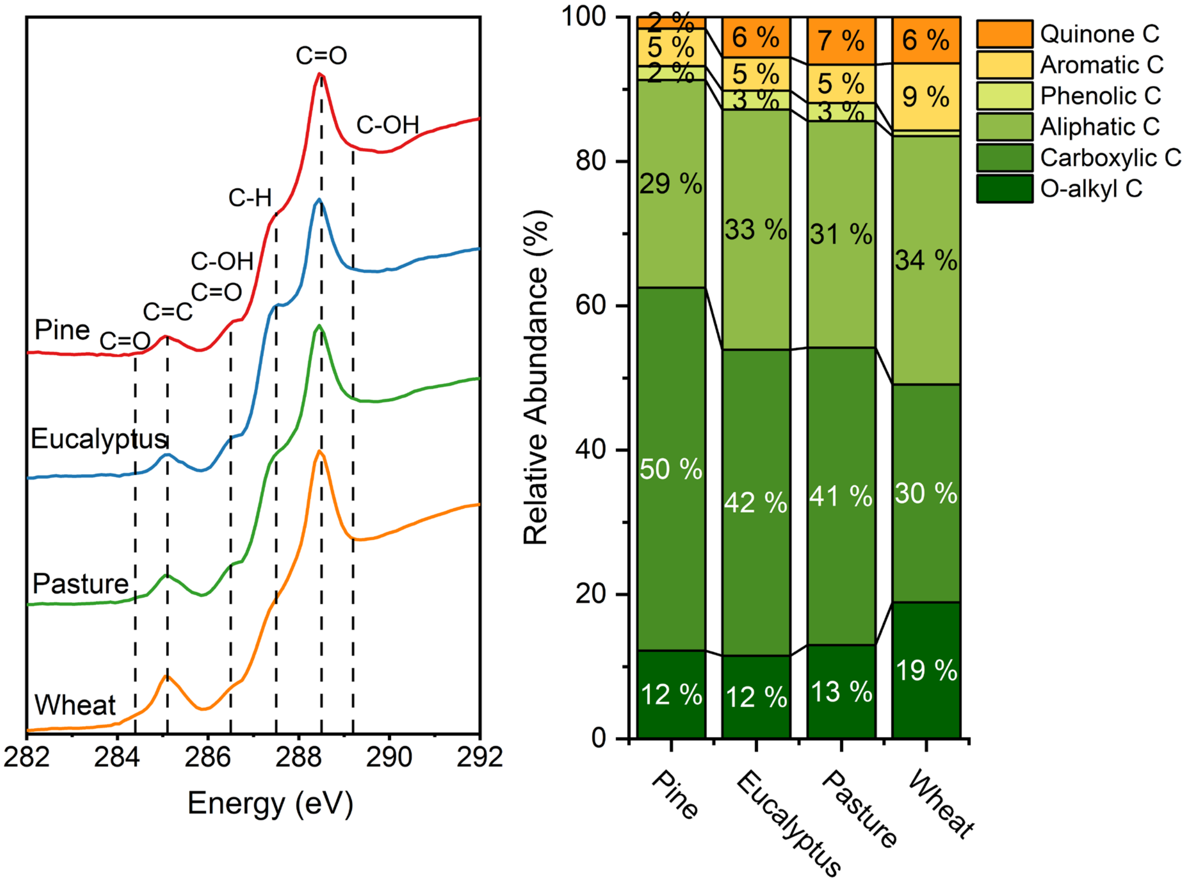

Figure 3.1 (a) Diffuse reflectance infrared Fourier transform (DRIFT) spectra of DOM extracted from pine, eucalyptus, pasture and wheat residues; (b) carbon-1s near edge X-ray absorption fine structure (NEXAFS) spectra of DOM samples; and (c) the relative abundance of assigned carbon functional groups in the DOM samples from NEXAFS analysis.

3.3.4 OC functional group composition of DOM by NEXAFS spectroscopy

The C-1s NEXAFS spectra of the four DOM were broadly similar, showing four distinct peaks at ~285.1 eV, 286.5 eV, 287.5 eV and 288.5 eV (Figure 3.1b). Deconvolution revealed two additional peaks at ~284.4 eV and 289.1 eV in all samples. The peak positions, along with their relative proportions and organic functional groups (Lehmann et al., 2009; Singh et al., 2014) are detailed in Figure 3.1c and Table S 3.5. The peak at 284.4 eV associated with C=O bonds from quinone and aromatic C had a similar relative abundance in pasture (6.6 %) and wheat (6.4 %) DOM, while it was much smaller in the pine DOM (1.6 %). A distinct peak at 285.1 eV was attributed to the C=C bonds of aromatic C and double-bonded alkyl C (Lehmann and Solomon, 2010), and it was much greater in the wheat DOM (9.3 %) compared to other samples. The peak at 286.5 eV was associated with the C-OH and C=O from aromatic structures with side chain C (Lehmann and Solomon, 2010), while some N-substituted aromatic C (e.g., C=N and C-N) may be also contributed to this peak (Lehmann et al., 2009). The contribution of the phenolic C was much smaller in the wheat DOM (0.8 %) than in the others. A sharp peak at 287.5 eV was mainly attributed to aliphatic C (i.e., CH, CH_2 and CH_3) had a similar abundance in all DOM samples. The peak at 288.5 eV was assigned to C=O bonds from carboxylic C (Lehmann and Solomon, 2010). A similar abundance of C=O bonds was observed in eucalyptus (42.4 %) and pasture (41.2 %) DOM samples, while there was a notable difference between pine (50.3%) and wheat (30.2%) DOM. The DOM samples extracted from pine, eucalyptus and pasture residues had similar relative abundance of C-OH (O-alkyl structures), while this bond was more abundant in the wheat DOM (18.9%).

In summary, carbon NEXAFS spectroscopy exhibited the highest abundance of carboxylic C in the pine DOM, while the eucalyptus DOM contained a greater abundance of phenolic C. Quinone C was enriched in the pasture DOM, whereas the wheat DOM showed the highest abundance of aromatic C, aliphatic C, and O-alkyl C, which was likely more complex.

3.3.5 Molecular composition of DOM by solution-state NMR spectroscopy

The 1D ^{1}H NMR spectra of DOM samples exhibited different intensity profiles with a combination of sharp and broad peaks in aromatic- and aliphatic-H regions, indicating the presence of a heterogeneous mixture of molecular species (Figure S 3.5). Pine and pasture DOM showed greater abundances of aromatic-H (10.1 % and 12.3 %), while eucalyptus and pasture DOM displayed elevated alkene-H contributions (5.4 % and 4.9 %) (Table S 3.6). Pasture and wheat DOM dominated organic compounds with ether-H (35.5% and 35.6 %), but the pasture DOM had the lowest abundance of aliphatic-H (17.7 % of XCCH and 29.6 % of CCCH). Generally, sharper or broader peaks in 1D ^{1}H NMR spectra indicate that the sample consists of smaller or larger molecular entities with different molecular weights. However, due to the inherent molecular heterogeneity of DOM, the samples likely consist of a wide range of structurally diverse compounds rather simple moieties (Minor et al., 2014). Some of the ^{1}H signals can overlap, limiting the peak assignments in 1D ^{1}H spectra (Claridge, 2016). To obtain high-resolution spectra, 2D NMR spectra were acquired. The 2D [^{1}H, ^{1}H]-TOCSY NMR spectra (Figure S 3.7) provided additional information on the correlation between protons within the same spin system, connected through scalar J-coupling in DOM molecules (Claridge, 2016). It revealed more detailed insights into the homogeneity of composition across DOM samples, while highlighting the structural differences in the ^{1}H environments of the molecules. For example, the eucalyptus DOM showed broader and sparser cross-peaks in the aliphatic region, suggesting that its molecules were either aggregated or contained extended aliphatic chains (Kelleher and Simpson, 2006). Pasture DOM exhibited larger and denser cross peaks in the aromatic region, implying the presence of complex aromatic structures (e.g., polycyclic or condensed aromatic compounds) (Kelleher and Simpson, 2006).

The 2D [^{13}C, ^{1}H]-HSQC NMR experiments (Figure S 3.7) were conducted to detect C-H couplings over one bond correlation and provided more detailed information on both C and H atoms in the moieties (Claridge, 2016). It should be noted that HSQC NMR is less sensitive than 1D ^{1}H and 2D [^{1}H, ^{1}H]-TOCSY NMR, since ^{13}C has only approximately 1.1 % natural abundance. This is because only a small proportion of C atoms in the DOM contributed to signals. Any exchangeable protons attached to oxygen (O-H) or nitrogen (N-H) cannot be observed by [^{13}C, ^{1}H]-HSQC NMR (Claridge, 2016). Since, the sensitivity of 2D [^{13}C, ^{1}H]-HSQC at natural ^{13}C abundance is significantly lower than that of 1D ^{1}H NMR, detecting peaks from low-concentration samples is challenging in 2D HSQC within short experimental times. Therefore, a perfect direct correlation between 1D ^{1}H NMR and 2D [^{13}C, ^{1}H]-HSQC NMR projections cannot be expected.

However, the HSQC NMR can still provide essential information on the abundance of specific organic compounds in DOM samples (Table S 3.7). Additionally, by comparing our results with a published database (Soucémarianadin et al., 2017), we were able to obtain more detailed information about different functional moieties of organic compounds in DOM samples (Figure 3.2 and Table S 3.8). In the alkyl C region (10-50/0.5-3.0 ppm), all four DOM samples exhibited abundant signals of alkyl C with long methylene chains attached to either carboxylic acids or esters. Although the abundance of alkyl C differed in pasture DOM (lowest with 48.5 %) and wheat DOM (highest with 62.2 %), the structure of alkyl C in both these samples was somewhat similar, showing more complex aliphatic groups containing additional methyl groups and alkenes compared to pine and eucalyptus DOM. The methylene (CH_2) and methyl (CH_3) units in the DOM may be derived from lipids, peptides and fatty acids (Hertkorn et al., 2016), reflecting rapid microbial turnover processes in the plant residues (Yan et al., 2018). In the O-alkyl C region (50-110/2.5-5.5 ppm), eucalyptus (42.7 %) and pasture (43.2 %) DOM exhibited a higher abundance of O-alkyl C, with a more complete set of internal cellulose signals compared to pine and wheat DOM. The O-alkyl C can be referred to a set of oxidized organic compounds including microbially derived carbohydrates and polysaccharides from cellulose, hemicelluloses, cutin and suberin (Kim and Ralph, 2014), which were also indicative of microbial activities (Almeida et al., 2023). Based on the reference database (Soucémarianadin et al., 2017), we observed a rich diversity of polysaccharides with identifiable hemicellulose structures (i.e., xylans, arabinofuranose and galactopyranose) in both pasture and wheat DOM, but these structures were less apparent in the pine and eucalyptus DOM. Pasture DOM also contained diverse cutin and suberin compounds, including methylene-O units adjacent to esters, methine in alcohols and glycerol, which were largely absent in the other DOM samples. Additionally, pine, pasture and wheat DOM exhibited strong signals from metabolized carbohydrates and polysaccharides derived from fungal activities (Soucémarianadin et al., 2017), with more features recognized as glycosidic linkage and glucans, whereas eucalyptus DOM lacked these signals. In the aromatic C region (105-140/6.0-8.5 ppm), the structure of phenylcoumaran, derived from lignin, tannin and other unsaturated aromatic compounds (Hedenström et al., 2009), was identified in all DOM samples. However, the abundance of aromatic C varied, with the highest observed in pasture DOM (8.4 %) and lowest in eucalyptus DOM (3.4 %). DOM from pasture and wheat residues contained more complex aromatic structures, with guaiacyl, hydroxyphenyl, and coumaryl units identified. It should be noted that comparing peak positions between the 2D HSQC-NMR spectra and the chemical shifts from a reference database cannot reveal all structural details, as a range of uncharacterized molecules remained unidentified due to the limitation of the database (Simpson et al., 2004). When using a reference database to assign signals in the HSQC-NMR spectra, a more comprehensive and expanded database is needed to improve structural interpretation. Additionally, one other limitation of solution NMR spectra is that spectra can only be recorded in specific solvents, typically either hydrophobic or aqueous. This means that molecules are not soluble in solvents like d_4-methanol may be absent from the analysis, leading to incomplete characterization of the sample. In contrast, solid-sate NMR can be used to acquire data from lyophilized DOM powder samples, potentially offering more direct correlation with XPS, NEXAFS and FTIR spectroscopy.

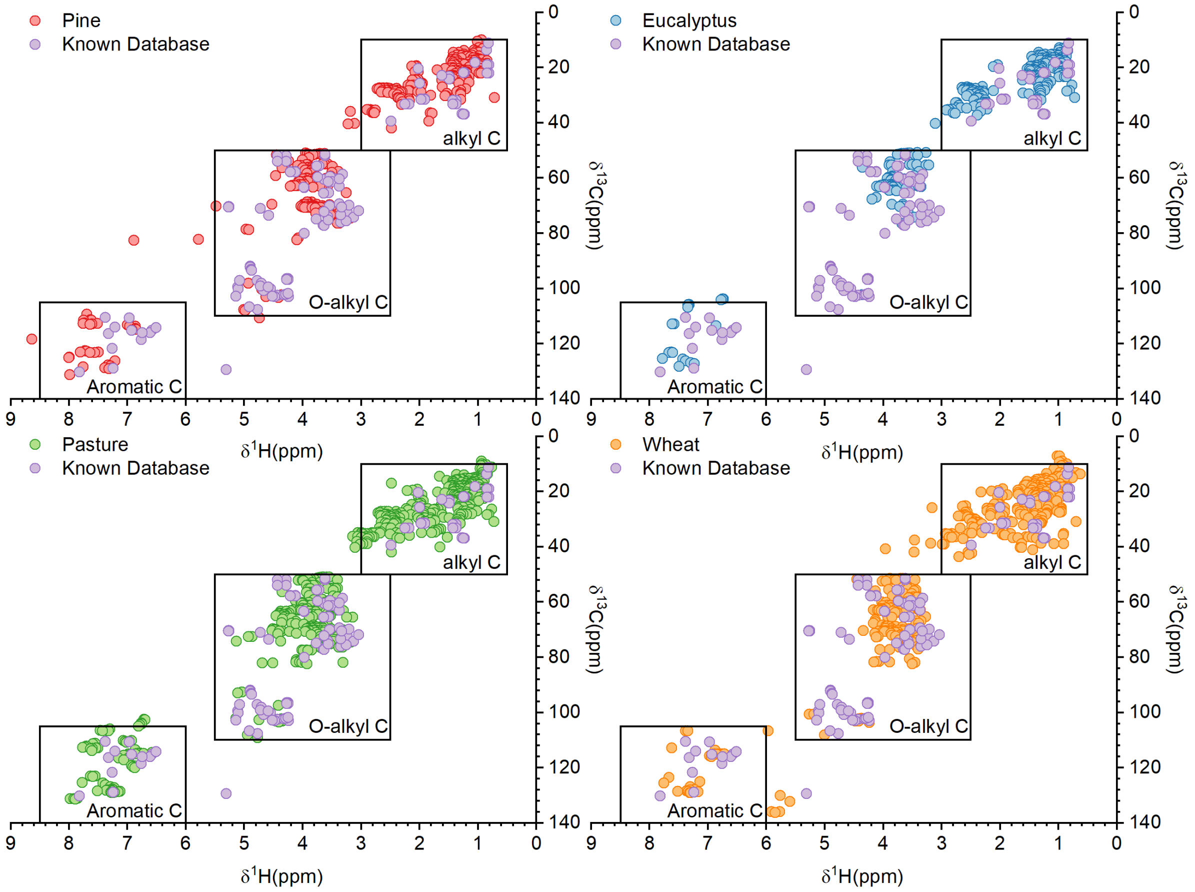

Figure 3.2 The comparison of observed peak position from 2D [^{13}C, ^{1}H]-HSQC spectra of DOM extracted from pine, eucalyptus, pasture and wheat against the reported chemical shits for various biochemical moieties.

3.3.6 Molecular composition of DOM by FT-ICR-MS analysis

We detected 1635 to 4286 molecular formulae across the DOM samples by combing negative- and positive-mode ICR results (Table S 3.10). The Venn diagram illustrates the 393 molecular formulae (9.2 % to 24.0 % of the total formulae detected in each DOM) shared across all four DOM samples (Figure 3.3a), with the proportion of unique compounds ranging from 27.7 to 50.5 % in total. Eucalyptus DOM showed the greatest number of formulae, including the most unique formulae, whereas wheat DOM had the fewest. Pasture DOM shared most formulae (72.3% in total) with other DOM samples. The molecular compounds of DOM were assigned into eight heteroatom subcategories of CHO, CHON, CHOS, CHOP, CHONS, CHONP, CHOSP, and CHONSP (Table S 3.10). The CHO, CHON, and CHOS compounds consisted of

75 % of total across DOM samples (Figure 3.3c). Pasture DOM had the greatest abundance of N-containing compounds (sum of CHON, CHONS, CHONP, and CHONSP), whereas wheat DOM exhibited the smallest abundance of both N- as well as of S-compounds (sum of CHOS, CHONS, CHOSP, CHONSP), and the greatest abundance of P-containing compounds (sum of CHOP, CHONP, CHOSP, CHONSP).

Despite similar clustering of molecular formulae in the van Krevelen diagram (Figure 3.3b), the abundance of assigned compound groups varied across the DOM samples (Figure 3.3c). The organic molecular composition of the four DOM samples showed the order: lignin-like > lipid-like > unsaturated hydrocarbon-like > aliphatic-like > tannin-like > condensed aromatic-like > peptide-like > carbohydrate > other (Figure 3.3c). The lignin-like group dominated the molecular composition of all DOM samples, constituting 37.1 % to 51.5 % of the total assigned compound groups, which are considered the second most abundant compounds of plant biomass and constitute about 30 % of OM in the biosphere (DiDonato et al., 2016). The abundance of lignin-like compounds varied in the order: pine (51.5 %) > eucalyptus (42.3 %) > pasture (42.1 %) > wheat (37.1 %). The abundance of such compounds is governed by the species of original plant residues, depending on the abundance and microbial resistance of lignin moieties between woody and herbaceous species (Campbell and Sederoff, 1996; Gleixner et al., 2001). The lignin-like compounds in DOM may exhibit similar structural units (e.g., phenylcoumaran and hydroxyphenyl) with aryl-ether linkage (Table S 3.8), which derived from macromolecular lignin polymers that have undergone similar microbial degradation and oxidation (Guggenberger et al., 1994; Kögel-Knabner, 2002).

The relative abundance of the lipid-like compounds was the second largest, accounting for 16.9-27.3 % of the total compounds in each sample. DOM extracted from pine and eucalyptus residues had a similar abundance of approximately 17 %, while slightly higher abundance in pasture (20.7 %) and wheat (27.3 %) DOM. The lipid-like compounds consist of fatty acid, terpenoids and sterols, which can be derived from plant residues, microbes and animals, depending on their length of alkyl chains (Dinel et al., 1990; Wiesenberg et al., 2010). In the NMR spectra, we consistently observed the presence of methyl, methylene, and methine groups across all DOM samples, indicating the contribution of plant and microbial processes to the abundance of alkyl C (Kögel-Knabner et al., 1992; Wang et al., 2015). The alkyl C also includes aliphatic-like and peptide-like compounds, and their abundance varied among DOM samples. Pine DOM had the smallest abundances of aliphatic-like (7.0 %) and peptide-like (2.2 %) compounds, whereas wheat DOM had the greatest (14.1 and 3.6 %). Wheat DOM showed a greater abundance of lipid-like, aliphatic-like, and peptide-like compounds, which is consistent with the greater alkyl C observed in the NMR analysis. These results suggest that wheat plant residues were either less resistant to microbial decomposition or exhibited greater microbial activity than the other plant residues (Baumann et al., 2009; Marschner et al., 2011).

The unsaturated hydrocarbon-like compounds were the third largest group present in the DOM samples, with values ranging from 7.9-12.6 %, suggesting high unsaturation condition of DOM samples with abundant double bonds (i.e., C=C and C=O) and/or aromatic rings (i.e., phenolic). The abundance of unsaturated hydrocarbon-like compounds varied across the DOM samples, with pasture and pine DOM exhibited greater proportions (12.6 and 11.9 %), but wheat DOM showed the lowest (7.9 %). As plant residues undergo decomposition or humification, microbes readily utilize unsaturated hydrocarbon-like compounds, driving the transition of molecules from unsaturated to more saturated states (Freeman et al., 2024; Pan et al., 2024). However, the abundance of carbohydrate-like compounds was extremely low across DOM samples, with fewer than 3 % of formulae assigned. These saturated low molecular weight compounds are primarily composed of plant-derived substances and are more water-soluble or labile undergoing oxidation and biodegradation (Guggenberger and Zech, 1994; Kaiser et al., 2002; Pizzeghello et al., 2006). It is possible that most of the carbohydrate-like compounds may have been rapidly utilized by microbes or washed away and leached into soil with rainfall (Kaiser and Guggenberger, 2000).

The abundance of tannin-like compounds in DOM samples ranged from 4.4-6.4 %. These include polyphenols and polycyclic aromatic compounds with aliphatic chains (Koch and Dittmar, 2006). As secondary metabolites derived from plant biomass, they tend to be recalcitrant to microbial processes (Chomel et al., 2016). Eucalyptus DOM exhibited the greatest abundance of tannin-like compounds (6.4 %), followed by wheat (5.5 %), pasture (4.8 %) and pine (4.4 %) DOM. Condensed aromatic-like compounds were less abundant compared to tannin-like compounds, ranging from 2.4-5.2 %. These compounds, often referred to as polycyclic aromatic or black carbon formed primarily through bush fires, have been assumed to be recalcitrant or refractory OM persisting in soil for centuries to millennia (Marschner et al., 2008). Bushfires can lead to the loss of lignocellulosic material from plant biomass and an increase in condensed C structures through dehydration and cyclisation reactions, resulting in the formation of polycyclic aromatic structures (Jiménez-Morillo et al., 2020). Eucalyptus DOM contained the highest proportion of condensed aromatic-like compounds (5.2 %), which is consistent with the frequent exposure of eucalyptus to bushfires at sampling locations (Wang et al., 2022).

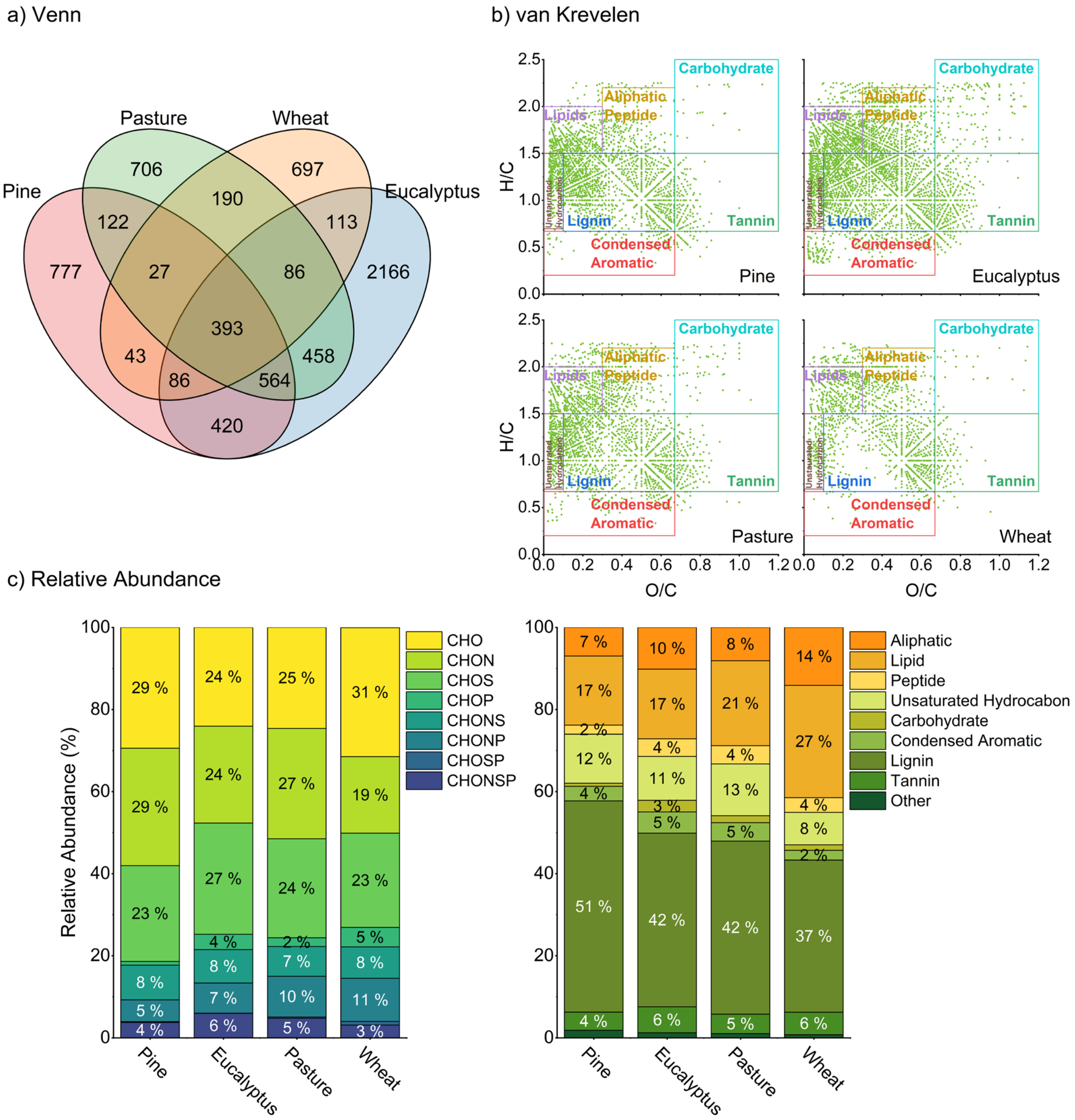

Figure 3.3 (a) The Vann diagram of chemical formulae in the four DOM extracted from pine, eucalyptus, pasture and wheat residues; (b) the van Krevelen diagram of assigned formulae in DOM samples; and (c) the relative abundance of chemical elemental formulae and assigned organic groups among in the DOM samples.

3.3.7 Integration of data obtained from different techniques by multivariate analysis

Different techniques provided some similar, yet still different information about the DOM composition from different plant residues. We performed principal coordinate analysis (PCoA) using Bray-Cutis dissimilarity matrix to present the variability in the relative abundance of functional groups or organic compounds in the DOM samples (Figure 3.4a). The PCoA plot showed that PCoA1 (74.7 %) and PCoA2 (14.3 %) collectively explained 89.0 % of the variability in DOM composition across different spectroscopic techniques. The closer the DOM samples are in the PCoA plot, the more similar they are in their chemical compositions. The length of each arrow reflects the contribution of the corresponding functional groups or families to the DOM composition. The contribution of C-H in FTIR, carboxylic C in XPS, and tannin-like and carbohydrate-like compounds in FT-ICR-MS had minimal influence on DOM composition with negligible arrows of these variables observed in the PCoA plot (Figure 3.4a).

DOM extracted from eucalyptus and pasture residues showed some similarities in specific aromatic compositions compared to other DOM samples. Eucalyptus DOM contained more ketone C and unsaturated compounds, while the pasture DOM had a greater abundance of more condensed aromatic, phenolic and O-alkyl C compounds with C=O/C=C functional groups. Different unsaturated or condensed aromatic structures of eucalyptus and pasture DOM samples could result from the differences in their organic litter quality and composition of the microbial communities (Prescott, 2010). Herbaceous residues generally decompose faster than woody residues under similar climatic and edaphic conditions (Wang et al., 2004). Eucalyptus DOM is expected to have a greater abundance of aromatic compounds because eucalyptus litter contains high amounts of recalcitrant lignin, tannins, polyphenols and terpenes (Wang et al., 2019). In addition, the higher C:N ratio of eucalyptus DOM may have inhibited continued microbial utilization of DOM (Ho et al., 2023). The unsaturated structures observed in eucalyptus DOM may reflect intensive activity of fungi communities such as white-rot fungi, which can metabolize the abundant lipids and sterols in eucalyptus residues and generate unsaturated products (Gutiérrez et al., 2002; Picariello et al., 2021). In contrast, pasture litter is structurally less robust and can be decomposed by microbes, yielding larger amounts of labile hydrolysates (e.g., O-alkyl C) (Prescott, 2010). However, these products can be either continued to be utilized by microbes or leached to deeper soil layers by rainfall, leaving recalcitrant and persistent aromatic compounds in the surface layer (Kaiser and Guggenberger, 2000; Kaiser and Kalbitz, 2012).

The DOM extracted from pine residues was more aromatic and carboxyl-rich, dominated by lignin-like compounds bearing C=O and C-O/O-H functional groups. The degradation of lignin is a primary control on DOM releasing from decaying pine litters (Kalbitz et al., 2006; Maria et al., 2019). White-rot and brown-rot fungi are the most common wood-rooting microbes in coniferous residues, and they can degrade lignin under the action of unspecific and extracellular enzymes (Bugg et al., 2011). Lignin consists of phenylpropanoid units, such as guaiacyl, syringyl, and hydroxyphenyl, which can undergo oxidative breakdown by microbial activity (Thevenot et al., 2010). The oxidative cleavage of aromatic rings in phenylpropanoid units can release low molecular weight products, including carboxylic acids and other aromatic acids, into the soil and sediments (Chen et al., 1983; Otto and Simpson, 2006; Bugg et al., 2011), which is consistent with the greater abundance of carboxylic C in pine DOM.

The DOM extracted from wheat residues differed substantially from the other DOM samples, showing enrichment in both lipid, aliphatic and O-alkyl compounds with C-H and O-H functional groups. In contrast to the other DOM samples, soil microbes contributed more to wheat DOM by repeatedly processing large macromolecular plant materials into smaller molecules, including lipids, carbohydrates and proteins (Freeman et al., 2024). The small C:N ratio in the wheat DOM (Table S 3.1) supported the presence of highly active microbial processing. Decomposable carbohydrates and proteins were degraded and lost rapidly during decomposition, leaving only microbial-derived and recalcitrant lipid or aliphatic compounds in the wheat DOM (Erhagen et al., 2013). The finding is consistent with previous studies showing that the deposition of wheat straw residues increased alkyl C abundance in SOM (Chen et al., 2017; Drosos et al., 2020).

The turnover of DOM from plant residues is complex and influenced by interactive effects among plants, soil microbes, and soil minerals in soil environments. However, the interactions of DOM with soil minerals were minimal in our study samples, and thus were not discussed further. Plants provide C substrate, while microbes accelerate the degradation, changing the original composition of DOM. Although we did not directly assess the degradation degree of each plant residue, the biochemical composition of the DOM can still reflect, to some extent, the microbial process involved in decomposition (Angst et al., 2021; Allain et al., 2023). Labile polysaccharide or carbohydrate compounds (e.g., cellulose and hemicellulose) are initially decomposed by microbes, resulting in the accumulation of aromatic-like compounds with higher O content, greater oxidation, and lower saturation, such as lignin, lipids and waxes (Klotzbücher et al., 2013; Thieme et al., 2019). As biodegradation progresses and labile substrates are exhausted, aromatic compounds begin to depolymerize through the activities of ligninolytic microbes, leading to the increase in saturated, reduced and oxygen-depleted aliphatic compounds of microbial origin, along with the persistence of more recalcitrant compounds such as cyclic or condensed aromatics left (Ingwersen et al., 2008; Hertkorn et al., 2016; Lange et al., 2024). Biodegradation and other processes (e.g., mineral interactions) contribute to the homogenization of the organic compounds in DOM and reduce the influence of the original plant materials (Davenport et al., 2023; Freeman et al., 2024). The compositional comparison among DOM samples was based on the relative abundance of identified functional groups or compound families as determined by each analytical technique. No unique organic composition was identified in any of the DOM samples, which is consistent with the chemical convergence hypothesis (Davenport et al., 2023; Freeman et al., 2024), which states that the decomposition by microbial communities proceeds, DOM from plant residues with different initial biochemistry may converge toward a common chemical composition.

Different spectroscopic techniques complemented each other to provide a more comprehensive understanding of the DOM composition. It should be noted that the varying information about the composition of DOM from each of the techniques does not imply that the results from a particular technique are incorrect but could be partial information. A Spearman rank correlation matrix was generated from the DOM datasets to evaluate the contribution of different techniques to characterize DOM composition based on the relative abundance of functional groups or organic compound families (Figure 3.4b). Positive correlation was observed among aliphatic-like compounds in FT-ICR-MS, alkyl C-H in FTIR and aliphatic C in NEXAFS, indicating their similar capability in identifying aliphatic moieties. Lipid-like compounds in FT-ICR-MS were positively associated with aromatic and O-alkyl C in NEXAFS, due to the presence of steroids or terpenoids compounds derived from plant waxes and cuticular materials (Otto and Simpson, 2005). Positive correlation was observed among unsaturated hydrocarbon-like compounds in FT-ICR-MS, ketone C in XPS and C=O/C=C in FTIR, suggesting similar sensitivity to unsaturated structures of DOM compounds. Condensed aromatic-like compounds in FT-ICR-MS were positively associated with phenolic C in NEXAFS, which may be attributed to the presence of O-containing moieties in both polycyclic aromatic and phenolic structures. Lignin-like compounds in FT-ICR-MS were positively correlated with FTIR C-O/O-H bonds, and with carboxylic in NEXAFS and aromatic C in XPS, indicating that lignin-like compounds may not only contain aromatic rings but also alcohol and carboxyl functionalities. Notably, a positive correlation was observed between O-alkyl C in NMR and aromatic C-H in FTIR. Although O-alkyl C groups in NMR is typically associated with carbohydrates and polysaccharides compounds with methoxy and ether moieties (Kim and Ralph, 2014), lignin compounds can contain alkyl aryl ether linkages between monomers (Lu et al., 2020). We also observed β-aryl ether linkages in the NMR results (Table S 3.8), which may underline this positive correlation. Positive correlation observed between quinone C in NEXAFS and C-O in FTIR likely reflected the redox reactions between quinones and phenols, with semiquinone radicals as the intermediates (Cory and McKnight, 2005).Carboxylic C in NEXAFS was positively associated with C-O/O-H in FTIR and with aromatic C in XPS, which was expected because carboxylic groups contain C-O and O-H functionalities, and the aromatic C signal in XPS often reflected aromatic acids with C-O (Singh et al., 2014). A positive correlation was observed between aliphatic C in XPS and C-O-C and O-H in FTIR, suggesting association of alcohol or ether moieties with aliphatic chains. The carboxylic C in XPS was correlated with C-H in FTIR, consistent with the presence of carboxylic acid in DOM samples.

Integrating different techniques to characterize DOM at the molecular level remains challenging, due to differences in both sampling methodologies and underlying theoretical principles (Nebbioso and Piccolo, 2013; Chen and Yu, 2021; Lv et al., 2022). FT-ICR-MS has rapidly become one of the primary instruments for DOM characterization because of its ultrahigh resolution and accuracy in identifying the chemical compounds and their associated compound classes (Bahureksa et al., 2021). However, the limitations in discrimination of molecule structures in FT-ICR-MS techniques should be considered, and any non-ionizable molecules and large molecules (>1000 Da) cannot be identified as larger molecules often ionizes less efficiently (Nebbioso and Piccolo, 2013). Additionally, high mass ions move more slowly in the ICR cell, leading to low signal-to-noise and mass accuracy. Therefore, NMR spectroscopy has been used in conjunction with FT-ICR-MS to provide more information about the molecular structures (Hertkorn et al., 2013). Due to the complexity and polyfunctionality of DOM compounds, some interpretations of spectroscopy results can be obscured by significant overlapping of characteristic spectral features. Ideally, NMR can elucidate the molecular structures if each H and C in molecules has a unique, discernible chemical shift. However, in many cases, except for very small molecules in DOM, the overlap of signals from large or aggregated molecules could limit the identification of structures (Minor et al., 2014).

Although both FT-ICR-MS and NMR are highly sensitive techniques, they still present certain limitations in DOM characterization, therefore, they are always integrated with other analytical methods (Allain et al., 2023). Both FT-ICR-MS and NMR required DOM solutions to be desalinated and concentrated through pre-treatment (e.g., solid phase extraction with PPL cartridge), which can result in the removal of a portion of N-containing molecules from DOM (Dittmar et al., 2008; Jerusalén-Lleó et al., 2023). In contrast, the DOM samples prepared for NEXAFS, XPS and FTIR were lyophilized into solid powders and directly analysed using X-ray or infrared spectroscopy. Considering the differences in DOM properties depending on the format used for analysis, contradictory information may arise when integrating different techniques.

Additionally, some contradictory information resulted due to the differences in quantitative interpretation of compound groups across different techniques. For example, assigned O-alkyl C compounds from NEXAFS and NMR showed negative correlation in the correlation matrix (Figure 3.4b). NEXAFS spectroscopy can generate high-quality spectra qualitatively showing different C functional groups, but an absolute quantitative interpretation of NEXAFS spectra remains a challenge (Solomon et al., 2005). It has been reported that the quantification of different OC functional groups was less precise in NEXAFS spectroscopy than in NMR spectroscopy, particularly for the contribution of O-alkyl C (Prietzel et al., 2018). Due to uncertainties in absolute intensity response of electron transitions and the effect of σ^* and π^* bond-bond interactions (Nefedov and Wöll, 2013), an absolute quantification of NEXAFS results has not yet been achieved. The semi-quantitative approach used in NEXAFS spectroscopy may have provided contradictory information when compared with other techniques. We also observed the negative correlation of aromatic C between XPS and NEXAFS spectroscopy. NEXAFS spectroscopy captures total carbon information of samples, whereas XPS provides surface specific quantitative analysis (depth < 10nm) and has a lower resolution, particularly in distinguishing between single and double-bond C (Singh et al., 2014). Therefore, the use of these analytical techniques should always be carefully considered to ensure accurate and relevant interpretation of DOM. Given the limitations mentioned above, we strongly recommend using multiple analytical techniques for OM characterization.

The integration of results from different analytical techniques is fruitful. The complementarity and differences in various techniques can provide more insights into the structural and functional features of DOM. Through Spearman's correlation matrix, we observed consistent interpretations of certain organic compounds, such as alkyl and unsaturated structures, across different spectroscopic techniques (Figure 3.4). This demonstrates the utility of integrating data from multiple spectroscopic techniques to decipher DOM composition. A better understanding of the nature of DOM will enhance our knowledge of its fate and pathways in the soil environment. This insight is essential for developing broad-scale decision-making frameworks to assess how DOM influences the stabilization of OC in response to climate change.

a) PCoA

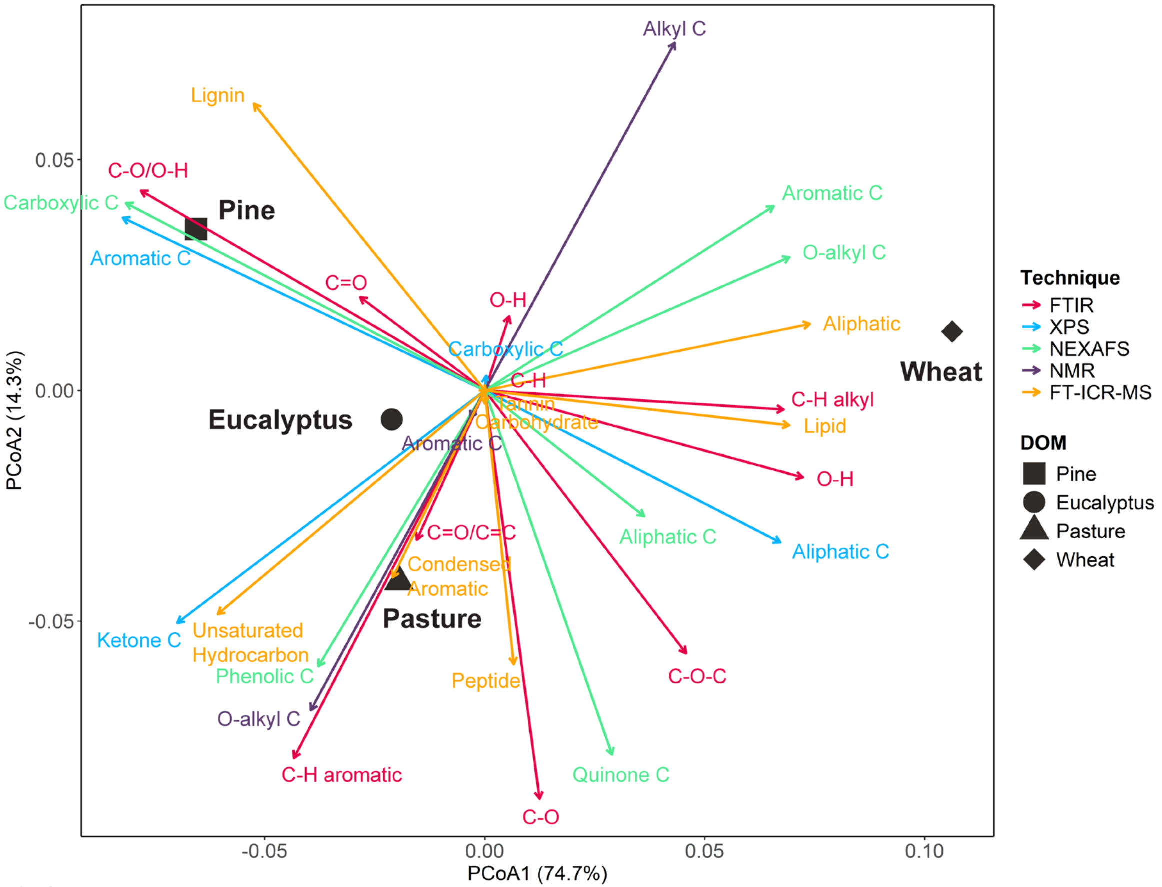

b) Correlation matrix

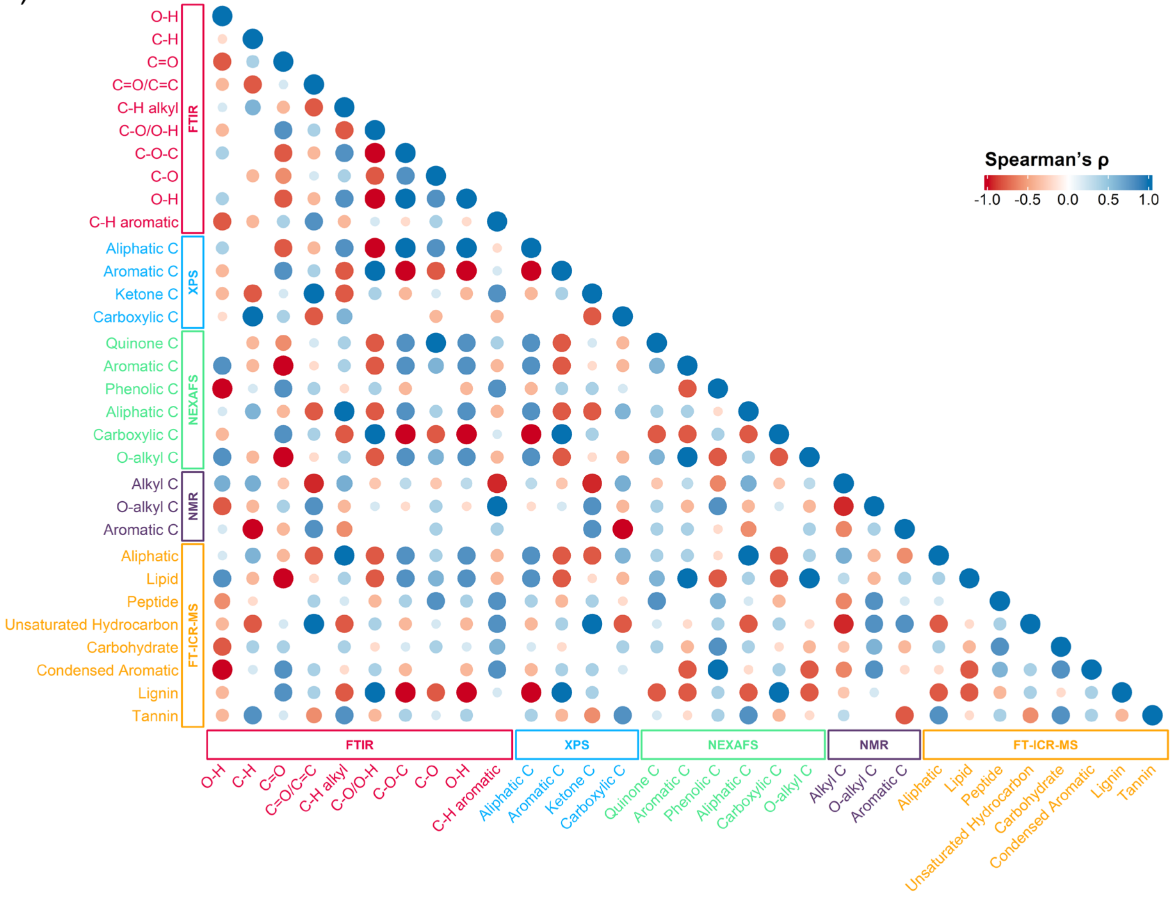

Figure 3.4 (a) The principal coordinates analysis (PCoA) plot depicting the Bray-Curtis dissimilarity of DOM chemical composition derived from XPS, FTIR, NEXAFS, 2D [^{13}C, ^{1}H]-HSQC NMR and FT-ICR-MS techniques. The spatial distance among four DOM samples reflects their original dissimilarity, with closer positions indicating greater similarity, while the direction and length of variable arrows reflect their contributions to DOM composition. And (b) the heatmap of Spearman rank correlation matrix for the normalized relative abundance of organic functional groups and compound families detected from FTIR, XPS, NEXAFS, 2D [^{13}C, ^{1}H]-HSQC NMR and FT-ICR-MS techniques. The size of dots in matrix reflects the magnitude of Spearman's ρ and cells are left blank when ρ=0.

3.4 Conclusions

The molecular composition of DOM extracted from four plant residues was influenced by the biochemical characteristics of the original plant residues, stage of degradation, and surrounding environmental conditions. The OC concentration in the DOM samples was in the sequence: pine > eucalyptus > wheat > pasture, with the highest C:N ratio in eucalyptus DOM and the lowest in wheat DOM. Different techniques yield varying levels of details due to differences in detection principles, sample preparation and quantitative methods, which can result in ambiguous outcomes, such as the overlapping spectral signals and less quantitative precisions. No single analytical technique can fully capture the molecular complexity of DOM, and this limitation is expected to persist in the foreseeable future. However, the integration of multiple spectroscopic techniques with multivariate statistical tools, such as PCoA and correlation matrix, significantly improved our ability to reconcile diverse spectroscopic data on functional groups and compound families, thus enables a comprehensive understanding of the DOM composition. In this study, PCoA integration revealed that eucalyptus and pasture DOM exhibited some similarities in aromatic compounds but differed in saturation and O-containing structures, with eucalyptus DOM exhibiting more unsaturated (e.g., ketone) and pasture DOM exhibiting more condensed and O-alkyl (e.g., phenol), reflecting differences in their origin and decomposition processes. Pine DOM was enriched in aromatic and carboxylic compounds, closely related to its plant material composition, while wheat DOM had abundant lipid and aliphatic compounds, with possibly resulting from intensive microbial processing. Spearman's correlation analysis showed that different techniques provided both consistent and contrasting information about specific organic moieties in the DOM samples. Integrated data from these techniques provided more comprehensive details on DOM composition compared to any single technique.

Although differences in the relative abundance of specific functional groups or compound families were observed among DOM samples, their general composition was broadly similar, likely due to similar microbial decomposition processes. We did not observe any unique molecular composition in any of DOM samples. The differences were largely in the relative abundance of organic groups. In addition, similarity in the assigned groups does not imply that all molecules are identical, and different molecules could share similarity in their functional groups, bonding environment or elemental composition. The overall molecular structures may still differ and perhaps too complex to fully decipher.

We encourage soil biogeochemists to adopt a cautious approach in interpreting results based on one single or two analytical techniques. To obtain a comprehensive understanding of DOM compositions and generate reliable and accurate information, it is essential to employ multiple techniques together. This allows cross-checking the validity and reliability of results and yields a comprehensive picture of DOM molecular composition.

Acknowledgements

This research was funded by the Australian Research Council (ARC) Discovery Project (DP220103026) and the University of Sydney. The authors acknowledge Dr. Lars Thomsen at the Australian Synchrotron (Proposal 20075) for his expertise in NEXAFS analysis. The authors also thank Dr. Michelle Wood for her support with FTIR analysis, Dr. Nicholas Proschogo for his support with FT-ICR-MS analysis at Sydney Analytical and Sydney Mass Spectrometry, University of Sydney, and Dr. Bin Gong for his assistance with XPS analysis at the Surface Analysis Laboratory, University of New South Wales. The authors additionally acknowledge Sydney analytical, University of Sydney, for access to the high-field 800 MHz NMR spectrometer.

3.5 Appendix

3.5.1 Basic properties of plant residues and DOM samples.

Table S 3.1 Some properties of plant residues and DOM extracted from pine, eucalyptus, pasture and wheat residues.

Properties	Pine	Eucalyptus	Pasture	Wheat
Plant residues				
OC (mg g^{-1})	254.6	271.5	162.1	186.1
TN (mg g^{-1})	10.5	11.1	6.6	12.0
C:N	24.2	24.5	24.6	15.5
DOM				
pH (1:10)	6.5	6.4	7.2	7.5
EC (mS m^{-1})	56.5	5.8	13.5	53.3
DOC - solution (mg L^{-1})	351.6	162.9	69.4	81.2
TOC - freeze dried (%)	38.4	36.6	30.7	15.4
TDN (mg g^{-1})	49.8	14.6	10.0	93.8
C:N	7.1	11.2	6.9	0.9
Na (mg L^{-1})	0.1	0.1	0.1	0.1
K (mg L^{-1})	0.1	0.1	0.6	0.2
Ca (mg L^{-1})	0.1	0.1	0.1	0.2
Mg (mg L^{-1})	0.1	0.0	0.1	0.1

Table S 3.2 The parameters of DOM samples obtained from UV-visible analysis.

DOM	Pine	Eucalyptus	Pasture	Wheat
SUVA$_{254}$ (L mg^{-1} m^{-1})	1.0	1.0	1.1	0.1
SUVA$_{260}$ (L mg^{-1} m^{-1})	1.1	1.2	1.1	0.2
E2:E3	0.4	0.4	0.1	0.4
Slope between 300 and 375 nm	0.02	0.02	0.02	0.02

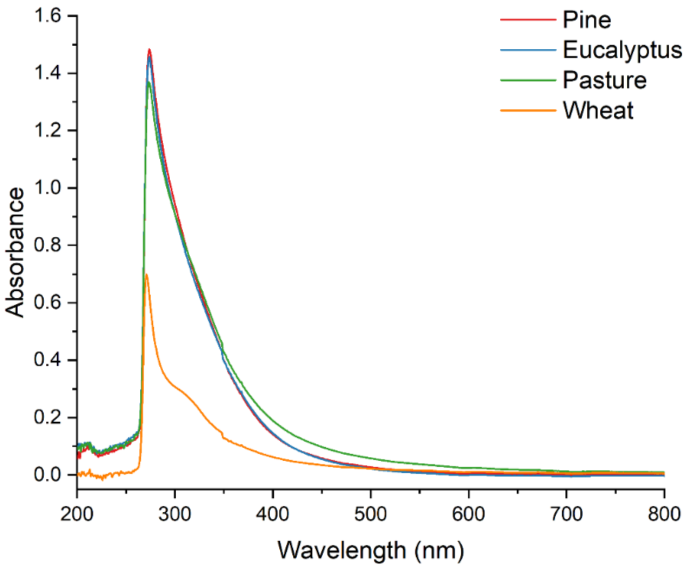

Figure S 3.1 The UV-vis absorbance spectra of DOM extracted from pine, eucalyptus, pasture and wheat residues.

3.5.2 XPS analysis of DOM samples.

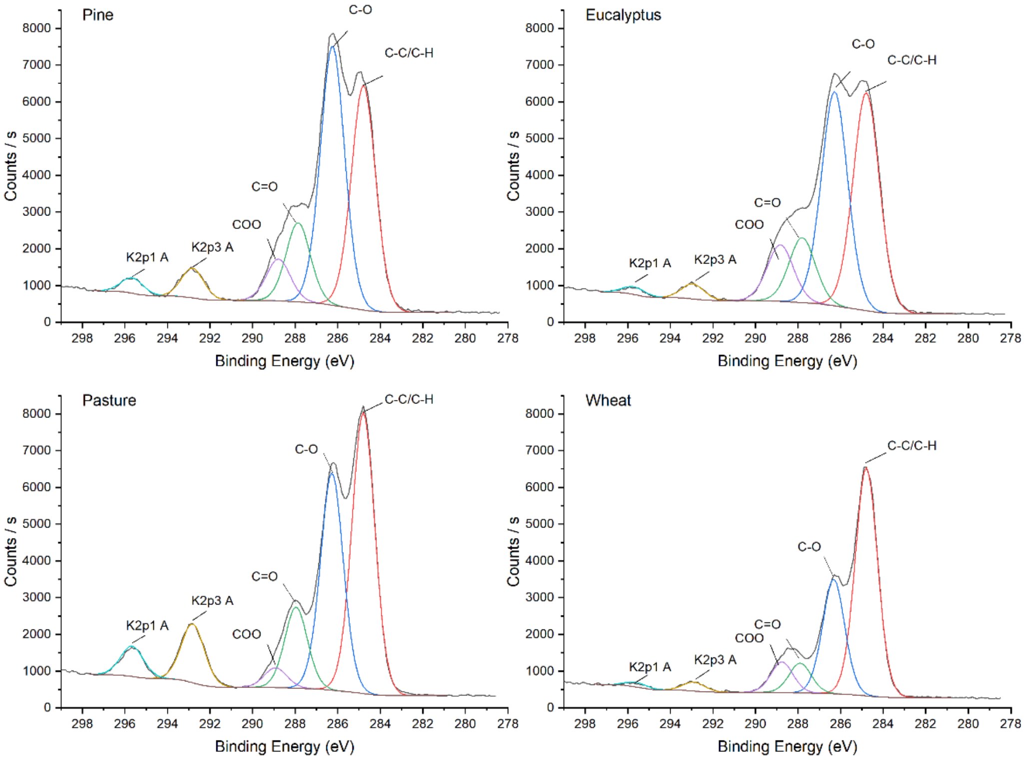

Figure S 3.2 The high-resolution spectra for the C-1s region in the DOM extracted from pine, eucalyptus, pasture and wheat residues.

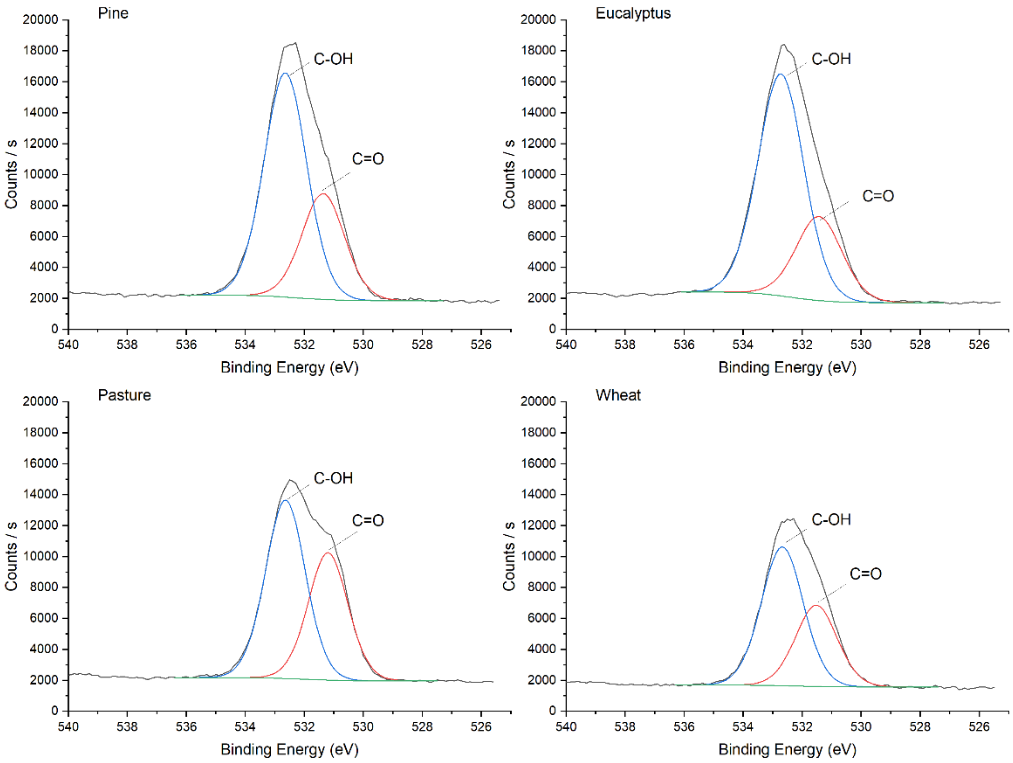

Figure S 3.3 The high-resolution spectra for the O-1s region in the DOM extracted from pine, eucalyptus, pasture and wheat residues.

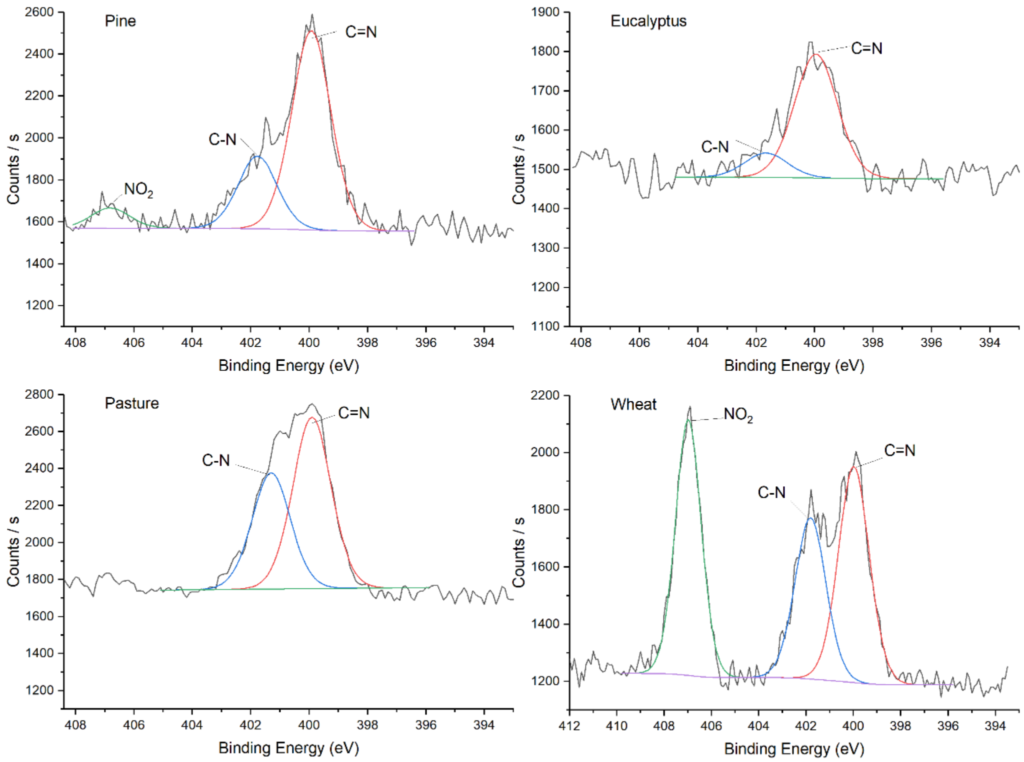

Figure S 3.4 The high-resolution spectra for the N-1s region in the DOM extracted from pine, eucalyptus, pasture and wheat residues.

Table S 3.3 The relative abundance of carbon, oxygen and nitrogen functional groups obtained from the XPS of the DOM extracted from four plant residues.

Relative Abundance (%)	Energy (eV)	Functional Groups	Pine	Eucalyptus	Pasture	Wheat
C 1s	284.8	**C**-C/**C**-H	37.1	39.4	46.9	56.6
	286.3	**C**-O	42.9	38.7	36.3	28.4
	287.9	**C**=O	13.1	11.7	13.5	7.4
	288.8	O=**C**-O	6.9	10.2	3.3	7.6
O 1s	531.4	C=**O**	32.1	27.4	41.6	36.9
	532.7	C-**O**H	67.9	72.6	58.4	63.1
N 1s	399.9	C=**N**	68.3	83.6	59.6	36.6
	401.8	C-**N**	24.9	16.4	40.4	27.3
	406.9	**NO**$_2$	6.9	-	-	36.1

3.5.3 FTIR analysis of DOM samples.

Table S 3.4 Potential region assignment for organic functional groups and their relative proportion in the FTIR spectra of the four DOM samples.

Wavenumber (cm^{-1})	Functional Groups and Vibration	Organic Components	Pine	Eucalyptus	Pasture	Wheat
3700-3100	O-H stretch; N-H stretch	Carboxylic acids, alcohols and phenols; Amines and amides	43.4	36.7	40.1	44.8
2950	C-H asymmetric stretch	Alkyl groups (CH, CH_2, CH_3) in aliphatic structures	1.3	8.1	1.3	6.3*
2877	C-H symmetric stretch		0.3	0.3	0.1	
1764, 1720	C=O stretch	Carboxylates, amides, aldehydes, ketones and esters	6.1	6.9	3.4	2.0
1630, 1606	C=O stretch; C=C stretch	Carboxylates, amide I, quinones, ketones and olefins; Unsaturated aromatic structures	13.7	11.7	16.4	10.5
1454	C-H bend	Alkyl groups (CH, CH_2, CH_3) in aliphatic structure (e.g., polysaccharides) and phenolic lignin;	6.0	7.0	3.0	4.1
1400, 1385			3.5	4.9	5.9	6.3
1343			0.0	0.0	1.7	3.5
1266	C-O stretch; O-H bend	Phenolic-OH in aromatic structures and aryl methyl ethers; Carboxyl groups	12.7	8.9	8.7	4.1
1118	C-O-C stretch	Carbohydrates and polysaccharides in cellulose and hemicellulose	2.1	2.4	3.1	3.4
1039	C-O stretch	Polysaccharides or polysaccharide-like substances	9.2	11.0	12.9	11.2
914	O-H bend	Carboxylic acids	0.9	1.1	2.1	3.8
823	C-H bend	Carbohydrates and aromatic structures	0.8	0.9	1.3	0.1

*The asymmetric and symmetric stretching of C-H in wheat DOM were shifted to 3014 cm^{-1}.

3.5.4 Carbon NEXAFS analysis of the DOM samples.

Table S 3.5 The photon energy positions, assigned organic carbon (OC) functional groups, and their relative proportions in the DOM samples*.

Energy (eV)	OC Forms	OC Bonds	Transition	Pine	Eucalyptus	Pasture	Wheat
283.0-284.5	Quinone C and aromatic C	C=O	1s-π*	1.6	5.6	6.6	6.4
284.9-285.5	Aromatic C and double-bonded alkyl C	C=C	1s-π*	5.2	4.6	5.3	9.3
286.0-287.4	Aromatic C with side chain and N-substituted aromatic C	C-OH C=O R-(C=O)-R’ C=N, C-N	1s-π*	1.9	2.6	2.5	0.8
287.0-287.8	Aliphatic C	C-H	1s-3ρ/σ*	28.8	33.3	31.4	34.4
288.0-288.7	Carboxylic C	R-COOH COO C=O	1s-π*	50.3	42.4	41.2	30.2
289.2-289.5	*O*-alkyl C	C-OH	1s-π* 1s-3ρ/σ*	12.2	11.5	13.0	18.9

*Peak assignments of the NEXAFS spectra were based on the published data (Lehmann et al., 2005; Solomon et al., 2005; Lehmann et al., 2009; Solomon et al., 2009; Keiluweit et al., 2012; Singh et al., 2014; Prietzel et al., 2018).

3.5.5 NMR analysis of DOM samples.

The 1D ^{1}H NMR spectra were acquired with a relaxation delay of 10s with 128 scans and a time domain of 64K complex points. An exponential window function with a line broadening factor of 0.3 Hz was applied before the Fourier transformation. The 2D [^{1}H,^{1}H]-TOCSY experiments were performed using uniform sampling with the following parameters: 128 dummy scans, 64 scans, a relaxation delay of 1.5 s, receiver gain set to 128, and an acquisition time of 102 ms with a time domain of 2048 points. In an HSQC experiment, the magnetization is initially excited on ^{1}H and then transferred to ^{13}C, where the ^{13}C chemical shifts evolve during the indirect dimension. The magnetization is subsequently transferred back to ^{1}H for detection. Thus, in the resulting 2D HSQC spectrum, the 13C chemical shifts appear along F1 (the indirect dimension), while the ^{1}H signals are recorded along F2 (the direct dimension). Therefore, we have defined the nomenclature of [^{13}C(F1),^{1}H(F2)]-HSQC as [^{13}C,^{1}H]-HSQC. The spectral width was set at 12.5 ppm in both the direct ^{1}H acquisition dimension (F2) and the indirect ^{1}H TOCSY dimension (F1). The carrier frequency was set at 4.83 ppm in both F2 and F1. The experiments included 512 increments in F1 with a TOCSY mixing time of 80 ms, resulting in a total acquisition time of approximately 16h. A 90° shifted squared sine bell function was applied to both dimensions and zero-filling to 1024 points was applied in F_1 before Fourier transformation.

The [^{13}C, ^{1}H]-HSQC NMR spectra were acquired with non-uniform sampling (NUS), by using 1024 scans; relaxation delay of 1s; $^{1}J^{CH}$ of 145 Hz; 128 receiver gain; spectral widths of 15 ppm in ^{1}H direct dimension (F2) with an acquisition time of 85 ms and 135 ppm in the indirect ^{13}C dimension (F1); carrier frequency was set at 4.83 ppm (^{1}H) and 72.5 ppm (^{13}C). The spectra were acquired with a time domain of 2048 in the ^{1}H dimension. 50% of 300 complex points were collected with a random sampling scheme (default setup in Topspin), resulting in a total acquisition time of approximately 48h. A 90° shifted squared sine bell function was applied in both dimensions and only zero filling of 1024 points was applied in F1 before the Fourier transformation.

NUS spectra were reconstructed using the compressed algorithm in Topspin. The baselines in 2D spectra were corrected using automated routines in Topspin before spectral analysis. The integration of peak volumes in 1D ^{1}H spectra was performed using the integration routine in the Bruker software Topspin. All NMR spectra were analysed using Topspin 3.7 (Bruker Biospin). For spectra collected in *d₄*-methanol, ^{1}H and ^{13}C chemical shifts were referenced to residual non-deuterated methanol ^{1}H and ^{13}C signal at 3.33 ppm and 49.15 ppm, respectively.

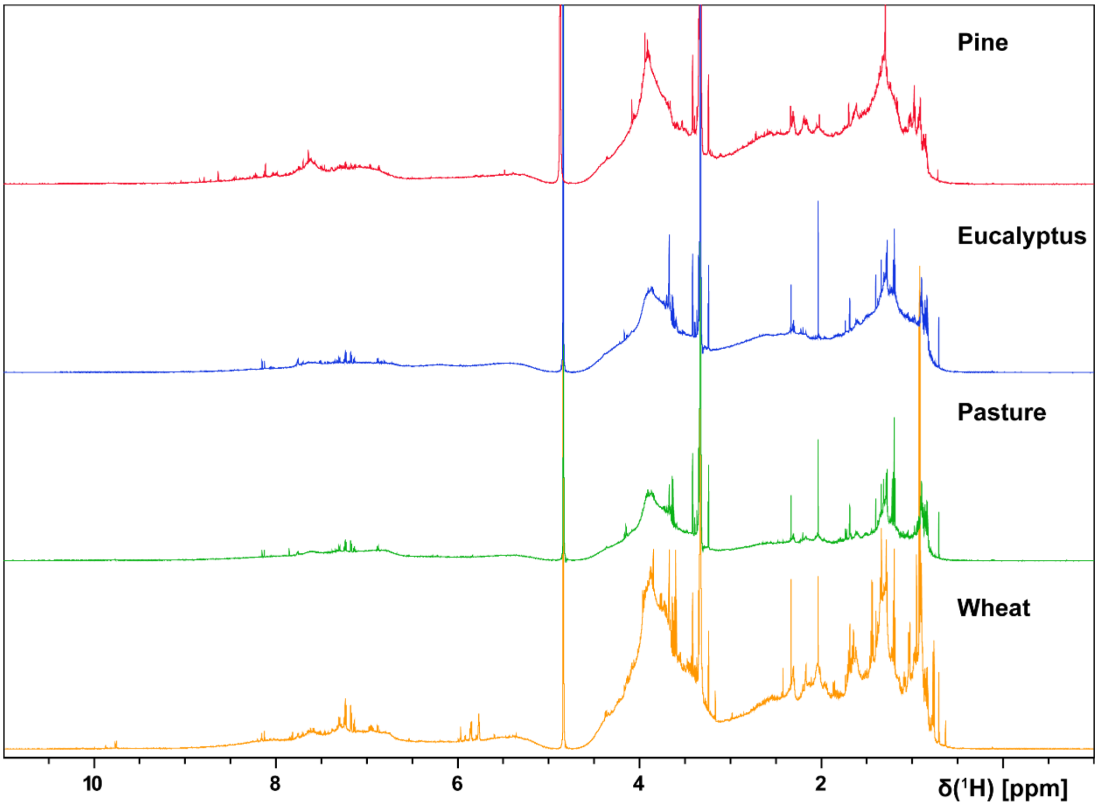

Figure S 3.5 1 D ^{1}H NMR spectra of the DOM samples extracted pine, eucalyptus, pasture, and wheat. The NMR data were acquired on an 800 MHz spectrometer equipped with a Z-gradient triple resonance CryoProbe at 298 K in *d*$_4$-methanol. All spectra were acquired using the same acquisition parameters and processed identically.

Table S 3.6 The relative abundance of 1D ^{1}H NMR section integral for major hydrogen moieties of the DOM extracted from pine, eucalyptus, pasture, and wheat residues. Hydrogen atom peak assignments and their relative abundance from 1D ^{1}H NMR spectra were categorized into five regions: aromatic protons (H_{ar}, 10.5-6.5 ppm), alkene/olefin protons (C=CH, O2CH, 6.5-5.0 ppm), ether/oxomethylene protons (OCH, 4.6-3.3 ppm), and aliphatic protons (XCCH, 3.1-1.9 ppm and CCCH, 1.9-0.0 ppm) (Hertkorn et al., 2016) .

H groups	H_{ar}	C=CH, O_2H	OCH	XCCH	CCCH
δ(^{1}H) [ppm]	10.5-6.5	6.5-5.0	4.6-3.1	3.1-1.9	1.9-0.0
Pine	10.1	4.2	31.8	22.8	31.1
Eucalyptus	8.2	5.4	30.5	22.1	33.8
Pasture	12.3	4.9	35.5	17.7	29.6
Wheat	9.1	4.3	35.6	19.4	31.6

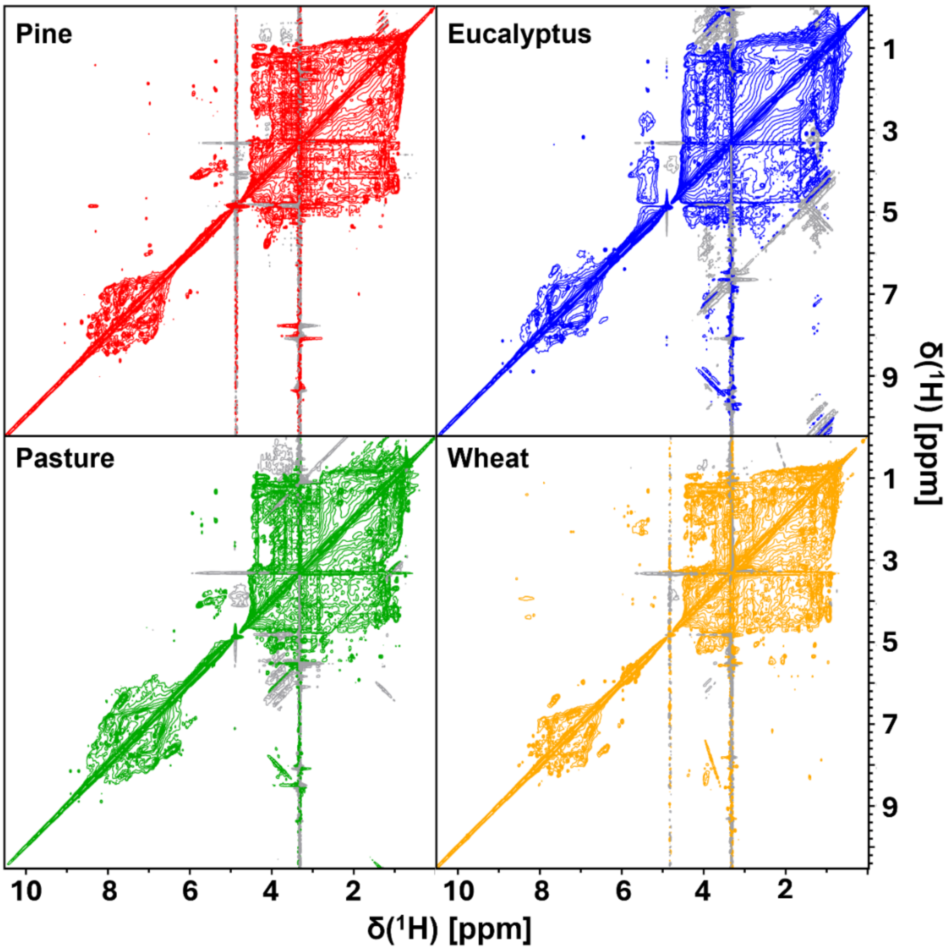

Figure S 3.6 2D [^{1}H, ^{1}H]-TOCSY NMR spectra (TOCSY mixing time of 80 ms) of DOM extracted from pine, eucalyptus, pasture and wheat. The NMR data were acquired on an 800 MHz spectrometer equipped with a Z-gradient triple resonance CryoProbe at 298 K in d_4-methanol. All spectra were acquired using the same acquisition parameters and processed identically. The artefacts along the ^{1}H-TOCSY indirect dimension arise from T1-ridge effects caused by strong signals from the residual methanol proton at 3.33 ppm and the water signal at 4.83 ppm.

Table S 3.7 The relative abundance of 2D [^{13}C, ^{1}H]-HSQC NMR section integral for major organic carbon groups of the DOM extracted from pine, eucalyptus, pasture, and wheat residues.

C groups	Alkyl C	O-alkyl C	Aromatic C
δ_C/δ_H [ppm]	10-5/0.5-3.0	50-110/2.5-5.5	105-150/6.0-8.5
Pine	53.9	39.4	6.7
Eucalyptus	53.9	42.7	3.4
Pasture	48.5	43.2	8.4
Wheat	62.2	33.7	4.1

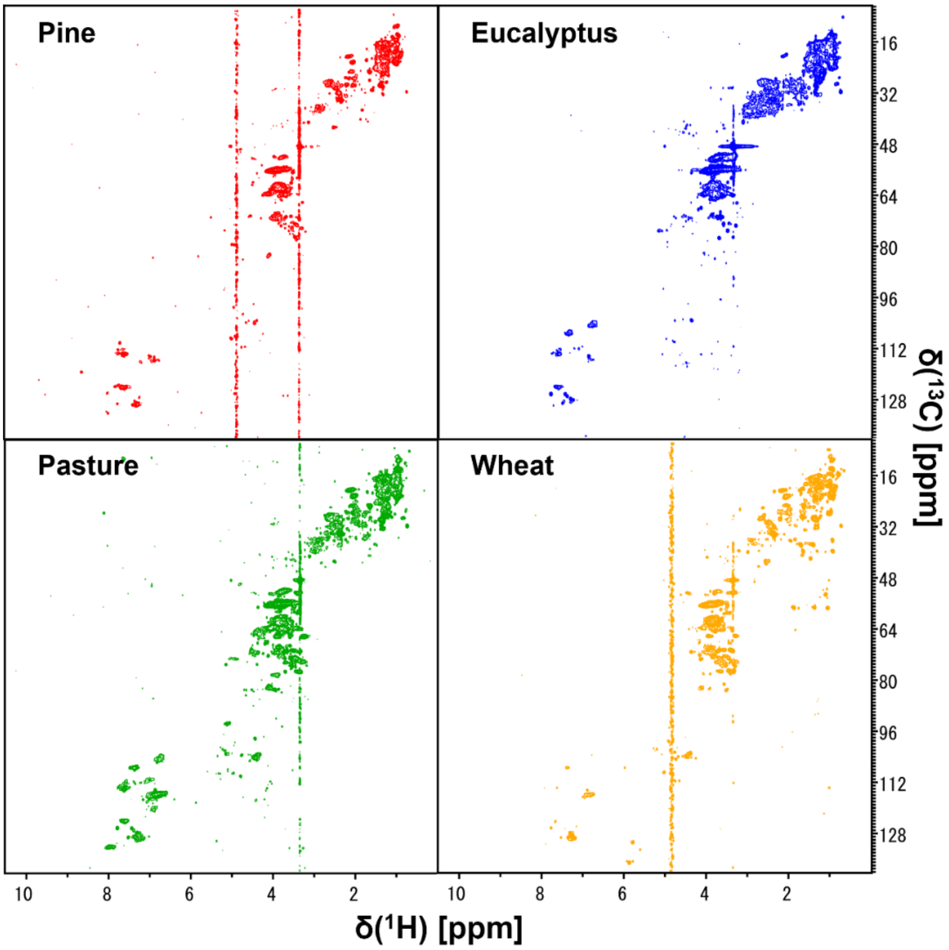

Figure S 3.7 2D [^{13}C, ^{1}H]-HSQC spectra of DOM extracted from pine, eucalyptus, pasture and wheat. The NMR data were acquired on an 800 MHz spectrometer equipped with a Z-gradient triple resonance CryoProbe at 298 K in d_4-methanol. All spectra were acquired using the same acquisition parameters and processed identically. The artefacts along the ^{13}C-dimension arise from T1-ridge effects caused by strong signals from the residual methanol proton at 3.33 ppm and the water signal at 4.83 ppm. Although the [^{13}C,^{1}H]-HSQC spectra were acquired using an edited pulse sequence to discriminate between different types of carbon environments, the CH, CH_2 and CH_3 cross peaks are displayed in the same phase for clarity.

Table S 3.8 The identified organic compounds and their potential structures of DOM from 2D [^{13}C, ^{1}H]-HSQC spectra by comparing a synthetic spectrum based on the a database provide by Soucémarianadin et al. (2017).

Organic Components	Pine	Eucalyptus	Pasture	Wheat
Alkyl C	· Methylene units α to carboxyl acid or carbonyl of an ester · Methylene units in aliphatic chains β and γ to acid or ester · Methyl groups from amino acids in peptides/proteins, fatty acids, lipids, hemicelluloses · Methylene and methine groups in aliphatic chains: polymethylene chains mainly from lipids/fatty acids and waxes · Methylene units adjacent to alkene · Methylene β in a primary alcohol chain in waxes	· Methylene units α to carboxyl acid or carbonyl of an ester · Methylene units in aliphatic chains β and γ to acid or ester · Methylene β in a primary alcohol chain in waxes · Methylene and methine groups in aliphatic chains: polymethylene chains mainly from lipids/fatty acids and waxes	· Methylene units α to carboxyl acid or carbonyl of an ester · Methylene units in aliphatic chains β and γ to acid or ester · Methyl groups from amino acids in peptides/proteins, fatty acids, lipids, hemicelluloses · Methylene and methine groups in aliphatic chains: polymethylene chains mainly from lipids/fatty acids and waxes · Methylene units adjacent to alkene · Methylene β in a primary alcohol chain in waxes	· Methylene units α to carboxyl acid or carbonyl of an ester · Methylene units in aliphatic chains β and γ to acid or ester · Methyl groups from amino acids in peptides/proteins, fatty acids, lipids, hemicelluloses · Methylene and methine groups in aliphatic chains: polymethylene chains mainly from lipids/fatty acids and waxes · Methylene units adjacent to alkene · Methylene β in a primary alcohol chain in waxes
Cellulose	· C_1/H_1 of cellulose · C_2/H_2 of reducing end (β) of cellulose · C_5/H_5 of cellulose · C_6/H_6 of internal cellulose	· C_1/H_1 of cellulose · C_2/H_2 of cellulose · C_3/H_3 of internal cellulose · C_4/H_4 of internal cellulose · C_6/H_6 of internal cellulose · C_6/H_6 of glucan	· C_1/H_1 of cellulose · C_2/H_2 of reducing end (β) of cellulose · C_3/H_3 of internal cellulose · C_4/H_4 of internal cellulose · C_5/H_5 of cellulose · C_6/H_6 of internal cellulose · C_6/H_6 of glucan	· C_1/H_1 of cellulose · C_3/H_3 of internal cellulose · C_5/H_5 of cellulose · C_6/H_6 of glucan

Hemicellulose	· C_1/H_1 of xylans · C_2/H_2 of the β-D-galactopyranose · C_3/H_3 of internal xylan · C_3/H_3 of the β-D-galactopyranose · C_5/H_5 of α-arabinofuranose	· C_1/H_1 of xylans · C_3/H_3 of the β-D-galactopyranose · C_5/H_5 of internal xylan · C_5/H_5 of α-arabinofuranose	· C_1/H_1 of xylans · C_2/H_2 of the β-D-galactopyranose · C_3/H_3 of internal xylan · C_3/H_3 of the β-D-galactopyranose · C_4/H_4 of internal xylan · C_5/H_5 of internal xylan · C_5/H_5 of α-arabinofuranose	· C_1/H_1 of xylans · C_3/H_3 of internal xylan · C_3/H_3 of the β-D-galactopyranose · C_4/H_4 of internal xylan · C_4/H_4 of non-reducing end xylan · C_5/H_5 of internal xylan · C_5/H_5 of α-arabinofuranose
Lignin	· Phenylcoumaran (C_β/H_β) · β-aryl ether linkages of the lignin units ($\gamma = C_\gamma/H_\gamma$) · C_2/C_6 of p- hydroxyphenyl unit	· Phenylcoumaran (C_β/H_β) · β-aryl ether linkages of the lignin units ($\gamma = C_\gamma/H_\gamma$)	· Phenylcoumaran (C_β/H_β) · C_2/C_6 of p-hydroxyphenyl unit	· Phenylcoumaran (C_β/H_β) · β-aryl ether linkages of the lignin units ($\gamma = C_\gamma/H_\gamma$) · C_2/C_6 of p-hydroxyphenyl unit
Cutin and suberin	· Methine group α in mid-chain alcohols · C_5 of guaiacyl unit	· Methylene directly attached to singly bonded ester O	· Methylene directly attached to singly bonded ester O · Methine group α in mid-chain alcohols · Glycerol · C_2 of guaiacyl unit · C_5 of guaiacyl unit	· Methylene directly attached to singly bonded ester O · C_5 of guaiacyl unit
Proteins and amino acids	· C_α/H_α in amino acids			· C_α/H_α in amino acids
Fungal signals	· Glycosidic linkages of glucans in 3-O- and 3,6-di-O-substituted residues (C_1/H_1) · Internal C_1/H_1 units in α of (1 → 3, 1 → 6)-linked β-D-glucans		· Glycosidic linkages of glucans in 3-O- and 3,6-di-O-substituted residues (C_1/H_1) · Internal C1/H1 units in α of (1 → 3, 1 → 6)-linked β-D-glucans	· Glycosidic linkages of glucans in 3-O- and 3,6-di-O-substituted residues (C_1/H_1) · Internal C1/H1 units in α of (1 → 3, 1 → 6)-linked β-D-glucans

3.5.6 FT-ICR-MS analysis of DOM samples.

Table S 3.9 The instrument parameter setting of negative and positive ESI FT-ICR-MS analysis for the DOM samples*.

	Parameter	Values	Unit
API source	Capillary	3500 (-) 4500 (+)	V
	End plate offset	-500	V
	Nebuliser	1.0	bar
	Dry gas	4.0	L min^{-1}
	Dry temp	200	°C
Source optics	Capillary exit	-200.0 (-) 200.0 (+)	V
	Deflector plate	-200.0 (-) 200.0 (+)	V
	Funnel 1	-150.0 (-) 150.0 (+)	V
	Skimmer 1	-15.0 (-) 15.0 (+)	V
	Funnel RF amplitude	100.0	Vpp
Octopole	Frequency	2	MHz
	RF amplitude	350.0	Vpp
Quadrupole	Q1 mass	200	m/z
	Collision voltage	2.5 (-) -1.5 (+)	V
	DC extract bias	-0.5 (-) 1.1 (+)	V
	RF frequency	2	MHz
	Collision RF amplitude	1000.0	Vpp
Transfer optics	Time of flight	0.800	ms
	Frequency	6	MHz
	RF amplitude	350.0	Vpp
Gas control	Flow	35.0	%
Analyser	Transfer exit lens	20.0 (-) -20.0 (+)	V
	Analyser entrance	10.0 (-) -10.0 (+)	V
	Side kick	2.5 (-) -6.0 (+)	V
	Side kick offset	1.5 (-) -2.0 (+)	V
	Front trap plate	-1.500 (-) 1.500 (+)	V
	Back trap plate	-1.500 (-) 1.500 (+)	V

	Back trap plate quench	30.0 (-) 5.0 (+)	V
	Sweep excitation power	18.0	%

* (-) and (+) represent the negative and positive ESI mode.

Table S 3.10 The molecular formulae and assigned chemical subcategories and organic compound groups in DOM from FT-ICR-MS*.

DOM	Pine	Eucalyptus	Pasture	Wheat
Molecular formulae	2439	4286	2546	1635
Mass$_w$	441.97	474.50	448.07	429.08
H/C$_w$	1.33	1.40	1.42	1.46
O/C$_w$	0.30	0.29	0.29	0.35
DBE$_w$	9.17	9.05	8.30	7.11
DBE/C$_W$	0.42	0.38	0.38	0.35
DBE/H$_W$	0.39	0.36	0.36	0.32
DBE/O$_W$	2.75	2.73	2.64	1.93
KM$_W$	442.07	474.61	448.18	429.18
NKM$_W$	441.78	474.30	447.88	428.89
KMD$_W$	0.28	0.31	0.30	0.29
AImod$_w$	0.27	0.18	0.19	0.16
NOSC$_W$	-0.45	-0.54	-0.55	-0.56
CHO (%RA)	29.44	24.08	24.63	31.44
CHON (%RA)	28.62	23.59	26.87	18.65
CHOS (%RA)	23.33	27.11	24.12	22.94
CHOP (%RA)	0.90	3.71	2.16	4.83
CHONS (%RA)	8.45	8.19	7.23	7.65
CHONP (%RA)	5.33	7.30	9.94	10.52
CHOSP (%RA)	0.21	0.07	0.27	0.86
CHONSP (%RA)	3.73	5.95	4.79	3.12
CRAM (%RA)	23.33	20.56	20.86	25.32
Aliphatic-like (%RA)	6.97	10.20	8.13	14.13
Lipid-like (%RA)	16.85	16.94	20.70	27.34
Peptide-like (%RA)	2.21	4.32	4.44	3.61
Unsaturated hydrocarbon-like (%RA)	11.93	10.66	12.61	7.89
Carbohydrate-like (%RA)	0.74	2.85	1.69	1.35
Condensed aromatic-like (%RA)	3.57	5.18	4.52	2.39
Lignin-like (%RA)	51.46	42.30	42.14	37.06
Tannin-like (%RA)	4.43	6.35	4.75	5.50
Other (%RA)	1.85	1.21	1.02	0.73

*$_w$ indicates intensity weighted average; %RA is the relative abundance.

References

Abe, T.,Watanabe, A., 2004. X-ray photoelectron spectroscopy of nitrogen functional groups in soil humic acids. *Soil Science 169*(1).

Allain, A., Alexis, M.A., Bridoux, M.C., Humbert, G., Agnan, Y.,Rouelle, M., 2023. Fingerprinting the elemental composition and chemodiversity of vegetation leachates: consequences for dissolved organic matter dynamics in Arctic environments. *Biogeochemistry 164*(1), 73-98.

Almeida, L.F.J., Souza, I.F., Hurtarte, L.C.C., Teixeira, P.P.C., Inagaki, T.M., Silva, I.R.,Mueller, C.W., 2023. Molecular diversity and the fate of biochemical fractions of eucalypt tissues in soil. *Geoderma 432*, 116404.

Angst, G., Mueller, K.E., Nierop, K.G.J.,Simpson, M.J., 2021. Plant- or microbial-derived? A review on the molecular composition of stabilized soil organic matter. *Soil Biology and Biochemistry 156*, 108189.

Augusto, L., De Schrijver, A., Vesterdal, L., Smolander, A., Prescott, C.,Ranger, J., 2015. Influences of evergreen gymnosperm and deciduous angiosperm tree species on the functioning of temperate and boreal forests. *Biological Reviews 90*(2), 444-466.

Bahureksa, W., Tfaily, M.M., Boiteau, R.M., Young, R.B., Logan, M.N., McKenna, A.M.,Borch, T., 2021. Soil organic matter characterization by Fourier transform ion cyclotron resonance mass spectrometry (FTICR MS): a critical review of sample preparation, analysis, and data interpretation. *Environmental Science & Technology 55*(14), 9637-9656.

Baumann, K., Marschner, P., Smernik, R.J.,Baldock, J.A., 2009. Residue chemistry and microbial community structure during decomposition of eucalypt, wheat and vetch residues. *Soil Biology and Biochemistry 41*(9), 1966-1975.

Bellamy, L.J., 1975. Esters and lactones. In: L. J. Bellamy (Ed.), *The Infra-red Spectra of Complex Molecules.* Springer Netherlands, pp. 203-228.

Bugg, T.D.H., Ahmad, M., Hardiman, E.M.,Rahmanpour, R., 2011. Pathways for degradation of lignin in bacteria and fungi. *Natural Product Reports 28*(12), 1883-1896.

Campbell, M.M.,Sederoff, R.R., 1996. Variation in lignin content and composition (mechanisms of control and implications for the genetic improvement of plants). *Plant Physiology 110*(1), 3-13.

Chen, C.-L., Chang, H.-M.,Kirk, T.K., 1983. Carboxylic acids produced through oxidative cleavage of aromatic rings during degradation of lignin in spruce wood by phanerochaete chrysosporium. *Journal of Wood Chemistry and Technology 3*(1), 35-57.

Chen, W.,Yu, H.-Q., 2021. Advances in the characterization and monitoring of natural organic matter using spectroscopic approaches. *Water Research 190*, 116759.

Chen, X., Mao, A., Zhang, Y., Zhang, L., Chang, J., Gao, H.,Thompson, M.L., 2017. Carbon and nitrogen forms in soil organic matter influenced by incorporated wheat and corn residues. *Soil Science and Plant Nutrition 63*(4), 377-387.

Chomel, M., Guittonny-Larchevêque, M., Fernandez, C., Gallet, C., DesRochers, A., Paré, D., Jackson, B.G.,Baldy, V., 2016. Plant secondary metabolites: a key driver of litter decomposition and soil nutrient cycling. *Journal of Ecology 104*(6), 1527-1541.

Claridge, T.D.W., 2016. Chapter 13 - Structure elucidation and spectrum assignment. In: T. D.

W. Claridge (Ed.), *High-Resolution NMR Techniques in Organic Chemistry (Third Edition).* Elsevier, pp. 499-525.

Cory, R.M.,McKnight, D.M., 2005. Fluorescence spectroscopy reveals ubiquitous presence of oxidized and reduced quinones in dissolved organic matter. *Environmental Science & Technology 39*(21), 8142-8149.

Craig, M.E., Geyer, K.M., Beidler, K.V., Brzostek, E.R., Frey, S.D., Stuart Grandy, A., Liang, C.,Phillips, R.P., 2022. Fast-decaying plant litter enhances soil carbon in temperate forests but not through microbial physiological traits. *Nature Communications 13*(1), 1229.

Davenport, R., Bowen, B.P., Lynch, L.M., Kosina, S.M., Shabtai, I., Northen, T.R.,Lehmann, J., 2023. Decomposition decreases molecular diversity and ecosystem similarity of soil organic matter. *Proceedings of the National Academy of Sciences 120*(25), e2303335120.

DiDonato, N., Chen, H., Waggoner, D.,Hatcher, P.G., 2016. Potential origin and formation for molecular components of humic acids in soils. *Geochimica et Cosmochimica Acta 178*, 210-222.

Dinel, H., Schnitzer, M.,Mehuys, G.R. (1990). *Soil lipids: origin, nature, content, decomposition, and effect on soil physical properties*.

Dittmar, T., Koch, B., Hertkorn, N.,Kattner, G., 2008. A simple and efficient method for the solid-phase extraction of dissolved organic matter (SPE-DOM) from seawater. *Limnology and Oceanography: Methods 6*(6), 230-235.

Drosos, M., Vinci, G., Spaccini, R.,Piccolo, A., 2020. Molecular dynamics of organic matter in a tilled soil under short term wheat cultivation. *Soil and Tillage Research 196*, 104448.

Erhagen, B., Öquist, M., Sparrman, T., Haei, M., Ilstedt, U., Hedenström, M., Schleucher, J.,Nilsson, M.B., 2013. Temperature response of litter and soil organic matter decomposition is determined by chemical composition of organic material. *Global Change Biology 19*(12), 3858-3871.

Freeman, E.C., Emilson, E.J.S., Dittmar, T., Braga, L.P.P., Emilson, C.E., Goldhammer, T., Martineau, C., Singer, G.,Tanentzap, A.J., 2024. Universal microbial reworking of dissolved organic matter along environmental gradients. *Nature Communications 15*(1), 187.

Fu, Q.-L., Fujii, M.,Kwon, E., 2022. Development of an internal calibration algorithm for ultrahigh-resolution mass spectra of dissolved organic matter. *Analytical Chemistry 94*(30), 10589-10594.

Gann, E., McNeill, C.R., Tadich, A., Cowie, B.C.C.,Thomsen, L., 2016. Quick AS NEXAFS Tool (QANT): a program for NEXAFS loading and analysis developed at the Australian Synchrotron. *Journal of Synchrotron Radiation 23*(1), 374-380.

Gleixner, G., Czimczik, C.J., Kramer, C., Lühker, B.,Schmidt, M.W.I., 2001. 1.15 - Plant compounds and their turnover and stabilization as soil organic matter. In: E.-D. Schulze, M. Heimann, S. Harrison, E. Holland, J. Lloyd, I. C. Prentice, and D. Schimel (Eds.), *Global Biogeochemical Cycles in the Climate System.* Academic Press, pp. 201-215.

Goranov, A.I., Sleighter, R.L., Yordanov, D.A.,Hatcher, P.G., 2023. TEnvR: MATLAB-based toolbox for environmental research. *Analytical Methods 15*(40), 5390-5400.

Guggenberger, G.,Kaiser, K., 2003. Dissolved organic matter in soil: challenging the paradigm of sorptive preservation. *Geoderma 113*(3), 293-310.

Guggenberger, G.,Zech, W., 1994. Dissolved organic carbon in forest floor leachates: simple degradation products or humic substances? *Science of The Total Environment 152*(1), 37-47.

Guggenberger, G., Zech, W.,Schulten, H.-R., 1994. Formation and mobilization pathways of dissolved organic matter: evidence from chemical structural studies of organic matter fractions in acid forest floor solutions. *Organic Geochemistry 21*(1), 51-66.

Gutiérrez, A., del Río José, C., Martínez-Íñigo María, J., Martínez María, J.,Martínez Ángel, T., 2002. Production of new unsaturated lipids during wood decay by ligninolytic basidiomycetes. *Applied and Environmental Microbiology 68*(3), 1344-1350.

Haynes, R.J., 2005. Labile organic matter fractions as central components of the quality of agricultural soils: an overview. In: *Advances in Agronomy.* Academic Press, pp. 221-268.

Hedenström, M., Wiklund-Lindström, S., Öman, T., Lu, F., Gerber, L., Schatz, P., Sundberg, B.,Ralph, J., 2009. Identification of lignin and polysaccharide modifications in *Populus* wood by chemometric analysis of 2D NMR spectra from dissolved cell walls. *Molecular Plant 2*(5), 933-942.

Hertkorn, N., Harir, M., Cawley, K.M., Schmitt-Kopplin, P.,Jaffé, R., 2016. Molecular characterization of dissolved organic matter from subtropical wetlands: a comparative study through the analysis of optical properties, NMR and FTICR/MS. *Biogeosciences 13*(8), 2257-2277.

Hertkorn, N., Harir, M., Koch, B.P., Michalke, B.,Schmitt-Kopplin, P., 2013. High-field NMR spectroscopy and FTICR mass spectrometry: powerful discovery tools for the molecular level characterization of marine dissolved organic matter. *Biogeosciences 10*(3), 1583-1624.

Ho, P.-C., Nakajima, S.,Urabe, J., 2023. Stoichiometry of carbon, nitrogen, and phosphorus released from the leaf litter of various temperate tree species. *Ecology and Evolution 13*(7), e10372.

Hockaday, W.C., Purcell, J.M., Marshall, A.G., Baldock, J.A.,Hatcher, P.G., 2009. Electrospray and photoionization mass spectrometry for the characterization of organic matter in natural waters: a qualitative assessment. *Limnology and Oceanography: Methods 7*(1), 81-95.

Ingwersen, J., Poll, C., Streck, T.,Kandeler, E., 2008. Micro-scale modelling of carbon turnover driven by microbial succession at a biogeochemical interface. *Soil Biology and Biochemistry 40*(4), 864-878.

Jerusalén-Lleó, E., Nieto-Cid, M., Fuentes-Santos, I., Dittmar, T.,Álvarez-Salgado, X.A., 2023. Solid phase extraction of ocean dissolved organic matter with PPL cartridges: efficiency and selectivity. *Frontiers in Marine Science 10*.

Jiménez-Morillo, N.T., Almendros, G., De la Rosa, J.M., Jordán, A., Zavala, L.M., Granged, A.J.P.,González-Pérez, J.A., 2020. Effect of a wildfire and of post-fire restoration actions in the organic matter structure in soil fractions. *Science of The Total Environment 728*, 138715.

Johnston, C.T.,Aochi, Y.O., 1996. Fourier transform infrared and raman spectroscopy. In: *Methods of Soil Analysis.* pp. 269-321.

Jones, D.L.,Willett, V.B., 2006. Experimental evaluation of methods to quantify dissolved organic nitrogen (DON) and dissolved organic carbon (DOC) in soil. *Soil Biology and Biochemistry 38*(5), 991-999.

Kaczmarczyk, B., 2013. FTIR study of conjugation in selected aromatic polyazomethines. *Journal of Molecular Structure 1048*, 179-184.

Kaiser, K.,Guggenberger, G., 2000. The role of DOM sorption to mineral surfaces in the preservation of organic matter in soils. *Organic Geochemistry 31*(7), 711-725.

Kaiser, K., Guggenberger, G., Haumaier, L.,Zech, W., 1997. Dissolved organic matter sorption on sub soils and minerals studied by 13C-NMR and DRIFT spectroscopy. *European Journal of Soil Science 48*(2), 301-310.

Kaiser, K., Guggenberger, G., Haumaier, L.,Zech, W., 2002. The composition of dissolved organic matter in forest soil solutions: changes induced by seasons and passage through the mineral soil. *Organic Geochemistry 33*(3), 307-318.

Kaiser, K.,Kalbitz, K., 2012. Cycling downwards – dissolved organic matter in soils. *Soil Biology and Biochemistry 52*, 29-32.

Kalbitz, K., Kaiser, K., Bargholz, J.,Dardenne, P., 2006. Lignin degradation controls the production of dissolved organic matter in decomposing foliar litter. *European Journal of Soil Science 57*(4), 504-516.

Kalembasa, S.,Kalembasa, D., 2016. Conversions and pathways of organic carbon and organic nitrogen in soils. In: L. W. Szajdak (Ed.), *Bioactive Compounds in Agricultural Soils.* Springer International Publishing, pp. 53-90.

Keiluweit, M., Bougoure, J.J., Zeglin, L.H., Myrold, D.D., Weber, P.K., Pett-Ridge, J., Kleber, M.,Nico, P.S., 2012. Nano-scale investigation of the association of microbial nitrogen residues with iron (hydr)oxides in a forest soil O-horizon. *Geochimica et Cosmochimica Acta 95*, 213-226.

Keiluweit, M., Nico, P.S., Johnson, M.G.,Kleber, M., 2010. Dynamic molecular structure of plant biomass-derived black carbon (Biochar). *Environmental Science & Technology 44*(4), 1247-1253.

Kelleher, B.P.,Simpson, A.J., 2006. Humic substances in soils: are they really chemically distinct? *Environmental Science & Technology 40*(15), 4605-4611.

Kim, H.,Ralph, J., 2014. A gel-state 2D-NMR method for plant cell wall profiling and analysis: a model study with the amorphous cellulose and xylan from ball-milled cotton linters. *RSC Advances 4*(15), 7549-7560.

Klotzbücher, T., Kaiser, K., Filley, T.R.,Kalbitz, K., 2013. Processes controlling the production of aromatic water-soluble organic matter during litter decomposition. *Soil Biology and Biochemistry 67*, 133-139.

Koch, B.P.,Dittmar, T., 2006. From mass to structure: an aromaticity index for high-resolution mass data of natural organic matter. *Rapid Communications in Mass Spectrometry 20*(5), 926-932.

Kögel-Knabner, I., 2002. The macromolecular organic composition of plant and microbial residues as inputs to soil organic matter. *Soil Biology and Biochemistry 34*(2), 139-162.

Kögel-Knabner, I., de Leeuw, J.W.,Hatcher, P.G., 1992. Nature and distribution of alkyl carbon in forest soil profiles: implications for the origin and humification of aliphatic biomacromolecules. *Science of the Total Environment 117-118*, 175-185.

Lange, D.F., Schröter, S.A., da Luz, F.M., Pires, E., Santos, Y.R., da Silva, J.S., Hildmann, S., Hoffmann, T., Ferreira, S.J.F., Schäfer, T., Quesada, C.A., Simon, C.,Gleixner, G., 2024. Cycling of dissolved organic nutrients and indications for nutrient limitations in contrasting Amazon rainforest ecosystems. *Biogeochemistry 167*(12), 1567-1588.

Lange, M., Roth, V.-N., Eisenhauer, N., Roscher, C., Dittmar, T., Fischer-Bedtke, C., González Macé, O., Hildebrandt, A., Milcu, A., Mommer, L., Oram, N.J., Ravenek, J., Scheu, S., Schmid, B., Strecker, T., Wagg, C., Weigelt, A.,Gleixner, G., 2021. Plant diversity enhances production and downward transport of biodegradable dissolved organic matter. *Journal of Ecology 109*(3), 1284-1297.

Lehmann, J., Hansel, C.M., Kaiser, C., Kleber, M., Maher, K., Manzoni, S., Nunan, N., Reichstein, M., Schimel, J.P., Torn, M.S., Wieder, W.R.,Kögel-Knabner, I., 2020. Persistence of soil organic carbon caused by functional complexity. *Nature Geoscience 13*(8), 529-534.

Lehmann, J., Liang, B., Solomon, D., Lerotic, M., Luizão, F., Kinyangi, J., Schäfer, T., Wirick, S.,Jacobsen, C., 2005. Near-edge X-ray absorption fine structure (NEXAFS) spectroscopy for mapping nano-scale distribution of organic carbon forms in soil: application to black carbon particles. *Global Biogeochemical Cycles 19*(1).

Lehmann, J.,Solomon, D., 2010. Chapter 10 - Organic carbon chemistry in soils observed by synchrotron-based spectroscopy. In: B. Singh and M. Gräfe (Eds.), *Developments in Soil Science.* Elsevier, pp. 289-312.

Lehmann, J., Solomon, D., Brandes, J., Fleckenstein, H., Jacobson, C.,Thieme, J., 2009. Synchrotron-based near-edge X-ray spectroscopy of natural organic matter in soils and sediments. In: *Biophysico-Chemical Processes Involving Natural Nonliving Organic Matter in Environmental Systems.* pp. 729-781.

Lu, Y.-C., Lu, Y.,Fan, X., 2020. Structure and characteristics of lignin. In: S. Sharma and A. Kumar (Eds.), *Lignin: Biosynthesis and Transformation for Industrial Applications.* Springer International Publishing, pp. 17-75.

Lv, J., Huang, Z., Luo, L., Zhang, S.,Wang, Y., 2022. Advances in molecular and microscale characterization of soil organic matter: current limitations and future prospects. *Environmental Science & Technology 56*(18), 12793-12810.

Maria, E., Crançon, P., Lespes, G.,Bridoux, M.C., 2019. Spatial variation in the molecular composition of dissolved organic matter from the podzol soils of a temperate pine forest. *ACS Earth and Space Chemistry 3*(8), 1685-1696.

Marschner, B., Brodowski, S., Dreves, A., Gleixner, G., Gude, A., Grootes, P.M., Hamer, U., Heim, A., Jandl, G., Ji, R., Kaiser, K., Kalbitz, K., Kramer, C., Leinweber, P., Rethemeyer, J., Schäffer, A., Schmidt, M.W.I., Schwark, L.,Wiesenberg, G.L.B., 2008. How relevant is recalcitrance for the stabilization of organic matter in soils? *Journal of Plant Nutrition and Soil Science 171*(1), 91-110.

Marschner, P., Umar, S.,Baumann, K., 2011. The microbial community composition changes rapidly in the early stages of decomposition of wheat residue. *Soil Biology and Biochemistry 43*(2), 445-451.

Michael, R.B., 1968. Infrared spectra of adsorbed molecules. *Applied Spectroscopy Reviews 1*(2), 289-378.

Minor, E.C., Swenson, M.M., Mattson, B.M.,Oyler, A.R., 2014. Structural characterization of dissolved organic matter: a review of current techniques for isolation and analysis. *Environmental Science: Processes & Impacts 16*(9), 2064-2079.

Nebbioso, A.,Piccolo, A., 2013. Molecular characterization of dissolved organic matter (DOM): a critical review. *Analytical and Bioanalytical Chemistry 405*(1), 109-124.

Nefedov, A.,Wöll, C., 2013. Advanced applications of NEXAFS spectroscopy for functionalized surfaces. In: G. Bracco and B. Holst (Eds.), *Surface Science Techniques.* Springer Berlin Heidelberg, pp. 277-303.

Nicolardot, B., Recous, S.,Mary, B., 2001. Simulation of C and N mineralisation during crop residue decomposition: a simple dynamic model based on the C:N ratio of the residues. *Plant and Soil 228*(1), 83-103.

Ohno, T.,Ohno, P.E., 2013. Influence of heteroatom pre-selection on the molecular formula assignment of soil organic matter components determined by ultrahigh resolution mass spectrometry. *Analytical and Bioanalytical Chemistry 405*(10), 3299-3306.

Otto, A.,Simpson, M.J., 2005. Degradation and Preservation of Vascular Plant-derived Biomarkers in Grassland and Forest Soils from Western Canada. *Biogeochemistry 74*(3), 377-409.

Otto, A.,Simpson, M.J., 2006. Evaluation of CuO oxidation parameters for determining the source and stage of lignin degradation in soil. *Biogeochemistry 80*(2), 121-142.

Pan, Y., Meng, L., Wu, Y., Zhang, S., Wu, Z., Zhao, C., Yang, G., Xu, J., Ren, Y., Huang, T., Bian, Z., Jiang, Q., Zhou, J., Yang, H., Yu, Z., Yuan, L., Liu, H.,Huang, C., 2024. Molecular composition limits the reaction kinetics of riverine dissolved organic matter decomposition. *Science of the Total Environment 950*, 175454.

Parfitt, R.L., Fraser, A.R.,Farmer, V.C., 1977. Adsorption on hydrous oxides. III. Fulvic acid and humic acid on goethie, gibbsite and imogolite. *Journal of Soil Science 28*(2), 289-296.

Pedersen, J.A., Simpson, M.A., Bockheim, J.G.,Kumar, K., 2011. Characterization of soil organic carbon in drained thaw-lake basins of Arctic Alaska using NMR and FTIR photoacoustic spectroscopy. *Organic Geochemistry 42*(8), 947-954.

Picariello, E., Baldantoni, D., Izzo, F., Langella, A.,De Nicola, F., 2021. Soil organic matter stability and microbial community in relation to different plant cover: a focus on forests characterizing Mediterranean area. *Applied Soil Ecology 162*, 103897.

Pizzeghello, D., Zanella, A., Carletti, P.,Nardi, S., 2006. Chemical and biological characterization of dissolved organic matter from silver fir and beech forest soils. *Chemosphere 65*(2), 190-200.

Prescott, C.E., 2010. Litter decomposition: what controls it and how can we alter it to sequester more carbon in forest soils? *Biogeochemistry 101*(1), 133-149.

Prietzel, J., Müller, S., Kögel-Knabner, I., Thieme, J., Jaye, C.,Fischer, D., 2018. Comparison of soil organic carbon speciation using C NEXAFS and CPMAS 13C NMR spectroscopy. *Science of The Total Environment 628-629*, 906-918.

Qi, Y., Xie, Q., Wang, J.-J., He, D., Bao, H., Fu, Q.-L., Su, S., Sheng, M., Li, S.-L., Volmer, D.A., Wu, F., Jiang, G., Liu, C.-Q.,Fu, P., 2022. Deciphering dissolved organic matter by Fourier transform ion cyclotron resonance mass spectrometry (FT-ICR MS): from bulk to fractions and individuals. *Carbon Research 1*(1), 3.

Ramette, A., 2007. Multivariate analyses in microbial ecology. *FEMS Microbiology Ecology 62*(2), 142-160.

Roth, V.-N., Lange, M., Simon, C., Hertkorn, N., Bucher, S., Goodall, T., Griffiths, R.I., Mellado-Vázquez, P.G., Mommer, L., Oram, N.J., Weigelt, A., Dittmar, T.,Gleixner, G., 2019. Persistence of dissolved organic matter explained by molecular changes during its passage through soil. *Nature Geoscience 12*(9), 755-761.

Schmidt, M.W.I., Torn, M.S., Abiven, S., Dittmar, T., Guggenberger, G., Janssens, I.A., Kleber, M., Kögel-Knabner, I., Lehmann, J., Manning, D.A.C., Nannipieri, P., Rasse, D.P., Weiner, S.,Trumbore, S.E., 2011. Persistence of soil organic matter as an ecosystem property. *Nature 478*(7367), 49-56.

Seidel, M., Vemulapalli, S.P.B., Mathieu, D.,Dittmar, T., 2022. Marine dissolved organic matter shares thousands of molecular formulae yet differs structurally across major water masses. *Environmental Science & Technology 56*(6), 3758-3769.

Simpson, A.J., Lefebvre, B., Moser, A., Williams, A., Larin, N., Kvasha, M., Kingery, W.L.,Kelleher, B., 2004. Identifying residues in natural organic matter through spectral prediction and pattern matching of 2D NMR datasets. *Magnetic Resonance in Chemistry 42*(1), 14-22.

Singh, B., Fang, Y., Cowie, B.C.C.,Thomsen, L., 2014. NEXAFS and XPS characterisation of carbon functional groups of fresh and aged biochars. *Organic Geochemistry 77*, 1-10.

Smolander, A.,Kitunen, V., 2002. Soil microbial activities and characteristics of dissolved organic C and N in relation to tree species. *Soil Biology and Biochemistry 34*(5), 651-660.

Solomon, D., Lehmann, J., Kinyangi, J., Liang, B., Heymann, K., Dathe, L., Hanley, K., Wirick, S.,Jacobsen, C., 2009. Carbon (1s) NEXAFS spectroscopy of biogeochemically relevant reference organic compounds. *Soil Science Society of America Journal 73*(6), 1817-1830.

Solomon, D., Lehmann, J., Kinyangi, J., Liang, B.,Schäfer, T., 2005. Carbon K-edge NEXAFS and FTIR-ATR spectroscopic investigation of organic carbon speciation in soils. *Soil Science Society of America Journal 69*(1), 107-119.

Soucémarianadin, L.N., Erhagen, B., Nilsson, M.B., Öquist, M.G., Immerzeel, P.,Schleucher, J., 2017. Two dimensional NMR spectroscopy for molecular characterization of soil organic matter: application to boreal soils and litter. *Organic Geochemistry 113*, 184-195.

Thevenot, M., Dignac, M.-F.,Rumpel, C., 2010. Fate of lignins in soils: a review. *Soil Biology and Biochemistry 42*(8), 1200-1211.

Thieme, L., Graeber, D., Hofmann, D., Bischoff, S., Schwarz, M.T., Steffen, B., Meyer, U.N., Kaupenjohann, M., Wilcke, W., Michalzik, B.,Siemens, J., 2019. Dissolved organic matter characteristics of deciduous and coniferous forests with variable management: different at the source, aligned in the soil. *Biogeosciences 16*(7), 1411-1432.

Traversa, A., D'Orazio, V., Mezzapesa, G.N., Bonifacio, E., Farrag, K., Senesi, N.,Brunetti, G., 2014. Chemical and spectroscopic characteristics of humic acids and dissolved organic matter along two Alfisol profiles. *Chemosphere 111*, 184-194.

Wang, B., Spessa, A.C., Feng, P., Hou, X., Yue, C., Luo, J.-J., Ciais, P., Waters, C., Cowie, A., Nolan, R.H., Nikonovas, T., Jin, H., Walshaw, H., Wei, J., Guo, X., Liu, D.L.,Yu, Q.,

2022. Extreme fire weather is the major driver of severe bushfires in southeast Australia. *Science Bulletin 67*(6), 655-664.

Wang, H., Liu, S., Chang, S.X., Wang, J., Shi, Z., Huang, X., Wen, Y., Lu, L.,Cai, D., 2015. Soil microbial community composition rather than litter quality is linked with soil organic carbon chemical composition in plantations in subtropical China. *Journal of Soils and Sediments 15*(5), 1094-1103.

Wang, W.J., Baldock, J.A., Dalal, R.C.,Moody, P.W., 2004. Decomposition dynamics of plant materials in relation to nitrogen availability and biochemistry determined by NMR and wet-chemical analysis. *Soil Biology and Biochemistry 36*(12), 2045-2058.

Wang, Y., Zheng, J., Boyd, S.E., Xu, Z.,Zhou, Q., 2019. Effects of litter quality and quantity on chemical changes during eucalyptus litter decomposition in subtropical Australia. *Plant and Soil 442*(1), 65-78.

Whalen, E.D., Grandy, A.S., Sokol, N.W., Keiluweit, M., Ernakovich, J., Smith, R.G.,Frey, S.D., 2022. Clarifying the evidence for microbial- and plant-derived soil organic matter, and the path toward a more quantitative understanding. *Global Change Biology 28*(24), 7167-7185.

Wiesenberg, G.L.B., Dorodnikov, M.,Kuzyakov, Y., 2010. Source determination of lipids in bulk soil and soil density fractions after four years of wheat cropping. *Geoderma 156*(3), 267-277.

Yan, J., Wang, L., Hu, Y., Tsang, Y.F., Zhang, Y., Wu, J., Fu, X.,Sun, Y., 2018. Plant litter composition selects different soil microbial structures and in turn drives different litter decomposition pattern and soil carbon sequestration capability. *Geoderma 319*, 194-203.

Chapter 4 Dissolved organic matter composition and mineral surface chemistry modulate carbon sequestration in soils

This chapter has been submitted *Geoderma* journal:

Yang, Z., Thomsen, L., Dijkstra, F.A., Guggenberger, G., Singh, B. (2025). Dissolved organic matter composition and mineral surface chemistry modulate carbon sequestration in soils. *Geoderma*. Under review.

Graphical abstract

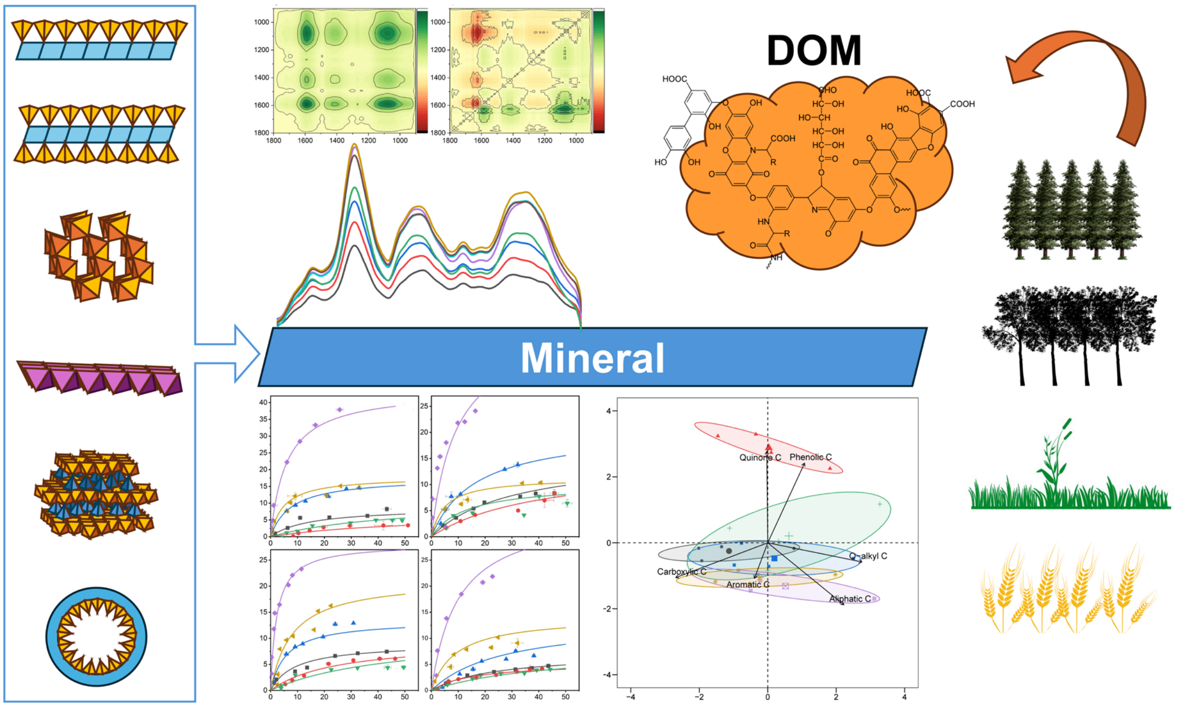

Highlights

- Mineral surface chemistry and DOM composition jointly controlled interactions.
- C=C/C=O, C-O-C and C-O groups consistently dominated at mineral-organic interfaces.
- Adsorption sequence and preferential selection of OM varied among minerals.
- Multilayer assembly formed via mineral-organic and organic-organic interactions.
- Reactive group abundances in DOM governed their adsorption capacity.

Abstract

The interaction between dissolved organic matter (DOM) and minerals governs OM stabilisation in soils. Heterogeneous composition of DOM and diverse mineral surface characteristics in soils make it extremely difficult to determine reaction mechanisms at mineral-organic interfaces. To determine the relationship between DOM and mineral characteristics in interactions at mineral-organic interfaces, we conducted adsorption experiments with four DOM extracts from pine, eucalyptus, pasture and wheat residues and a set of minerals with different charge characteristics, structural order and specific surface area (i.e., kaolinite, montmorillonite, goethite, birnessite, ferrihydrite and allophane). With the help of attenuated total reflectance Fourier transform infrared (ATR-FTIR) and near edge X-ray absorption fine structure (NEXAFS) spectroscopies, the adsorption sequence of functional groups differed with mineral surface chemistry, but C=C/C=O, C-O-C and C-O groups were consistently the most abundant adsorbed moieties. Adsorption involved both mineral-organic and organic-organic interactions, with the latter appearing with increased OM loading, yielding different mineral-OM assemblages depending on OM loading and mineral characteristics. Carboxylic, aromatic and aliphatic organic components predominantly adsorbed on the surfaces of ferrihydrite, allophane, goethite, and kaolinite, whereas quinone and phenolic organic components were preferentially adsorbed on birnessite and montmorillonite. Variations in the molecular composition within DOM also modulate adsorption behaviour at mineral-organic interfaces. The adsorption capacity of wheat DOM on mineral surfaces was lower than that of the other DOM due to its less abundance of reactive functional groups. Our results provide a robust explanatory foundation for predicting and monitoring soil carbon sequestration in relation to DOM sources and mineral assemblage.

Keywords

Dissolved organic matter, mineral, adsorption, mineral-organic interface, ATR-FTIR, 2D-COS, NEXAFS

4.1 Introduction

Being the largest organic carbon (OC) pool in the terrestrial system, soil organic matter (SOM) plays an important role in the global carbon cycle and in mitigating climate change (Tao et al., 2023; Friedlingstein et al., 2025). Although it comprises only a small fraction (<2%) of the total SOM (Guo et al., 2020), dissolved organic matter (DOM) is the most labile and reactive component of OM in soil (Marschner and Kalbitz, 2003; Nebbioso and Piccolo, 2013). With the translocation of DOM through the soil profile, it actively participates in the OC cycling by influencing its bioavailability and compositions through physicochemical interactions with plants, microbes and minerals in the pedosphere (Marschner and Kalbitz, 2003; Angst et al., 2018; Sokol et al., 2019). Particularly the interactions between DOM and soil minerals, including phyllosilicates and metal oxides (the term used to include oxyhydroxides, hydroxides, and oxides in this paper), have been highlighted as a major controlling factor in SOM stabilisation (Hemingway et al., 2019).

Not all organic components in DOM exhibit equal capabilities to interact with mineral surfaces. The reactivity of DOM is largely related to its type and abundance of active functional groups (Guggenberger and Kaiser, 2003; Curti et al., 2021). Recent studies have shown that hydrophobic, aromatic, and carboxylic-rich compounds exhibit greater affinity to mineral surfaces than other structures (Eusterhues et al., 2011; Lv et al., 2016; Avneri-Katz et al., 2017; Coward et al., 2019), resulting in the molecular fractionation of DOM and subsequently influencing the stabilisation and bioavailability of OM in the terrestrial ecosystem (Kögel-Knabner et al., 2008). Due to differences in surface charge characteristics, soil minerals exhibit different capacities and preferentially retain certain organic compounds through multiple reaction mechanisms, including ligand exchange, electrostatic attraction, cation bridging, hydrogen bonding, hydrophobic interaction, and van der Waals forces (Amrhein and Suarez, 1988; Kubicki et al., 1999; Arnarson and Keil, 2000). Organic compounds containing both aliphatic and phenolic structures are preferentially adsorbed onto phyllosilicates (Wang and Xing, 2005; Lombardi et al., 2006; Han et al., 2021), whereas crystalline Fe oxides tend to preferentially adsorb aromatic acids (Ghosh et al., 2009; Yeasmin et al., 2014; Wan et al., 2019). Also, high molecular weight, oxygen-rich, carboxyl-rich and aromatic compounds have been shown to preferentially bind to amorphous or short range ordered Fe oxides and aluminosilicates (Chen et al., 2014; Lv et al., 2016; Sowers et al., 2019; Lenhardt et al., 2022). Redox-active metal oxides, such as Mn oxides, not only preferentially adsorb aromatic compounds with high molecular weight, but can also oxidise phenolic compounds by either polymerisation or depolymerisation (Ma et al., 2020; Zhang et al., 2021; Ding et al., 2022).

Interactions between DOM and minerals at the mineral-organic interfaces are complex and diverse, often proceeding through a sequential assembly of specific organic components. Sequential adsorption of DOM on Fe oxides, beginning with the primary adsorption of aromatic-like compounds, followed by lignin-like, then aliphatic compounds and carboxylate-rich compounds have been observed (Coward et al., 2019; Ye et al., 2023; Lin et al., 2025). In contrast, phyllosilicates initially interact with oxygen-rich aliphatic moieties, such as proteins and carbohydrates (Han et al., 2021; Ruiz et al., 2024). However, due to the presence of hydrophobic groups in organic compounds, DOM compounds can undergo organic-organic interactions without direct contact with mineral surfaces through hydrophobic partitioning (Possinger et al., 2020; Underwood et al., 2024; Azimzadeh and Martínez, 2025). These interactions can assemble multilayer OM-OM structures coatings at the mineral-organic interfaces, resulting to the final composition of organic components retained on minerals difficult to estimate and predict.

Most previous studies have either focused on model organic compounds and/or examined only one or two minerals, which cannot capture the diversity and complexity of the assemblages between DOM and minerals in natural soil environments. In this study, DOM with distinct biomolecular structures were extracted from four plant residues - eucalyptus, pine, pasture and wheat - representing common land use systems in Australia. Six common soil minerals (i.e., kaolinite, montmorillonite, goethite, birnessite, ferrihydrite, and allophane) were selected for batch adsorption experiments with the four DOM samples. *In-situ* attenuated total reflection Fourier transform infrared (ATR-FTIR) spectroscopy coupled with two-dimensional correlation spectroscopy (2D-COS) was employed to monitor the temporal evolution of functional group interactions at mineral-organic interfaces. Carbon near-edge X-ray absorption fine structure (NEXAFS) spectroscopy was employed to investigate the preferential adsorption and fractionation of the organic-mineral complexes formed. The objectives of this study were (1) to determine the role of both DOM compositions and minerals in OM preservation; (2) to characterise the interactions at mineral-organic interfaces by tracking the adsorption of organic functional groups; and (3) to identify the preferential retention of organic components by minerals in the resulting mineral-organic complexes. The findings from this study will provide a better understanding and more reliable mechanistic framework to predict affinity of OM to minerals and clarify the associated mechanisms at mineral-organic interfaces in soils.

4.2 Materials and methods

4.2.1 *Dissolved organic matter*

Dissolved organic matter (DOM) was obtained by extraction of four decomposed plant residues (i.e., pine, eucalyptus, pasture and wheat) that represent common land use systems in Australia. Plant residues were shaken with Milli-Q water (1:10 w/v) for 3 hours at room temperature and filtrated through a 0.45 µm syringe filter (Shimadzu, PTFE membrane). Extracts were characterised for pH, EC, OC, point of zero charge (PZC) and elemental composition. The DOM samples were stored separately in liquid form and as freeze-dried powder at 4 °C for additional experiments and analyses. Important chemical properties of DOM samples are shown in Table S 4.1 in Section 4.6.1. The details obtained from FTIR and NEXAFS spectroscopy for DOM samples are also provided in Section 4.6.1.

4.2.2 *Minerals*

Six minerals representing different surface charge characteristics and specific surface area of minerals in soils were used in this study.

Two phyllosilicates, i.e., kaolinite KGa-2 (a variable charge mineral), and Na-rich montmorillonite SWy-2 (a permanent charge mineral), were obtained from the Clay Minerals Society Source Clay Repository. Both minerals were saturated with Na^+, dried and finely ground before use in the adsorption experiments. A well-crystalline Fe oxide with variable charge, i.e., goethite (α-FeOOH), and a poorly crystalline and meta-stable Fe oxide with variable charge, i.e., 2-line ferrihydrite ($Fe_{10}O_{14}(OH)_2$), were synthesised following the procedures described by Schwertmann and Cornell (2000). Manganese oxide (i.e., birnessite, δ-MnO_2), a variable charge nano-crystalline Mn oxide, was synthesised following the method developed by McKenzie (1971). The synthesis of allophane, ($(OH)_3Al_2O_3Si(OH)$)), a short-range ordered aluminosilicate common in volcanic ash soils, was synthesised following the procedure described by Ohashi et al. (2002).

Mineral identification was done by powder X-ray diffraction (XRD) analysis using a PANalytical X'Pert Pro powder diffractometer (Malvern Panalytical, Malvern, United Kingdom) with Cu Kα radiation. Specific surface area (SSA) was determined by N_2 adsorption BET method with Autosorb iQ gas adsorption analyser (Anton Paar GmbH, Graz, Austria) and PZC was determined by electrophoretic measurements with Malvern Zetasizer Nano ZS

(Malvern Panalytical, Malvern, United Kingdom). Detailed information of minerals is provided in the Section 4.6.2 of Appendix.

4.2.3 Batch adsorption experiments

The four DOM samples extracted from decomposed residues of pine, eucalyptus, pasture and wheat were each diluted in Mili-Q water to obtain initial OC concentrations of 0, 10, 20, 30, 40, 50, 60, 70, and 80 mg L^{-1}. All minerals were also suspended separately in Milli-Q water with ultrasonic treatment to obtain 1% (10 g L^{-1}) suspensions. Batch adsorption experiments were carried out in duplicate by mixing 1 mL of mineral suspensions with 4 mL of a series of DOM solutions (0-80 mg L^{-1}) in 15 mL centrifuge tubes. Both mineral suspensions and DOM solutions were initially acidified to pH 4. 10 mM NaCl was used as a background electrolyte. Sodium azide (NaN_3) was also added to the solutions to inhibit microbial activity from DOM extracts (Yeasmin et al., 2014). The Na^+ background electrolyte was used to minimise precipitation of organic substances (Arnarson and Keil, 2000). It was also ineffective at cation bridging during adsorption due to the monovalent cations primarily neutralised the mineral surface charge rather than forming bridges (Theng, 2012). The DOM-mineral suspensions were shaken in the dark at 4 °C for 16 hours on a horizontal shaker at 150 rpm to achieve equilibrium. The equilibrium solutions were centrifuged at 3000 × g for 30 mins and filtered through a 0.45 μm nylon membrane filter. The supernatant solutions were stored in the dark at 4 °C until the total organic carbon (TOC) analysis (within 24 hours). Langmuir and Freundlich isotherm models were used to describe the adsorption capacity of DOM onto each soil mineral. The Akaike information criterion (AIC) was calculated to compare the two models.

4.2.4 Attenuated total reflectance Fourier transform infrared (ATR-FTIR) spectroscopy

The ATR-FTIR spectra were obtained using a Bruker Vertex 80v spectrometer (Bruker Optiks GmbH, Ettlingen, Germany) equipped with a deuterated L-alanine doped triglycine sulphate (DLaTGS) MIR detector. A horizontal flow-through ATR trough plate equipped with a 45° ZnSe crystal was mounted in sample assembly. The spectra were collected at room temperature between 900 and 1900 cm^{-1} at a resolution of 4 cm^{-1} and 256 scans were averaged for each spectrum. Mineral suspensions (1 %) were prepared, adjusted to pH 4 and 10 mM NaCl was used as the background electrolytpe. Each mineral suspension was evenly spread across the ZnSe crystal surface to load approximately 1 mg of the mineral, dried overnight at room temperature, and rinsed with Mili-Q water to remove any detached minerals. A 10 mM NaCl solution was initially circulated over the mineral surface at a rate of 0.4 mL min^{-1} until no further spectral changes were observed in the successive spectra, and then the final spectrum was set as the background. Pine DOM sample (the highest DOC concentration) was selected for the adsorption experiments to ensure sufficient DOM interacting with mineral surfaces. The DOM solution was then circulated over the mineral surface at same rate, and spectra were collected every 10 min for about 140 min when the steady state was reached.

4.2.5 Two-dimensional correlation spectroscopy (2D-COS) analysis

The 2D-COS analysis of the ATR-FTIR adsorption spectra was done using with 2D Correlation Spectroscopy Analysis package in OriginPro 2021 software. The basic mathematical principle and conceptual framework of 2D-COS plots, i.e., synchronous and asynchronous correlation spectra, have been well explained in the Noda's rules (Noda and Ozaki, 2004). Briefly, the changes of functional groups adsorption can be inferred from the position of auto-peaks (located at the diagonal) and cross-peaks (located off the diagonal), denoted as spectral variables (ν_1, ν_2), and their correlation sign, shown as green (+) and red (-) regions in synchronous and asynchronous spectra.

The auto-peaks in synchronous spectrum are always positive. Spectral variable (ν) exhibits greater intensity changes over adsorption time will show a stronger auto-peak, while those that remain constant or change very little displays weaker or no auto-peaks. The positive cross-peaks in synchronous spectrum reflect the simultaneous changes in which both ν_1 and ν_2 increase or decrease over time, while the negative synchronous cross-peaks suggest that changes in opposite direction (i.e., non-simultaneous changes) in both variables. There are no auto-peaks in the asynchronous spectra, and cross-peaks develop only when the intensities of two spectral variables change out of phase with each other. A positive cross-peak in asynchronous spectra indicate that the intensity changes at ν_1 occurs predominantly before that at ν_2 in the sequential order of time. Conversely, a negative cross-peak suggests that changes at ν_2 occur before ν_1. However, these sign rules in asynchronous spectra will be reversed if the corresponding synchronous correlation at the same coordinate is negative.

4.2.6 Carbon near edge X-ray absorption fine structure (NEXAFS) spectroscopy

Carbon 1s K-edge NEXAFS spectroscopy was conducted at the soft X-ray spectroscopy beamline of the Australian Synchrotron. The beam operated in top-up mode with the storage ring beam current of 200 mA. Mineral-organic complexes from batch adsorption experiments were freeze-dried and ground. The complexes with the highest OM loading were selected and mounted on to a sample loading ruler using a double-sided tape and placed inside a high throughput NEXAFS vacuum chamber for analysis. The nominal beam size at sample under the operating conditions was 1 × 1 mm. The NEXAFS spectra were collected in the total electron yield (TEY) and partial electron yield (PEY) modes at an angle of 55° to the beam. The settings for C scanning signals of PEY were 200 eV on channeltron front detector (CHF) and 100 eV on hemispherical analyser (HA) with the flood gun off. C-1s K-edge spectra were collected in the 270-340 eV energy range using a step size of 0.1 eV and the dwell time of 0.8 s. The drain current from TEY was used in this study because of their higher quality, and were double normalised with I_0 (incident beam) and photodiode background spectra, and corrected with C reference spectra on the Quick AS NEXAFS Tool (QANT) v1.13 (Gann et al., 2016). The normalised spectra were scaled by setting the pre-edge (at 280.0 eV) to zero and the post-edge (at 320.0 eV) to one. Six peaks were identified and assigned to quinone C (284.4 eV), aromatic C (285.1 eV), phenolic C (286.5 eV), aliphatic C (287.5 eV), carboxylic C (288.5 eV) and O-alkyl C (289.2 eV) (Singh et al., 2014). The relative abundances of each organic groups were fitted Gaussian function with an expected error of 1-3 %. The principal component analysis (PCA) was applied to determine the relationship of adsorbed organic functional groups and each mineral by using *vegan* package in R 4.5.1.

4.3 Results

4.3.1 *DOM properties*

Organic carbon concentration in the DOM samples differed from their original plant residues and followed the order: pine (553 mg L^{-1}) > pasture (142 mg L^{-1}) > wheat (100 mg L^{-1}) and eucalyptus (87 mg L^{-1}) (Table S 4.1). Although they may have retained a fraction of positively charged polymers, all DOM samples carried a net negative charge (Figure S 4.1). The FTIR and NEXAFS analysis of the DOM samples (Figure S 4.2 and Figure S 4.3) showed a broadly similar molecular composition of functional groups, such as, C=C, C=O, C-C, C-O, C-H, and O-H, across the samples. However, some differences were observed in the relative abundance of assigned organic groups in the FTIR (Table S 4.2) and NEXAFS (Table S 4.3) spectra. Compared to the other DOM sources, the DOM extracted from pine residues exhibited a greater abundance of carboxylic compounds, with substantial C=O and O-H functional groups. Eucalyptus DOM was more diverse and enriched in phenolic and aliphatic compounds, containing prominent C-H, C=O, and C-O functional groups. Pasture DOM also showed a large abundance of phenolic compounds with conjugated C=O/C=C and C-O functional groups. Wheat DOM was dominated by oxygen-rich compounds, including O-alkyl C and quinone structures, with abundant C-O-C and O-H functional groups.

4.3.2 *Adsorption isotherm of DOM on minerals*

DOM adsorption onto all six soil minerals was well described by both Langmuir and Freundlich isotherm models (Figure 4.1 and Table S 4.5). The Langmuir adsorption maximum (Q_{max}) of DOM on minerals followed the order: ferrihydrite (Fh) > allophane (Allo) > goethite (Goe) > kaolinite (Kao) > birnessite (Bir) > montmorillonite (Mont) (Figure 4.1). This order was consistent with the adsorption capacity (K_F) derived from the Freundlich model (Table S 4.5).

The highest maximum adsorption capacities were observed for Fh (Q_{max}: 28.2-43.9 mg g^{-1}; K_F: 4.9-10.2 mg^{1-n} L^n g^{-1}) followed by Allo (Q_{max}: 11.4-21.4 mg g^{-1}; K_F: 1.7-4.1 mg^{1-n} L^n g^{-1}) (Figure 4.1 and Table S 4.5). At pH 4, the single coordinated hydroxyl dominated in Fe polyhedra of Fh and the outer gibbsite sheets of Allo are mostly protonated to $\equiv FeOH_2^+$ and $AlOH_2^+$ (< PZC of Fh 7.4 and PZC of Allo 7.6, Table S 4.4) (Hiemstra and Zhao, 2016; Boily and Song, 2020; Lenhardt et al., 2022). Similar coordinated surface hydroxyl groups to Fh can be expected to Goe surfaces, but their proportion of the most reactive hydroxyl groups was lower than that on Fh, as indicated by its higher PZC (PZC of Goe being 8.8) (Hiemstra and Zhao, 2016; Boily and Song, 2020). However, the lower DOM adsorption capacity was observed on Goe with Q_{max} 13.5-20.4 mg g^{-1} and K_F 0.5-4.4 mg^{1-n} L^n g^{-1} related to Fh and Allo.

Both phyllosilicates (i.e., Kao and Mont) and the Mn oxide (i.e., Bir) exhibited low maximum adsorption capacity at pH4. In particular, Mont showed the lowest DOM adsorption capacity among all minerals, with Q_{max} 5.4-14.4 mg g^{-1} and K_F 0.2-0.6 mg^{1-n} L^n g^{-1}, while Bir showed the lowest bonding energy (K_L) (approximately 0.02 L g^{-1}). At pH 4, adsorption of DOM on these mineral surfaces is expected to be weak due to the presence of electrostatic repulsion between negatively charged surfaces (PZC < 3.0) and negatively charged organic molecules. Although aluminol and silanol groups on the edge sites of phyllosilicates can be protonated at pH 4, occurring as $Al\text{-}OH_2^+$ ($pK_a = 5.7$) and $Si\text{-}OH_2^+$ ($pK_a = 8.7$), respectively (Liu et al., 2013), the limited abundance of edge hydroxyl sites is unlikely to support substantial adsorption progresses (Tombácz and Szekeres, 2006). Adsorption may not be the primary interactions occurred between Bir and DOM due to the presence of highly oxidised Mn species (e.g., Mn^{4+} and Mn^{3+}) in Mn oxide, which can promote redox reactions with organic molecules (Zhang et al., 2021; Ding et al., 2024).

The composition of DOM derived from different plant residues also played an important role in its adsorption behaviour onto minerals. We observed differences in the maximum adsorption capacity of DOM samples on the same mineral (Figure S 4.6). At similar amount of DOC input, Eucalyptus DOM exhibited the highest adsorption on most minerals, except for Fh and Allo, which adsorbed more pine and pasture DOM, respectively. However, wheat DOM consistently showed the lowest adsorption across all minerals. The abundance of reactive organic functional groups in DOM that are aligned to the surface reactivity of the minerals can directly influence its adsorption and leads to DOM fractionation (Ding et al., 2019; Sowers et al., 2019; Hu et al., 2024). Eucalyptus DOM contained a diverse composition of aliphatic and phenolic compounds with abundant C=O and C-O functional groups, which likely promotes affinity for a wide range of mineral surfaces. In contrast, pine and pasture DOM were enriched in carboxylic and aromatic acid compounds, respectively, which preferentially retained by Fh and Allo. Wheat DOM was dominated by O-alkyl C and quinone compounds, which are generally less reactive than carboxylic and phenolic compounds on mineral surfaces.

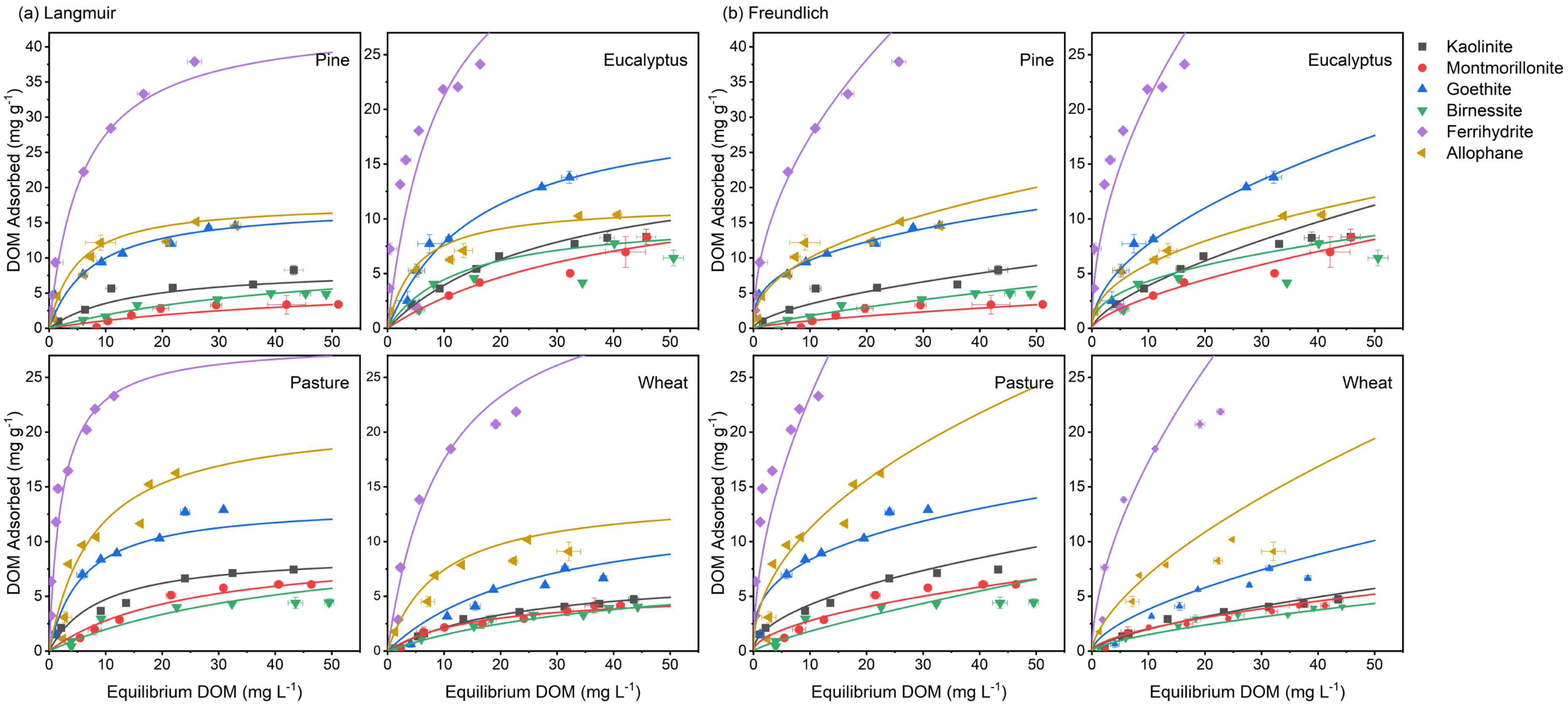

Figure 4.1 Adsorption isotherms of the four DOM samples (i.e., pine, eucalyptus, pasture and wheat) onto six minerals (i.e., kaolinite, montmorillonite, goethite, birnessite, ferrihydrite, and allophane). Various symbols represent the mean of experimental data points with error bars (n=2), and the solid lines represent Langmuir (a) and Freundlich (b) isotherm model fitted to the experimental data.

4.3.3 ATR-FTIR coupled with 2D-COS analysis for interaction mechanisms

The ATR-FTIR spectroscopy coupled with 2D-COS analysis were employed to elucidate the specific reaction mechanisms and sequential adsorption of DOM functional groups. While the composition of DOM can influence the abundance of reactive functional groups available for interaction, the specific reactions occurring at mineral-organic interfaces are primarily determined by the mineral surface chemistry (Xu et al., 2022). Therefore, we selected only one DOM source (i.e., pine DOM) to investigate functional groups interactions across different mineral surfaces.

Organic compounds containing C=O (1623 cm^{-1}) and conjugated C=C/C=O (1600 cm^{-1}) were predominantly adsorbed on the Kao surface over time, whereas on Mont surfaces, organic compounds containing C=C/C=O (1598 cm^{-1}) and C-O (1032 and 1014 cm^{-1}) were primarily involved in adsorption (Figure 4.2). Based on the Noda's rule, the dynamic adsorption sequence on the Kao surface began with the simultaneous appearance of C=O (1700 cm^{-1}), C=C (1510 cm^{-1}), C-O/O-H (1269 cm^{-1}), C-O-C (1142 cm^{-1}) and C-O (1077cm^{-1}), followed by C=O (1623 cm^{-1}), then C=C/C=O (1600 cm^{-1}), and C-H (1422, 1385 cm^{-1}) appeared last (Figure 4.3 and Table S 4.7). A similar sequential adsorption order was observed on Mont: C=O (1717 cm^{-1}) → C-O-C (1116 cm^{-1}) → C-O (1014 cm^{-1}) → C-O/O-H (1269 cm^{-1}) → C-O (1032 cm^{-1}) → C=C/C=O (1598 cm^{-1}) → C-H (1455 and 1418 cm^{-1}) (Figure 4.3 and Table S 4.8). It should be noted that the fingerprint region (after ~1050 cm^{-1}) in the ATR-FTIR spectra of Kao was noisy (not shown in Figure 4.2), which may have attributed to a low signal-to-noise ratio for low DOM loading onto Kao. Also, Kao particles may have been dislodged in the flow-through system during the experiment, leading to weak absorbance intensities of functional groups.

Four distinct bands at 1589 cm^{-1} (C=C/C=O), 1418 cm^{-1} (C-H), 1129 cm^{-1} (C-O-C) and 1075 cm^{-1} (C-O) were observed on Goe surfaces over time (Figure 4.2). The sequential order of adsorption of functional groups on the Goe was: C-H (1418 cm^{-1}) → C-O-C (1129 cm^{-1}) → C-O (1075 cm^{-1}) → C=C/C=O (1589 cm^{-1}) → C=O (1717 cm^{-1}), C-O/O-H (1269 cm^{-1}) and C=C (1510 cm^{-1}) (Figure 4.3 and Table S 4.9). Unexpectedly, alkyl groups (C-H) and O-alkyl groups (C-O-C and C-O) interacted prior to carboxyl groups (C=O). Organic groups C=C/C=O (1595 cm^{-1}), C-O-C (1081 cm^{-1}) and C-O (1030 cm^{-1}) dominated the DOM adsorption on Bir surfaces over time (Figure 4.2). The 2D-COS analysis showed an initial adsorption of alkyl groups (C-H), followed by the conjugated C=C/C=O groups, then carboxyl groups (C=O), with simultaneous adsorption of O-alkyl groups (C-O-C and C-O) occurring last (Figure 4.3 and Table S 4.10).

The DOM functional groups on Fh and Allo showed similar predominant moieties over time, including C=C/C=O (1592 or 1595 cm^{-1}), C-O-C (1112 or 1129 cm^{-1}), and C-O (1063 or 1086 cm^{-1}) (Figure 4.2). The sequential order of functional groups on Fh was: C=O (1753 cm^{-1}) and C-H (1405 cm^{-1}) → C-O/O-H (1269 cm^{-1}) → C-O-C (1112 cm^{-1}) → C=C/C=O (1592 cm^{-1}) → C-O (1063 cm^{-1}) (Figure 4.3 and Table S 4.11). While the sequence on Allo surface was: C=O (1717 cm^{-1}) → C-O-C (1129 cm^{-1}) and C-O (1086 cm^{-1}) → C-H (1455 cm^{-1}) → C=C/C=O (1595 cm^{-1}) → C-H (1410 cm^{-1}) and C-O/O-H (1272 cm^{-1}) (Figure 4.3 and Table S 4.12).

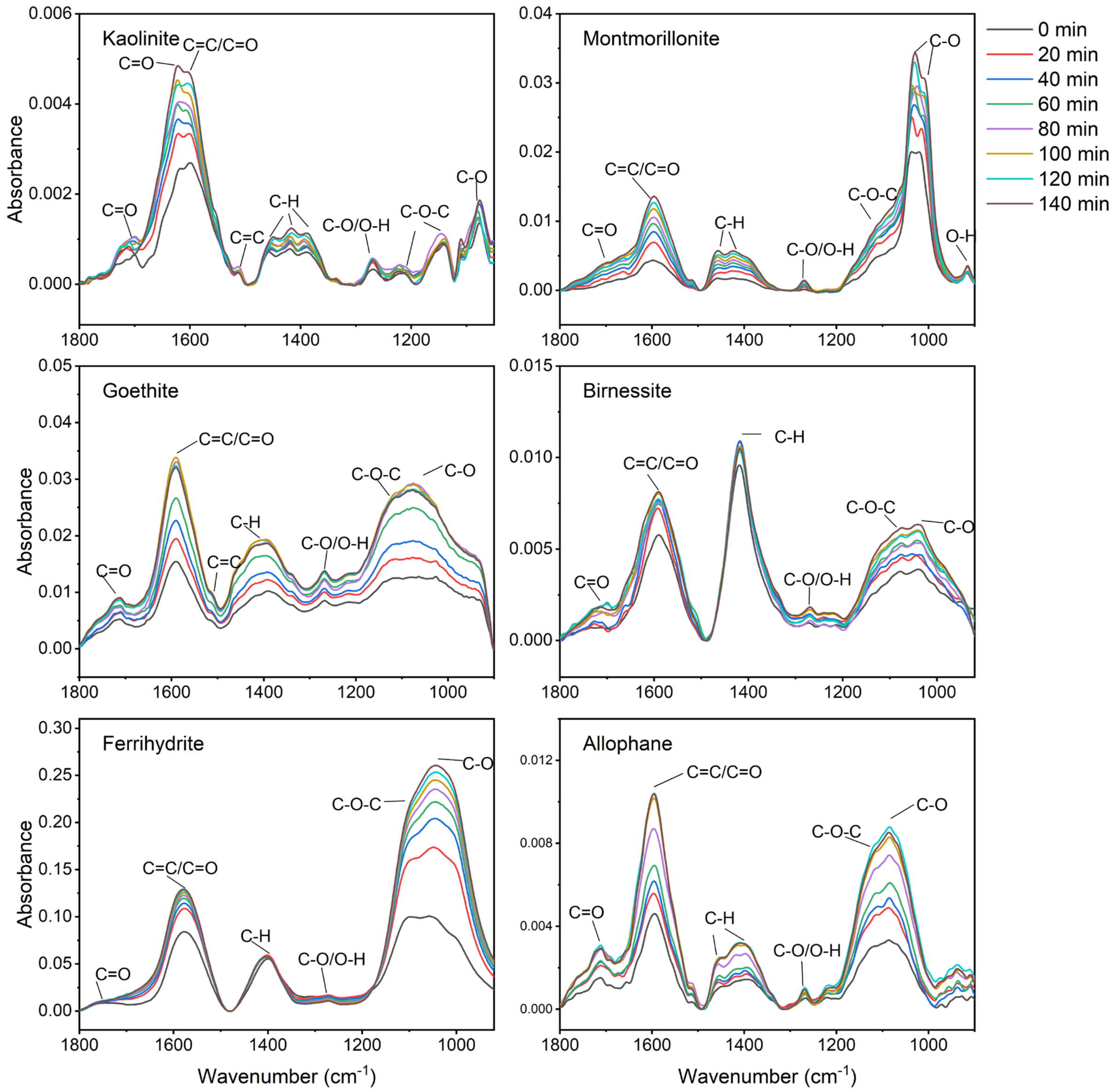

Figure 4.2 ATR-FTIR spectra of DOM adsorption onto different minerals with increasing absorption time from 0 to 140 min at pH 4 in 0.01 M NaCl background electrolyte, shown for the 1800-900 cm^{-1} (1800-1050 cm^{-1} for kaolinite due to very nosy spectra after 1050 cm^{-1}). Each ATR-FTIR spectrum was baseline corrected with scattering correction. The absorbance bands were assigned to frequency positions of C=O, C=C/C=O, C-H, C-O/O-H, C-O-C, and C-O.

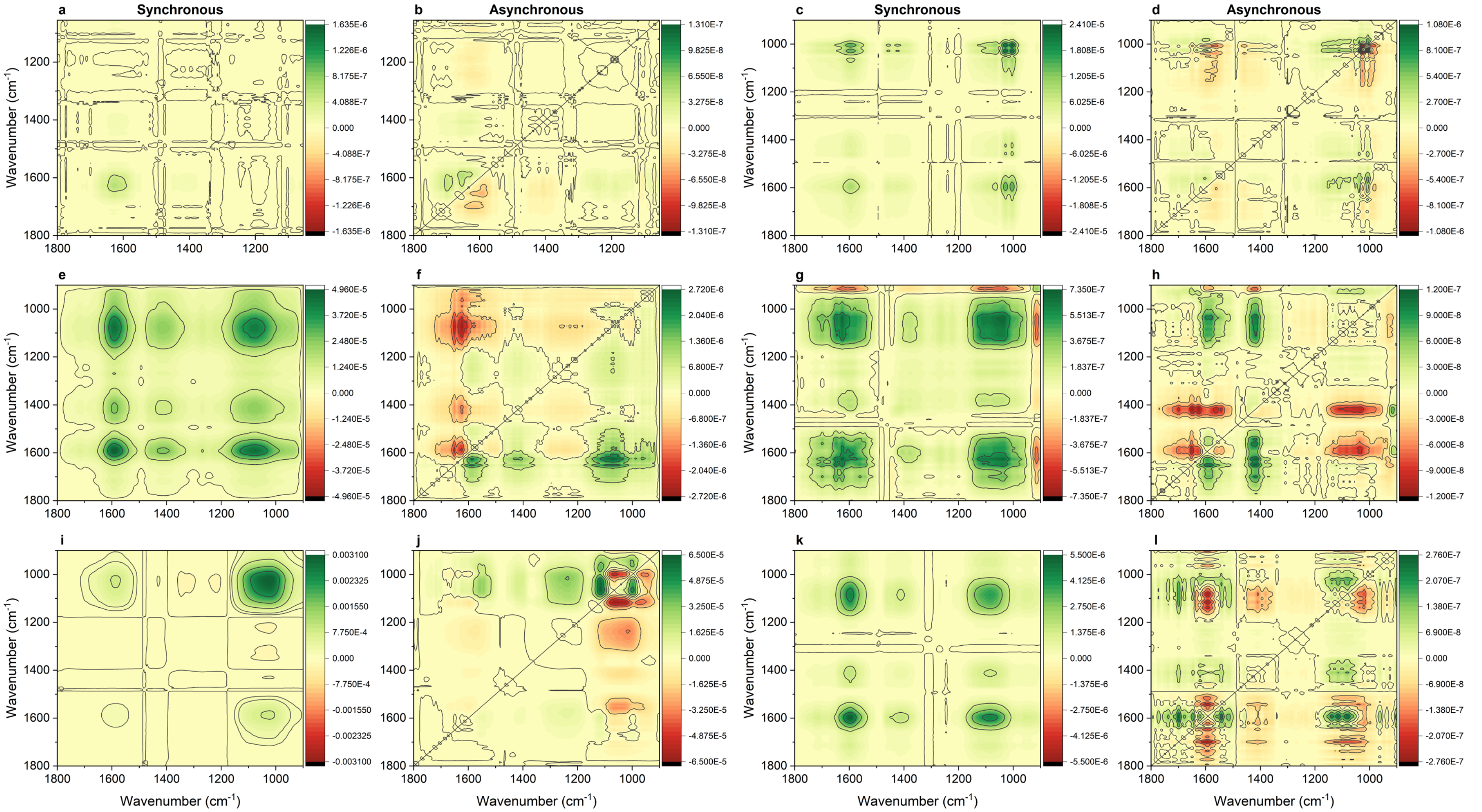

Figure 4.3 Synchronous (a, c, e, g, i, k) and asynchronous (b, d, f, h, j, l) 2D-FTIR-COS spectra of pine DOM adsorption onto kaolinite (a and b), montmorillonite (c and d), goethite (e and f), birnessite (g and h), ferrihydrite (i and j), and allophane (k and l) with interaction time from 0-140 min in the 1800-900 cm^{-1} region (1800-1050 cm^{-1} for kaolinite due to very noisy spectra after 1050 cm^{-1}). The colours of auto- and cross-peak in both synchronous and asynchronous spectra represented the correlation results from 2D-COS analysis: green - positive (+) and red - negative (-).

4.3.4 OM characterisation of mineral-organic complexes by NEXAFS spectroscopy

Due to the complexity and heterogeneous characteristics of the DOM used, the OM adsorbed onto minerals consisted of a range of compounds, with intricate structures and multiple functional groups in various abundance (Table S 4.13). Therefore, the organic groups identified by NEXAFS spectroscopy referred to the most representative functional groups on the mineral-organic complexes with specific characteristics, rather than indicating the adsorption of only a single functional group.

Organic compounds in Kao- and Mont-organic complexes contained more quinone C and aromatic C, but less aliphatic C and O-alkyl C compared to other minerals (Table S 4.13). Notably, the highest abundances of quinone (16.0-19.2 %) and phenolic C (5.4-9.0 %) was observed in Mont-organic complexes (Figure 4.4). Compared to Mont, Kao-organic complexes showed higher abundances of carboxylic C (5.7-6.6 %) and aliphatic C (26.1-35.5 %). Compared to other minerals, organic compounds adsorbed onto Goe exhibited more diverse characteristics with a greater abundance of carboxylic C (28.4-46.2 %), aromatic C (8.2-11.3%), aliphatic C (27.0-36.5 %) and O-alkyl C (10.0-18.3 %) (Table S 4.13). Bir adsorbed DOM with greater abundance of quinine C (3.2-7.2 %), phenolic C (3.1-10.2 %) and aliphatic C (26.6-37.1 %) (Table S 4.13). Organic compounds adsorbed onto Fh and Allo exhibited similar abundances of carboxylic, aromatic and aliphatic C (Figure 4.4). Fh showed the highest relative abundance of aromatic C (9.9-16.9 %) and aliphatic C (30.2-39.8 %) among all minerals (Table S 4.13). Preferential adsorption of organic compounds with carboxylic C occurred on Allo, with the highest relative abundance ranging from 35.9-52.4 % among the minerals (Table S 4.13).

OM in mineral-organic complexes derived from pine, eucalypt, and pasture DOM overlapped in the PCA analysis (Figure 4.4b), with similar contributions of quinone, aromatic, phenolic and carboxylic C in their adsorption. Although the abundance of these organic compounds varied in the DOM samples, minerals preferentially interacted with the carboxyl groups of these organic compounds (Kleber et al., 2021). Organic compounds adsorbed from wheat DOM exhibited a greater abundance of aliphatic and O-alkyl C on minerals (Figure 4.4b). These compounds were more saturated, lacked carboxyl groups, and contained mainly C-O-C and -OH functional groups, which were less reactive and less preferentially adsorbed onto mineral surfaces (Table S 4.2 and Table S 4.3). Aliphatic and O-alkyl C have been reported to weakly interact with adsorbed organic compounds or self-assembly on mineral surfaces at hydrophobic zone (Kleber et al., 2007; Gao et al., 2020). Despite similar C concentrations in DOM, differences in their composition could lead to variable behaviour due to preferential and selective interactions of certain functional groups with mineral surfaces (Sanderman et al., 2014; Avneri-Katz et al., 2017). The wheat DOM consistently exhibited relatively lower adsorption, likely due to its limited content of reactive functional groups capable of interacting with mineral surfaces. This is in contrast with the other three DOM samples, where adsorption was largely mineral dependent.

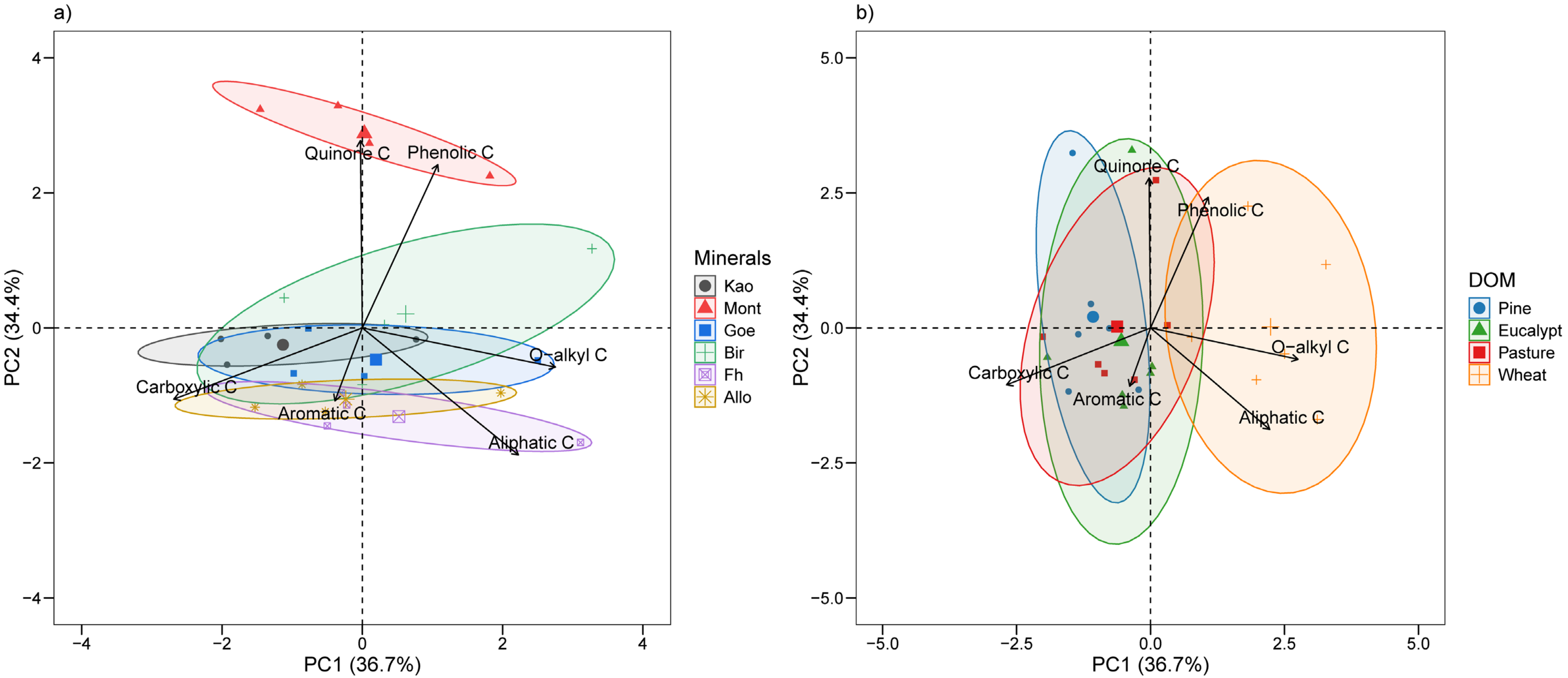

Figure 4.4 Principal component analysis (PCA) of the relationship of adsorbed functional groups between minerals (a) and dissolved organic matter extracted from four plant residues (b). The loading vector variables (arrows) represent the organic groups assigned from C NEXAFS: quinone C, aromatic C, phenolic C, aliphatic C, carboxylic C and O-alkyl C.

4.4 Discussion

4.4.1 *Interaction mechanisms between DOM and minerals*

The adsorption isotherm results showed that the surface characteristics of adsorbent (i.e., minerals) and the composition of adsorbate (i.e., DOM) jointly influenced the adsorption behaviour of DOM (Guggenberger and Kaiser, 2003; Xu et al., 2022).

The large maximum adsorption capacities observed for Fh and Allo are consistent with other studies, with the adsorption capacities of amorphous or short range ordered Fe/Al minerals always higher than other minerals, likely due to their positively charged surfaces, relatively high SSA (186 $m^2 g^{-1}$ and 145.8 $m^2 g^{-1}$, Table S 4.4), disordered pore structures and surface morphologies (Chevallier et al., 2010; Eusterhues et al., 2011; Filimonova et al., 2016; Voggenreiter et al., 2024). The primary adsorption mechanisms for DOM on Fh and Allo likely involved electrostatic attractions, ligand exchange and H-bonding (Chevallier et al., 2010; Eusterhues et al., 2011; Filimonova et al., 2016). Due to the presence of positively charged hydroxyl groups on Fh and Allo, electrostatic attraction between anionic functional groups in DOM, particularly carboxyl groups (i.e., COO^-) (Kleber et al., 2015; Voggenreiter et al., 2024), and mineral surface hydroxyl sites promotes the adsorption process. Strong polar Fe/Al-O-C bonds can also be formed via ligand exchange reactions, whereby the organic ligands formed chelated with Fh and Allo as inner-sphere complexes (Kleber et al., 2015). Furthermore, outer-sphere complexes may be formed via surface H-shared ion pair interactions (i.e., H-bonding) between the oxygen atoms in organic functional groups and surface hydroxyl groups on Fh and Allo (Johnson et al., 2004; Norén and Persson, 2007). Similar adsorption mechanisms, including electrostatic attraction, ligand exchange and H-bonding, between DOM and Goe surfaces can be deduced from its similar structures to Fh (Norén and Persson, 2007; Kleber et al., 2015). The lower DOM adsorption capacity observed for Goe relative to Fh may result from a lower intensity of reactive surface hydroxyl sites and its smaller SSA (31.8 $m^2 g^{-1}$), which together reduce the number of available reactive sites for DOM adsorption.

Kao possesses heterogeneous surface charges with a small amount of constant charge and the predominantly variable charge on the edges arising from the protonation or deprotonation of surface hydroxyl groups (Zhou and Gunter, 1992). Mont surfaces are relatively homogeneous and carry substantial permanent negative charge due to isomorphous substitution within its structure, with comparatively few reactive hydroxyl groups at edge sites (Li et al., 2022b). Cation bridging through multivalent cations has been suggested as an important process in the

DOM adsorption onto Kao and Mont (Varadachari et al., 1991; Ahmed et al., 2002). However, such bridging was not expected in our system (with Na^+ in the background solution). Instead, at pH 4, protonated hydroxyl groups at edges can form covalent bonds with DOM compounds via ligand exchange (Chen et al., 2020), or participate in H-bonding interactions to form loosely bound outer-sphere complexes on Kao and Mont (Chorover and Amistadi, 2001; Han et al., 2021). Adsorption can be established through π-π interactions via electron donor-acceptor (EDA) systems between benzene rings of DOM compounds and Kao and Mont surfaces, forming either inner- or outer-sphere complexes (Keiluweit and Kleber, 2009).

Adsorption of DOM compounds onto Bir can occur via ligand exchange, hydrophobic partitioning and electrostatic interactions (Li et al., 2021). However, DOM compounds adsorbed onto Bir surfaces are also known to be oxidised and form new compounds (Zhang et al., 2021; Ding et al., 2024). The negatively charged Bir surface at pH 4 (PZC < 3.0) may have promoted redox reactions, which has been observed in previous studies where the transformation of DOM compounds through fragmentation and polymerisation reached a maximum at pH 4 (Wu et al., 2020). Oxidised forms of Mn^{4+} and Mn^{3+} in Mn oxides can accept electrons from DOM compounds (Ma et al., 2020; Zhang et al., 2021), especially phenolic compounds, reducing to a lower valence state of Mn^{3+} and Mn^{2+}. The reduced Mn cations on Bir surfaces not only provide cation-bridging sites, but also screen the intrinsic negative surface charge, thus substantially enhancing the adsorption of DOM (Wang et al., 2019; Li et al., 2021).

The SSA of minerals is known to play an important role in their DOM adsorption capacity by influencing the availability and number of reactive sites (Chevallier et al., 2010; Hiemstra and Zhao, 2016; Calvelo Pereira et al., 2019). However, the amorphous or short range ordered Fe/Al minerals (i.e., Fh and Allo) exhibited the lowest adsorption capacity per unit of SSA compared to other minerals, with the order being - Goe > Kao > Bir > Mont > Fh > Allo (Figure S 4.6 and Table S 4.6). This contrasts with previous studies reporting higher absorption capacity per SSA for Fe/Al hydrous oxides than for metal oxides (Fe/Al or Mn) or clay minerals (Kaiser and Guggenberger, 2003; Li et al., 2022a). It is possible that freeze-drying collapsed Fh and Allo structures and reduced their porosity (Figure S 4.8), leading to more condensed structures and occlusion of some reactive surface sites (Calvelo Pereira et al., 2019; Gu et al., 2022). Although the minerals were dispersed using ultrasonic treatment, the condensed structures might not have been restored to their original forms, resulting in fewer reactive sites available for interaction with DOM compounds. Another contributing factor may be the filling or clogging of micro-pores in minerals by adsorbed OM compounds (Kaiser and Guggenberger, 2003; Mikutta et al., 2004). It has been reported that DOM compounds can enter the interior spaces within tiny allophane nanoparticles or aggregates during the adsorption (Ding et al., 2019). The adsorbed OM compounds may cover the amorphous minerals as aggregates, inhibiting accessibility to reactive sites for further DOM adsorption (Kaiser and Guggenberger, 2000).

4.4.2 Sequential adsorption of organic functional groups at mineral surfaces

Based on the synchronous and asynchronous spectra of DOM adsorption on minerals, the sequence of organic functional group adsorption at mineral-organic interfaces varied among mineral surfaces.

The DOM compounds adsorbed on Kao surfaces appeared more complex in this study, with the simultaneous appearance of multiple functional groups, compared with previous studies using humic acid where the adsorption sequence was carboxylate, aliphatic and carboxylic acid (Chen et al., 2020). The carboxyl group (COO^-) was likely to be the first functional group interacting with protonated aluminol groups on the edges of Kao through ligand exchange (Chen et al., 2020). However, the surface hydroxyl groups can be easily saturated due to the limited space at the edges (Tombácz et al., 2004). Subsequently, the permanently negatively siloxane surface would interact with organic compounds containing oxygen-rich structures, such as carbohydrates (C-O-C), polysaccharides (C-O) and phenols (C-O/O-H) through H-bonding and hydrophobic attractions (Ghosh et al., 2009; Han et al., 2021). The aromatic structures (e.g., phenolic or quinone C) were likely to be adsorbed at later stages through aromatic-π EDA interactions (Keiluweit and Kleber, 2009), and aliphatic structures via hydrophobic interactions (Kretzschmar et al., 1997; Lombardi et al., 2006). In this study, the sequence on Mont contrasted with previous studies, where it was reported that Mont initially adsorbed aliphatic, protein, and phenolic compounds, followed by aliphatic and aromatic structures (Mitchell et al., 2018). This can be explained by the absence of divalent cation bridging in our system, where hydrophobic interactions between unsaturated and aromatic compounds (with C=C/C=O and C-O functional groups) and hydrophobic patches possibly dominated (Lützow et al., 2006).

On the Geo surface, ligand exchange or electrostatic attraction between surface hydroxyl groups ($FeOH_2^+$) and carboxyl groups (COO^-) are known to occur first (Chorover and Amistadi, 2001; Han et al., 2021). However, it is possible that under acidic condition (pH 4), the extent of surface hydration-shared ion pairs formation between surface coordinated groups (i.e., -

FeOH, $=Fe_2OH$, and $\equiv Fe_3OH$) and O-alkyl groups (especially C-O) was greater than that of ligand exchange with carboxyl groups (C=O), thus forming outer-sphere complexes (Norén and Persson, 2007; Azimzadeh and Martínez, 2025). This has also been reported in acid subsoils by some studies where O-alkyl C or sugars were preferentially stabilised by Fe oxides (Spielvogel et al., 2008). Additionally, carboxyl groups may have interacted first, but the abundance of alkyl and O-alkyl groups (e.g., C-H, C-O-C and C-O) overshadowed the C=O signals, resulting in their apparent earlier appearance in the 2D-COS analysis.

On the Bir surface, the early C-H signals may either be subsidiary structures associated with reactive carboxyl groups, or directly adsorbed onto the Bir surface through hydrophobic attraction (Allard et al., 2017). The interaction mechanisms of DOM on Bir were markedly different from other minerals, possibly due to redox reactions. Oxidised Mn^{4+} and Mn^{3+}, located either at the edges or vacancies on Bir, can be reduced to Mn^{2+}, which can act as a bridge for DOM adsorption (Wang et al., 2019). It should be noted that the change of intensity of phenolic compounds (C-O/O-H) was minimal on Bir (Figure 4.2), likely due to Mn oxidation. Oxidation reactions can break down aromatic structures into carboxylic acids or induce polymerisation into more condensed aromatic structures (e.g., quinones) (Ma et al., 2020; Zhang et al., 2021; Ding et al., 2022). The condensed aromatic structures (C=C/C=O) can accept electrons from Mn^{2+} and adsorb onto Bir through a Mn^{2+}-π system (Keiluweit and Kleber, 2009). The depolymerised carboxylates from DOM may subsequently adsorb via ligand exchange reactions (Johnson et al., 2015). Oxygen-rich compounds with C-O-C and C-O functional groups, such as polysaccharides and carbohydrates, may either form complexes with Mn^{2+} or accumulate as multilayer arrangements through hydrophobic attractions on the Bir surface (Reardon et al., 2018).

On the surfaces of Fh and Allo, the carboxyl groups (C=O), either from aromatic acids or from carboxylic acids, initially interacted with mineral surface hydroxyl groups via ligand exchange and electrostatic attraction, forming a strong polar metal-O-C bonds on the Fh and Allo surfaces (Coward et al., 2019; Ding et al., 2019; Gao et al., 2020; Lenhardt et al., 2022). However, subsequently adsorbed functional groups differed between Fh and Allo. The adsorption of phenolic compounds (C-O/O-H) dominated on Fh, whereas carbohydrates and polysaccharides (C-O-C and C-O) were dominantly adsorbed on Allo. Both minerals ultimately adsorbed aromatic compounds with oxygen-rich functional groups (C=C/C=O or C-O/O-H) as the last moieties. The adsorption of C=O appeared first on both Fh and Allo surfaces tended to reach saturation rapidly, showing minimal or negligible changes over time. This suggests that although Fh and Allo exhibit amorphous structures with high SSA, the availability of reactive sites on their surfaces (i.e., hydroxyl groups) may be limited due to the structural compaction after deposition on the ZnSe crystal in the ATR-FTIR analysis (Gu et al., 2022) or blockage by previously adsorbed organic compounds (Mikutta et al., 2004; Chen et al., 2022). Consequently, further interactions between remaining reactive functional groups and mineral surfaces would be inhibited. Organic-organic interactions then gradually dominated the adsorption process through hydrophobic or polar interactions instead of solely mineral-organic interactions (Begill et al., 2023; Underwood et al., 2024), with oxygen-rich organic compounds continuing to adsorb via the formation of multilayer OM-OM structures in the hydrophobic zone (Kleber et al., 2007; Gao et al., 2020; Ye et al., 2023; Lin et al., 2025).

4.4.3 Preferential retention of organic families in mineral-organic complexes

After mineral-organic and organic-organic interactions during absorption, the mineral-organic complexes formed from different minerals exhibited distinct preferential retention of organic compounds.

Substantial abundance of quinone and phenolic C observed on Mont-organic complexes in our study. It has been reported that 2:1 phyllosilicates (e.g., Mont) preferentially adsorbed aliphatic and carbohydrate (or O-alkyl C) organic compounds via cation bridging interactions (Wang and Xing, 2005; Ghosh et al., 2009; Han et al., 2021). However, as discussed earlier, such preferential selection was not apparent due to the absence of multivalent cations in our study. Instead, the π-π EDA interactions and hydrophobic attractions between aromatic-like compounds with Mont might have been the primary interaction mechanism (Keiluweit and Kleber, 2009). Similar interactions can be expected on Kao surfaces, thus, quinone C and aromatic C were also observed in Kao-organic complexes. However, Kao-organic complexes also showed higher abundances of carboxylic C and aliphatic C, which is consistent with our 2D-COS results that adsorbed organic compounds contained aromatic and aliphatic structures with carboxyl groups from amide or carboxylic acids (Kretzschmar et al., 1997; Lombardi et al., 2006).

We observed chemically diverse organic features in Geo-organic complexes compared to other complexes. Previous studies have reported that different patterns of preferential adsorption on Goe, including carboxyl and aromantic groups, polysaccharides, aliphatic compounds, and peptides (Spielvogel et al., 2008; Ghosh et al., 2009; Wan et al., 2019). These differences suggest that Fe oxides can retain a wide range of organic compounds due to their high surface reactivity (Ghosh et al., 2009; Chassé et al., 2015; Han et al., 2021). Due to the dominant progresses can shift between mineral-organic and organic-organic interactions during complex formation, the apparent selectivity for specific organic groups by Goe can also vary substantially across adsorption stages. Quinine C, phenolic C and aliphatic C were the predominant organic families observed in Bir-organic complex, which can be attributed to the oxidation progress. Phenolic compounds are highly susceptible to oxidation, leading to either polymerisation from radicals to polymeric products (e.g., quinones) or the opening of their benzene rings into lower molecular weight structures (e.g., aliphatic compounds) (Ma et al., 2020; Zhang et al., 2021; Ding et al., 2022). Newly formed organic molecules and remaining phenolic compounds then can be absorbed onto Bir surfaces through ligand exchange, hydrophobic partitioning and electrostatic interactions.

Compared with the other minerals, complexes formed with Fh and Allo exhibited the highest abundance of aromatic, aliphatic C and carboxylic C, respectively. This feature appears to contrast with our 2D-COS analysis, which showed phenolic carbohydrate components dominated on Fh and Allo surfaces during adsorption. However, these findings can be reconciled because both minerals finally retained aromatic compounds enriched in oxygen-containing functional groups as the last moieties. This is consistent with previous studies reporting a high affinity of highly unsaturated or oxygen-rich aromatic compounds for Fh and Allo (Chen et al., 2014; Lv et al., 2016; Sowers et al., 2019; Lenhardt et al., 2022). The final organic characterisation of mineral-organic complexes is therefore not determined by a single reaction progress, but instead reflects the jointly influences of mineral-organic and organic-organic interactions during complex formation. This increases the chemical complexity of mineral-organic complexes and make it difficult to examine interactions solely from bulk end-point measurements.

4.5 Conclusion

The mineral surface charge characteristics and specific surface area in tandem with DOM functional group composition jointly modulate the stabilisation of OM in soils. Our results showed that minerals with net positive charge and high SSA adsorbed large amounts of DOM. Large adsorption capacities exhibited by Fh, Allo and Goe underscores the potential and importance of Fe oxides and poorly ordered minerals in preserving OC in soils. Although the adsorption conditions in this study did not replicate natural soil environments, the observations still align well with field evidence, where OC stocks associated with Fe oxides accounted for 18 % to 48 % of the total OC stock and more than 50 % of the mineral associated organic matter in topsoils (Kramer and Chadwick, 2018; Jia et al., 2024). Mineralogical composition contributes to differences in SOM sequestration capacity and potential among soil types. This possibly explains that certain regions, such as tropical forests, with adequate soil moisture and sustained high biomass production and high weathered soils often exhibit large stocks of mineral associated OC and serve as significant carbon sinks (Georgiou et al., 2022; Bramble et al., 2025).

Depending on the structural properties including crystal order and defects, different minerals can associate with distinct OM fractions (Kaiser et al., 2016; Hall et al., 2018). Regardless of the source, labile DOM can undergo fractionation as a result of the adsorption process with minerals (Avneri-Katz et al., 2017; Underwood et al., 2024). Variable charge minerals, i.e., Fh, Allo, Goe, Kao, that were positively charged under acidic conditions predominantly accumulated DOM components possessing carboxylic, aromatic, and aliphatic C groups, whereas negatively charged minerals (Bir and Mont) adsorbed more quinone and phenolic C components. Differing compositions of the resulting mineral-organic complexes supports the hypothesis that the fate of DOM largely depends on the dominant mineral phases present in soils (Zhao et al., 2020; Xu et al., 2022). Both surface hydroxyl groups and siloxane surfaces on minerals can interact with various DOM functional groups through multiple reaction mechanisms. The abundance of reactive surface sites on minerals determines the sequential assembly order of organic groups as observed in our study. The functional groups C=C/C=O, C-O-C and C-O consistently dominated in adsorbed moieties at the mineral-organic interfaces. Interactions between minerals and organic matter, together with interactions among organic molecules, synergistically controlled DOM adsorption behaviour. With increasing occupancy of most reactive sites on minerals, organic-organic interactions involving hydrophobic attractions occurred (Azimzadeh and Martínez, 2025), consistent with the hypothesis of kinetic architecture of multilayer formation in mineral-organic complexes (Chen et al., 2022). The organic-organic interactions have been considered important in the assemblage of organic multilayers at mineral-organic interfaces (Kleber et al., 2007; Kleber et al., 2021). Our data also supported the assertion the contribution of DOM molecular composition and properties in selective preservation of OM (Sanderman et al., 2014). Eucalyptus DOM, having a diverse composition of aliphatic and aromatic structures consisting of C=O, C-O and C-H functional groups, was adsorbed in largest amount. In contrast, adsorption of wheat DOM was limited due to the lack of reactive functional groups, in particular carboxyl groups.

The formation of mineral associated organic matter involved both mineral-organic and organic-organic interactions. It is important to explicitly integrate properties of both DOM and minerals in SOM models to better predict SOM stability and OC sequestration potential in soils.

Acknowledgements

This research was funded by the Australian Research Council (ARC) Discovery Project (DP220103026) and the University of Sydney. Carbon NEXAFS spectroscopy analysis was supported by the Australian Synchrotron (AS232/SXR/20075). The authors thank Dr. Michelle Wood for her scientific and technical assistance with ATR-FTIR analysis, which was carried out at Sydney Analytical, a core research facility at the University of Sydney.

4.6 Appendix

4.6.1 Extracted dissolved organic matter (DOM)

Table S 4.1 Important chemical properties of the DOM extracted from four decomposed plant residues, i.e., pine, eucalypt, pasture and wheat.

DOM	Pine	Eucalypt	Pasture	Wheat
Solution				
pH (1:10 H_2O)	6.5	6.4	7.2	7.5
EC (mS m^{-1})	56.5	5.8	13.5	53.3
TOC (mg L^{-1})	553.7	86.6	141.7	99.7
Na (mg L^{-1})	0.12	0.09	0.13	0.05
K (mg L^{-1})	0.13	0.07	0.59	0.22
Ca (mg L^{-1})	0.08	0.06	0.14	0.21
Mg (mg L^{-1})	0.05	0.03	0.08	0.08
Freeze-dried				
^{13}C	-26.2	-28.7	-19.3	-26.0
OC (%)	30.7	36.6	38.4	15.4

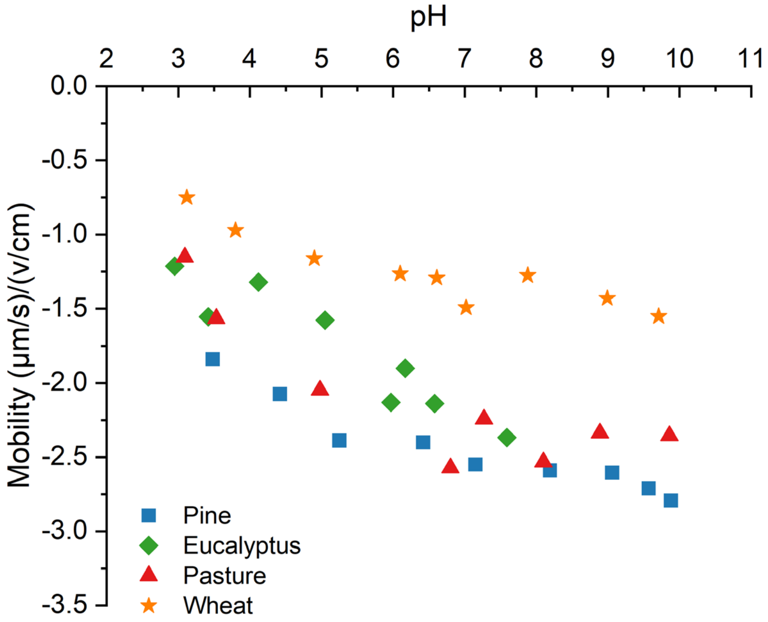

Figure S 4.1 Electrophoretic mobility ((μm s^{-1}) (v cm^{-1})$^{-1}$) of four DOM samples as a function of pH measured in 0.1 M $NaNO_3$ solution (Zelazny et al., 1996; Osei and Singh, 1999).

FTIR analysis

To determine the chemical composition of the extracted DOM samples at the molecular level, diffuse reflectance infrared Fourier transform (DRIFT) spectroscopy was used to characterise the functional group composition of the DOM samples. Briefly, the freeze-dried DOM samples were diluted with KBr (mixed and finely ground with spectroscopic-grade KBr in a ratio of 1:100) to collect DRIFT spectra using a Bruker Vertex 80V spectrometer (Bruker, Karlsruhe Germany). The spectra were recorded in the frequency region from 4000 to 600 cm^{-1} with the co-addition of 256 scans at a spectral resolution of 4 cm^{-1}. The sample chamber was evacuated prior to spectral acquisition to minimise atmospheric contributions from CO_2 and moisture (still two small CO_2 peaks remaining between 2500 and 2400 cm^{-1}). The peaks obtained from the spectra were assigned and fitted using a Gaussian function, with an expected error of 1-3%, to determine the relative proportions of various functional groups.

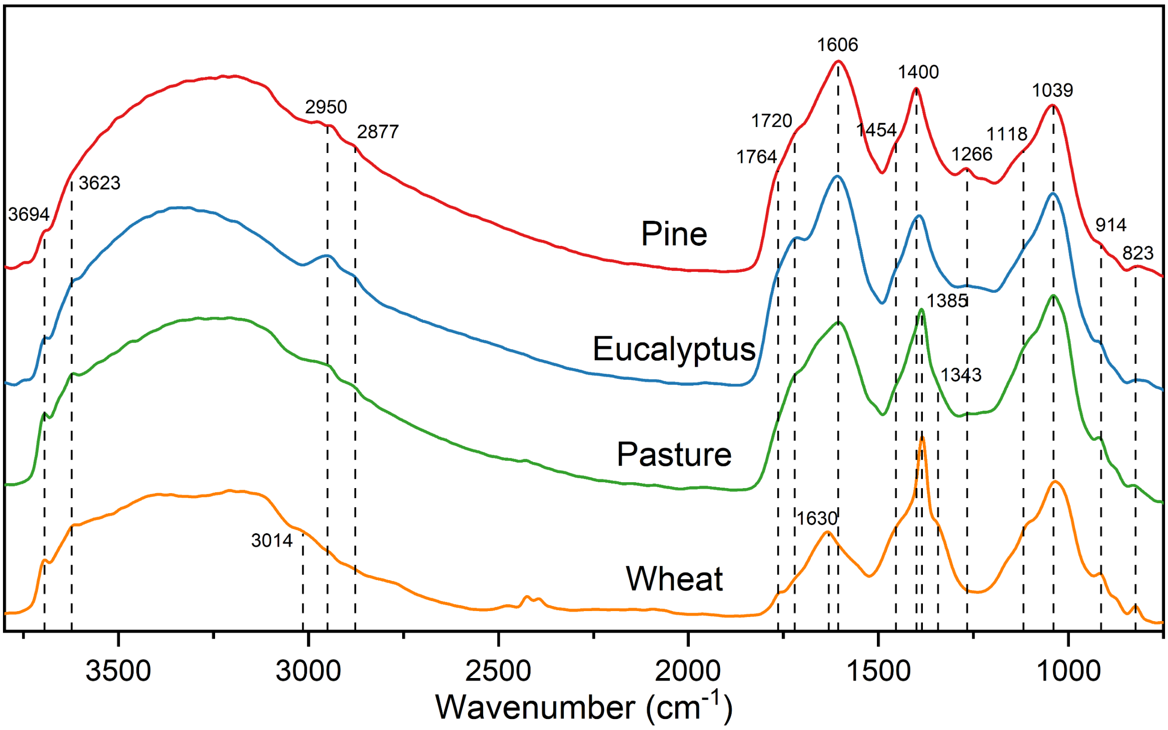

Figure S 4.2 The DRIFT spectra of DOM samples extracted from pine (PI), eucalypt (E), pasture (PA) and wheat (W) residues.

Table S 4.2 Assignment for band frequencies (cm^{-1}) for organic functional groups and their relative proportion in the four DOM samples from the FTIR analysis*.

Wavenumber (cm^{-1})	Functional Groups and Vibration	Organic Components	Pine	Eucalypt	Pasture	Wheat
3700-3100	O-H stretch; N-H stretch	Carboxylic acids, alcohols and phenols; amines and amides	43.4	36.7	40.1	44.8
2950	C-H asymmetric stretch	Alkyl groups (CH, CH_2, CH_3) in aliphatic structures	1.3	8.1	1.3	6.3*
2877	C-H symmetric stretch		0.3	0.3	0.1	
1764, 1720	C=O stretch	Carboxylates, amides, aldehydes, ketones and esters	6.1	6.9	3.4	2.0
1630, 1606	C=O stretch; C=C stretch	Carboxylates, amide I, quinones, ketones and olefins; Unsaturated aromatic structures	13.7	11.7	16.4	10.5
1454	C-H bend	Alkyl groups (CH, CH_2, CH_3) in aliphatic structure (e.g., polysaccharides) and phenolic lignin;	6.0	7.0	3.0	4.1
1400, 1385			3.5	4.9	5.9	6.3
1343			0.0	0.0	1.7	3.5
1266	C-O stretch; O-H bend	Phenolic-OH in aromatic structures and aryl methyl ethers; Carboxyl groups	12.7	8.9	8.7	4.1
1118	C-O-C stretch	Carbohydrates and polysaccharides in cellulose and hemicellulose	2.1	2.4	3.1	3.4
1039	C-O stretch	Polysaccharides or polysaccharide-like substances	9.2	11.0	12.9	11.2
914	O-H bend	Carboxylic acids	0.9	1.1	2.1	3.8
823	C-H bend	Carbohydrates and aromatic structures	0.8	0.9	1.3	0.1

*The asymmetric and symmetric stretching of C-H in wheat DOM shifted to 3014 cm^{-1}. Peak assignments were based on published studies (Chen et al., 2002; Solomon et al., 2005; Artz et al., 2008; Pedersen et al., 2011; Singh et al., 2016; Dhillon et al., 2017; Yeasmin et al., 2017).

NEXAFS analysis

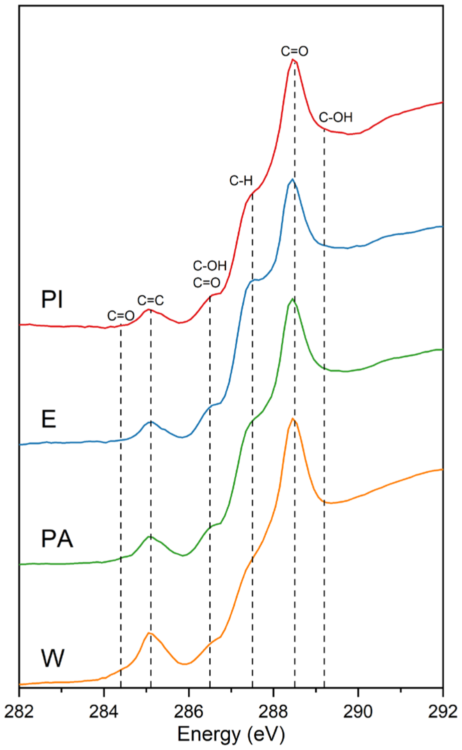

Figure S 4.3 The C-1s K-edge NEXAFS spectra of the DOM samples extracted from pine (PI), eucalypt (E), pasture (PA) and wheat (W) residues.

Table S 4.3 The photon energy positions, assigned functional groups, and their relative proportions within each peak region of the four DOM samples*.

Energy (eV)	OC Forms	OC Bonds	Transition	Pine	Eucalypt	Pasture	Wheat
283.0-284.5	Quinone C and aromatic C	C=O	1s-π*	1.6	5.6	6.6	6.4
284.9-285.5	Aromatic C and double-bonded alkyl C	C=C	1s-π*	5.2	4.6	5.3	9.3
286.0-287.4	Aromatic C with side chain and N-substituted aromatic C	C-OH C=O R-(C=O)-R’ C=N, C-N	1s-π*	1.9	2.6	2.5	0.8
287.0-287.8	Aliphatic C	C-H	1s-3ρ/σ*	28.8	33.3	31.4	34.4
288.0-288.7	Carboxylic C	R-COOH COO C=O	1s-π*	50.3	42.4	41.2	30.2
289.2-289.5	*O*-alkyl C	C-OH	1s-π* 1s-3ρ/σ*	12.2	11.5	13.0	18.9

*Peak assignments in the NEXAFS spectra were based on the published data (Lehmann et al., 2005; Solomon et al., 2005; Lehmann et al., 2009; Solomon et al., 2009; Singh et al., 2014; Prietzel et al., 2018).

4.6.2 Clay minerals properties

Table S 4.4 The specific surface area and pore characteristics and point of zero charge (PZC) of clay minerals used in this study.

Mineral	Kaolinite	Montmorillonite	Goethite	Birnessite	Ferrihydrite	Allophane
Specific Surface Area (m^2 g^{-1})	20.5	46.4	31.8	23.0	186.2	145.8
Point of Zero Charge (PZC)	< 3.0	negative	8.8	< 3.0	7.4	7.6

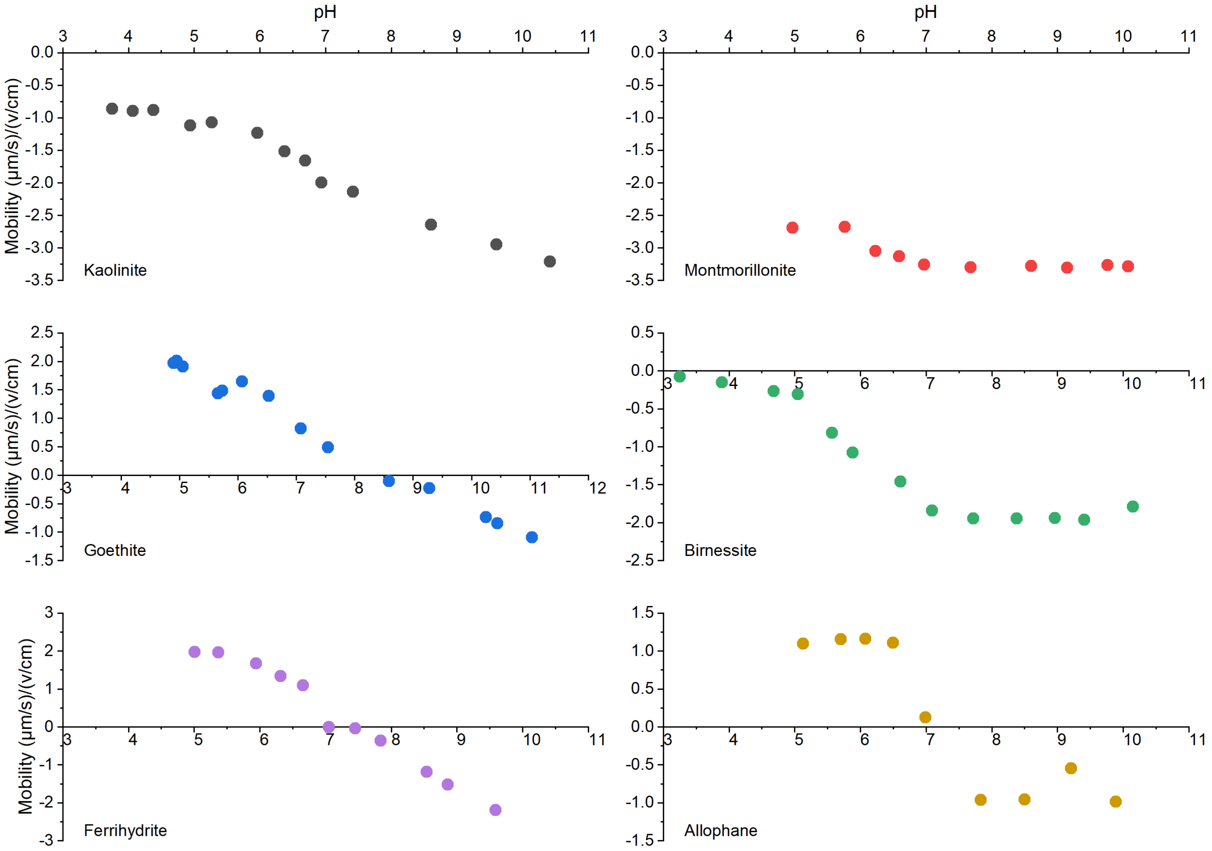

Figure S 4.4 Electrophoretic mobility ((µm s^{-1}) (v cm^{-1})$^{-1}$) of the six minerals as a function of pH measured in 0.1 M $NaNO_3$ solution.

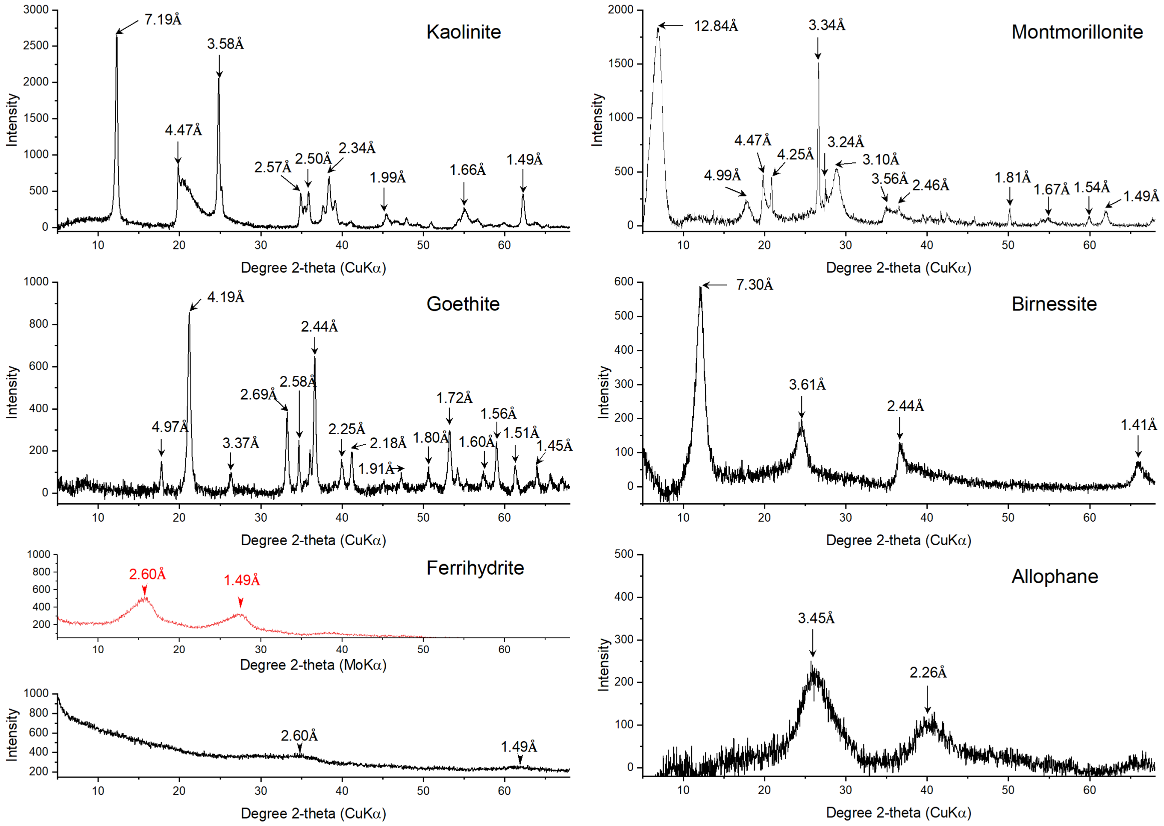

Figure S 4.5 Random powder X-ray diffraction patterns of the minerals used in the study.

4.6.3 Adsorption isotherm and mechanisms

The adsorption data of DOM were fitted to Langmuir and Freundlich equations (Eq.1 and Eq.2) (Gu et al., 1994; Azizian and Eris, 2021), respectively, to estimate the adsorption capacity:

$$Q_e = Q_{max} \frac{K_L C_e}{1 + K_L C_e} \qquad (Eq. 1)$$

$$Q_e = K_F C_e^n \qquad (Eq. 2)$$

in *Eq. 1*, where Q_e represents the equilibrium amount of adsorbed DOM (mg g^{-1}); Q_{max} represents the maximum amount of adsorbed DOM at equilibrium (mg g^{-1}); C_e represents the equilibrium concentration of OC (mg L^{-1}); K_L is a constant related to bonding energy (L g^{-1}). in *Eq.2*, where Q_e represents the equilibrium amount of adsorbed DOM (mg g^{-1}); K_F represent the number of adsorption sites ($mg^{1-n} \cdot L^n$ g^{-1}); C_e represents the equilibrium concentration of OC (mg L^{-1}); n represents the heterogeneity constants of the type of adsorption sites (L mg^{-1}) at which adsorption occurs (dimensionless).

The Akaike information criterion (AIC) was calculated to compare the quality of two isotherm model for the adsorption of DOM samples onto minerals.

Table S 4.5 The Langmuir and Freundlich isotherm model parameters (±SE) of the DOM adsorption onto minerals*.

DOM	Mineral	Langmuir Isotherm				Freundlich Isotherm			
		Q_{max}	K_L	R^2	AIC	K_F	n	R^2	AIC
Pine	Kaolinite	8.73±1.03	0.07±0.01	0.99	19.54	1.21±0.59	0.49±0.15	0.96	21.08
	Montmorillonite	7.01±2.73	0.02±0.01	0.91	37.01	0.17±0.15	1.32±0.39	0.99	19.86
	Goethite	17.67±2.07	0.13±0.05	0.78	31.46	4.37±0.23	0.34±0.02	0.87	11.61
	Birnessite	10.92±1.84	0.02±0.01	0.97	46.83	0.35±0.18	0.70±0.14	0.99	20.04
	Ferrihydrite	43.87±2.31	0.17±0.03	0.99	29.91	8.76±0.90	0.47±0.04	0.94	35.97
	Allophane	17.92±0.46	0.21±0.03	0.98	28.83	4.13±0.84	0.38±0.07	0.93	34.67
Eucalypt	Kaolinite	15.77±1.94	0.03±0.01	0.93	4.57	1.31±0.25	0.50±0.06	0.98	14.12
	Montmorillonite	14.40±3.03	0.02±0.01	0.98	16.86	0.56±0.21	0.68±0.11	0.99	15.31
	Goethite	20.69±1.11	0.06±0.02	0.96	18.78	2.13±0.49	0.54±0.07	0.99	21.99
	Birnessite	10.20±0.97	0.08±0.03	0.93	24.06	1.32±0.80	0.42±0.17	0.98	24.27
	Ferrihydrite	40.94±17.93	0.11±0.10	0.74	32.35	9.49±0.76	0.35±0.04	0.92	32.87
	Allophane	11.35±0.89	0.20±0.06	0.80	16.12	2.54±0.25	0.39±0.03	0.92	10.61
Pasture	Kaolinite	9.00±1.13	0.11±0.04	0.87	15.97	1.55±0.14	0.40±0.03	0.95	9.92
	Montmorillonite	9.55±1.33	0.04±0.01	0.97	12.72	0.47±0.14	0.70±0.09)	0.99	17.23
	Goethite	13.46±0.80	0.17±0.04	0.85	17.52	2.76±0.52	0.46±0.06	0.95	22.74
	Birnessite	10.93±6.05	0.02±0.02	0.88	8.86	0.82±0.25	0.46±0.09	0.97	14.32

	Ferrihydrite	28.19±1.85	0.44±0.07	0.80	30.21	10.10±0.98	0.36±0.05	0.94	38.09
	Allophane	21.39±4.22	0.13±0.05	0.96	38.18	2.68±0.91	0.58±0.13	0.99	39.49
Wheat	Kaolinite	7.25±0.88	0.04±0.01	0.95	1.19	0.53±0.12	0.59±0.07	0.99	9.19
	Montmorillonite	5.37±1.17	0.06±0.02	0.95	6.54	0.48±0.12	0.58±0.07	0.98	7.46
	Goethite	13.64±4.20	0.04±0.02	0.84	46.82	0.45±0.27	0.79±0.19	0.99	27.68
	Birnessite	7.96±1.22	0.02±0.01	0.92	0.73	0.49±0.12	0.56±0.07	0.97	5.69
	Ferrihydrite	34.61±7.02	0.10±0.04	0.90	35.70	4.87±1.04	0.49±0.07	0.97	38.89
	Allophane	14.23±1.21	0.11±0.02	0.89	28.92	1.73±0.67	0.52±0.13	0.97	33.14

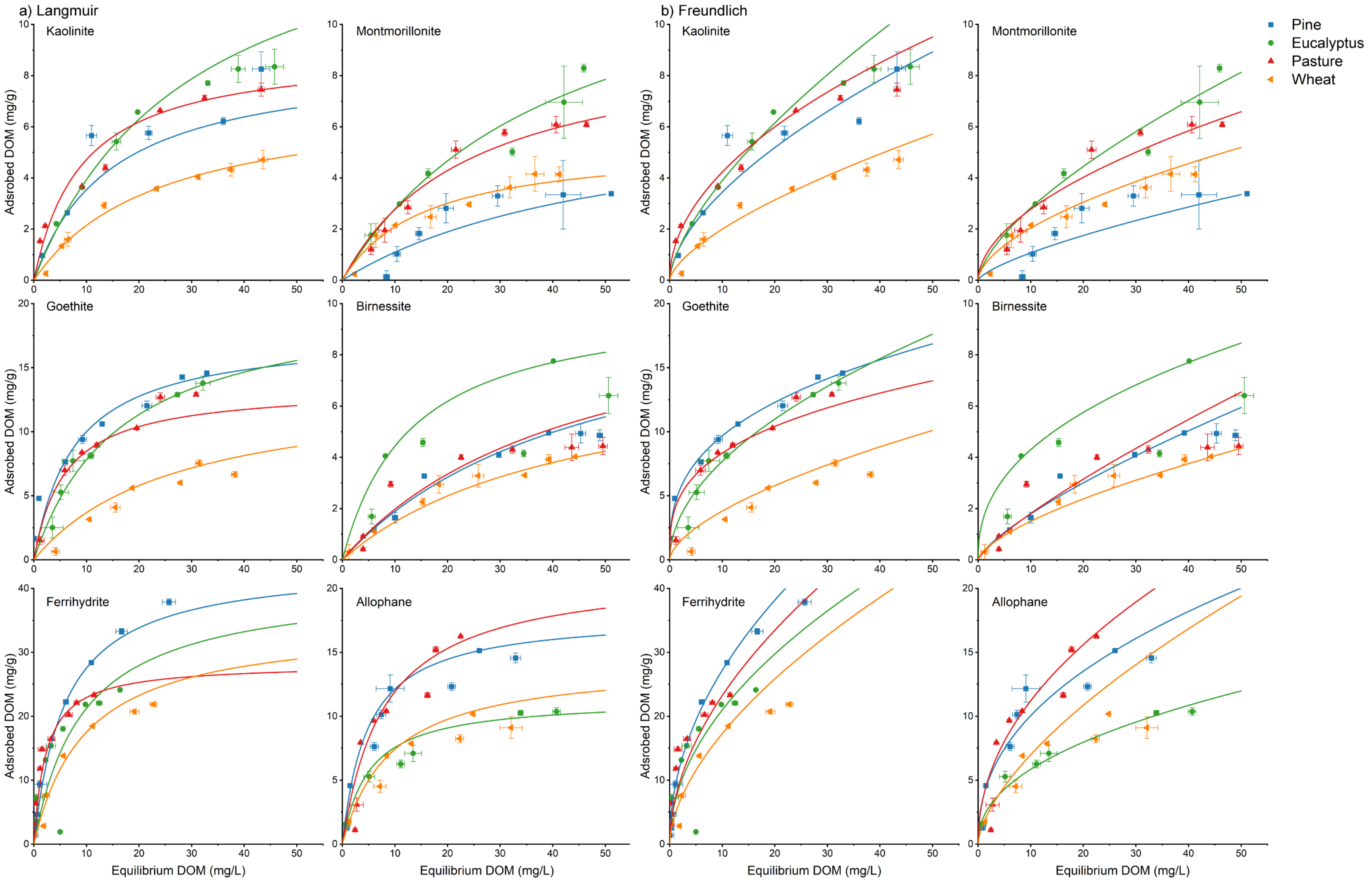

Figure S 4.6 Adsorption isotherm of the four DOM (i.e., pine, eucalypt, pasture and wheat) onto six minerals (i.e., kaolinite, montmorillonite, goethite, birnessite, ferrihydrite, and allophane).

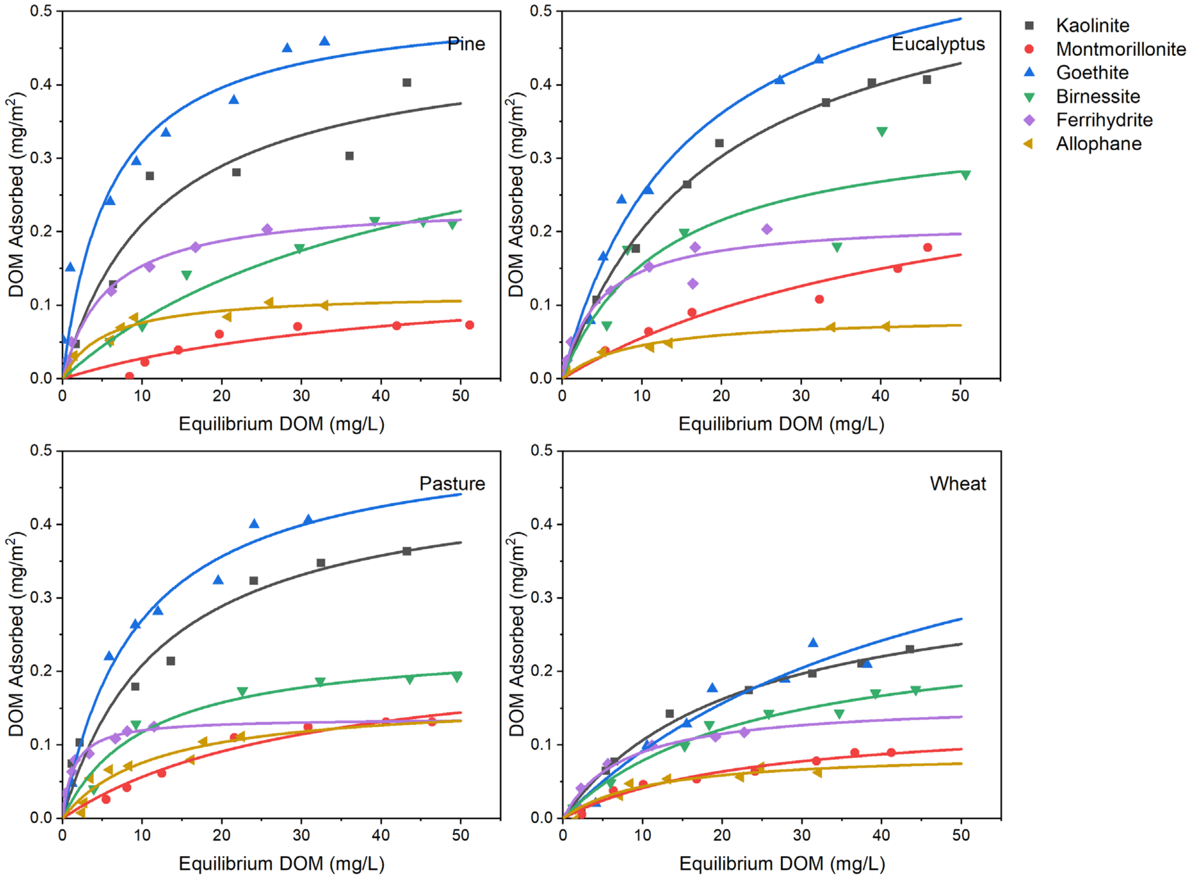

Figure S 4.7 Adsorption isotherm of the four DOM samples (extracted from pine, eucalypt, pasture and wheat) based on the specific surface area of six minerals (i.e., kaolinite, montmorillonite, goethite, birnessite, ferrihydrite, and allophane) fitted to the Langmuir isotherm model.

Table S 4.6 The maximum adsorption parameters (Q_{max}) (mg m^{-2}) from the Langmuir isotherm model, representing the amount of DOM adsorbed onto minerals, normalised by specific surface area.

DOM	Kaolinite	Montmorillonite	Goethite	Birnessite	Ferrihydrite	Allophane
Pine	0.47	0.15	0.52	0.42	0.24	0.12
Eucalypt	0.60	0.34	0.64	0.35	0.22	0.09
Pasture	0.47	0.24	0.52	0.24	0.14	0.17
Wheat	0.34	0.14	0.53	0.27	0.16	0.09

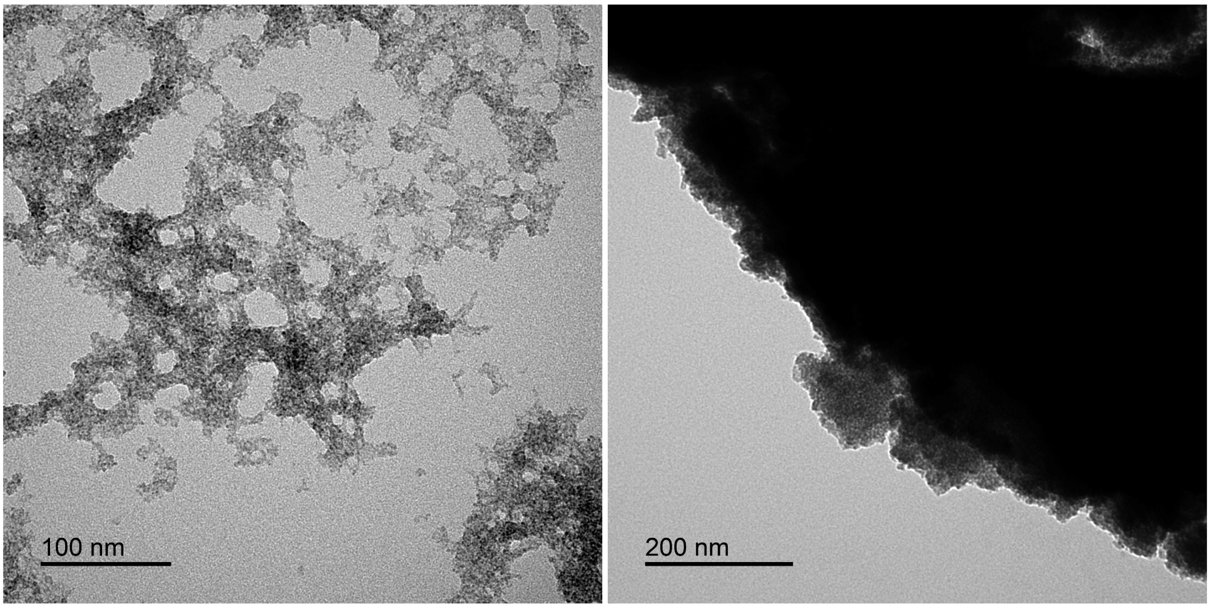

Figure S 4.8. The transmission electron microscopy (TEM) images of changes in the crystallinity of a poorly crystalline mineral (e.g., ferrihydrite) in suspension (Left) and after freeze-drying (Right).

4.6.4 Dynamic interactions of functional groups via 2D-FTIR-COS analysis

Table S 4.7 Results of 2D-FTIR-COS analysis for DOM adsorption on kaolinite, showing synchronous and asynchronous cross-peak signs and the corresponding sequence of spectral changes*.

Minerals	Spectral variables (v_1, v_2)	1717	1623	1600	1510	1455	1422	1385	1269	1142	1077	The sequences of spectral change
Kaolinite	1717	0 (0)	+ (+)	0 (0)	0 (0)	0 (0)	0 (0)	0 (0)	0 (0)	0 (0)	0 (0)	1717→1623
	1623		auto-peak	+ (+)	0 (-)	0 (0)	+ (+)	+ (+)	0 (-)	0 (-)	0 (-)	1623→1600,1510→1623, 1623→1422,1623→1385, 1269→1623,1142→1623, 1077→1623
	1600			auto-peak	0 (-)	0 (0)	+ (+)	+ (+)	0 (-)	0 (-)	0 (-)	1510→1600,1600→1422, 1600→1385,1269→1600, 1142→1600,1077→1600
	1510				0 (0)	0 (0)	0 (0)	0 (0)	0 (0)	0 (0)	0 (0)	
	1455					0 (0)	0 (0)	0 (0)	0 (0)	0 (0)	0 (0)	
	1422						0 (0)	0 (0)	0 (0)	0 (0)	0 (0)	
	1385							0 (0)	0 (0)	0 (0)	0 (0)	
	1269								0 (0)	0 (0)	0 (0)	
	1142									0 (0)	0 (0)	
	1077										0 (0)	
	1717,1510,1269,1142,1077→1623→1600→1422,1385 C=O, C=C, C-O/O-H, C-O-C, C-O→C=O→C=C/C=O→C-H											

*"0" represents no cross peak appears; the sign in "()" represents the results from synchronous (and asynchronous) spectra; "=" or "&" represents the peaks appeared simultaneously; "→" represents the sequential order of peaks appeared.

Table S 4.8 Results of 2D-FTIR-COS analysis for DOM adsorption on montmorillonite, showing synchronous and asynchronous cross-peak signs and the corresponding sequence of spectral changes*.

Minerals	Spectral variables (v_1, v_2)	1717	1598	1455	1418	1269	1116	1032	1014	915	The sequences of spectral change
Montmorillonite	1717	auto-peak	+ (+)	+ (+)	+ (+)	0 (+)	0 (0)	+ (+)	+ (+)	0 (0)	1717→1598,1717→1455 1717→1418,1717→1269 1717→1032,1717→1014
	1598		auto-peak	+ (+)	+ (+)	0 (-)	+ (-)	+ (-)	+ (-)	0 (0)	1598→1455,1598→1418, 1269→1598, 1116→1598,1032→1598, 1014→1598
	1455			auto-peak	+ (0)	0 (0)	+ (-)	+ (-)	+ (-)	0 (0)	1455=1418,1116→1455, 1032→1455,1014→1455
	1418				auto-peak	0 (0)	+ (-)	+ (-)	+ (-)	0 (0)	1116→1418,1032→1418 1014→1418
	1269					0 (0)	0 (0)	0 (0)	0 (0)	0 (0)	
	1116						auto-peak	+ (+)	+ (+)	0 (0)	1116→1032,1116→1014
	1032							auto-peak	+ (-)	0 (0)	1014→1032
	1014								auto-peak	0 (0)	
	915									0 (0)	
	1717→1116→1014→1269→1032→1598→1455=1418 C=O→C-O-C→C-O→C-O/O-H→C-O→C=C/C=O→C-H										

*"0" represents no cross peak appears; the sign in "()" represents the results from synchronous (and asynchronous) spectra; "=" or "&" represents the peaks appeared simultaneously; "→" represents the sequential order of peaks appeared.

Table S 4.9 Results of 2D-FTIR-COS analysis for DOM adsorption on goethite, showing synchronous and asynchronous cross-peak signs and the corresponding sequence of spectral changes*.

Minerals	Spectral variables (v_1, v_2)	1717	1589	1510	1418	1269	1129	1075	The sequences of spectral change
Goethite	1717	0 (0)	+ (-)	0 (0)	+ (-)	+ (0)	+ (-)	+ (-)	1589→1717,1418→1717, 1717=1269,1129→1717, 1075→1717
	1589		auto-peak	0 (+)	+ (-)	+ (+)	+ (-)	+ (-)	1589→1510,1418→1589, 1589→1269, 1129→1589, 1075→1589
	1510			auto-peak	0 (0)	0 (0)	0 (0)	0 (-)	1075→1510
	1418				auto-peak	0 (+)	+ (+)	+ (+)	1418→1269,1418→1129, 1418→1075
	1269					0 (0)	+ (-)	+ (-)	1129→1269,1075→1269
	1129						auto-peak	+ (+)	1129→1075
	1075							auto-peak	
	1418→1129→1075→1589→1717=1269,1510 C-H→C-O-C→C-O→C=C/C=O→C=O&C-O/O-H,C=C								

*"0" represents no cross peak appears; the sign in "()" represents the results from synchronous (and asynchronous) spectra; "=" or "&" represents the peaks appeared simultaneously; "→" represents the sequential order of peaks appeared.

Table S 4.10 Results of 2D-FTIR-COS analysis for DOM adsorption on birnessite, showing synchronous and asynchronous cross-peak signs and the corresponding sequence of spectral changes*.

Minerals	Spectral variables (v_1, v_2)	1700	1595	1418	1269	1081	1030	The sequences of spectral change
Birnessite	1700	auto-peak	+ (-)	- (-)	0 (0)	+ (+)	+ (+)	1595→1700,1418→1700, 1700→1081,1700→1030
	1595		auto-peak	+ (-)	0 (0)	+ (+)	+ (+)	1418→1595,1595→1081 1595→1030
	1418			0 (0)	0 (0)	0 (+)	0 (+)	1418→1081,1418→1030
	1269				0 (0)	0 (0)	0 (0)	
	1081					auto-peak	+ (0)	1081=1030
	1030						auto-peak	
	1418→1595→1700→1081=1030 C-H→C=C/C=O→C=O→C-O-C&C-O							

*"0" represents no cross peak appears; the sign in "()" represents the results from synchronous (and asynchronous) spectra; "=" or "&" represents the peaks appeared simultaneously; "→" represents the sequential order of peaks appeared.

Table S 4.11 Results of 2D-FTIR-COS analysis for DOM adsorption on ferrihydrite, showing synchronous and asynchronous cross-peak signs and the corresponding sequence of spectral changes*.

Minerals	Spectral variables (v_1, v_2)	1753	1592	1405	1269	1112	1063	The sequences of spectral change
Ferrihydrite	1753	0 (0)	0 (+)	0 (0)	0 (0)	0 (+)	0 (+)	1753→1592,1753→1112, 1753→1063
	1592		auto-peak	0 (-)	0 (-)	+ (-)	+ (+)	1405→1592,1269→1592, 1112→1592,1592→1063
	1405			0 (0)	0 (0)	0 (+)	0 (+)	1405→1112,1405→1063
	1269				0 (0)	0 (+)	0 (+)	1269→1112,1269→1063
	1112					0 (0)	+ (+)	1112→1063
	1063						auto-peak	
	1753,1405→1269→1112→1592→1063 C=O, C-H→C-O/O-H→C-O-C→C=C/C=O→C-O							

*“0” represents no cross peak appears; the sign in “()” represents the results from synchronous (and asynchronous) spectra; “=” or “&” represents the peaks appeared simultaneously; “→” represents the sequential order of peaks appeared.

Table S 4.12 Results of 2D-FTIR-COS analysis for DOM adsorption on allophane, showing synchronous and asynchronous cross-peak signs and the corresponding sequence of spectral changes*.

Minerals	Spectral variables (v_1, v_2)	1717	1595	1455	1410	1272	1129	1086	The sequences of spectral change
Allophane	1717	auto-peak	+ (+)	+ (+)	+ (+)	0 (0)	+ (0)	+ (+)	1717→1595,1717→1455, 1717→1410, 1717→1129, 1717→1086
	1595		auto-peak	+ (-)	+ (+)	0 (+)	+ (-)	+ (-)	1455→1595,1595→1410, 1595→1272,1129→1595 1086→1595
	1455			auto-peak	+ (+)	0 (0)	+ (-)	+ (-)	1455→1410,1129→1455, 1086→1455
	1410				auto-peak	0 (0)	+ (-)	+ (-)	1129→1410,1086→1410
	1272					0 (0)	0 (0)	0 (0)	
	1129						auto-peak	+ (0)	1129=1086
	1086							auto-peak	
	1717→1129=1086→1455→1595→1410,1272 C=O→C-O-C&C-O→C-H→C=C/C=O→C-H, C-O/O-H								

*"0" represents no cross peak appears; the sign in "()" represents the results from synchronous (and asynchronous) spectra; "=" or "&" represents the peaks appeared simultaneously; "→" represents the sequential order of peaks appeared.

4.6.5 Preferential adsorption of organic carbon compounds on minerals via NEXAFS spectroscopy

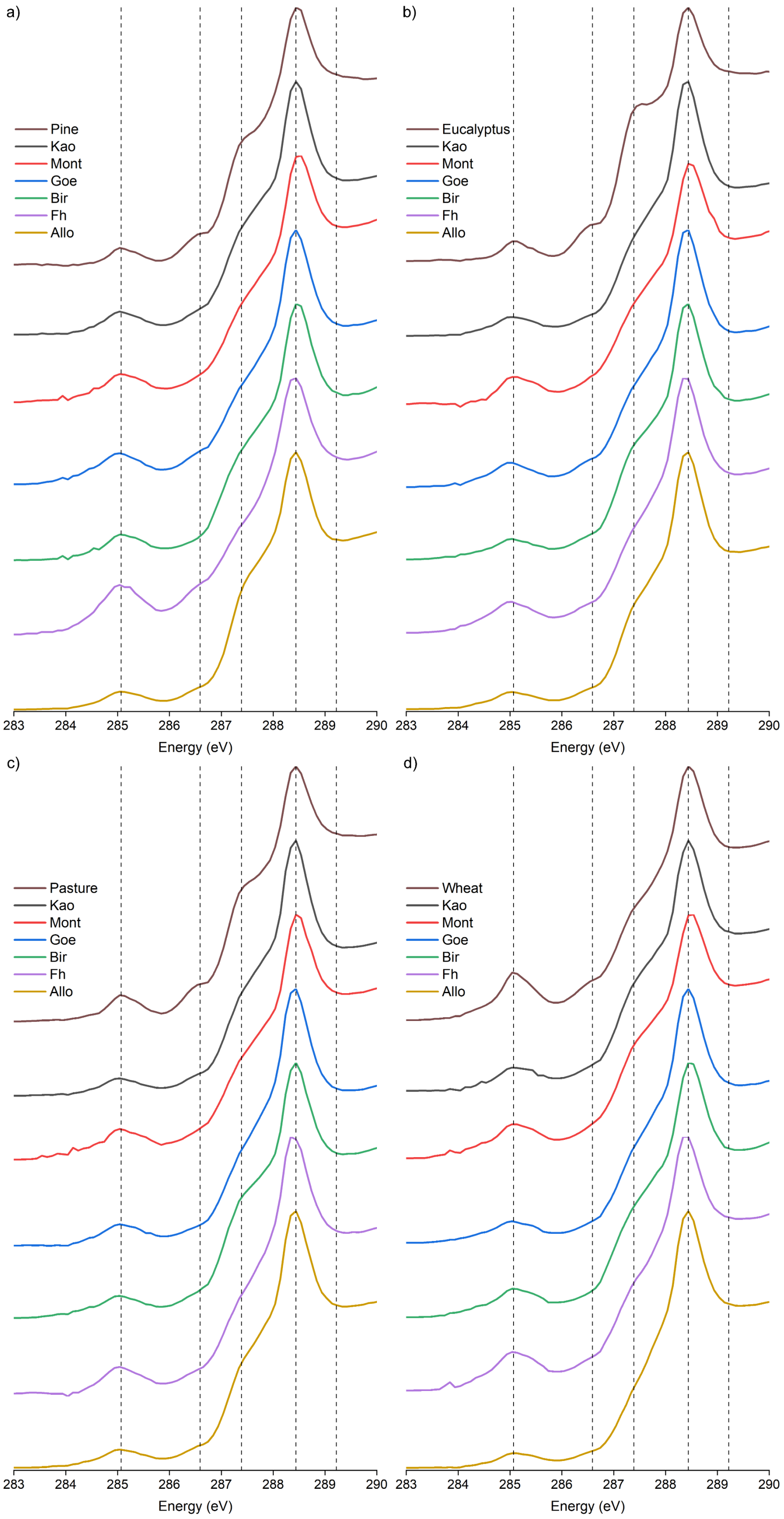

Figure S 4.9 The C-1s K-edge NEXAFS spectra of DOM extracted from pine (a), eucalypt (b), pasture (c) and wheat (d), adsorbed on different minerals after adsorption.

Table S 4.13 The assigned functional groups and their relative abundance (based on peak area using Gaussian function) in the NEXAFS spectra of original DOM and DOM adsorbed onto minerals.

Gaussian Peak	G1	G2	G3	G4	G5	G6
Peak Position	284.4	285.1	286.5	287.5	288.5	289.2
OC Groups	Quinone C	Aromatic C	Phenolic C	Aliphatic C	Carboxylic C	O-alkyl C
Pine						
Original DOM	1.6	5.2	1.9	28.8	50.3	12.2
Kaolinite	5.4	11.7	3.2	28.2	44.9	6.6
Montmorillonite	16.0	8.7	8.7	19.3	41.0	6.2
Goethite	5.3	11.3	3.4	27.0	42.9	10.0
Birnessite	3.2	7.8	5.5	26.6	48.3	8.5
Ferrihydrite	0.0	16.9	4.2	31.7	38.1	9.2
Allophane	0.0	8.4	1.3	30.0	52.4	8.0
Eucalypt						
Original DOM	5.6	4.6	2.6	33.3	42.4	11.5
Kaolinite	6.0	16.3	1.8	26.1	44.2	5.7
Montmorillonite	17.2	11.0	9.0	19.3	33.2	10.3
Goethite	2.1	11.2	3.0	29.9	41.1	12.7
Birnessite	3.8	11.5	2.0	31.9	39.6	11.2
Ferrihydrite	0.0	12.6	1.6	31.3	43.8	10.6
Allophane	0.0	12.1	2.0	29.7	44.6	11.6
Pasture						
Original DOM	6.6	5.3	2.5	31.4	41.2	13
Kaolinite	9.0	10.4	0.3	26.8	47.7	5.8
Montmorillonite	19.2	7.4	5.4	22.8	33.0	12.2
Goethite	3.4	10.6	1.5	27.4	46.2	10.8
Birnessite	7.2	8.3	3.1	31.7	38.2	11.6
Ferrihydrite	0.0	9.9	2.8	30.2	45.1	12.1
Allophane	1.9	10.1	1.8	28.2	46.9	11.1
Wheat						
Original DOM	6.4	9.3	0.8	34.4	30.2	18.9
Kaolinite	13.0	10.5	0.4	35.5	30.1	10.5
Montmorillonite	17.6	12.6	7.7	31.0	19.2	11.8
Goethite	5.6	8.2	3.0	36.5	28.4	18.3
Birnessite	5.1	6.8	10.2	37.1	24.1	16.7
Ferrihydrite	0.0	15.6	3.8	39.8	22.3	18.5
Allophane	0.0	7.9	3.0	32.4	35.9	20.8

References

Ahmed, N., Varadachari, C.,Ghosh, K., 2002. Soil clay-humus complexes. II. Bridging cations and DTA studies. *Soil Research 40*(4), 705-713.

Allard, S., Gutierrez, L., Fontaine, C., Croué, J.-P.,Gallard, H., 2017. Organic matter interactions with natural manganese oxide and synthetic birnessite. *Science of The Total Environment 583*, 487-495.

Amrhein, C.,Suarez, D.L., 1988. The use of a surface complexation model to describe the kinetics of ligand-promoted dissolution of anorthite. *Geochimica et Cosmochimica Acta 52*(12), 2785-2793.

Angst, G., Messinger, J., Greiner, M., Häusler, W., Hertel, D., Kirfel, K., Kögel-Knabner, I., Leuschner, C., Rethemeyer, J.,Mueller, C.W., 2018. Soil organic carbon stocks in topsoil and subsoil controlled by parent material, carbon input in the rhizosphere, and microbial-derived compounds. *Soil Biology and Biochemistry 122*, 19-30.

Arnarson, T.S.,Keil, R.G., 2000. Mechanisms of pore water organic matter adsorption to montmorillonite. *Marine Chemistry 71*(3), 309-320.

Artz, R.R.E., Chapman, S.J., Jean Robertson, A.H., Potts, J.M., Laggoun-Défarge, F., Gogo, S., Comont, L., Disnar, J.-R.,Francez, A.-J., 2008. FTIR spectroscopy can be used as a screening tool for organic matter quality in regenerating cutover peatlands. *Soil Biology and Biochemistry 40*(2), 515-527.

Avneri-Katz, S., Young, R.B., McKenna, A.M., Chen, H., Corilo, Y.E., Polubesova, T., Borch, T.,Chefetz, B., 2017. Adsorptive fractionation of dissolved organic matter (DOM) by mineral soil: macroscale approach and molecular insight. *Organic Geochemistry 103*, 113-124.

Azimzadeh, B.,Martínez, C.E., 2025. Dynamic sorption and interfacial assembly of polysaccharide on hydrophobic vs hydrophilic surfaces. *ACS Earth and Space Chemistry 9*(5), 1030-1042.

Azizian, S.,Eris, S., 2021. Chapter 6 - Adsorption isotherms and kinetics. In: M. Ghaedi (Ed.), *Interface Science and Technology.* Elsevier, pp. 445-509.

Begill, N., Don, A.,Poeplau, C., 2023. No detectable upper limit of mineral-associated organic carbon in temperate agricultural soils. *Global Change Biology 29*(16), 4662-4669.

Boily, J.-F.,Song, X., 2020. Direct identification of reaction sites on ferrihydrite. *Communications Chemistry 3*(1), 79.

Bramble, D.S.E., Schöning, I., Brandt, L., Poll, C., Kandeler, E., Ulrich, S., Mikutta, R., Mikutta, C., Silver, W.L., Totsche, K.U., Kaiser, K.,Schrumpf, M., 2025. Land use and mineral type determine stability of newly formed mineral-associated organic matter. *Communications Earth & Environment 6*(1), 415.

Calvelo Pereira, R., Camps Arbestain, M., Kelliher, F.M., Theng, B.K.G., McNally, S.R., Macías, F.,Guitián, F., 2019. Assessing the pore structure and surface area of allophane-rich and non-allophanic topsoils by supercritical drying and chemical treatment. *Geoderma 337*, 805-811.

Chassé, A.W., Ohno, T., Higgins, S.R., Amirbahman, A., Yildirim, N.,Parr, T.B., 2015. Chemical force spectroscopy evidence supporting the layer-by-layer model of organic matter binding to iron (oxy)hydroxide mineral surfaces. *Environmental Science &*

Technology 49(16), 9733-9741.

Chen, C., Dynes, J.J., Wang, J.,Sparks, D.L., 2014. Properties of Fe-organic matter associations via coprecipitation versus adsorption. *Environmental Science & Technology 48*(23), 13751-13759.

Chen, H., Li, Q., Wang, M., Ji, D.,Tan, W., 2020. XPS and two-dimensional FTIR correlation analysis on the binding characteristics of humic acid onto kaolinite surface. *Science of The Total Environment 724*, 138154.

Chen, J., Gu, B., LeBoeuf, E.J., Pan, H.,Dai, S., 2002. Spectroscopic characterization of the structural and functional properties of natural organic matter fractions. *Chemosphere 48*(1), 59-68.

Chen, S., Klotzbücher, T., Lechtenfeld, O.J., Hong, H., Liu, C., Kaiser, K., Mikutta, C.,Mikutta, R., 2022. Legacy effects of sorption determine the formation efficiency of mineral-associated soil organic matter. *Environmental Science & Technology 56*(3), 2044-2053.

Chevallier, T., Woignier, T., Toucet, J.,Blanchart, E., 2010. Organic carbon stabilization in the fractal pore structure of Andosols. *Geoderma 159*(1), 182-188.

Chorover, J.,Amistadi, M.K., 2001. Reaction of forest floor organic matter at goethite, birnessite and smectite surfaces. *Geochimica et Cosmochimica Acta 65*(1), 95-109.

Coward, E.K., Ohno, T.,Sparks, D.L., 2019. Direct evidence for temporal molecular fractionation of dissolved organic matter at the iron oxyhydroxide interface. *Environmental Science & Technology 53*(2), 642-650.

Curti, L., Moore, O.W., Babakhani, P., Xiao, K.-Q., Woulds, C., Bray, A.W., Fisher, B.J., Kazemian, M., Kaulich, B.,Peacock, C.L., 2021. Carboxyl-richness controls organic carbon preservation during coprecipitation with iron (oxyhydr)oxides in the natural environment. *Communications Earth & Environment 2*(1), 229.

Dhillon, G.S., Gillespie, A., Peak, D.,Van Rees, K.C.J., 2017. Spectroscopic investigation of soil organic matter composition for shelterbelt agroforestry systems. *Geoderma 298*, 1-13.

Ding, Y., Lu, Y., Liao, P., Peng, S., Liang, Y., Lin, Z., Dang, Z.,Shi, Z., 2019. Molecular fractionation and sub-nanoscale distribution of dissolved organic matter on allophane. *Environmental Science: Nano 6*(7), 2037-2048.

Ding, Z., Ding, Y., Liu, F., Yang, J., Li, R., Dang, Z.,Shi, Z., 2022. Coupled sorption and oxidation of soil dissolved organic matter on manganese oxides: nano/sub-nanoscale distribution and molecular transformation. *Environmental Science & Technology 56*(4), 2783-2793.

Ding, Z., Hu, S., Zhu, L., Xiao, J., Ye, Q., Liu, T.,Shi, Z., 2024. Multiple effects of iron oxides on the adsorption and oxidation of dissolved organic matter by manganese oxides. *Geochimica et Cosmochimica Acta 384*, 213-227.

Eusterhues, K., Rennert, T., Knicker, H., Kögel-Knabner, I., Totsche, K.U.,Schwertmann, U., 2011. Fractionation of organic matter due to reaction with ferrihydrite: coprecipitation versus adsorption. *Environmental Science & Technology 45*(2), 527-533.

Filimonova, S., Kaufhold, S., Wagner, F.E., Häusler, W.,Kögel-Knabner, I., 2016. The role of allophane nano-structure and Fe oxide speciation for hosting soil organic matter in an allophanic Andosol. *Geochimica et Cosmochimica Acta 180*, 284-302.

Friedlingstein, P., O'Sullivan, M., Jones, M.W., Andrew, R.M., Hauck, J., Landschützer, P., Le Quéré, C., Li, H., Luijkx, I.T., Olsen, A., Peters, G.P., Peters, W., Pongratz, J., Schwingshackl, C., Sitch, S., Canadell, J.G., Ciais, P., Jackson, R.B., Alin, S.R., Arneth, A., Arora, V., Bates, N.R., Becker, M., Bellouin, N., Berghoff, C.F., Bittig, H.C., Bopp, L., Cadule, P., Campbell, K., Chamberlain, M.A., Chandra, N., Chevallier, F., Chini, L.P., Colligan, T., Decayeux, J., Djeutchouang, L.M., Dou, X., Duran Rojas, C., Enyo, K., Evans, W., Fay, A.R., Feely, R.A., Ford, D.J., Foster, A., Gasser, T., Gehlen, M., Gkritzalis, T., Grassi, G., Gregor, L., Gruber, N., Gürses, Ö., Harris, I., Hefner, M., Heinke, J., Hurtt, G.C., Iida, Y., Ilyina, T., Jacobson, A.R., Jain, A.K., Jarníková, T., Jersild, A., Jiang, F., Jin, Z., Kato, E., Keeling, R.F., Klein Goldewijk, K., Knauer, J., Korsbakken, J.I., Lan, X., Lauvset, S.K., Lefèvre, N., Liu, Z., Liu, J., Ma, L., Maksyutov, S., Marland, G., Mayot, N., McGuire, P.C., Metzl, N., Monacci, N.M., Morgan, E.J., Nakaoka, S.I., Neill, C., Niwa, Y., Nützel, T., Olivier, L., Ono, T., Palmer, P.I., Pierrot, D., Qin, Z., Resplandy, L., Roobaert, A., Rosan, T.M., Rödenbeck, C., Schwinger, J., Smallman, T.L., Smith, S.M., Sospedra-Alfonso, R., Steinhoff, T., Sun, Q., Sutton, A.J., Séférian, R., Takao, S., Tatebe, H., Tian, H., Tilbrook, B., Torres, O., Tourigny, E., Tsujino, H., Tubiello, F., van der Werf, G., Wanninkhof, R., Wang, X., Yang, D., Yang, X., Yu, Z., Yuan, W., Yue, X., Zaehle, S., Zeng, N.,Zeng, J., 2025. Global carbon budget 2024. *Earth Syst. Sci. Data 17*(3), 965-1039.

Gann, E., McNeill, C.R., Tadich, A., Cowie, B.C.C.,Thomsen, L., 2016. Quick AS NEXAFS Tool (QANT): a program for NEXAFS loading and analysis developed at the Australian Synchrotron. *Journal of Synchrotron Radiation 23*(1), 374-380.

Gao, J., Mikutta, R., Jansen, B., Guggenberger, G., Vogel, C.,Kalbitz, K., 2020. The multilayer model of soil mineral–organic interfaces—a review. *Journal of Plant Nutrition and Soil Science 183*(1), 27-41.

Georgiou, K., Jackson, R.B., Vindušková, O., Abramoff, R.Z., Ahlström, A., Feng, W., Harden, J.W., Pellegrini, A.F.A., Polley, H.W., Soong, J.L., Riley, W.J.,Torn, M.S., 2022. Global stocks and capacity of mineral-associated soil organic carbon. *Nature Communications 13*(1), 3797.

Ghosh, S., Wang, Z.-Y., Kang, S., Bhowmik, P.C.,Xing, B.S., 2009. Sorption and fractionation of a peat derived humic acid by kaolinite, montmorillonite, and goethite. *Pedosphere 19*(1), 21-30.

Gu, B., Schmitt, J., Chen, Z., Liang, L.,McCarthy, J.F., 1994. Adsorption and desorption of natural organic matter on iron oxide: mechanisms and models. *Environmental Science & Technology 28*(1), 38-46.

Gu, X., Wu, W., Lin, D.,Yang, K., 2022. Adsorption of soil organic matter by gel-like ferrihydrite and dense ferrihydrite. *Science of The Total Environment 835*, 155507.

Guggenberger, G.,Kaiser, K., 2003. Dissolved organic matter in soil: challenging the paradigm of sorptive preservation. *Geoderma 113*(3), 293-310.

Guo, Z., Wang, Y., Wan, Z., Zuo, Y., He, L., Li, D., Yuan, F., Wang, N., Liu, J., Song, Y., Song, C.,Xu, X., 2020. Soil dissolved organic carbon in terrestrial ecosystems: Global budget, spatial distribution and controls. *Global Ecology and Biogeography 29*(12), 2159-2175.

Hall, S.J., Berhe, A.A.,Thompson, A., 2018. Order from disorder: do soil organic matter composition and turnover co-vary with iron phase crystallinity? *Biogeochemistry 140*(1), 93-110.

Han, L., Yang, Y., Sun, K., Zhang, B., Chen, Y., Fang, L.,Xing, B., 2021. Different mechanisms driving the preferential adsorption of dissolved organic matter by goethite and montmorillonite. *Chemical Geology 585*, 120560.

Hemingway, J.D., Rothman, D.H., Grant, K.E., Rosengard, S.Z., Eglinton, T.I., Derry, L.A.,Galy, V.V., 2019. Mineral protection regulates long-term global preservation of natural organic carbon. *Nature 570*(7760), 228-231.

Hiemstra, T.,Zhao, W., 2016. Reactivity of ferrihydrite and ferritin in relation to surface structure, size, and nanoparticle formation studied for phosphate and arsenate. *Environmental Science: Nano 3*(6), 1265-1279.

Hu, Z., McKenna, A.M., Wen, K., Zhang, B., Mao, H., Goual, L., Feng, X.,Zhu, M., 2024. Controls of mineral solubility on adsorption-induced molecular fractionation of dissolved organic matter revealed by 21 T FT-ICR MS. *Environmental Science & Technology 58*(5), 2313-2322.

Jia, N., Li, L., Guo, H.,Xie, M., 2024. Important role of Fe oxides in global soil carbon stabilization and stocks. *Nature Communications 15*(1), 10318.

Johnson, K., Purvis, G., Lopez-Capel, E., Peacock, C., Gray, N., Wagner, T., März, C., Bowen, L., Ojeda, J., Finlay, N., Robertson, S., Worrall, F.,Greenwell, C., 2015. Towards a mechanistic understanding of carbon stabilization in manganese oxides. *Nature Communications 6*(1), 7628.

Johnson, S.B., Yoon, T.H., Kocar, B.D.,Brown, G.E., 2004. Adsorption of organic matter at mineral/water interfaces. 2. outer-sphere adsorption of maleate and implications for dissolution processes. *Langmuir 20*(12), 4996-5006.

Kaiser, K.,Guggenberger, G., 2000. The role of DOM sorption to mineral surfaces in the preservation of organic matter in soils. *Organic Geochemistry 31*(7), 711-725.

Kaiser, K.,Guggenberger, G., 2003. Mineral surfaces and soil organic matter. *European Journal of Soil Science 54*(2), 219-236.

Kaiser, M., Zederer, D.P., Ellerbrock, R.H., Sommer, M.,Ludwig, B., 2016. Effects of mineral characteristics on content, composition, and stability of organic matter fractions separated from seven forest topsoils of different pedogenesis. *Geoderma 263*, 1-7.

Keiluweit, M.,Kleber, M., 2009. Molecular-level interactions in soils and sediments: the role of aromatic π-systems. *Environmental Science & Technology 43*(10), 3421-3429.

Kleber, M., Bourg, I.C., Coward, E.K., Hansel, C.M., Myneni, S.C.B.,Nunan, N., 2021. Dynamic interactions at the mineral–organic matter interface. *Nature Reviews Earth & Environment 2*(6), 402-421.

Kleber, M., Eusterhues, K., Keiluweit, M., Mikutta, C., Mikutta, R.,Nico, P.S., 2015. Chapter one - Mineral–organic associations: formation, properties, and relevance in soil environments. In: D. L. Sparks (Ed.), *Advances in Agronomy.* Academic Press, pp. 1-140.

Kleber, M., Sollins, P.,Sutton, R., 2007. A conceptual model of organo-mineral interactions in soils: self-assembly of organic molecular fragments into zonal structures on mineral surfaces. *Biogeochemistry 85*(1), 9-24.

Kögel-Knabner, I., Guggenberger, G., Kleber, M., Kandeler, E., Kalbitz, K., Scheu, S., Eusterhues, K.,Leinweber, P., 2008. Organo-mineral associations in temperate soils: integrating biology, mineralogy, and organic matter chemistry. *Journal of Plant Nutrition and Soil Science 171*(1), 61-82.

Kramer, M.G.,Chadwick, O.A., 2018. Climate-driven thresholds in reactive mineral retention of soil carbon at the global scale. *Nature Climate Change 8*(12), 1104-1108.

Kretzschmar, R., Sticher, H.,Hesterberg, D., 1997. Effects of adsorbed humic acid on surface charge and flocculation of kaolinite. *Soil Science Society of America Journal 61*(1), 101-108.

Kubicki, J.D., Schroeter, L.M., Itoh, M.J., Nguyen, B.N.,Apitz, S.E., 1999. Attenuated total reflectance Fourier-transform infrared spectroscopy of carboxylic acids adsorbed onto mineral surfaces. *Geochimica et Cosmochimica Acta 63*(18), 2709-2725.

Lehmann, J., Liang, B., Solomon, D., Lerotic, M., Luizão, F., Kinyangi, J., Schäfer, T., Wirick, S.,Jacobsen, C., 2005. Near-edge X-ray absorption fine structure (NEXAFS) spectroscopy for mapping nano-scale distribution of organic carbon forms in soil: application to black carbon particles. *Global Biogeochemical Cycles 19*(1).

Lehmann, J., Solomon, D., Brandes, J., Fleckenstein, H., Jacobson, C.,Thieme, J., 2009. Synchrotron-based near-edge X-ray spectroscopy of natural organic matter in soils and sediments. In: *Biophysico-Chemical Processes Involving Natural Nonliving Organic Matter in Environmental Systems.* pp. 729-781.

Lenhardt, K.R., Breitzke, H., Buntkowsky, G., Mikutta, C.,Rennert, T., 2022. Interactions of dissolved organic matter with short-range ordered aluminosilicates by adsorption and co-precipitation. *Geoderma 423*, 115960.

Li, H., Santos, F., Butler, K.,Herndon, E., 2021. A critical review on the multiple roles of manganese in stabilizing and destabilizing soil organic matter. *Environmental Science & Technology 55*(18), 12136-12152.

Li, Y., Gong, X., Sun, Y., Shu, Y., Niu, D.,Ye, H., 2022a. High molecular weight fractions of dissolved organic matter (DOM) determined the adsorption and electron transfer capacity of DOM on iron minerals. *Chemical Geology 604*, 120907.

Li, Y., Koopal, L.K., Tan, W., Chai, Y., Chen, Y., Wu, C.,Tang, X., 2022b. Effect of humic acid on lysozyme interaction with montmorillonite and kaolinite. *Science of the Total Environment 834*, 155370.

Lin, C., Dong, B.,Xu, Z., 2025. Microscopic mechanism of organic carbon sequestration and redox properties influenced by iron (Oxyhydr)oxides. *Water Research 275*, 123220.

Liu, X., Lu, X., Sprik, M., Cheng, J., Meijer, E.J.,Wang, R., 2013. Acidity of edge surface sites of montmorillonite and kaolinite. *Geochimica et Cosmochimica Acta 117*, 180-190.

Lombardi, K.C., Mangrich, A.S., Wypych, F., Rodrigues-Filho, U.P., Guimarães, J.L.,Schreiner, W.H., 2006. Sequestered carbon on clay mineral probed by electron paramagnetic resonance and X-ray photoelectron spectroscopy. *Journal of Colloid and Interface Science 295*(1), 135-140.

Lützow, M.v., Kögel-Knabner, I., Ekschmitt, K., Matzner, E., Guggenberger, G., Marschner, B.,Flessa, H., 2006. Stabilization of organic matter in temperate soils: mechanisms and their relevance under different soil conditions – a review. *European Journal of Soil Science 57*(4), 426-445.

Lv, J., Zhang, S., Wang, S., Luo, L., Cao, D.,Christie, P., 2016. Molecular-scale investigation with ESI-FT-ICR-MS on fractionation of dissolved organic matter induced by adsorption on iron oxyhydroxides. *Environmental Science & Technology 50*(5), 2328-2336.

Ma, D., Wu, J., Yang, P.,Zhu, M., 2020. Coupled manganese redox cycling and organic carbon degradation on mineral surfaces. *Environmental Science & Technology 54*(14), 8801-8810.

Marschner, B.,Kalbitz, K., 2003. Controls of bioavailability and biodegradability of dissolved organic matter in soils. *Geoderma 113*(3), 211-235.

McKenzie, R.M., 1971. The synthesis of birnessite, cryptomelane, and some other oxides and hydroxides of manganese. *Mineralogical Magazine 38*(296), 493-502.

Mikutta, C., Lang, F.,Kaupenjohann, M., 2004. Soil organic matter clogs mineral pores. *Soil Science Society of America Journal 68*(6), 1853-1862.

Mitchell, P.J., Simpson, A.J., Soong, R.,Simpson, M.J., 2018. Nuclear magnetic resonance analysis of changes in dissolved organic matter composition with successive layering on clay mineral surfaces. *Soil Systems 2*(1), 8.

Nebbioso, A.,Piccolo, A., 2013. Molecular characterization of dissolved organic matter (DOM): a critical review. *Analytical and Bioanalytical Chemistry 405*(1), 109-124.

Noda, I.,Ozaki, Y. (2004). *Two-dimensional correlation spectroscopy - applications in vibrational and optical spectroscopy*: John Wiley & Sons, Ltd.

Norén, K.,Persson, P., 2007. Adsorption of monocarboxylates at the water/goethite interface: the importance of hydrogen bonding. *Geochimica et Cosmochimica Acta 71*(23), 5717-5730.

Ohashi, F., Wada, S.I., Suzuki, M., Maeda, M.,Tomura, S., 2002. Synthetic allophane from highconcentration solutions: nanoengineering of the porous solid. *Clay Minerals 37*(3), 451-456.

Osei, B.A.,Singh, B., 1999. Electrophoretic mobility of some tropical soil clays: effect of iron oxides and organic matter. *Geoderma 93*(3), 325-334.

Pedersen, J.A., Simpson, M.A., Bockheim, J.G.,Kumar, K., 2011. Characterization of soil organic carbon in drained thaw-lake basins of Arctic Alaska using NMR and FTIR photoacoustic spectroscopy. *Organic Geochemistry 42*(8), 947-954.

Possinger, A.R., Zachman, M.J., Enders, A., Levin, B.D.A., Muller, D.A., Kourkoutis, L.F.,Lehmann, J., 2020. Organo–organic and organo–mineral interfaces in soil at the nanometer scale. *Nature Communications 11*(1), 6103.

Prietzel, J., Müller, S., Kögel-Knabner, I., Thieme, J., Jaye, C.,Fischer, D., 2018. Comparison of soil organic carbon speciation using C NEXAFS and CPMAS 13C NMR spectroscopy. *Science of The Total Environment 628-629*, 906-918.

Reardon, P.N., Walter, E.D., Marean-Reardon, C.L., Lawrence, C.W., Kleber, M.,Washton, N.M., 2018. Carbohydrates protect protein against abiotic fragmentation by soil minerals. *Scientific Reports 8*(1), 813.

Ruiz, F., Barreto, M.S.C., Rumpel, C., Nóbrega, G.N., Oliveira, H.A., Menandro, A.S., Péres, L.O., Montes, C.R.,Ferreira, T.O., 2024. Adsorption and thermal stability of dissolved organic matter on Ca- and Mg-exchanged montmorillonite: Implications for persistence in soils and sediments. *Chemical Geology 643*, 121813.

Sanderman, J., Maddern, T.,Baldock, J., 2014. Similar composition but differential stability of mineral retained organic matter across four classes of clay minerals. *Biogeochemistry 121*(2), 409-424.

Schwertmann, U.,Cornell, R.M. (2000). *Iron Oxides In The Laboratory: Preparation And Characterization*: WILEY-VCH Verlag GmbH.

Singh, B., Fang, Y., Cowie, B.C.C.,Thomsen, L., 2014. NEXAFS and XPS characterisation of carbon functional groups of fresh and aged biochars. *Organic Geochemistry 77*, 1-10.

Singh, B., Fang, Y.,Johnston, C.T., 2016. A Fourier-transform infrared study of biochar aging in soils. *Soil Science Society of America Journal 80*(3), 613-622.

Sokol, N.W., Sanderman, J.,Bradford, M.A., 2019. Pathways of mineral-associated soil organic matter formation: integrating the role of plant carbon source, chemistry, and point of entry. *Global Change Biology 25*(1), 12-24.

Solomon, D., Lehmann, J., Kinyangi, J., Liang, B., Heymann, K., Dathe, L., Hanley, K., Wirick, S.,Jacobsen, C., 2009. Carbon (1s) NEXAFS spectroscopy of biogeochemically relevant reference organic compounds. *Soil Science Society of America Journal 73*(6), 1817-1830.

Solomon, D., Lehmann, J., Kinyangi, J., Liang, B.,Schäfer, T., 2005. Carbon K-edge NEXAFS and FTIR-ATR spectroscopic investigation of organic carbon speciation in soils. *Soil Science Society of America Journal 69*(1), 107-119.

Sowers, T.D., Holden, K.L., Coward, E.K.,Sparks, D.L., 2019. Dissolved organic matter sorption and molecular fractionation by naturally occurring bacteriogenic iron (oxyhydr)oxides. *Environmental Science & Technology 53*(8), 4295-4304.

Spielvogel, S., Prietzel, J.,Kögel-Knabner, I., 2008. Soil organic matter stabilization in acidic forest soils is preferential and soil type-specific. *European Journal of Soil Science 59*(4), 674-692.

Tao, F., Huang, Y., Hungate, B.A., Manzoni, S., Frey, S.D., Schmidt, M.W.I., Reichstein, M., Carvalhais, N., Ciais, P., Jiang, L., Lehmann, J., Wang, Y.-P., Houlton, B.Z., Ahrens, B., Mishra, U., Hugelius, G., Hocking, T.D., Lu, X., Shi, Z., Viatkin, K., Vargas, R., Yigini, Y., Omuto, C., Malik, A.A., Peralta, G., Cuevas-Corona, R., Di Paolo, L.E., Luotto, I., Liao, C., Liang, Y.-S., Saynes, V.S., Huang, X.,Luo, Y., 2023. Microbial carbon use efficiency promotes global soil carbon storage. *Nature 618*(7967), 981-985.

Theng, B.K.G., 2012. Chapter 4 - Negatively charged polymers (polyanions). In: B. K. G. Theng (Ed.), *Developments in Clay Science.* Elsevier, pp. 111-127.

Tombácz, E., Libor, Z., Illés, E., Majzik, A.,Klumpp, E., 2004. The role of reactive surface sites and complexation by humic acids in the interaction of clay mineral and iron oxide particles. *Organic Geochemistry 35*(3), 257-267.

Tombácz, E.,Szekeres, M., 2006. Surface charge heterogeneity of kaolinite in aqueous suspension in comparison with montmorillonite. *Applied Clay Science 34*(1), 105-124.

Underwood, T.R., Bourg, I.C.,Rosso, K.M., 2024. Mineral-associated organic matter is heterogeneous and structured by hydrophobic, charged, and polar interactions. *Proceedings of the National Academy of Sciences 121*(46), e2413216121.

Varadachari, C., Mondal, A.H.,Ghosh, K., 1991. Some aspects of clay-humus complexation: effect of exchangeable cations and lattice charge. *Soil Science 151*(3).

Voggenreiter, E., Schmitt-Kopplin, P., ThomasArrigo, L., Bryce, C., Kappler, A.,Joshi, P., 2024. Emerging investigator series: preferential adsorption and coprecipitation of permafrost organic matter with poorly crystalline iron minerals. *Environmental Science: Processes & Impacts 26*(8), 1322-1335. 10.1039/D4EM00241E.

Wan, D., Ye, T., Lu, Y., Chen, W., Cai, P.,Huang, Q., 2019. Iron oxides selectively stabilize plant-derived polysaccharides and aliphatic compounds in agricultural soils. *European Journal of Soil Science 70*(6), 1153-1163.

Wang, K.,Xing, B., 2005. Structural and sorption characteristics of adsorbed humic acid on clay minerals. *Journal of Environmental Quality 34*(1), 342-349.

Wang, Q., Yang, P.,Zhu, M., 2019. Effects of metal cations on coupled birnessite structural transformation and natural organic matter adsorption and oxidation. *Geochimica et Cosmochimica Acta 250*, 292-310.

Wu, P., Fu, Q.-L., Zhu, X.-D., Liu, C., Dang, F., Müller, K., Fujii, M., Zhou, D.-M., Wang, H.-L.,Wang, Y.-J., 2020. Contrasting impacts of pH on the abiotic transformation of hydrochar-derived dissolved organic matter mediated by δ-MnO2. *Geoderma 378*, 114627.

Xu, Y., Liu, K., Yao, S., Zhang, Y., Zhang, X., He, H., Feng, W., Ndzana, G.M., Chenu, C., Olk, D.C., Mao, J.,Zhang, B., 2022. Formation efficiency of soil organic matter from plant litter is governed by clay mineral type more than plant litter quality. *Geoderma 412*, 115727.

Ye, Y., Wang, Z., Liu, L., Qi, K.,Xie, X., 2023. Novel insights into the temporal molecular fractionation of dissolved black carbon at the iron oxyhydroxide - water interface. *Water Research 229*, 119410.

Yeasmin, S., Singh, B., Johnston, C.T.,Sparks, D.L., 2017. Evaluation of pre-treatment procedures for improved interpretation of mid infrared spectra of soil organic matter. *Geoderma 304*, 83-92.

Yeasmin, S., Singh, B., Kookana, R.S., Farrell, M., Sparks, D.L.,Johnston, C.T., 2014. Influence of mineral characteristics on the retention of low molecular weight organic compounds: a batch sorption–desorption and ATR-FTIR study. *Journal of Colloid and Interface Science 432*, 246-257.

Zelazny, L.W., He, L.,Vanwormhoudt, A., 1996. Charge analysis of soils and anion exchange. In: *Methods of Soil Analysis.* pp. 1231-1253.

Zhang, J., McKenna, A.M.,Zhu, M., 2021. Macromolecular characterization of compound selectivity for oxidation and oxidative alterations of dissolved organic matter by manganese oxide. *Environmental Science & Technology 55*(11), 7741-7751.

Zhao, Q., Callister, S.J., Thompson, A.M., Kukkadapu, R.K., Tfaily, M.M., Bramer, L.M., Qafoku, N.P., Bell, S.L., Hobbie, S.E., Seabloom, E.W., Borer, E.T.,Hofmockel, K.S., 2020. Strong mineralogic control of soil organic matter composition in response to nutrient addition across diverse grassland sites. *Science of The Total Environment 736*, 137839.

Zhou, Z.,Gunter, W.D., 1992. The nature of the surface charge of kaolinite. *Clays and Clay Minerals 40*(3), 365-368.

Chapter 5 Direct characterisation of organic carbon at mineral-organic interface in the submicron level using optical photothermal infrared (OPTIR) microscopy

Abstract

Elucidating the composition of soil organic matter (SOM) and the mechanisms at mineral-organic interfaces is important to understanding SOM dynamics and stabilisation. However, due to the heterogeneous distribution of OM fractions and their fine-scale differences within soil mineral-organic complexes, critical interfacial organic information can be easily obscured by either mineral structures or non-reactive yet predominant organic structures in bulk analysis using conventional infrared spectroscopy. In this study, we evaluated optical photothermal infrared (OPTIR) microscopy as an alternative to attenuated total reflectance Fourier transform infrared (ATR-FTIR) spectroscopy for revealing the mineral-organic interfacial chemistry in synthetic systems and the organic compositions of OM fractions in soils. Synthetic mineral-organic interfaces were formulated or assembled by adsorbing model organic compounds with distinct functional groups onto mixtures of clay minerals, while particulate organic matter (POM) and mineral associated organic matter (MAOM) fractions were isolated from two soils with contrasting mineralogies. OPTIR can reveal key interfacial information on primary functional groups - such as carboxyl, hydroxyl, amine and aromatic groups - involved in electrostatic attraction, ligand exchange, H-bonding, π-π electron transfer, and hydrophobic attractions, which was hardly detected by ATR-FTIR analysis. OPTIR is a rapid, reliable, and powerful analytical tool for distinguish the spatial distribution of OM fractions within mineral-organic complexes at submicron level. OPTIR can be utilised to characterise mechanistic processes at mineral-organic interfaces in both simulated and natural systems, and its high spatial resolution should be further applied to identify specific mineral fractions and their associated organic compositions in future research. The application of OPTIR will provide deeper insights into long-term SOM stabilisation for mitigating climate change.

5.1 Introduction

In terrestrial environments, minerals act as unique anchors that regulate long-term soil organic matter (SOM) sequestration (Torn et al., 1997). Minerals can influence the quantity and quality of SOM, its turnover time, and even atmosphere-pedosphere CO_2 fluxes within organic carbon (OC) cycles (Cotrufo et al., 2019; Galvez et al., 2020; Georgiou et al., 2022). Mineral associated organic matter (MAOM) constitutes over half of the total OC in soils, especially in mineral soils and forested biomes (Kramer and Chadwick, 2018; Georgiou et al., 2022). Increasing research attention has focused on the processes of mineral-organic interactions in the context of increasing OC sequestration in soils (Newcomb et al., 2017; Kleber et al., 2021). Mineral-organic interactions have been considered into two broad categories - physical occlusion within aggregated mineral structures and adsorption interactions at molecular-scale among minerals, OM and microbes (Rae Cho et al., 2016; Possinger et al., 2020; Whalen et al., 2024). Although limited spatial accessibility caused by physical occlusion, intercalation, and encapsulation within soil aggregates can directly restrict microbial utilisation (Rae Cho et al., 2016; Chi et al., 2022), chemical interactions between OM and minerals remain the primary mechanism for OM stabilisation in soils (Avneri-Katz et al., 2017; Yang et al., 2021; Chen et al., 2022). The adsorption behaviour of OM onto mineral matrix is governed by interactions between functional groups of organic moieties and mineral characteristics, involving reactions such as ligand exchange, cation bridging, hydrogen bonding, electrostatic attraction, hydrophobic interactions, and van der Waals forces (Kleber et al., 2015; Kleber et al., 2021). Therefore, a comprehensive understanding of the mineral-organic interactions within MAOM and the related OM fractions is crucial for realising the OC sequestration potential of soils.

Directly observation of chemical interactions at mineral-organic interfaces in natural mineral-organic complexes is particularly challenging. It has been evidenced that the OM is not uniformly attached to mineral matrix, but is instead heterogeneously distributed in discrete patches and layers (Wan et al., 2007; Vogel et al., 2014). Identification of specific spatial localisation of individual organic moieties requires preservation of natural structures, thus wet chemistry approaches that can destroy their spatial architecture are not useful for this (Kelleher and Simpson, 2006; Kleber and Johnson, 2010). As a non-invasive analytical technique, Fourier transform infrared (FTIR) spectroscopy an effective technique that is widely used for characterising interactions between organic and minerals (Johnston and Aochi, 1996; Parikh et al., 2014). Traditionally, FTIR spectra are collected in transmission, diffuse reflectance infrared Fourier transform (DRIFT) and attenuated total reflectance Fourier transform infrared (ATR-

FTIR) modes. However, these approaches provide bulk analyses due to their limited resolution, and important OC information and reaction mechanisms at mineral-organic interfaces are often masked or unresolved in these analysis (Newcomb et al., 2017). Although the post-analysis procedure of spectral subtraction or ratio can help to reduce the influence of overlapping signals between OM and minerals, the limited resolution still makes it difficult to characterise specific OM components in the mineral-organic complexes.

Instrumental analysis methods have been advanced substantially in recent decades, enabling detailed investigation of the spatial heterogeneity of OM at the mineral-organic interfaces at the submicron level (Solomon et al., 2012; Weng et al., 2022; Amelung et al., 2024). For example, the synchrotron radiation-based Fourier infrared (SR-FTIR) spectroscopy can directly provide insights into the spatial distribution of OC functional groups in soils at a finer scale (10 μm) (Holman, 2010; Xiao et al., 2018). However, this technique require access to synchrotron facilities associated with high costs, and it is possible to analyses a limited number of samples often with no replication. Nanoscale secondary ion mass spectrometry (nanoSIMS) is a powerful technique that allows precise and spatially resolved molecular and isotopic analysis down to 50 nm (Lv et al., 2022; Li et al., 2023). However, resin embedding needed for surface polishing to obtain a flat surface presents a major hurdle in the application of NanoSIMS for mineral-organic associations. Also, the technique requires a high vacuum and probes only few nm of the surface layer. Recently, optical photothermal infrared (OPTIR) microscopy has been developed to map the molecular distributions of OC moieties in diverse environmental samples with a spatial resolution less than 500 nm (Olson et al., 2020; Jubb et al., 2023; Liu et al., 2024; Jamoteau et al., 2025). This novel non-invasive technique is capable of measuring the thermal expansion and change in the refractive index of a sample in response to IR absorbance, requiring only minimal sample preparation (Prater et al., 2024; Molina et al., 2025). Jubb et al. (2023) were the first to employ OPTIR to evaluate the structure of sedimentary organic matter, demonstrating the potential of this analytical approach for geologic material studies. Liu et al. (2024) reported the molecular fractionation of organic compounds within halite crystals using OPTIR spectroscopy. More recently, Jamoteau et al. (2025) investigated the detection sensitivity of mineral-organic associations, as well as sample preparation and instrument setting of OPTIR spectroscopy for the analysis of minerals and adsorbed organic compounds.

OPTIR spectroscopy allows the identification of OC at mineral-organic interfaces and provides detailed information on specific organic moieties interacting with minerals. In this study, we have compared the capability of OPTIR microscopy with ATR-FTIR spectroscopy in characterising OC at mineral-organic interfaces. Specifically, nine organic compounds with distinct functional groups (i.e., carboxyl, hydroxyl, amine, amide, ether, ester, and aromatic) were adsorbed onto crystalline mineral mixtures (i.e., comprising kaolinite, montmorillonite and goethite). In addition, OPTIR microscopy was applied to characterise OC in two OM fractions - mineral associated organic matter (MAOM) and particulate organic matter (POM) - which were isolated from a Ferralsol and a Vertisol. Laboratory-synthesised adsorption experiments were expected to provide further insights into mineral-organic interactions and to improve characterisation of the complex OC composition of soil OM fractions by using OPTIR spectroscopy. The OPTIR microscopy can represent a powerful, non-invasive analytical approach for probing the OC characteristics of MAOM and POM fractions at submicron scales, and it could be promoted as a novel analytical technique used to enhance monitoring of long-term SOM sequestration and stabilisation.

5.2 Materials and methods

5.2.1 Adsorption experiments of model organic compounds

Nine organic compounds, 1-hexanol, hexanoic acid, citric acid, phenol, benzoic acid, gallic acid, L-arginine, adenine, and pectin, each containing one or more particular functional groups (Table S 5.1), were selected for adsorption experiments. Organic compound solutions with C concentration from 235 to 308 mg L^{-1} were prepared for the adsorption experiments onto a mineral mixture. The mineral mixture comprised three common clay minerals with distinct surface characteristics, i.e., kaolinite, montmorillonite and goethite, in a ratio (wt. basis) of 2:2:1. Kaolinite (KGa-2) and montmorillonite (Swy-2) were obtained from the Source Clays Minerals Repository of the Clay Minerals Society, whereas goethite was synthesised in the laboratory following the procedure outlined by Schwertmann and Cornell (2000). Basic properties of selected minerals are presented in Table S 5.2.

Adsorption experiments were conducted by mixing 40 mL of each chemical solution with 200 mg of the mineral mixture at pH 6.0, using 0.01 M NaCl as the background electrolyte. The mixtures were shaken for 16 h in the dark at 4 °C, centrifuged (3000 × g, 30 min) and filtered using 0.45 μm PTFE membrane. The solid residues were washed by Milli-Q water to remove entrained solution and the solid residues were retained for further analysis.

5.2.2 Particulate organic matter and mineral-associated organic matter

The POM and MAOM fractions were isolated from two bulk soils (i.e., a Ferrasol and a Vertisol) based on density: <1.8 g/cm^3 (POM) and > 1.8g/cm^3 (MAOM), following procedure from Sollins et al. (2006) and Yeasmin et al. (2023). Briefly, 30 g of air-dried soil (<2 mm) was mixed with 125 mL of sodium polytungstate (SPT) solution (1.8 g/cm^3) in a 250 mL centrifuge bottle. The suspension was shaken for 3 h on a horizontal shaker (300 rpm) and then centrifuged for 30 min at 970 × g. The floating materials were aspirated and the supernatant SPT solution was filtered using a 0.7 µm glass fibre filter and returned to the same centrifuge bottle. The remaining mixtures were shaken again for 1 h, centrifuged and aspirated a second time. The two aspirated floating materials (i.e., POM, < 1.8 g/cm^3) were combined and rinsed with Milli-Q water on a 0.7 µm filter until EC was < 50 µS/cm. The remaining residue (i.e., MAOM, >1.8 g/cm^3) in the centrifuge bottle were also rinsed until EC < 50 µS/cm. All recovered fractions were oven-dried and ground (< 200 µm) for further analysis.

5.2.3 Attenuated total reflectance Fourier transform infrared (ATR-FTIR) spectroscopy

The ATR spectra of pure organic compounds, mineral mixture, mineral-organic complexes and isolated POM and MAOM were collected using a Bruker Vertex 80V spectrometer equipped with a MIRacle single reflection horizonal ATR accessory (Ge crystal) and a room-temperature DLaTGS detector in the Vibrational Spectroscopy Lab of the Sydney Analytical, the University of Sydney. Spectra were obtained in the 4000-600 cm^{-1} region with the co-addition of 128 scans at a spectral resolution of 4 cm^{-1}. The spectra processing, including atmospheric compensation, scattering baseline correction, normalisation and spectral ratio calculation, was performed using OPUS Software 8.7.31.

5.2.4 Optical photothermal infrared (OPTIR) spectroscopy

The OPTIR analysis was conducted using the photothermal mIRage-LS microscope with a MIRcat QT infrared laser, 532 nm dual Raman probe laser, an avalanche photodiode (APD) detector and a Cassegrain ×40 objective in the Vibrational Spectroscopy Lab of the Sydney Analytical, the University of Sydney. Prior to sample measurement, the objectives were calibrated, and the background spectra were collected. The organic compounds, mineral mixture, mineral-organic associations, and POM and MAOM fractions were prepared as powdered samples that were pressed between glass windows to obtain a flat surface (Jamoteau et al., 2025). Some organic compounds that were in liquid form samples were directly dropped on the glass window for measurement. OPTIR spectra were obtained in co-propagation mode with the settings: 1040 cm^{-1} as autofocus wavenumber, 25 % of IR laser power, 0.27 % of probe powder, averaging 3 IR scans over the region of 2993-771 cm^{-1} at a spectral resolution of 8 cm^{-1}, and sweep speed at 1000 cm^{-1}/s.

To acquire high quality spectra from the target OC moieties, a few spectra were initially collected at different locations on samples. Then, the identified band positions of organics (between 1800-1100 cm^{-1}) in analysed spectra (which varied among samples) were selected to map the ratio hotspots of organic peaks over a mineral peak (Si-O stretching at 1027 cm^{-1}) within the area of interest. The microscopy image of the scanned area and hot-spots mapped in synthetic mineral-organic complexes are presented in Figure S 5.1-Figure S 5.9. The hotspots identified on the mapping image were rescanned with a grid array to ensure the acquisition of the OC spectra from the sample (Figure S 5.1-Figure S 5.9), rather than background or detector artifacts. The spectra were linear baseline corrected, intensity normalised, and averaged to obtain final spectra using PTIR Studio software 4.6.1.

5.3 Results and Discussion

5.3.1 *Functional groups at synthetic mineral-organic interfaces by ATR-FTIR and OPTIR analysis*

The ATR spectra of the mineral mixture and mineral-organic complexes appeared similar, with prominent bands observed at 3697, 3651, 3623, 1115, 1027, 1007, 913, 790, 746, 689, and 602 cm^{-1} (Figure 5.1 and Table S 5.4). The peaks at 3697, 3651, and 3623 cm^{-1} can be attributed to OH stretching vibrations of structural surface groups (i.e., Al-OH, Si-OH and Fe-OH) from clay minerals (Farmer, 1974b; Ryskin, 1974). Bending vibrations of these surface hydroxyl groups appear at lower wavenumber region, with 913 cm^{-1} assigned to Si-OH or Al-OH and 790 cm^{-1} to Fe-OH. The shoulder peak at 1115 cm^{-1} is attributed to asymmetric stretching vibrations of Si-O from silicates. Two sharp peaks at 1027 and 1007 are associated with stretching of Si-O-Si or Si-O-Al, corresponding to oxygen bridges formed by condensation of Si and Al hydroxides, while bending of these oxygen bridges is associated with the peak at 746 cm^{-1} (Henmi et al., 1981). The stretching vibrations of metal-O, such as Fe-O and Al-O from goethite were observed at 689 and 602 cm^{-1} (Farmer, 1974a; Schwertmann and Cornell, 2000). Despite the substantial amount of organic C adsorbed from different organic compounds (Table S 5.3), only a small organic band was observed at 1195 cm^{-1} in all mineral-organic complexes. The band corresponds to vibrations of alcohol or phenol C-O (Bellamy, 1975a) and alkyl amine

C-N stretching (Bellamy, 1975c). The negligible presence of organic peaks in ATR spectra suggest that they may have been masked by the dominant contribution of mineral signals. It should be noted that additional organic peaks were observed in the adsorption of N-containing compounds at 1702, 1558, 1474, 1267 and 830 cm^{-1} for arginine, and 1702 and 1195 cm^{-1} for adenine (Figure 5.1g and h). The peak at 1702 cm^{-1} can be attributed to the carboxyl group (-COOH) from the amino group. The 1558 cm^{-1} peak in the mineral-organic complex spectra corresponds to deformation vibrations of protonated $-NH_3^+$ groups and the asymmetric stretching of deprotonated COO^- groups, which are considered the primary functional group involved in the mineral-organic interactions (Kitadai et al., 2009; Jaber et al., 2014). Minor peaks at 1474 cm^{-1} was possibly associated to symmetric stretching of deprotonated carboxylate and 1267 cm^{-1} associated with the deformation vibrations of C-O and C-N, while the peak at 830 cm^{-1} corresponded to C-N or C-H bending.

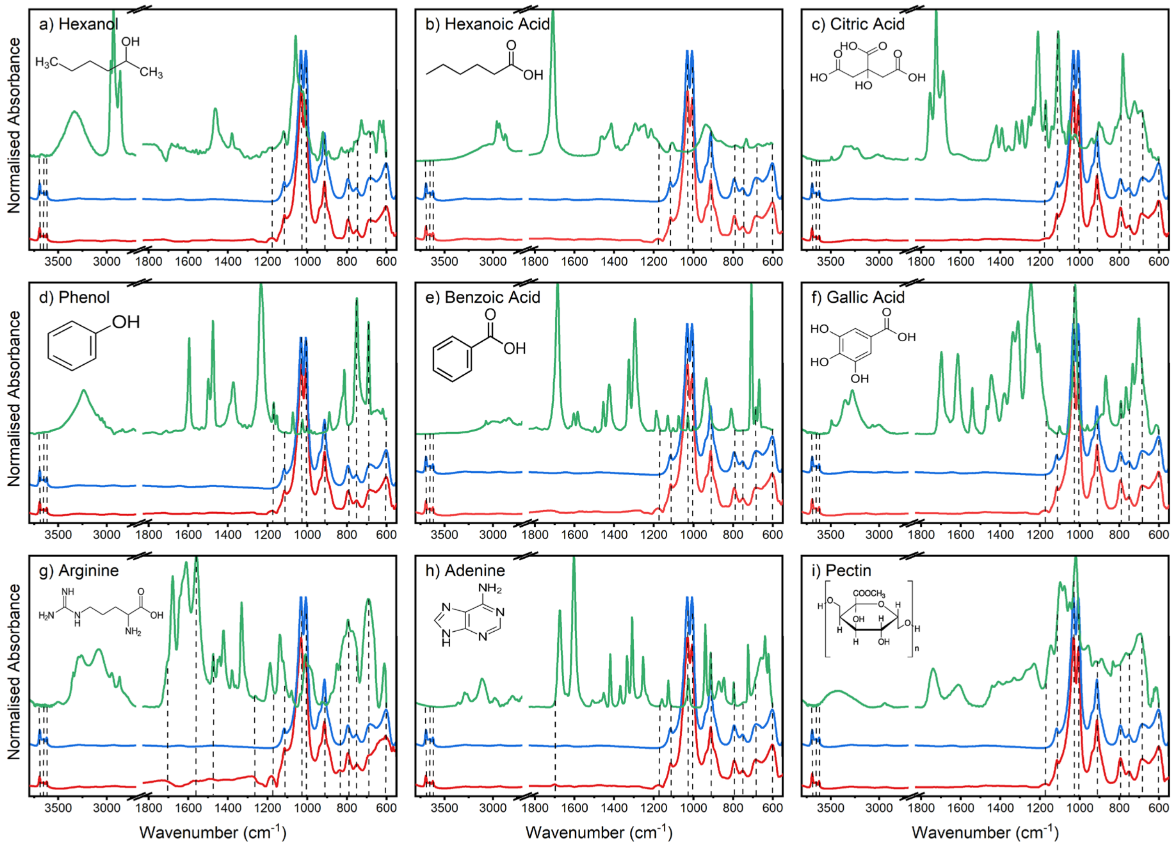

Figure 5.1 ATR-FTIR spectra of organic compounds (top, green), the mineral mixture (middle, blue) and mineral-organic complexes made by adsorbed organic compounds onto the mineral mixture (bottom, red) (a - hexanol; b - hexanoic acid; c - citric acid; d - phenol; e - benzoic acid; f - gallic acid; g - arginine; h - adenine; i - pectin).

In contrast to ATR-FTIR, the OPTIR spectroscopy specifically identified OC components in mineral-organic complexes, which were heterogeneously distributed as discrete patches across complexes (Figure S 5.1-Figure S 5.9). This is consistent with previous studies, which reported a patchy and disordered spatial distribution of OC adsorbed on minerals at nanoscale (Rae Cho et al., 2016; Possinger et al., 2020). The resolution of OPTIR results and selected scanning wavenumber varied across samples due to their distinct functional moieties.

Mineral bands still contributed significantly to the OPTIR spectra of mineral-organic complexes, but fewer mineral peaks than ATR spectra (Figure 5.2). The band frequencies at 1115, 1040, 1007, 913 and 796 cm^{-1} from mineral structures remained consistent across all mineral-organic complexes, which were attributed to the tetrahedral (i.e., Si-O and Si-O-Si) and octahedral (i.e., Al-O) sheets of kaolinite and montmorillonite (Farmer, 1974b). The absorbance signals of iron oxides were scarcely detected by OPTIR analysis. The OH bending vibration at 891 cm^{-1} from Fe-OH of goethite at 891 cm^{-1} (Cambier, 1986) was observed in the mineral-organic complexes obtained by adsorption of citric acid, gallic acid, and pectin, which contain both hydroxyl and carboxyl groups capable of binding with positively charged surface of goethite (Norén et al., 2008; Zhang et al., 2019). The less sensitivity of iron oxides in OPTIR analysis can be attributed to the lower crystallinity of goethite compared to kaolinite and montmorillonite. Jamoteau et al. (2025) also reported lower detection of poorly crystalline minerals relative to crystalline minerals, likely due to their potential recrystallisation in the OPTIR analysis.

The frequency of organic bands varied in OPTIR spectra of mineral-organic complexes (Figure 5.2 and Table S 5.4), reflecting the specific functional groups involved in the mineral-organic interactions. In hexanol adsorbed mineral-organic complex, only one frequency band at 1275 cm^{-1} was observed that was attributed to C-O stretching from alcohol moieties. Similarly, only one band at 1620 cm^{-1} was present in hexanoic acid adsorbed complexes that corresponded to deprotonated COO^{-} group. The frequency bands observed at 1787 and 1664 cm^{-1} in citric acid, gallic acid and pectin adsorbed complex were attributed to carboxyl (COOH) stretching and asymmetric stretching of deprotonated COO^{-} groups, respectively. In addition, the C=C from aromatic ring can also be associated with the frequency at 1664 cm^{-1}.

The C=C stretching bond in aromatic in the benzene ring structure was observed at 1664 or 1620 cm^{-1} in the adsorption complexes of phenol, benzoic acid and gallic acid. The inconsistent position of the aryl C can be attributed to the number and type of functional groups substituted in the benzene ring (Nikolova et al., 2014). Additional frequencies at 1195 and 1100 cm^{-1} of C-O stretching were observed in the complexes of phenol and benzoic acid, respectively.

Similar to the ATR spectra, additional bands in the OPTIR spectra of N-containing compound adsorption were observed, emphasising the important role of N functional groups (e.g., amino and amine groups) in the mineral-organic interactions. The band frequencies at 1664 (C=N stretching and COO^- asymmetric), 1620 (NH_3^+), 1474 (COO^- symmetric and $-CH_3$ asymmetric), 1400 ($-CH_3$ symmetric), and 841 (CH_2 rocking vibration) cm^{-1} were observed in arginine complexes (Chia et al., 2012; Yeasmin et al., 2014; Kasprzhitskii et al., 2022; Millman et al., 2024). In adenine complexes band frequencies were observed at 1702 (C=N and purine ring structure), 1620 (NH_3^+), 1452 (C-H), 1400 (C-H) and 1238 (-OH) cm^{-1}.

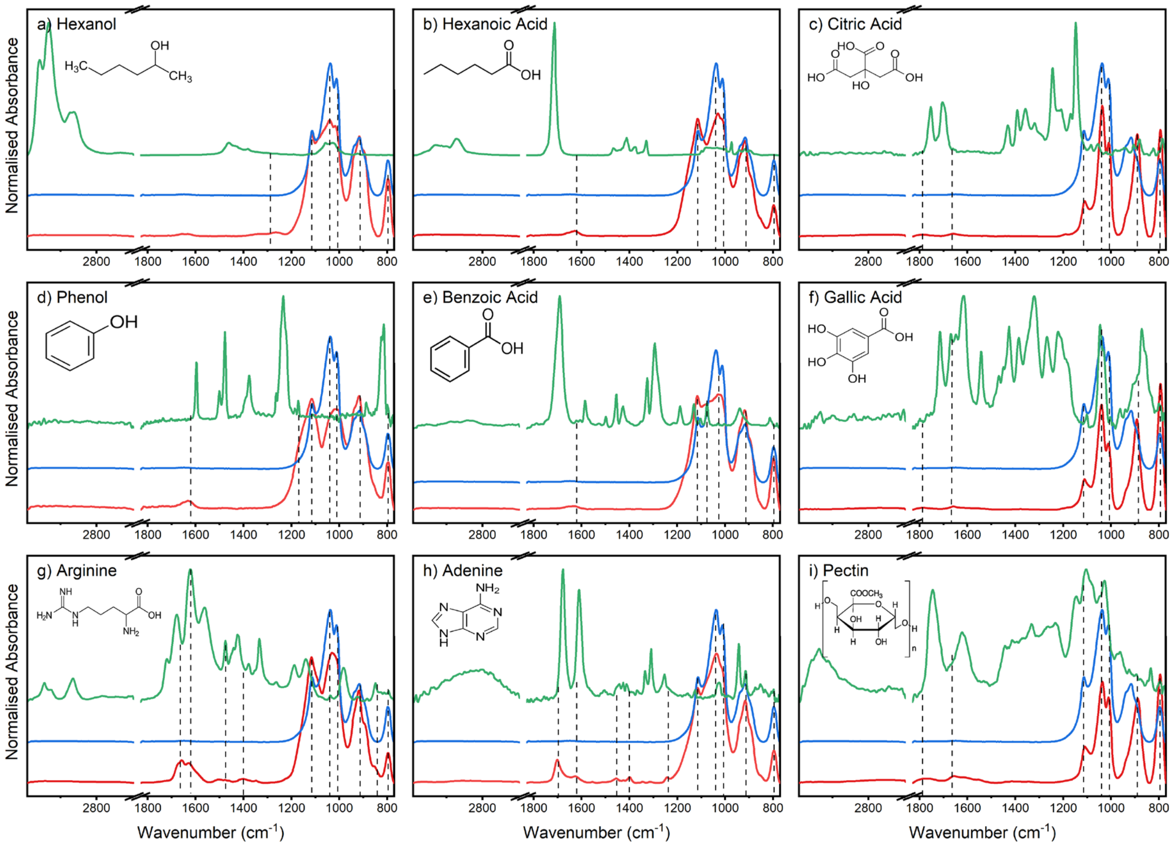

Figure 5.2 OPTIR spectra of organic compounds (top, green), the mineral mixture (middle, blue) and mineral-organic complexes made by adsorbed organic compounds onto the mineral mixture (bottom, red) (a - hexanol; b - hexanoic acid; c - citric acid; d - phenol; e - benzoic acid; f - gallic acid; g - arginine; h - adenine; i - pectin).

5.3.2 The capability of ATR-FTIR and OPTIR analysis in revealing OC characterisation

Compared to ATR that detected only few organic peaks, OPTIR analysis revealed more detailed information on the reactive functional groups involved in mineral-organic interactions. However, some organic bands were still obscured by strong mineral signals in the spectra. Therefore, to minimise the interference of mineral peaks and get better insights to organic functional groups involved in adsorption reaction, we ratioed both ATR and OPTIR spectra of mineral-organic complexes to their corresponding mineral mixture spectra (Figure 5.3), which identified additional organic bands.

The C-O stretching band at 1195 cm^{-1} observed in ATR spectra became highly prominent with the sharpest peak in all ratioed spectra. In hexanol adsorbed complex, minor peaks appeared at 1275 and 1144 cm^{-1} in the ATR spectra, which corresponded to C-OH moieties, and these were also observed in the OPTIR spectra. The hydroxyl groups of hexanol can interact with mineral surfaces through cation bridging and H-bonding reactions at pH 6 (Lock and Skipper, 2007; Guo et al., 2022). In contrast, OPTIR revealed additional alkyl C-H peaks at 1338, 975, 868, and 808 cm^{-1}. In hexanoic acid complex, minor peaks at 1720 cm^{-1} for COOH and 1580 cm^{-1} for symmetric COO^{-} were detected in the ATR spectrum, while an additional and a significant peak was observed at 1620 cm^{-1} (asymmetric COO^{-}) in the OPTIR spectrum, indicating the primary role of deprotonated COO^{-} in the adsorption reaction. The C-O band frequency observed in the 1300-1100 cm^{-1} region varied in the ATR and OPTIR spectra, with the band at 1275, 1195, and 1144 cm^{-1} in ATR spectrum and at 1238 and 1169 cm^{-1} in the OPTIR spectrum. A sharp peak at 841 cm^{-1} associated with methylene group (CH_2), was also observed by OPTIR, while this was a minor peak in ATR. Electrostatic attraction might have occurred between negatively charged carboxylic groups and positively charged sites on goethite surface and at the edges of the octahedral sheet of phyllosilicates at pH 6 (Kubicki et al., 1999). In addition, surface hydroxyl groups of minerals (such as goethite) can be replaced by the carboxyl groups through ligand exchange to form monodentate inner-sphere complexes or from outer-sphere complexes through H-bonding (Feng et al., 2005; Norén and Persson, 2007). It should be noted that only minor peaks were observed for citric acid adsorbed complex in both ATR and OPTIR spectra, particularly in the OPTIR spectrum. In the ATR spectrum, symmetric stretching of COO^{-} was observed at 1580 cm^{-1}, whereas bands at 1195 and 1100 cm^{-1} were associated with C-OH. However, OPTIR detected only C-H peaks at 868 and 816 cm^{-1}, along with two minor peaks at 1787 cm^{-1} for COOH and at 1664 cm^{-1} for asymmetric stretching of COO^{-}. In our study ($pH \leq pK_a3$), two carboxylic groups were deprotonated, while the third was partially deprotonated or protonated. The negatively carboxylate groups in citric acid can also participate in complex interactions with surface sites or surface hydroxyl groups through electrostatic attraction, cation-bridging, ligand exchange and H-bonding (Kubicki et al., 1999; Lackovic et al., 2003; Ramos and Huertas, 2014). In contrast to previous studies (Lackovic et al., 2003; Ramos and Huertas, 2014; Yeasmin et al., 2014), the position of carboxylate COO^{-} group shifted to lower frequencies in this study (values), indicating the intensive formation of inner-sphere complexes. Although a high amount of OC (30.7 mg g^{-1}) was adsorbed in citric acid adsorption, it was still difficult to detect distinct OC regions in OPTIR, with only a small OC area being found and scanned (Figure S 5.3). This can be attributed to the heterogeneous adsorption of citric acid, leading to a non-uniform distribution within the complexes. We hypothesise that esterification may occur between adsorbed citrate molecules on mineral surfaces and free citric acid, as the significant organic peak at 1195 cm^{-1} in ATR can also be attributed to the stretching of methyl ester ($COOCH_3$) groups (Doumenq et al., 1990). This self-assembly of citric acid could theoretically cause adsorbed components to accumulate in specific areas on the mineral surface, which may result on the difficulty to identify suitable scan regions for OPTIR analysis.

In phenol complex, ATR showed the C-O peaks at 1275, 1195 and 1144 cm^{-1} from the phenolic C-OH moiety, along with a peak at 841 cm^{-1} corresponding to C-H out-of-plane bending from the aromatic structure. Several additional bands were visible in the OPTIR spectrum of the phenol complex, such as the C=C stretching of aromatic structure at 1620 cm^{-1} by OPTIR and a minor peak at 1730 cm^{-1}, which can be attributed to quinone C=O groups rather than carboxylic groups in the phenol adsorption. The presence of Fe^{3+} in goethite may lead to the oxidation of phenol to phenoxy radicals appeared to be a potential pathway (McBride, 1987; Kung and McBride, 1988), which are primary intermediates that can undergo further oxidation to quinone structures (C=O) (Uchimiya and Stone, 2006; Jiang et al., 2015; Zhang et al., 2019). In addition, electron transfer can also occur between the benzene ring structure and the negatively charged phyllosilicate surfaces via π-π electron donor-acceptor (EDA) interactions (Keiluweit and Kleber, 2009; Li et al., 2024), with significant C-H peak from benzene rings detected by OPTIR at 1481, 1400, 1338, 975, and 841 cm^{-1}. In benzoic acid complex, carboxyl (C=O) band at 1720 cm^{-1} and at 1580 cm^{-1} for carboxylate (COO^-) were observed in the ATR spectrum, whereas only a single aromatic peak at 1620 cm^{-1} was observed by OPTIR. Phenolic groups can form donor hydrogen bonds with phyllosilicate surfaces at pH 6 (< pK_a 10.0) (Lock and Skipper, 2007; Praus et al., 2011; Li et al., 2024). Previous studies have also reported that mono- or bidentate complexes can form through H-bonding between carboxylic groups in benzoic acid and mineral surfaces (Kubicki et al., 1999; Li et al., 2018). The spectra of gallic acid complex were similar to those of citric acid, with only minor peaks observed by both ATR and OPTIR, and the absence of C-O bands in the 1300-1100 cm^{-1} region of OPTIR spectrum. The adsorption of gallic acid is therefore expected to be driven primarily by π-π interactions (Chefetz et al., 2011; Ahmat et al., 2019). Although deprotonated COO^- in gallic acid may still interact with mineral sites to form monodentate-mononuclear complexes (COO^- at 1660 cm^{-1}), such interactions were less favoured due to protonated COOH remaining at 1787 cm^{-1}.

Prominent organic peaks from amino, guanidine, and purine ring moieties of N-containing compounds, such as arginine and adenine, were revealed in both ATR and OPTIR spectra. In arginine adsorbed complex, additional frequencies at 1144, 975, and 841 cm^{-1} due to C-H group in ATR spectrum and at 1502 (N-H), 1223 (C-N and C-O), 1169 (C-H), and 975 (C-H) cm^{-1} in the OPTIR spectrum were observed. At pH 6, arginine can exhibit protonated amino and guanidine groups with NH_3^+, which can interact with deprotonated surface sites through electrostatic attraction or H-bonding. In addition, deprotonated COO^- groups of arginine can interact with protonated hydroxyl surface sites via electrostatic attraction, H-bonding and ligand exchange (Dong et al., 2018; Kasprzhitskii et al., 2022). In adenine adsorbed complex, ATR exhibited additional peaks at 1275 and 1238 cm^{-1} corresponding to C-N bonds, whereas OPTIR revealed additional C-H information at 1195, 1144 and 841 cm^{-1}. The ring structure of adenine has been reported as the primary moiety interacting with phyllosilicates through π-π interactions with electron donation to the surface sites (Plekan et al., 2007; Hashizume et al., 2010). At pH 6, the protonated NH_3^+ group may also interact with negatively charged phyllosilicate surface (e.g., montmorillonite) through electrostatic attraction or H-bonding (Baú et al., 2012). The adsorption of water may also accompany adenine adsorption, as evidenced by O-H bending at 1238 cm^{-1}. The ATR and OPTIR spectra of pectin complex exhibited patterns similar to citric acid and gallic acid, with the presence of both carboxyl and hydroxyl groups, which it may undergo reactions via electrostatic attraction, ligand exchange and H-bonding (Azimzadeh and Martínez, 2024). It should be noted that the pyranose rings and glycosidic bonds (i.e., C-O) of pectin in the region of 1200-1000 cm^{-1} disappeared after adsorption in the OPTIR spectrum. This can be attributed to interactions between hydroxyl groups from two adjacent rings interacting and mineral surfaces, forming eight-member ring complexes (Weisseborn et al., 1995; Wang et al., 2017). Such complexes can exert strain on the pyranose ring, causing its deformation and resulting in the signal elimination during the OPTIR analysis.

The capability of ATR to detect functional groups involved in adsorption reaction is limited. It primarily revealed C-O and C-N bonds that are prevalent in many mineral-organic complexes. However, the lack of key information on reactive functional groups in ATR analysis is insufficient for accurately interpreting and explaining diverse and complex mineral-organic interactions. OPTIR can address this limitation by directly detecting organic fractions at very fine scale, making it possible to identify the anchoring organic bond and functional groups that connect organic molecules with mineral surfaces.

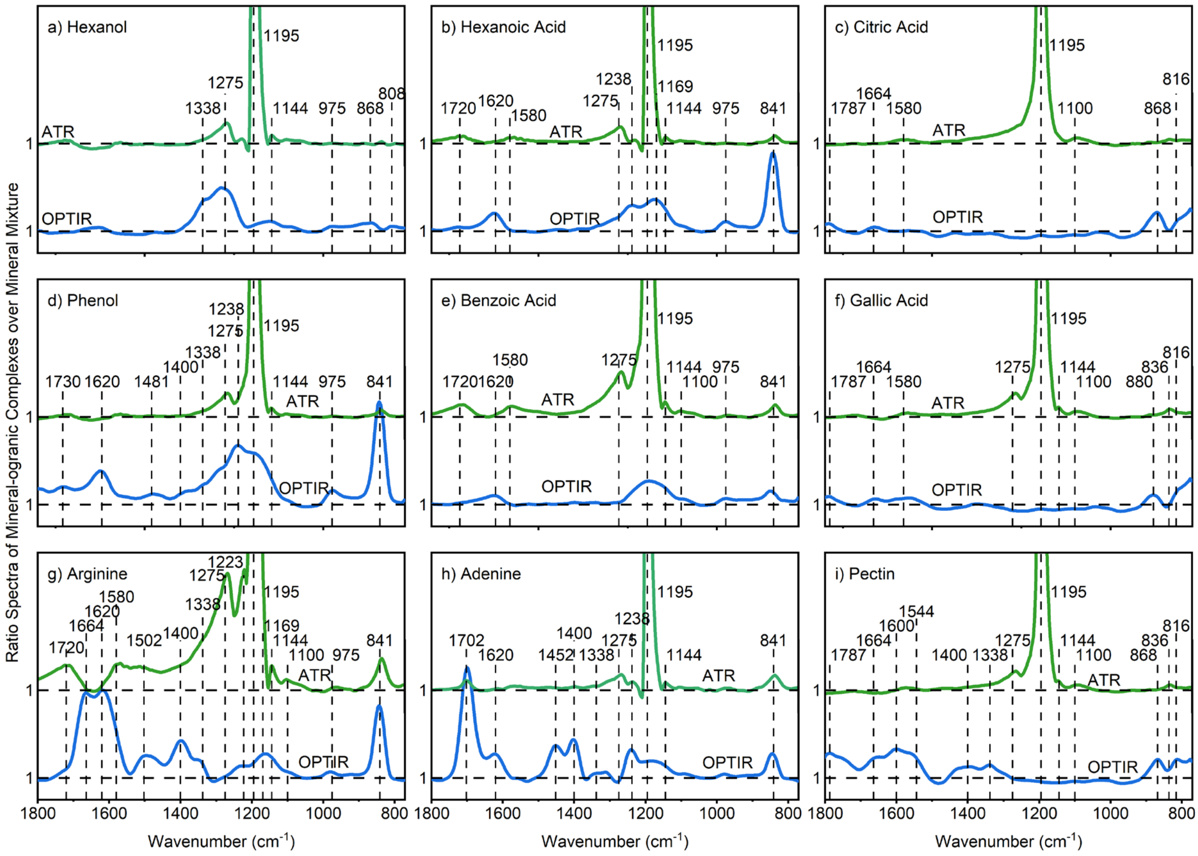

Figure 5.3 Ratioed ATR-FTIR (top green) and OPTIR (bottom blue) spectra of mineral-organic complexes to the mineral mixture (a - hexanol; b - hexanoic acid; c - citric acid; d - phenol; e - benzoic acid; f - gallic acid; g - arginine; h - adenine; i - pectin).

5.3.3 ATR-FTIR and OPTIR analysis of POM and MAOM fractions

Both Ferrasol and Vertisol exhibited high clay content but differed in dominant clay mineralogy (Fang et al., 2014; Jones and Singh, 2014). Ferrasol was enriched in Fe/Al oxides including goethite, hematite and gibbsite, whereas Vertisol was dominated by phyllosilicates such as smectite and montmorillonite. These mineralogical differences are expected to influence the composition of adsorbed organic compounds, both in terms of their quantity and molecular characteristics. Total OC and N concentration in the POM and MAOM fractions of surface and subsurface soils samples of Ferralsol and Vertisol are presented in Table S 5.3. The OC concentration was much greater in the POM and MAOM fractions of Ferrasol than of Vertisol, consistent with previous findings that Fe/Al oxides have a greater capacity for OC adsorption than phyllosilicates (Mikutta et al., 2007; Saidy et al., 2013). The POM fractions of both Ferrasol and Vertisol had higher OC concentration than the corresponding MAOM fractions of the two soils. However, the MAOM fraction of the subsurface Vertisol exhibited greater OC concentration than its corresponding POM fraction.

In the ATR-FTIR analysis (Figure 5.4a), similar inorganic spectra were consistently observed across all OM fractions. The stretching vibrations of surface hydroxyl groups appeared at 3697 and 3623 cm^{-1}, followed by Si-O at 1115 cm^{-1}, Si-O-Si or Al-O at 1027 and 1007 cm^{-1}, Fe-O at 913 cm^{-1}, and Si-O at 796 cm^{-1}, all of which can be attributed to the clay mineral crystal structures. Additional organic peaks at 3526 and 3443 cm^{-1}, corresponding to N-H stretching from primary amide moieties, were detected only in Ferrasol fractions. This indicates a greater abundance of N-containing compounds associated to the Ferrasol fractions than Vertisol fractions, consistent with their higher TN concentration (Table S 5.3). In the 1800-1500 cm^{-1} region, a broad peak was consistently observed across all OM fractions, which can be attributed to a mixture contribution of functional groups, including C=O stretching from carboxyl, carboxylate, amide I and conjugated ketone, as well as C=C vibration from aromatic compounds (Bu et al., 2010; Pedersen et al., 2011). However, only the Ferrasol fractions exhibited an additional smaller organic peak at 1400 cm^{-1}, corresponding to the deformation of aliphatic C-H groups and phenolic O-H groups (González-Pérez et al., 2008; Bu et al., 2010). No differences were observed between the POM and MAOM fractions, nor between surface and subsurface layers, in the ATR analysis.

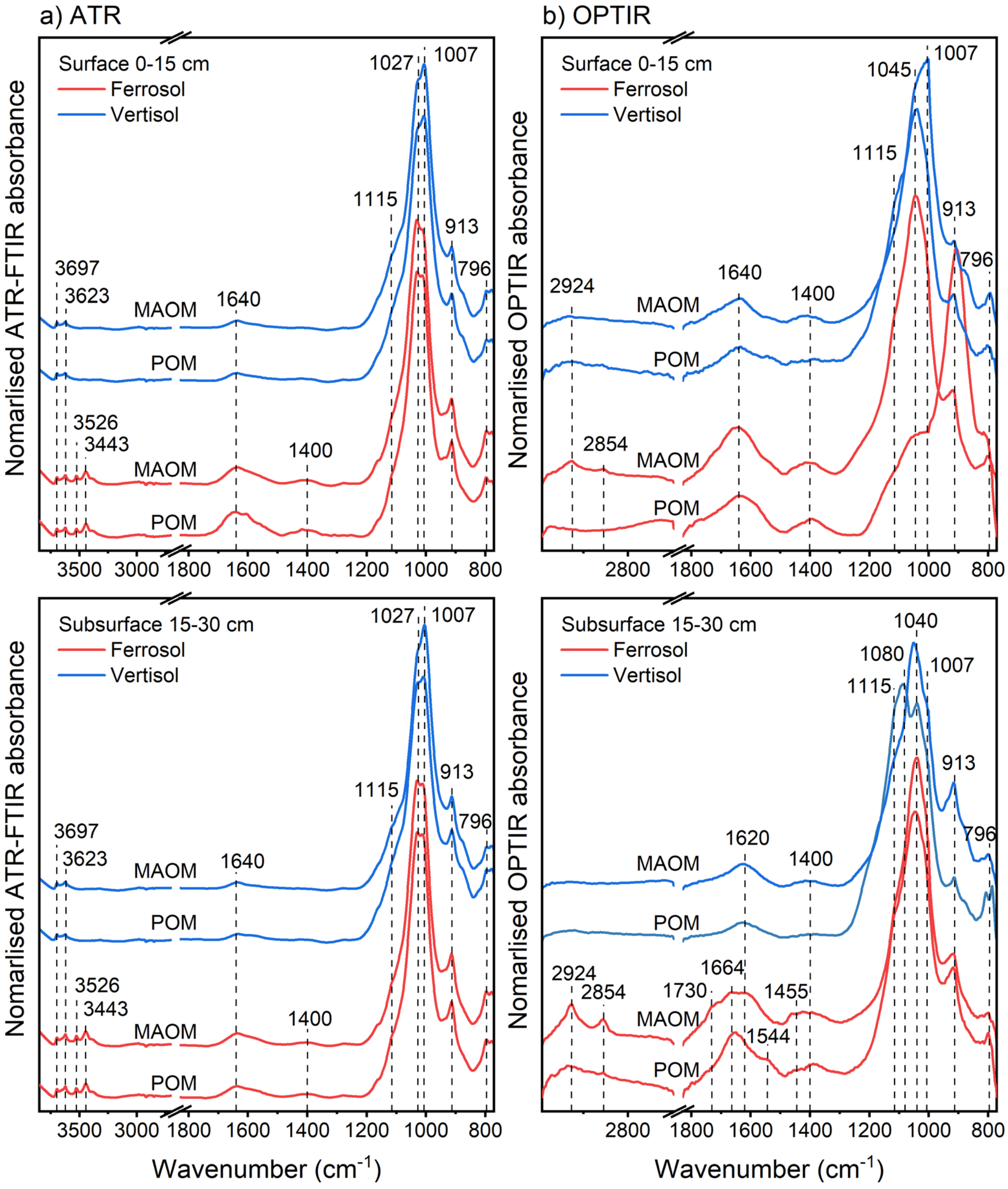

Figure 5.4 ATR-FTIR spectra (a) and OPTIR spectra (b) of particulate organic matter (POM) and mineral associated organic matter (MAOM) separated from surface (0-15 cm) and subsurface (15-30 cm) of a Ferrasol and a Vertisol.

OPTIR provided more information about the POM and MAOM fractions. In the Ferrasol (Figure 5.5), the spatial distribution of organic components in both POM and MAOM fractions appeared distinct and patchy. The OC compositions of POM and MAOM showed different in the organic region (2900-2800 and 1800-1300 cm^{-1}) (Figure 5.4b). Two sharp peaks were observed at 2924 and 2854 cm^{-1} in the MAOM fractions, which can be attributed to the asymmetric and symmetric stretching vibration of aliphatic alkyl groups (Bellamy, 1975b). In contrast, the corresponding region in the POM fractions either did not show any detectable peaks or a broad bump was only observed at 2924 cm^{-1}. Similar to the ATR-FTIR spectra, two broad peaks were observed at 1640 or 1664 and 1400 cm^{-1}. However, additional shoulder peaks of at 1730 cm^{-1} (COOH) and at 1544 (asymmetric) and 1455 (symmetric) cm^{-1} of carboxylate (COO^-) were only observed in the MAOM fraction of subsurface soils. Slight differences in the prominent mineral peaks were observed in the POM and MAOM fractions of surface Ferrasol, with the Si/Al-O peak from silicate sheets at 1045 cm^{-1} in MAOM fraction, and the Fe-O peak from Fe/Al oxides at 913 cm^{-1} in POM fraction. The nearby shoulder peaks associated with Si-O were similar to those in the ATR spectra at 1115, 1040, and 796 cm^{-1}.

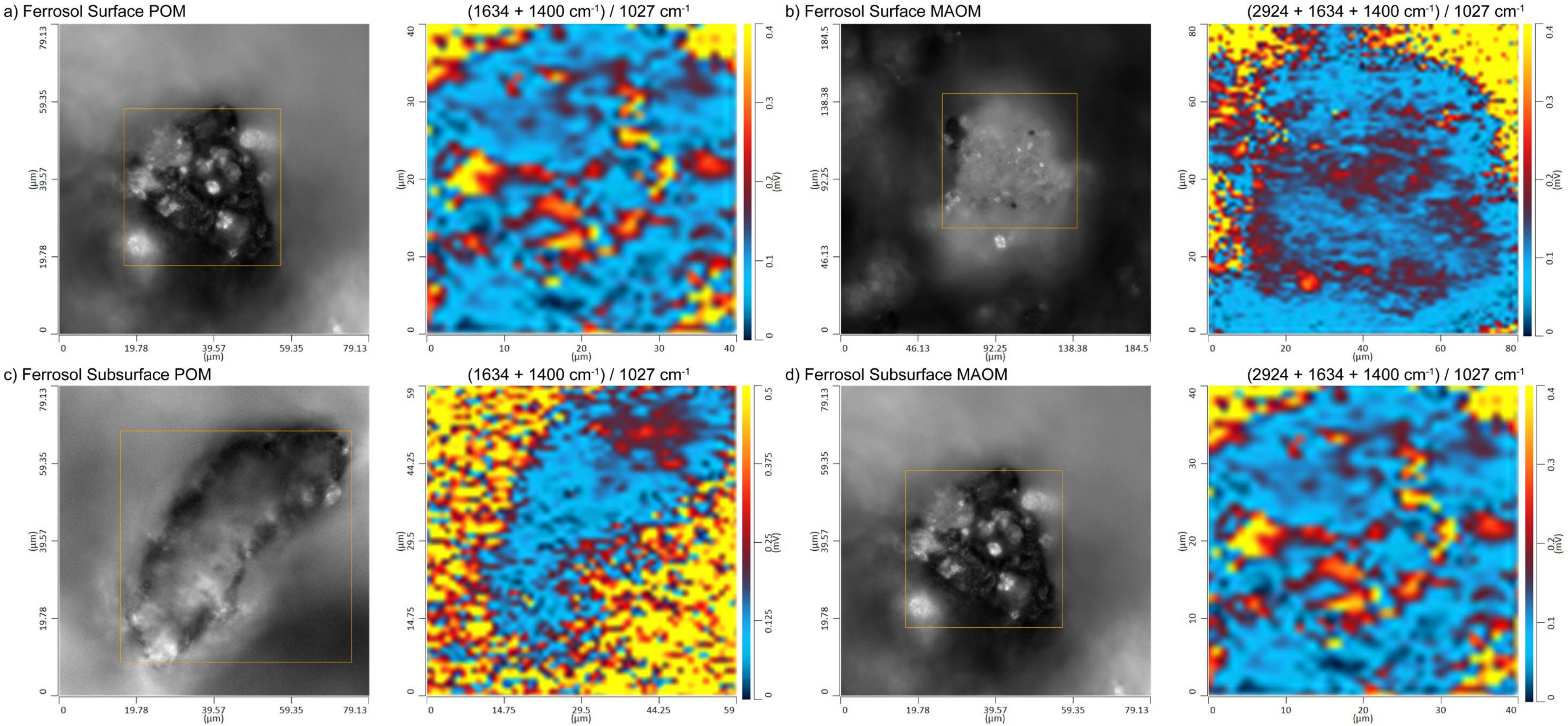

Figure 5.5 Microscopy images and organic hotspot mappings based on OPTIR absorbance ratios in the Ferrasol. The ratio (1634 + 1400 cm^{-1}) / 1027 cm^{-1} was employed for particulate organic matter (POM) and (2924 + 1634 + 1400 cm^{-1}) / 1027 cm^{-1} for mineral associated organic matter (MAOM) in surface (a, b) and subsurface (b, d) samples. Corresponding OPTIR data with average spectra and a zoomed-in view of the organic region are shown at the bottom.

In contrast to the Ferrasol, organic components were uniformly distributed in both the POM and MAOM fractions of the Vertisol (Figure 5.6). In the OPTIR spectra, only the surface fractions displayed the band at 2924 cm^{-1}, which was broad and minor, and while the broad peak in the 1800-1500 cm^{-1} region of Vertisol fractions was shifted to lower frequency at 1640 or 1620 cm^{-1}, which suggested that the binding mechanisms between mineral and organic fractions may be different from those in the Ferrasol (Figure 5.4b). The organic peak at 1400 cm^{-1} remained consistent, which was assigned to the deformation vibration of C-H or O-H bonds. Similar contribution of mineral peaks observed in the Vertisol fractions, with dominant Si-O and Al-O peaks from kaolinite and montmorillonite.

The OC composition varied between the two soil types, with the Ferrasol fractions exhibiting a greater abundance of aliphatic-, carboxylic- and amide-like compounds. This can be attributed to their greater OC concentration in the Ferralsol. Fe/Al oxides in Ferralsol play an important role to engage in more diverse interactions than phyllosilicates, owing to their variable changed surfaces and higher specific surface area (Barré et al., 2014; Filimonova et al., 2016). The OC concentrations in the MAOM and subsurface fractions were lower than those of POM and surface fractions, therefore, the greater abundance of these compounds may be attributed to intensive mineral-organic interactions governed by the differences in their mineralogical composition. There was a little minimal difference in the OC compositions of POM and MAOM fractions of the Vertisol. The slightly greater abundance of aliphatic-like compounds in the surface sample may be due to its higher OC concentration.

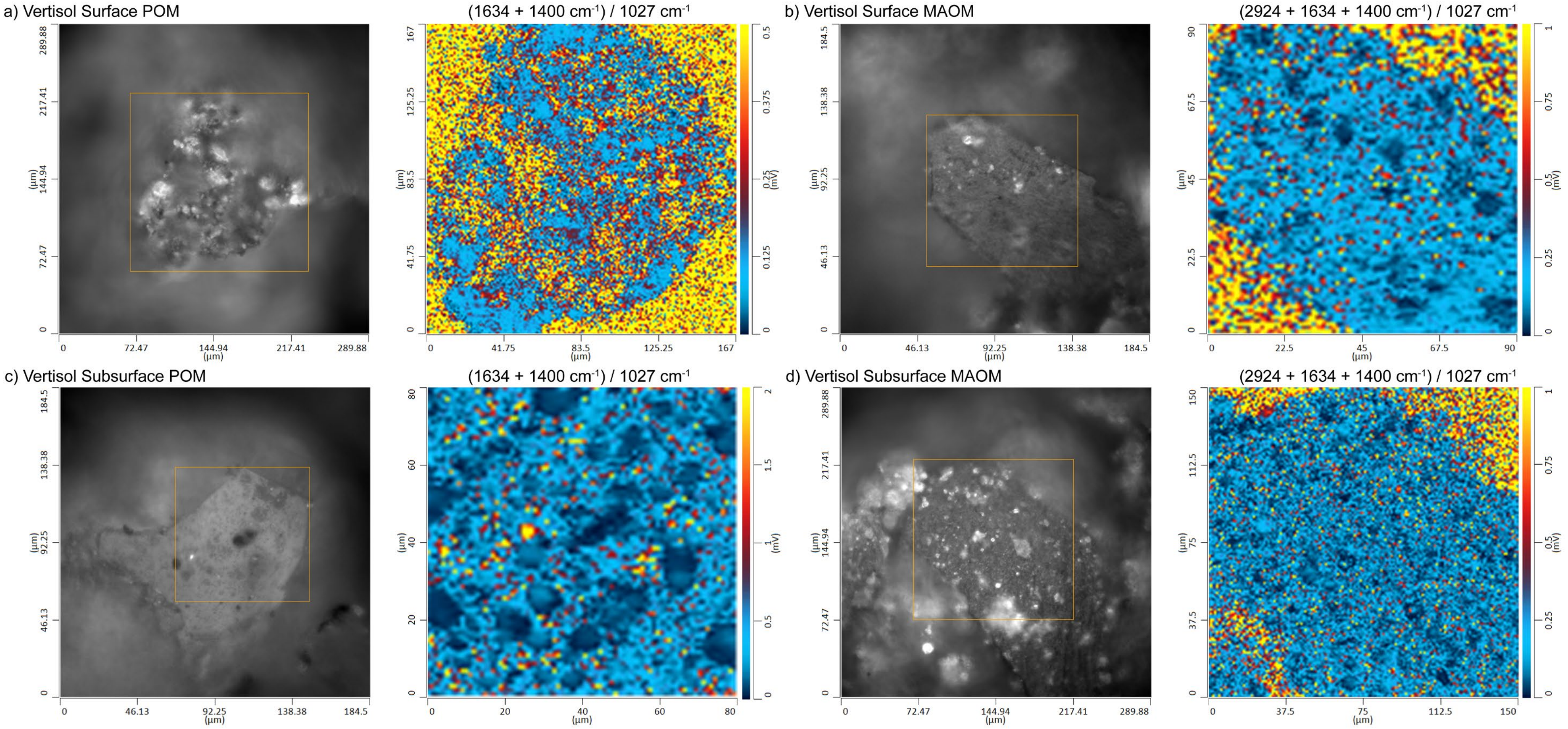

Figure 5.6 Microscopy images and organic bands hotspot mappings based on OPTIR absorbance ratios in the Vertisol. The ratio (1634 + 1400 cm^{-1}) / 1027 cm^{-1} was employed for particulate organic matter (POM) and (2924 + 1634 + 1400 cm^{-1}) / 1027 cm^{-1} for mineral associated organic matter (MAOM) in surface (a, b) and subsurface (b, d). Corresponding OPTIR data with average spectra and a zoomed-in view of organic region are shown at the bottom.

OPTIR directly revealed the key functional groups at synthetic mineral-organic complexes, where only low molecular weight model compounds were involved in the mineral-organic interactions. However, in natural mineral-organic complexes, the organic matter characteristics is very complex involving numerous compounds of varying compositions. OPTIR cannot clearly identify and distinguish organic compounds in the POM and MAOM fractions. This is consistent with Jamoteau et al. (2025) who demonstrated that OPTIR has lower detection sensitivity for higher molecular weight compounds compared to lower molecular weight compounds due to their different thermal diffusivity (Mandelis, 1991). Nevertheless, OPTIR identified additional organic band frequencies as compared to ATR-FTIR greater insights into the organic groups involved in mineral-organic complexes.

In this study, the POM and MAOM fractions pressed to obtain flat surfaces for OPTIR measurements and thus do not represent their natural state. OPTIR is a valuable technique to determine the spatial distribution of organic carbon fractions within natural mineral-organic complexes. It can image and distinguish the physical boundaries of mineral-organic interfaces at submicron level (< 0.5 μm) with minimal sample preparation (Olson et al., 2020; Jubb et al., 2023; Liu et al., 2024; Jamoteau et al., 2025). The spatial distribution of OC fractions within mineral matrix can be investigated using other advanced analytical techniques, such as NanoSIMS and synchrotron-based spectroscopies, including IR spectroscopy (e.g., SR-FTIR microspectroscopy) and X-ray adsorption spectroscopy (e.g., near edge X-ray adsorption fine structure, NEXAFS) coupled with scanning transmission X-ray microscopy (STXM) (Lehmann and Solomon, 2010). However, these methods inevitably require extensive sample preparation steps, including but not limited to cryopreservation, resins embedding, and thin sectioning, which are impractical for large sample sets in the SOC sequestration studies and limitations in terms of limits of detection levels (Lv et al., 2022; Amelung et al., 2024).

5.4 Conclusion

The application of OPTIR microscopy in our study directly revealed the mineral-organic interaction mechanisms occurred within synthetic mineral-organic interfaces at fine-scale resolution. Compared to the conventional ATR-FTIR technique, OPTIR provided more detailed OC information, particularly for the key reactive functional groups involved in mineral-organic interactions, making it a powerful and valuable analytical tool for simulating mineral-organic interfaces. In our study, it demonstrated the mechanisms of model organic compound adsorptions on mineral surfaces, including electrostatic attraction, ligand exchange, H-bonding, cation bridging, π-π electron transfer, oxidation, and hydrophobic attractions, depending on the functional groups involved. The mineral mixture of phyllosilicates and iron oxides exhibited both negatively and positively charged surface hydroxyl groups on crystal facet or at the edges of octahedral sheet, as well as hydrophobic tetrahedral sheet, which favoured electrostatic attraction or ligand exchange with NH_3^+ and COO^- groups and hydrophobic attractions with alkyl and aromatic structures. Hydrogen or cations can act as bridges, connecting organic hydroxyl and phenol -OH groups with mineral surface sites via H-bonding and cation-bridging. Possibility oxidation of organic compounds by iron oxides and the self-assembly of organic compounds themselves may also occurred at the synthetic mineral-organic interfaces. These potential mineral-organic interaction mechanisms identified at synthetic mineral-organic interfaces may provide deeper insights into the fate of natural organic fractions in soil systems, including their movement, dynamics and bioavailability. In addition, OPTIR microscopic imaging at the submicron level can help identify spatial distribution of OM fractions within natural mineral-organic complexes. Although OPTIR provided similarly broad information on complex OM components as ATR-FTIR in POM and MAOM fractions, further refinement of the boundaries between OC and minerals using OPTIR in future studies is both suggested and encouraged. By directly identifying different mineral fractions in soil complexes, it would be possible to the specific compositions of OM fractions associated with the individual mineral fractions in natural condition. This will ultimately improve our understanding of the nature of SOM in terrestrial ecosystems and enhance knowledge of OC pools and flexes in soil environment.

This study compared the capabilities of OPTIR microscopy and ATR-FTIR spectroscopy in both synthetic and natural mineral-organic complexes and demonstrated that OPTIR is a rapid, reliable, and advanced non-invasive analytical technique for SOM characterisation. With the help of OPTIR, we now have a powerful analytical tool for resolving some of the most complex unknowns in SOC sequestration and climate change with greater precision and efficiency.

Acknowledgement

This research was funded by the Australian Research Council (ARC) Discovery Project (DP220103026) and the University of Sydney. The authors thank Dr. Michelle Wood for assistance with ATR-FTIR and OPTIR analysis, which was carried out at Sydney Analytical, a core research facility of the University of Sydney.

5.5 Appendix

Table S 5.1 The basic information of organic chemical compounds.

Chemicals	Formula	Molecular weight (g/mol)	CAS number	TC (and TN) concentration (mg/L)	pK_a	Functional groups	Chemical structure
1-hexanol	$C_6H_{14}O$	102.2	111-27-3	255.1	16.8	-OH	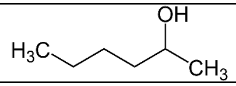
Hexanoic acid	$C_6H_{12}O_2$	116.2	142-62-1	285.5	4.9	-COOH	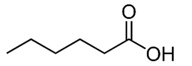
Citric acid	$C_6H_8O_7$	192.1	77-92-9	261.2	3.1 4.8 6.4	-COOH -OH	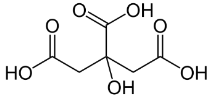
Phenol	C_6H_6O	94.1	108-95-2	308.2	10.0	-Ar* -OH	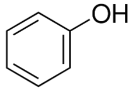
Benzoic acid	$C_7H_6O_2$	122.1	65-85-0	290.4	4.2	-Ar -COOH	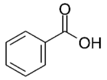
Gallic acid	$C_7H_6O_5$	170.1	149-91-7	260.2	4.0 8.7 11.4 13.0	-Ar -COOH -OH	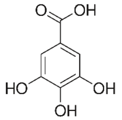
L-arginine	$C_6H_{14}N_4O_2$	174.2	74-79-3	235.3 (TN: 181.4)	13.8	$-NH_2$ -C=NH -COOH	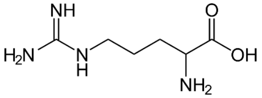
Adenine	$C_5H_5N_5$	135.1	73-24-5	295.6 (TN: 331.2)	3.6 10.3	$-NH_2$ -C=NH C=C	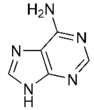
Pectin	$(C_6H_{10}O_7)_n$	50-150 kDa	9000-69-5	277.6	3.5	-OH -COOH C-O-C $-COOCH_3$	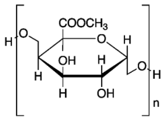

*Ar: aromatic ring.

Table S 5.2 The basic properties of selected minerals.

Minerals	TC (mg/g)	Specific Surface Area (m^2/g)	Pore Size Diameter (nm)	Pore Volume (cm^3/g)	Point of Zero Charge (PZC)
Kaolinite	3.2	20.5	30.9	0.43	<3.0
Montmorillonite	2.4	46.4	3.8	0.10	negative
Goethite	5.1	31.8	2.7	0.52	8.8

Table S 5.3 The organic and nitrogen contents (mg/g) of organic-mineral complexes, i.e., organic adsorbed onto mineral mixture after subtracting the OC content 3.3 mg/g of the mineral mixture and particulate organic matter (POM) and mineral associated organic matter (MAOM) separated from the surface (0-15 cm) and subsurface (15-30 cm) samples of a Ferralsol and a Vertisol.

Mineral organic associations		TC (mg/g)	TN (mg/g)
Hexanol		19.4	0.1
Hexanoic acid		15.5	0.2
Citric acid		30.7	0.3
Phenol		21.6	0.2
Benzoic acid		17.7	0.1
Gallic acid		19.0	0.4
Arginine		20.5	5.7
Adenine		35.9	12.2
Pectin		15.9	0.1
Ferralsol			
Surface	POM	91.7	7.3
	MAOM	67.3	5.7
Subsurface	POM	53.6	3.8
	MAOM	39.2	3.0
Vertisol			
Surface	POM	40.2	2.7
	MAOM	28.5	2.4
Subsurface	POM	17.5	0.9
	MAOM	20.1	1.5

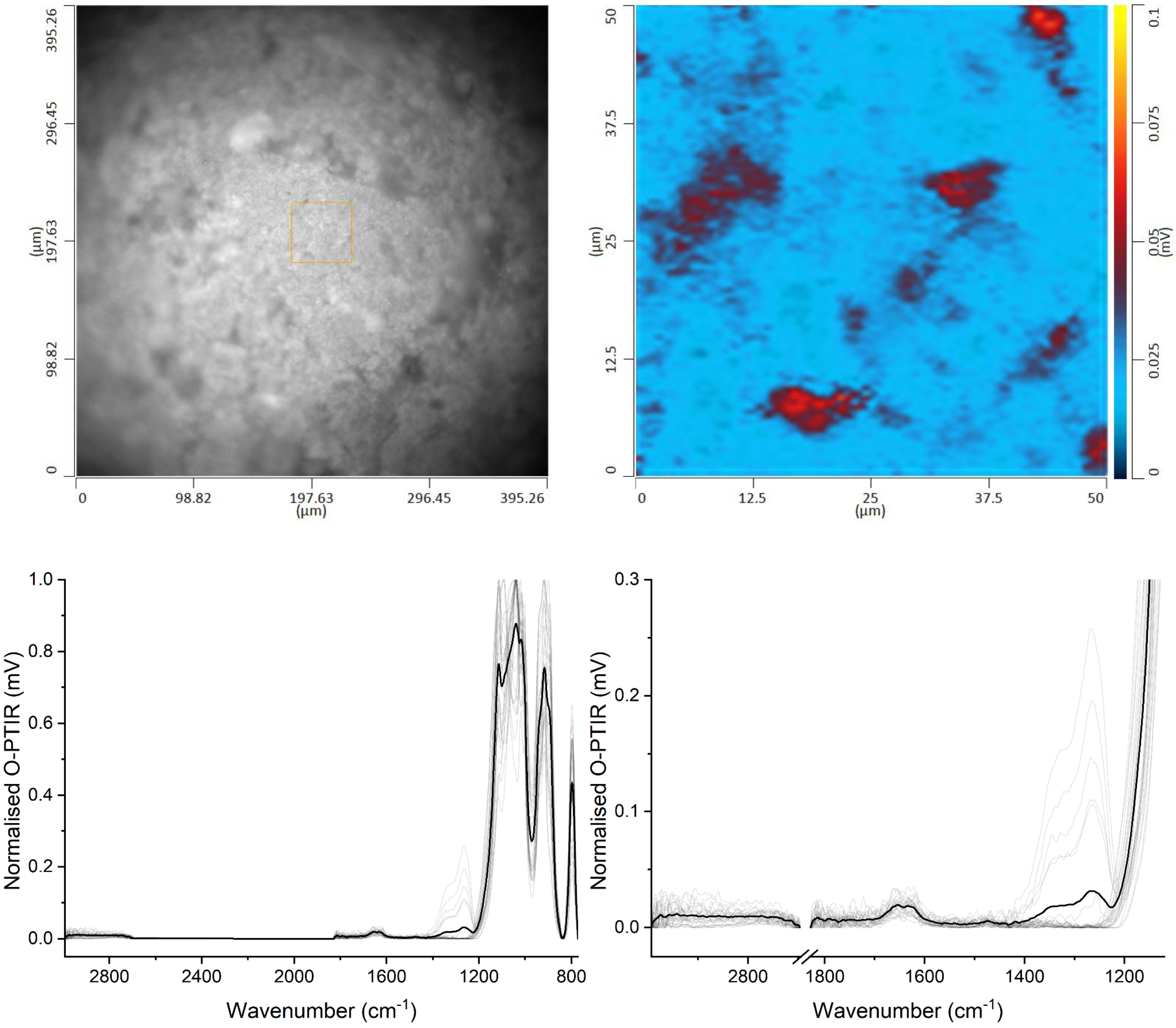

Figure S 5.1 Microscopy image of the mineral-organic complex of hexanol (top left), OPTIR spectral image derived from the ratio of (1660 + 1624 + 1337 + 1288 cm^{-1}) to 1027 cm^{-1} (top right), and associated OPTIR spectra for the hotspots of OC components between 2993 and 771 cm^{-1} (bottom left) and zoomed-in spectra (bottom right).

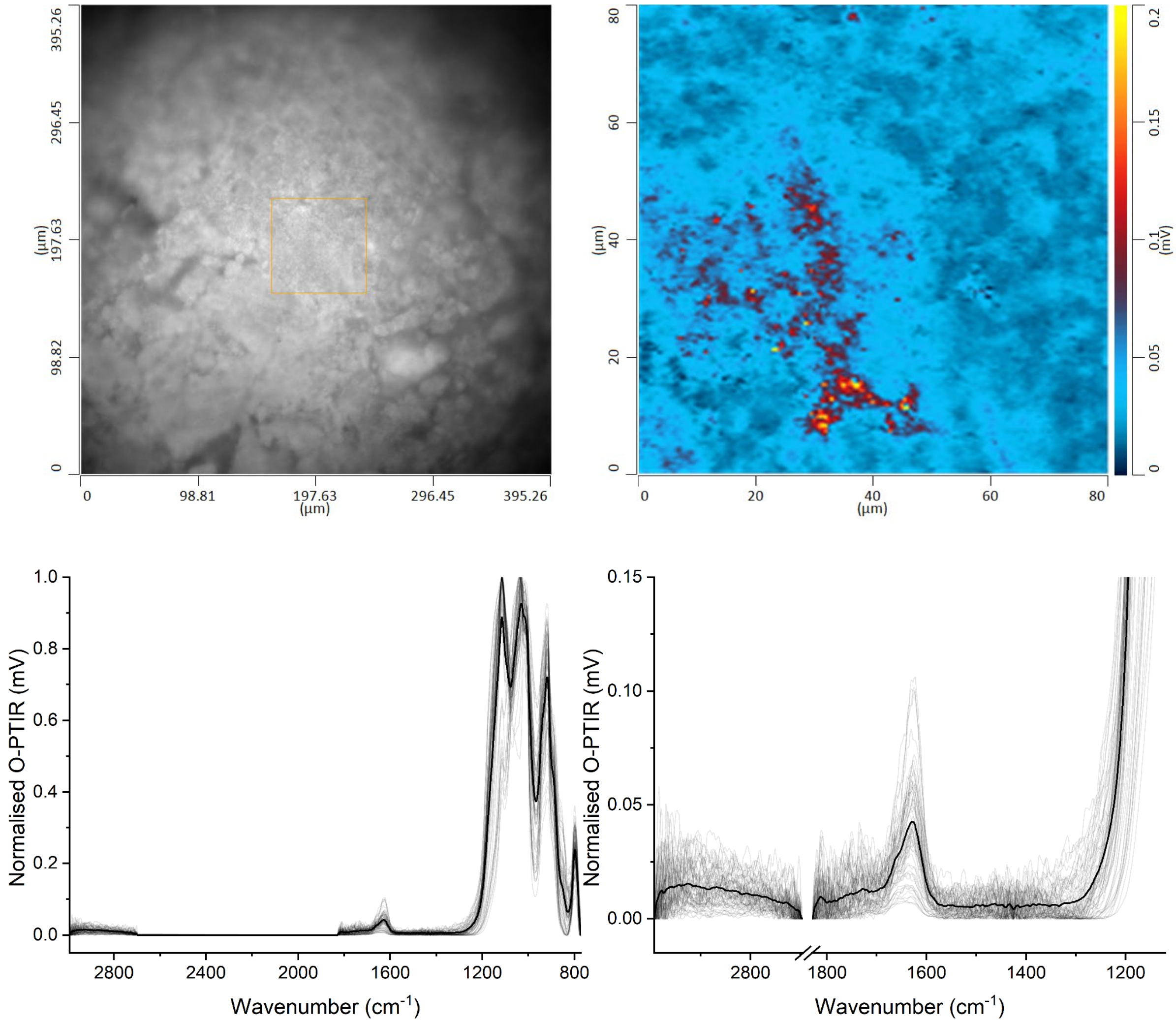

Figure S 5.2 Microscopy image of the mineral-organic complex of hexanoic acid (top left), OPTIR spectral image derived from the ratio of 1624 cm^{-1} to 1027 cm^{-1} (top right), and associated OPTIR spectra for the hotspots of OC components between 2993 and 771 cm^{-1} (bottom left) and zoomed-in spectra (bottom right).

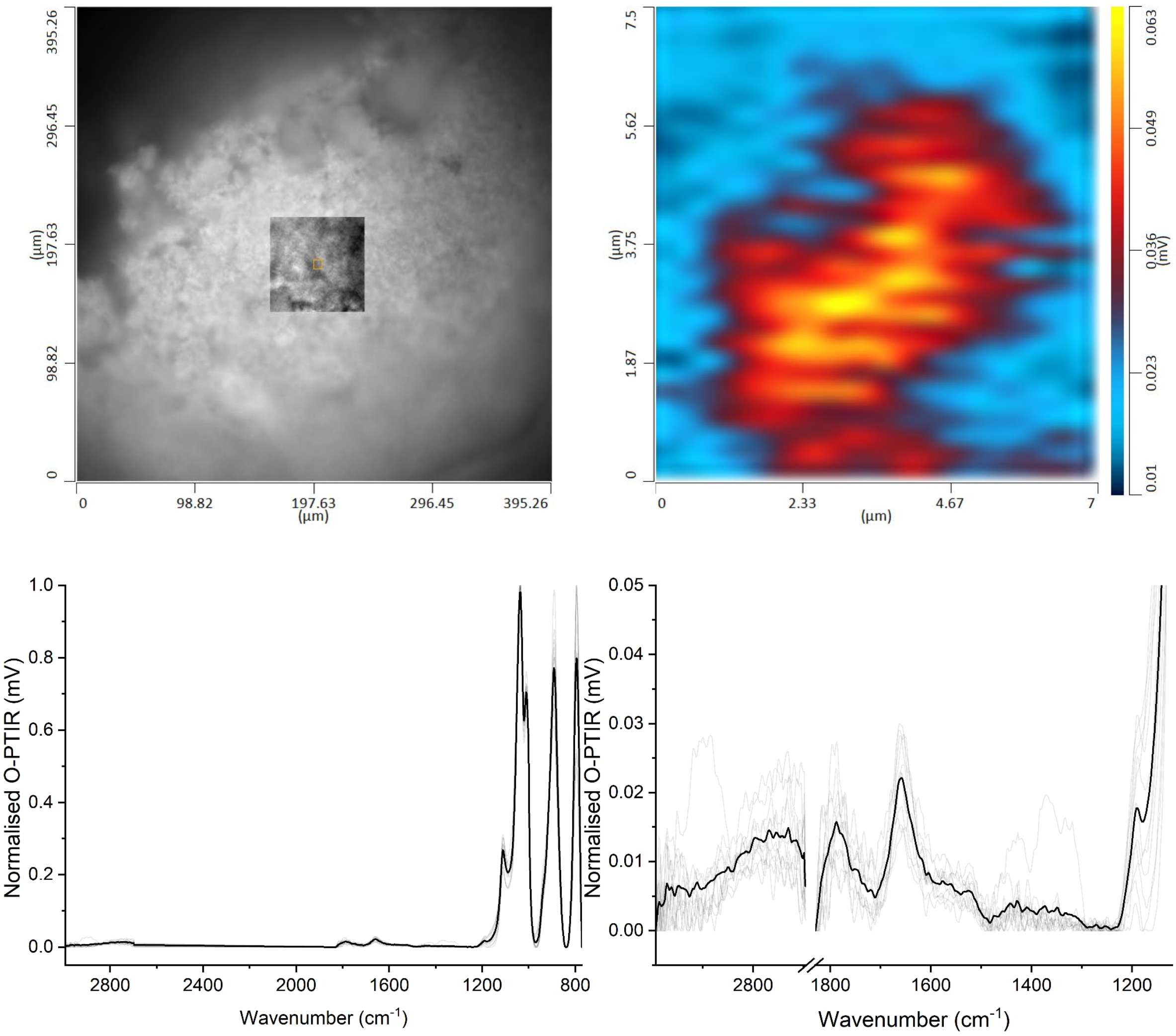

Figure S 5.3 Microscopy image of the mineral-organic complex of citric acid (top left), OPTIR spectral image derived from the ratio of (1788+1655 cm^{-1}) to 1027 cm^{-1} (top right), and associated OPTIR spectra for the hotspots of OC components between 2993 and 771 cm^{-1} (bottom left) and zoomed-in spectra (bottom right).

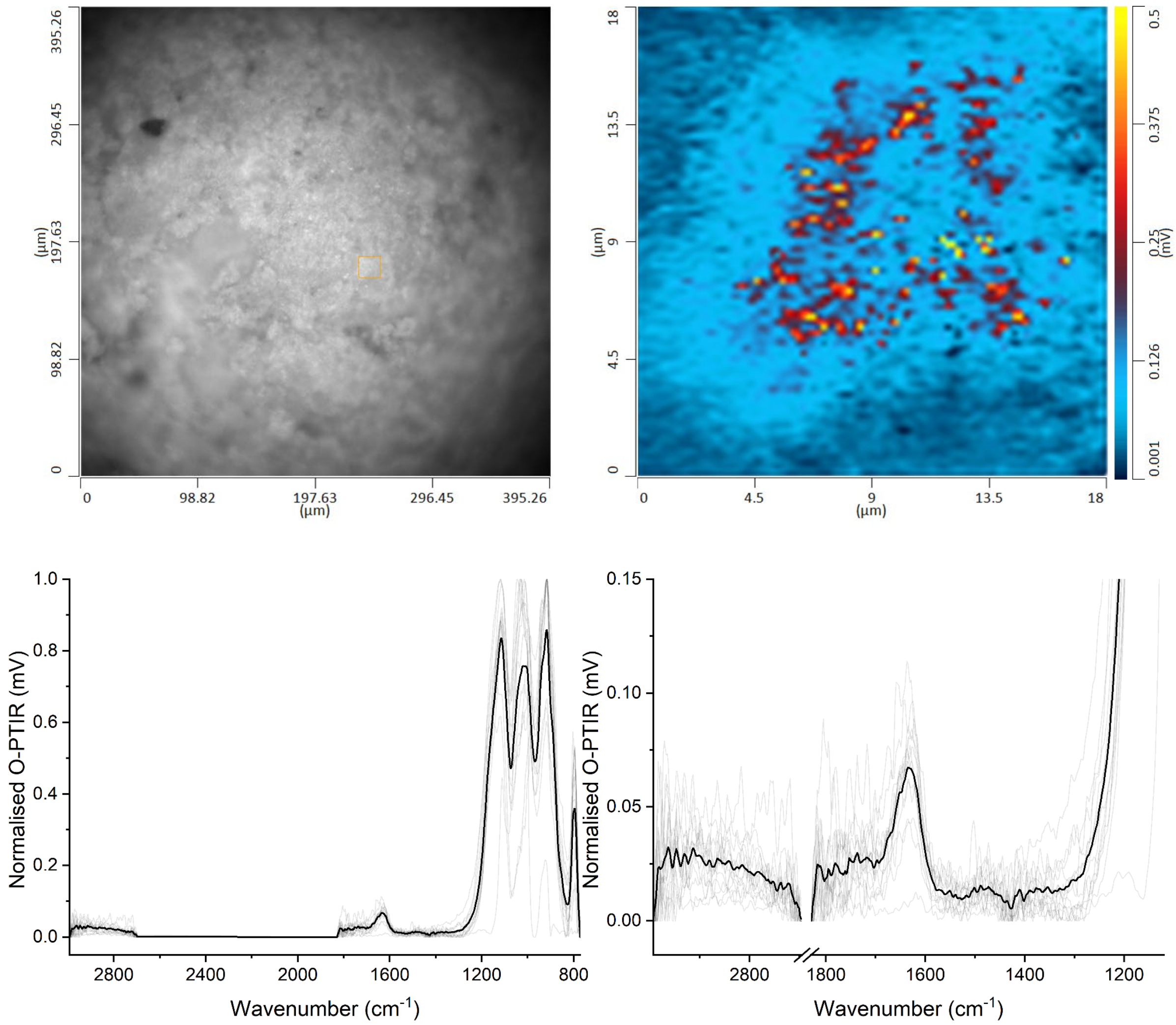

Figure S 5.4 Microscopy image of the mineral-organic complex of phenol (top left), OPTIR spectral image derived from the ratio of 1624 cm^{-1} to 1027 cm^{-1} (top right), and associated OPTIR spectra for the hotspots of OC components between 2993 and 771 cm^{-1} (bottom left) and zoomed-in spectra (bottom right).

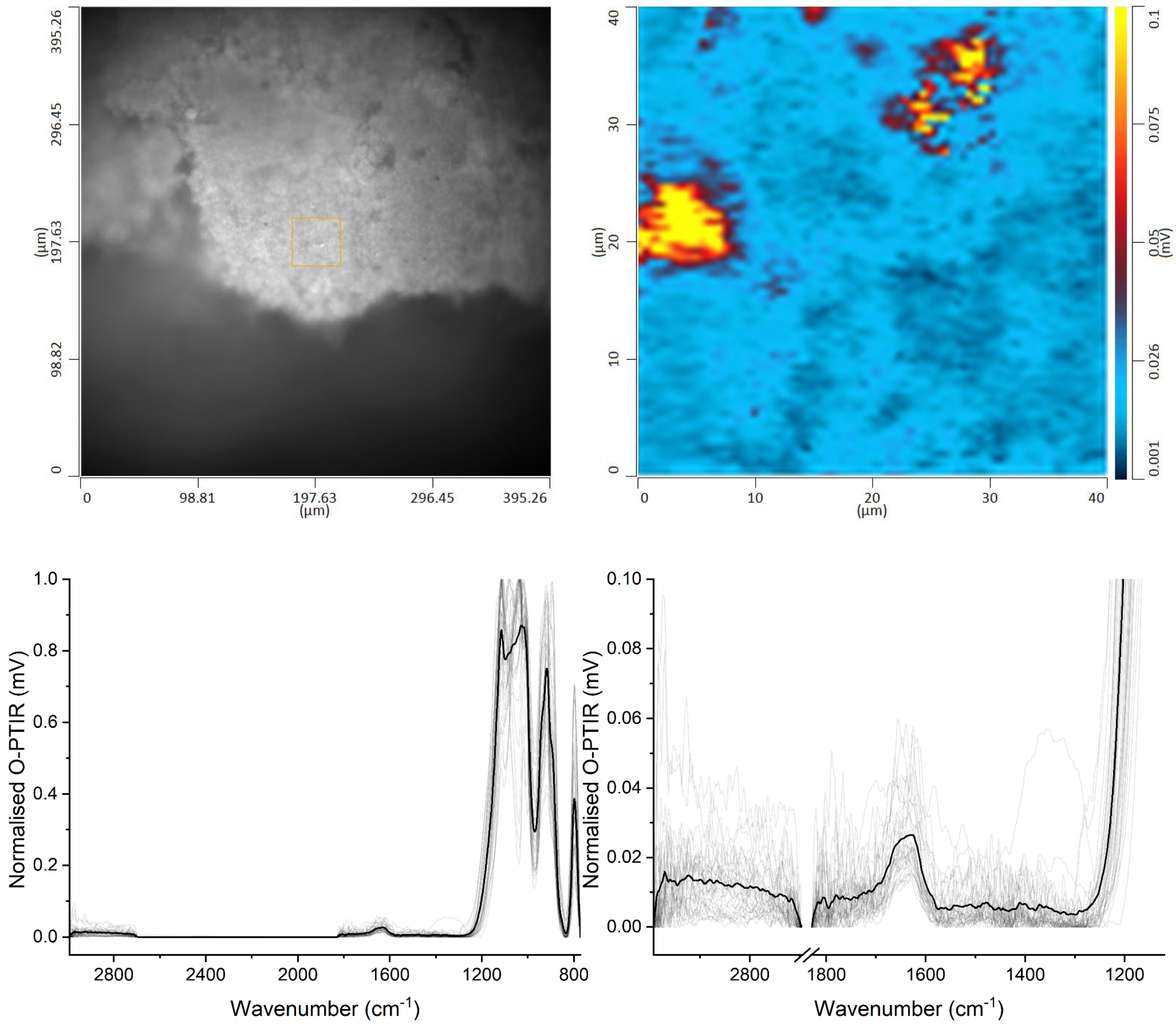

Figure S 5.5 Microscopy image of the mineral-organic complex of benzoic acid (top left), OPTIR spectral image derived from the ratio of 1624 cm^{-1} to 1027 cm^{-1} (top right), and associated OPTIR spectra for the hotspots of OC components between 2993 and 771 cm^{-1} (bottom left) and zoomed-in spectra (bottom right).

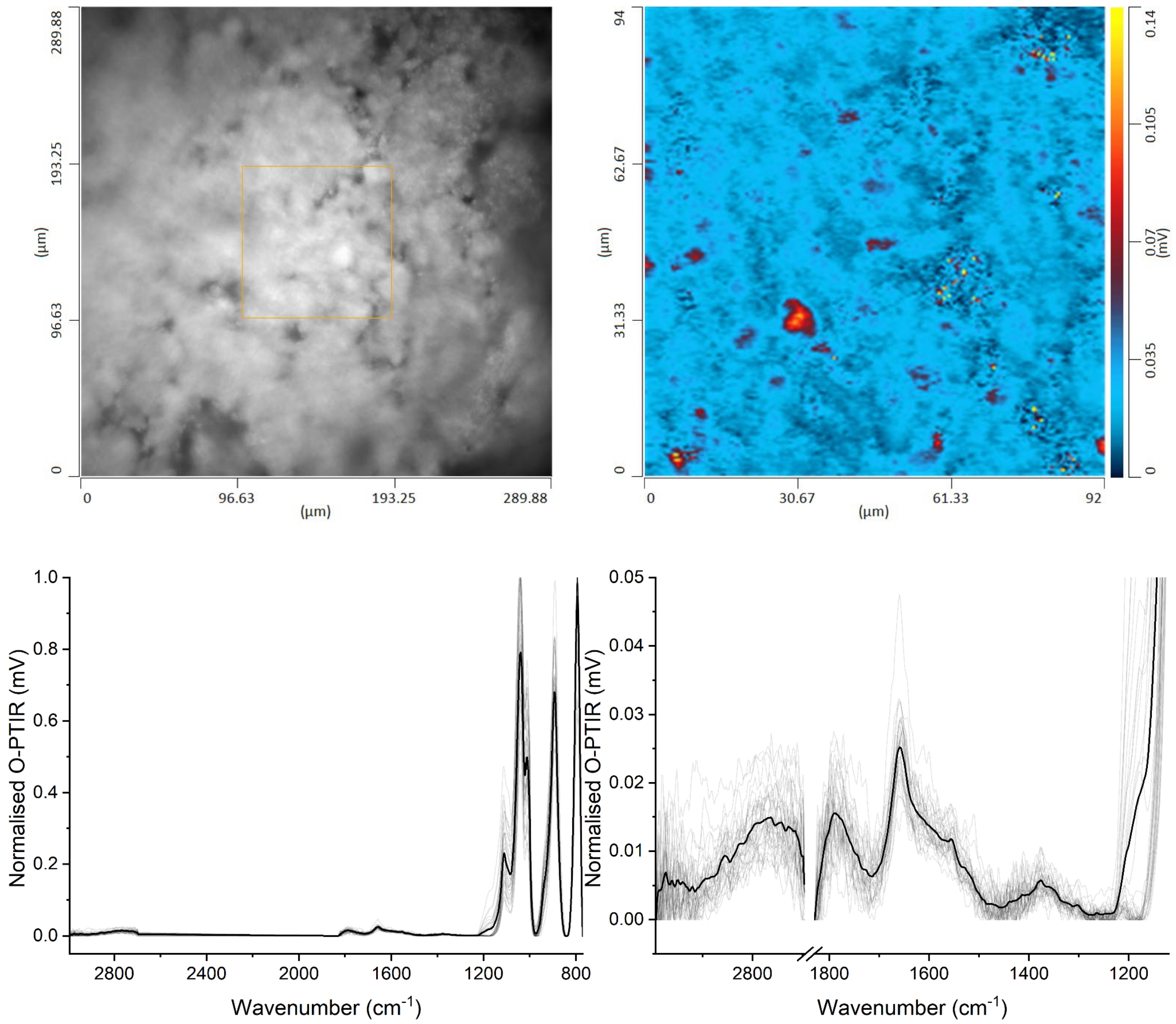

Figure S 5.6 Microscopy image of the mineral-organic complex of gallic acid (top left), OPTIR spectral image derived from the ratio of (1788 + 1660 cm^{-1}) to 1027 cm^{-1} (top right), and associated OPTIR spectra for the hotspots of OC components between 2993 and 771 cm^{-1} (bottom left) and zoomed-in spectra (bottom right).

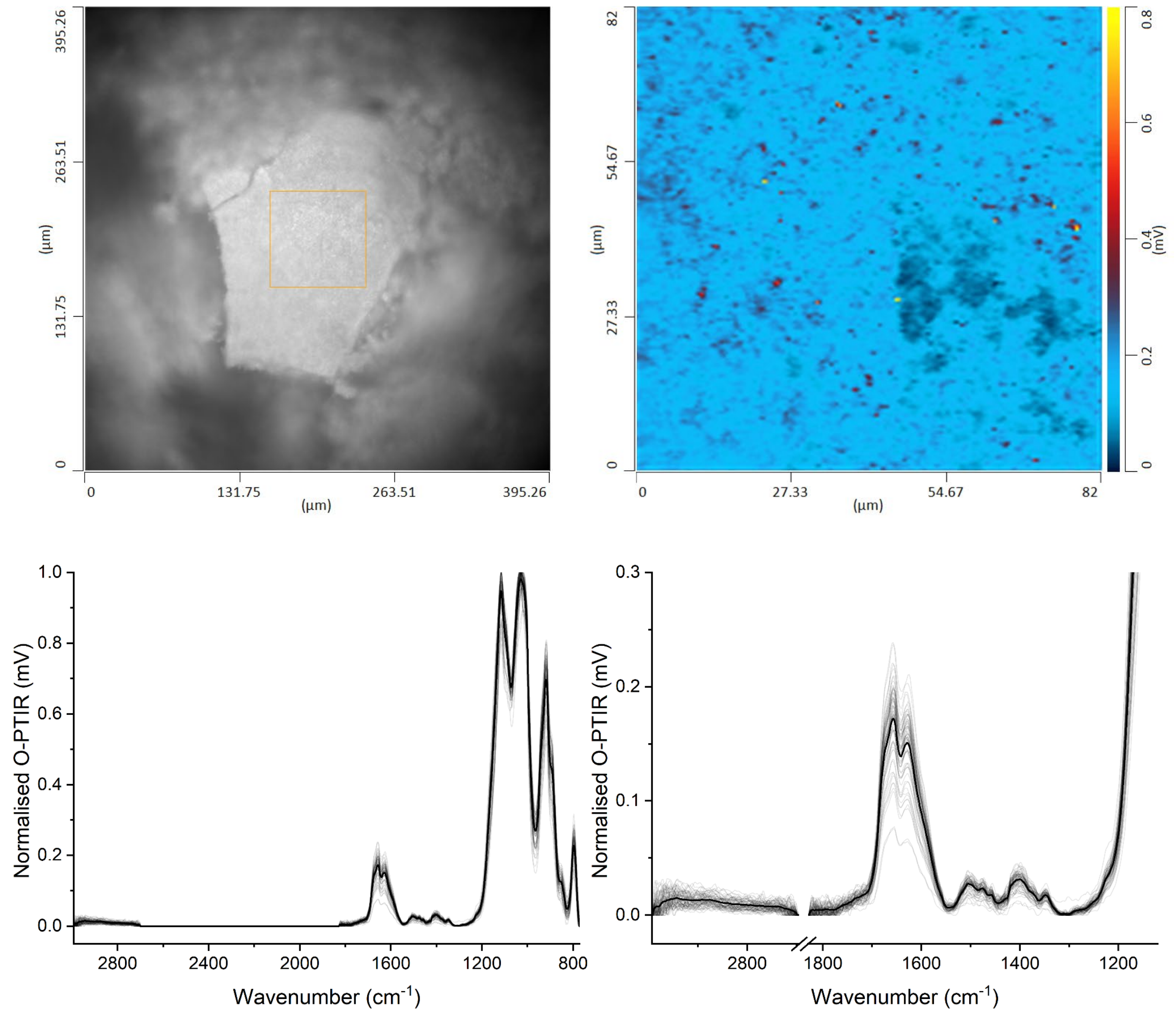

Figure S 5.7 Microscopy image of the mineral-organic complex of arginine (top left), OPTIR spectral image derived from the ratio of (1660 + 1624 + 1499 + 1400 + 1342 cm^{-1}) to 1027 cm^{-1} (top right), and associated OPTIR spectra for the hotspots of OC components between 2993 and 771 cm^{-1} (bottom left) and zoomed-in spectra (bottom right).

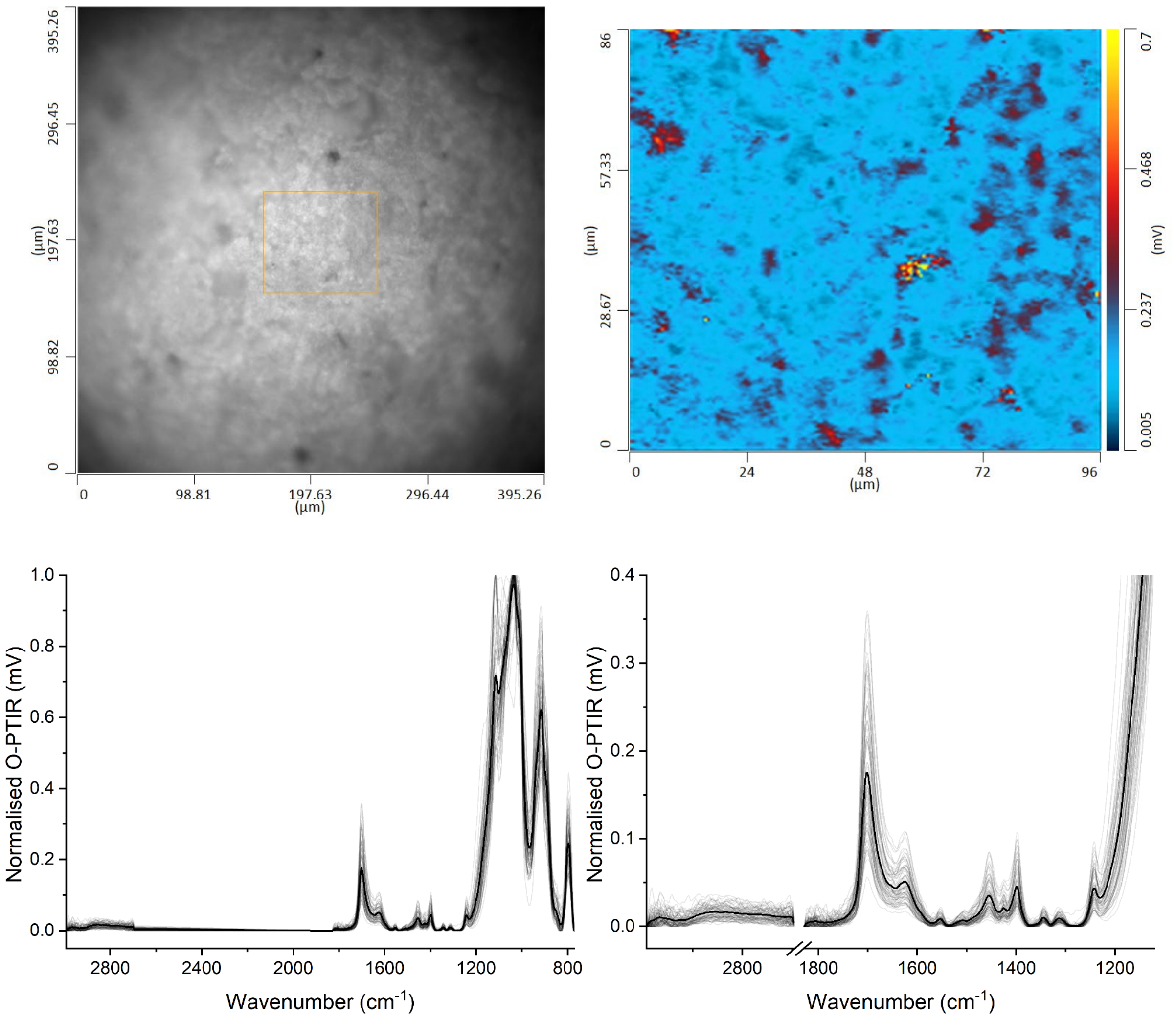

Figure S 5.8 Microscopy image of the mineral-organic complex of adenine (top left), OPTIR spectral image derived from the ratio of (1700 + 1624 + 1451 + 1400 + 1241 cm^{-1}) to 1027 cm^{-1} (top right), and associated OPTIR spectra for the hotspots of OC components between 2993 and 771 cm^{-1} (bottom left) and zoomed-in spectra (bottom right).

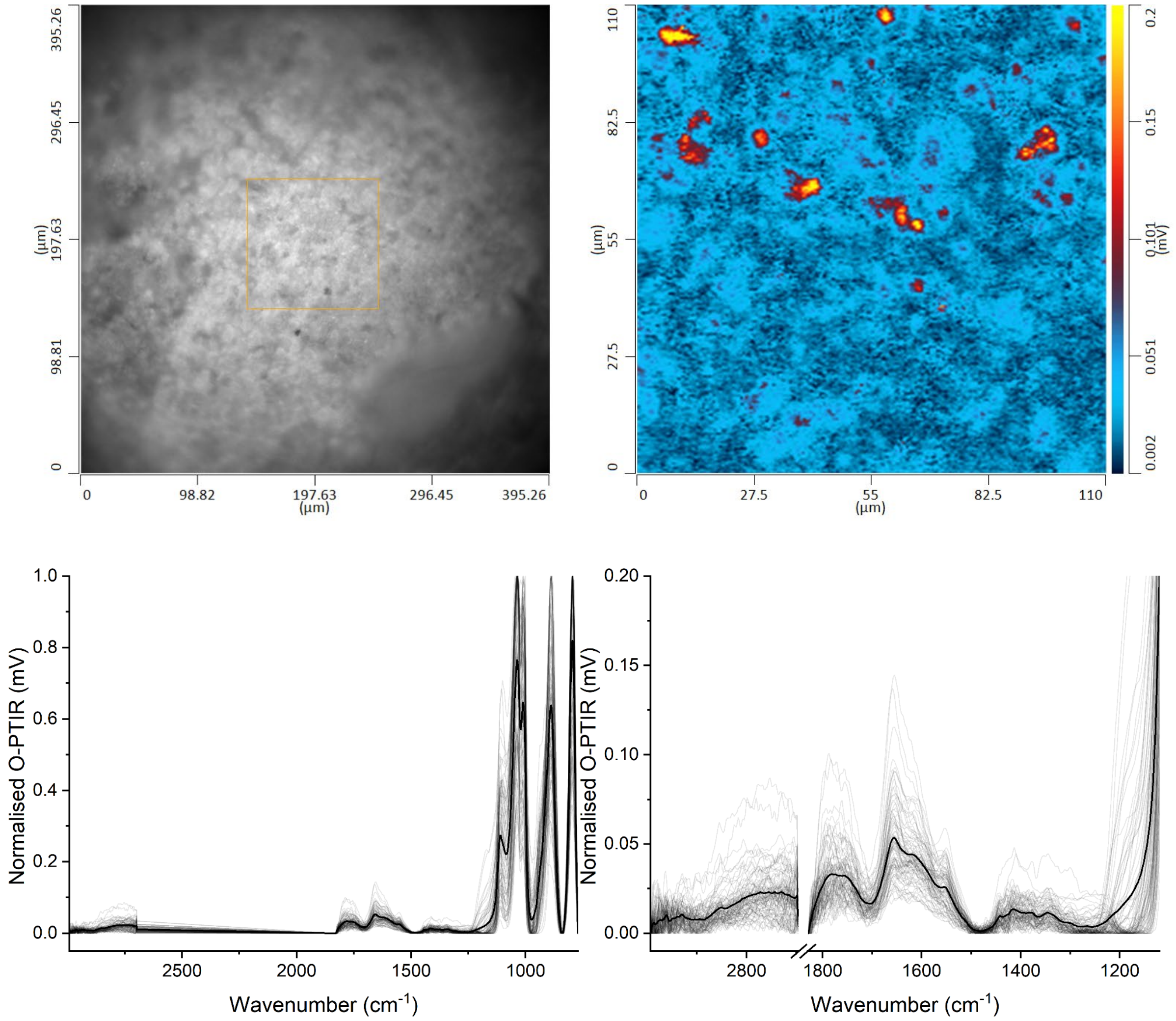

Figure S 5.9 Microscopy image of the mineral-organic complex of pectin (top left), OPTIR spectral image derived from the ratio of (1788 + 1660 cm^{-1}) to 1027 cm^{-1} (top right), and associated OPTIR spectra for the hotspots of OC components between 2993 and 771 cm^{-1} (bottom left) and zoomed-in spectra (bottom right).

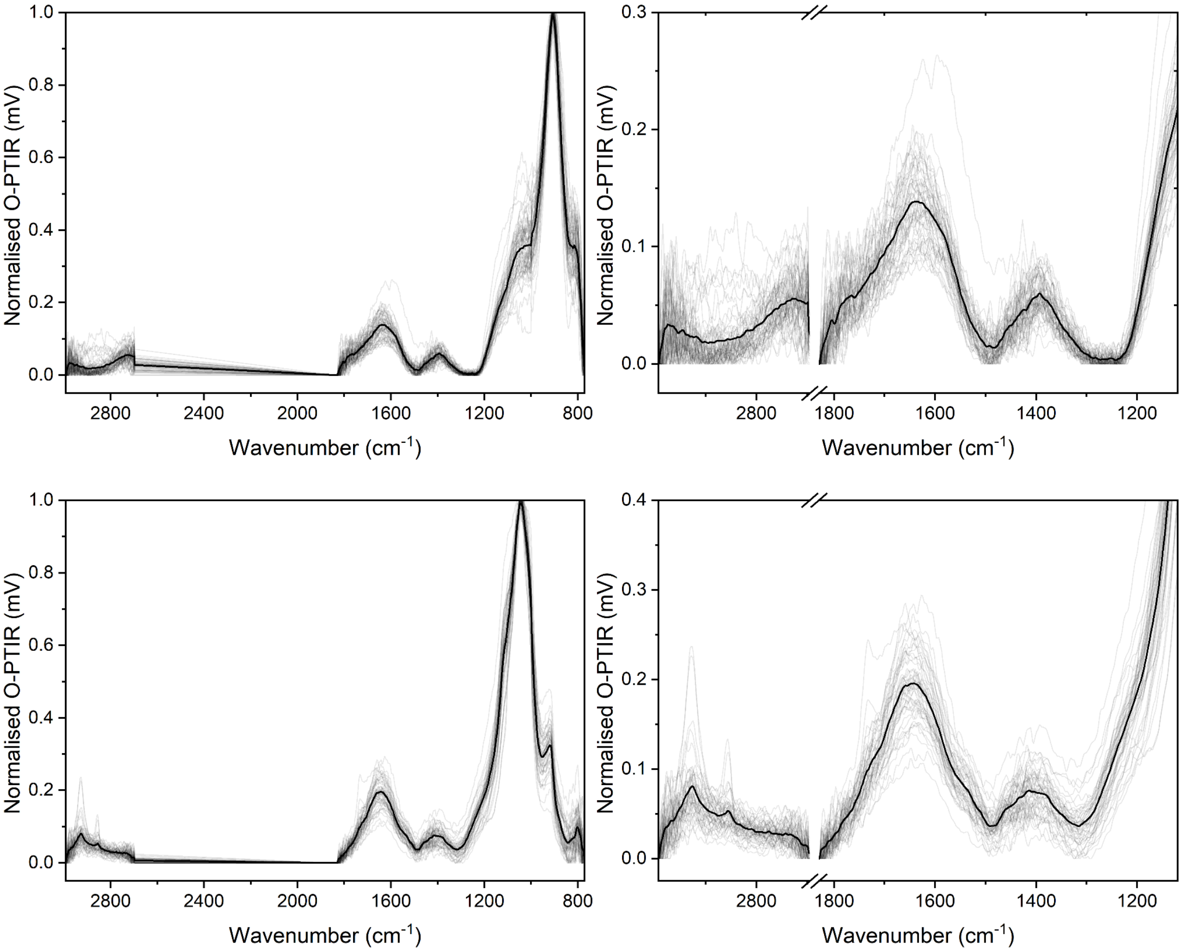

Figure S 5.10 OPTIR spectra for POM (top) and MAOM (bottom) fractions in surface Ferrasol between 2993-771 cm^{-1} and zoomed-in spectra.

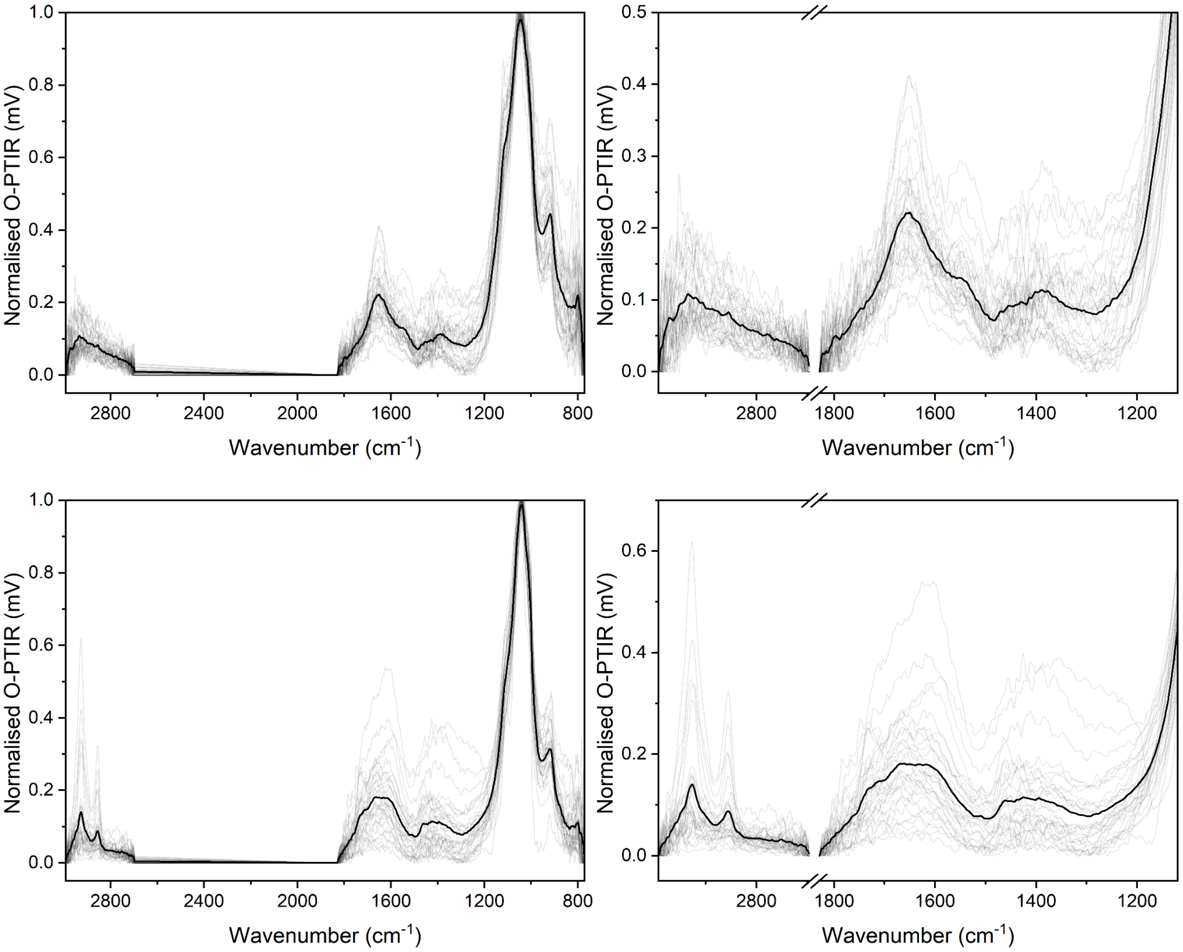

Figure S 5.11 OPTIR spectra for POM (top) and MAOM (bottom) fractions in subsurface Ferrasol between 2993-771 cm^{-1} and zoomed-in spectra.

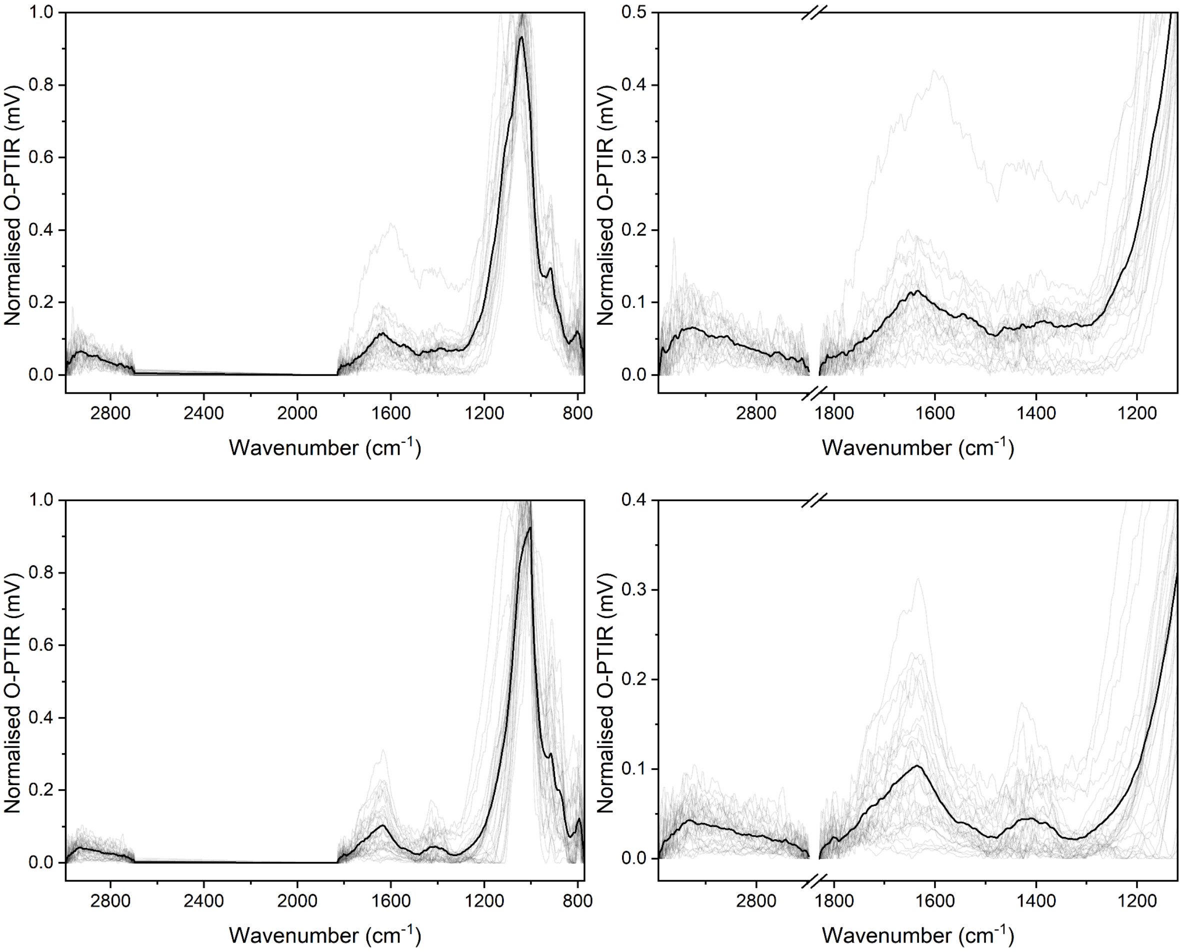

Figure S 5.12 OPTIR spectra for POM (top) and MAOM (bottom) fractions in surface Vertisol between 2993-771 cm^{-1} and zoomed-in spectra.

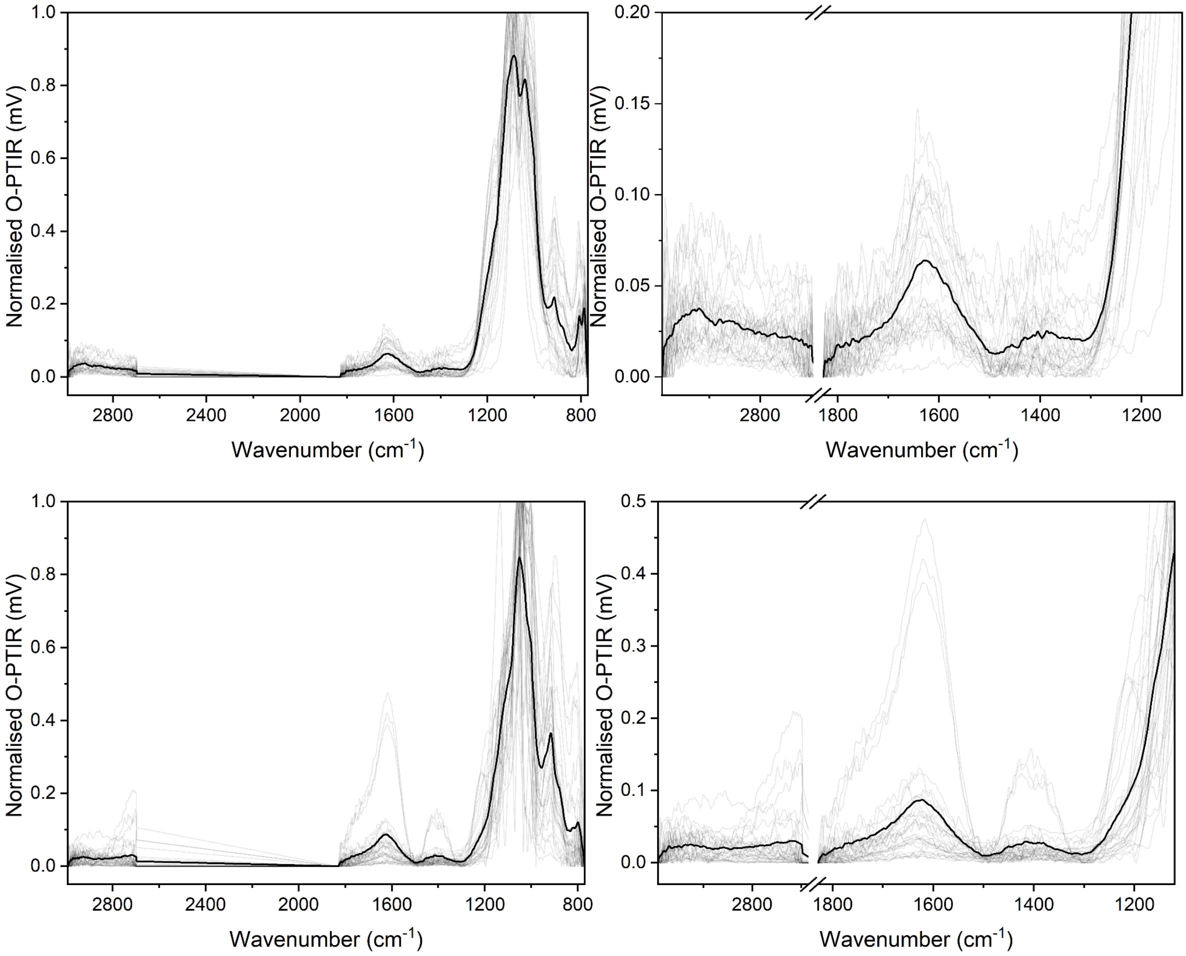

Figure S 5.13 OPTIR spectra for POM (top) and MAOM (bottom) fractions in subsurface Vertisol between 2993-771 cm^{-1} and zoomed-in spectra.

Table S 5.4 Band frequencies (cm^{-1}) of mineral and organic functional groups in mineral-organic complexes observed by ATR-FTIR and OPTIR spectroscopy.

Wavenumber (cm^{-1})	ATR-FTIR			OPTIR		
	Minerals	Organic	The ratio of complexes to minerals	Minerals	Organic	The ratio of complexes to minerals
Hexanol	3697, 3651, 3623, 1115, 1027, 1007, 913, 790, 746, 689, 602	1195	1275, 1195, 1144	1115, 1040, 1007, 913,796	1275	1338, 1275, 1144, 975, 868, 808
Hexanoic Acid	3697, 3651, 3623, 1115, 1027, 1007, 913, 790, 746, 689, 602	1195	1720, 1580, 1275, 1195, 1144, 841	1115, 1040, 1007, 913, 796	1620	1720, 1620, 1238, 1169, 975, 841
Citric Acid	3697, 3651, 3623, 1115, 1027, 1007, 913, 790, 746, 689, 602	1195	1580, 1195, 1100	1115, 1040, 1007, 891, 796	1787, 1664	1787, 1664, 868, 816
Phenol	3697, 3651, 3623, 1115, 1027, 1007, 913, 790, 746, 689, 602	1195	1275, 1195, 1144, 841	1115, 1040, 1007, 913, 796	1620, 1195	1730, 1620, 1481, 1400, 1338, 1275, 1238, 1195, 975, 841
Benzoic Acid	3697, 3651, 3623, 1115, 1027, 1007, 913, 790, 746, 689, 602	1195	1720, 1580, 1275, 1195, 1144, 1100, 841	1115, 1025, 913, 796	1620, 1100	1620, 1195, 1100, 975, 841
Gallic Acid	3697, 3651, 3623, 1115, 1027, 1007, 913, 790, 746, 689, 602	1195	1580, 1275, 1195, 1144, 1100, 836	1115, 1040, 1007, 891, 796	1787, 1664	1787, 1664, 1580, 880, 816
Arginine	3697, 3651, 3623, 1115, 1027, 1007, 913, 790, 746, 689, 602	1702, 1558, 1474, 1267, 1195, 830	1720, 1580, 1275, 1223, 1195, 1144, 1100, 975, 841	1115, 1040, 1007, 913, 796	1664, 1620, 1474, 1400, 841	1664, 1620, 1502, 1338, 1223, 1169, 975, 841
Adenine	3697, 3651, 3623, 1115, 1027, 1007, 913, 790, 746, 689, 602	1702, 1195	1702, 1275, 1238, 1195, 1144, 841	1115, 1040, 1007, 913, 796	1702, 1620, 1452, 1400, 1238	1702, 1620, 1452, 1400, 1338, 1238, 1195, 1144, 841
Pectin	3697, 3651, 3623, 1115, 1027, 1007, 913, 790, 746, 689, 602	1195	1275, 1195, 1144, 1100, 836	1115, 1040, 1007, 891, 796	1787, 1664	1787, 1664, 1600, 1544, 1400, 1338, 868, 816

References

Ahmat, A.M., Thiebault, T.,Guégan, R., 2019. Phenolic acids interactions with clay minerals: a spotlight on the adsorption mechanisms of gallic acid onto montmorillonite. *Applied Clay Science 180*, 105188.

Amelung, W., Tang, N., Siebers, N., Aehnelt, M., Eusterhues, K., Felde, V.J.M.N.L., Guggenberger, G., Kaiser, K., Kögel-Knabner, I., Klumpp, E., Knief, C., Kruse, J., Lehndorff, E., Mikutta, R., Peth, S., Ray, N., Prechtel, A., Ritschel, T., Schweizer, S.A., Woche, S.K., Wu, B.,Totsche, K.U., 2024. Architecture of soil microaggregates: advanced methodologies to explore properties and functions. *Journal of Plant Nutrition and Soil Science 187*(1), 17-50.

Avneri-Katz, S., Young, R.B., McKenna, A.M., Chen, H., Corilo, Y.E., Polubesova, T., Borch, T.,Chefetz, B., 2017. Adsorptive fractionation of dissolved organic matter (DOM) by mineral soil: macroscale approach and molecular insight. *Organic Geochemistry 103*, 113-124.

Azimzadeh, B.,Martínez, C.E., 2024. Unraveling the role of polysaccharide-goethite associations on glyphosate' adsorption–desorption dynamics and binding mechanisms. *Journal of Colloid and Interface Science 653*, 1283-1292.

Barré, P., Fernandez-Ugalde, O., Virto, I., Velde, B.,Chenu, C., 2014. Impact of phyllosilicate mineralogy on organic carbon stabilization in soils: incomplete knowledge and exciting prospects. *Geoderma 235-236*, 382-395.

Baú, J.P.T., Carneiro, C.E.A., de Souza Junior, I.G., de Souza, C.M.D., da Costa, A.C.S., di Mauro, E., Zaia, C.T.B.V., Coronas, J., Casado, C., de Santana, H.,Zaia, D.A.M., 2012. Adsorption of adenine and thymine on zeolites: FT-IR and EPR spectroscopy and X-ray diffractometry and SEM studies. *Origins of Life and Evolution of Biospheres 42*(1), 19-29.

Bellamy, L.J., 1975a. Alcohols and phenols. In: L. J. Bellamy (Ed.), *The Infra-red Spectra of Complex Molecules.* Springer Netherlands, pp. 107-128.

Bellamy, L.J., 1975b. Alkanes. In: L. J. Bellamy (Ed.), *The Infra-red Spectra of Complex Molecules.* Springer Netherlands, pp. 13-36.

Bellamy, L.J., 1975c. Amines and Imines. In: L. J. Bellamy (Ed.), *The Infra-red Spectra of Complex Molecules.* Springer Netherlands, pp. 277-293.

Bu, X., Wang, L., Ma, W., Yu, X., McDowell, W.H.,Ruan, H., 2010. Spectroscopic characterization of hot-water extractable organic matter from soils under four different vegetation types along an elevation gradient in the Wuyi mountains. *Geoderma 159*(1), 139-146.

Cambier, P., 1986. Infrared study of goethites of varying crystallinity and particle size: I. Interpretation of OH and lattice vibration frequencies. *Clay Minerals 21*(2), 191-200.

Chefetz, B., Eldad, S.,Polubesova, T., 2011. Interactions of aromatic acids with montmorillonite: Ca2+- and Fe3+-saturated clays versus Fe3+–Ca2+-clay system. *Geoderma 160*(3), 608-613.

Chen, S., Klotzbücher, T., Lechtenfeld, O.J., Hong, H., Liu, C., Kaiser, K., Mikutta, C.,Mikutta, R., 2022. Legacy effects of sorption determine the formation efficiency of mineral-associated soil organic matter. *Environmental Science & Technology 56*(3), 2044-2053.

Chi, J., Fan, Y., Wang, L., Putnis, C.V.,Zhang, W., 2022. Retention of soil organic matter by occlusion within soil minerals. *Reviews in Environmental Science and Bio/Technology 21*(3), 727-746.

Chia, C.H., Gong, B., Joseph, S.D., Marjo, C.E., Munroe, P.,Rich, A.M., 2012. Imaging of mineral-enriched biochar by FTIR, Raman and SEM–EDX. *Vibrational Spectroscopy 62*, 248-257.

Cotrufo, M.F., Ranalli, M.G., Haddix, M.L., Six, J.,Lugato, E., 2019. Soil carbon storage informed by particulate and mineral-associated organic matter. *Nature Geoscience 12*(12), 989-994.

Dong, F., Guo, Y., Liu, M., Zhou, L., Zhou, Q.,Li, H., 2018. Spectroscopic evidence and molecular simulation investigation of the bonding interaction between lysine and montmorillonite: Implications for the distribution of soil organic nitrogen. *Applied Clay Science 159*, 3-9.

Doumenq, P., Guiliano, M., Bertrand, J.C.,Mille, G., 1990. GC/FT-IR analysis of fatty acid methyl esters. *Applied Spectroscopy 44*(8), 1355-1359.

Fang, Y., Singh, B., Singh, B.P.,Krull, E., 2014. Biochar carbon stability in four contrasting soils. *European Journal of Soil Science 65*(1), 60-71.

Farmer, V.C., 1974a. The anhydrous oxide minerals. In: *The Infrared Spectra of Minerals.* Mineralogical Society of Great Britain and Ireland, pp. 0.

Farmer, V.C., 1974b. The layer silicates. In: *The Infrared Spectra of Minerals.* Mineralogical Society of Great Britain and Ireland, pp. 0.

Feng, X., Simpson, A.J.,Simpson, M.J., 2005. Chemical and mineralogical controls on humic acid sorption to clay mineral surfaces. *Organic Geochemistry 36*(11), 1553-1566.

Filimonova, S., Kaufhold, S., Wagner, F.E., Häusler, W.,Kögel-Knabner, I., 2016. The role of allophane nano-structure and Fe oxide speciation for hosting soil organic matter in an allophanic Andosol. *Geochimica et Cosmochimica Acta 180*, 284-302.

Galvez, M.E., Fischer, W.W., Jaccard, S.L.,Eglinton, T.I., 2020. Materials and pathways of the organic carbon cycle through time. *Nature Geoscience 13*(8), 535-546.

Georgiou, K., Jackson, R.B., Vindušková, O., Abramoff, R.Z., Ahlström, A., Feng, W., Harden, J.W., Pellegrini, A.F.A., Polley, H.W., Soong, J.L., Riley, W.J.,Torn, M.S., 2022. Global stocks and capacity of mineral-associated soil organic carbon. *Nature Communications 13*(1), 3797.

González-Pérez, M., Vidal Torrado, P., Colnago, L.A., Martin-Neto, L., Otero, X.L., Milori, D.M.B.P.,Gomes, F.H., 2008. 13C NMR and FTIR spectroscopy characterization of humic acids in spodosols under tropical rain forest in southeastern Brazil. *Geoderma 146*(3), 425-433.

Guo, F., Li, D., Fein, J.B., Xu, J., Wang, Y., Huang, Q.,Rong, X., 2022. Roles of hydrogen bond and ion bridge in adsorption of two bisphenols onto montmorillonite: an experimental and DFT study. *Applied Clay Science 217*, 106406.

Hashizume, H., van der Gaast, S.,Theng, B.K.G., 2010. Adsorption of adenine, cytosine, uracil, ribose, and phosphate by Mg-exchanged montmorillonite. *Clay Minerals 45*(4), 469-475.

Henmi, T., Tange, K., Minagawa, T.,Yoshinaga, N., 1981. Effect of SiO2/Al2O3 ratio on the thermal reactions of allophane. II. infrared and X-ray powder diffraction data. *Clays and Clay Minerals 29*(2), 124-128.

Holman, H.-Y.N., 2010. Chapter 4 - Synchrotron infrared spectromicroscopy for studying chemistry of microbial activity in geologic materials. In: B. Singh and M. Gräfe (Eds.), *Developments in Soil Science.* Elsevier, pp. 103-130.

Jaber, M., Georgelin, T., Bazzi, H., Costa-Torro, F., Lambert, J.-F., Bolbach, G.,Clodic, G., 2014. Selectivities in adsorption and peptidic condensation in the (arginine and glutamic acid)/montmorillonite clay system. *The Journal of Physical Chemistry C 118*(44), 25447-25455.

Jamoteau, F., Kansiz, M., Unger, M.,Keiluweit, M., 2025. Probing mineral-organic interfaces in soils and sediments using optical photothermal infrared microscopy. *Environmental Science & Technology 59*(1), 501-512.

Jiang, C., Garg, S.,Waite, T.D., 2015. Hydroquinone-mediated redox cycling of iron and concomitant oxidation of hydroquinone in oxic waters under acidic conditions: comparison with iron–natural organic matter interactions. *Environmental Science & Technology 49*(24), 14076-14084.

Johnston, C.T.,Aochi, Y.O., 1996. Fourier transform infrared and raman spectroscopy. In: *Methods of Soil Analysis.* pp. 269-321.

Jones, E.,Singh, B., 2014. Organo-mineral interactions in contrasting soils under natural vegetation. *Frontiers in Environmental Science 2*. Original Research.

Jubb, A.M., Rebecca Stokes, M., McAleer, R.J., Hackley, P.C., Dillon, E.,Qu, J., 2023. Mapping ancient sedimentary organic matter molecular structure at nanoscales using optical photothermal infrared spectroscopy. *Organic Geochemistry 177*, 104569.

Kasprzhitskii, A., Lazorenko, G., Kharytonau, D.S., Osipenko, M.A., Kasach, A.A.,Kurilo, I.I., 2022. Adsorption mechanism of aliphatic amino acids on kaolinite surfaces. *Applied Clay Science 226*, 106566.

Keiluweit, M.,Kleber, M., 2009. Molecular-level interactions in soils and sediments: the role of aromatic π-systems. *Environmental Science & Technology 43*(10), 3421-3429.

Kelleher, B.P.,Simpson, A.J., 2006. Humic substances in soils: are they really chemically distinct? *Environmental Science & Technology 40*(15), 4605-4611.

Kitadai, N., Yokoyama, T.,Nakashima, S., 2009. In situ ATR-IR investigation of L-lysine adsorption on montmorillonite. *Journal of Colloid and Interface Science 338*(2), 395-401.

Kleber, M., Bourg, I.C., Coward, E.K., Hansel, C.M., Myneni, S.C.B.,Nunan, N., 2021. Dynamic interactions at the mineral–organic matter interface. *Nature Reviews Earth & Environment 2*(6), 402-421.

Kleber, M., Eusterhues, K., Keiluweit, M., Mikutta, C., Mikutta, R.,Nico, P.S., 2015. Chapter one - Mineral–organic associations: formation, properties, and relevance in soil environments. In: D. L. Sparks (Ed.), *Advances in Agronomy.* Academic Press, pp. 1-140.

Kleber, M.,Johnson, M.G., 2010. Chapter 3 - Advances in understanding the molecular structure of soil organic matter: implications for interactions in the environment. In: D. L. Sparks (Ed.), *Advances in Agronomy.* Academic Press, pp. 77-142.

Kramer, M.G.,Chadwick, O.A., 2018. Climate-driven thresholds in reactive mineral retention of soil carbon at the global scale. *Nature Climate Change 8*(12), 1104-1108.

Kubicki, J.D., Schroeter, L.M., Itoh, M.J., Nguyen, B.N.,Apitz, S.E., 1999. Attenuated total reflectance Fourier-transform infrared spectroscopy of carboxylic acids adsorbed onto mineral surfaces. *Geochimica et Cosmochimica Acta 63*(18), 2709-2725.

Kung, K.H.,McBride, M.B., 1988. Electron transfer processes between hydroquinone and iron oxides. *Clays and Clay Minerals 36*(4), 303-309.

Lackovic, K., Johnson, B.B., Angove, M.J.,Wells, J.D., 2003. Modeling the adsorption of citric acid onto Muloorina illite and related clay minerals. *Journal of Colloid and Interface Science 267*(1), 49-59.

Lehmann, J.,Solomon, D., 2010. Chapter 10 - Organic carbon chemistry in soils observed by synchrotron-based spectroscopy. In: B. Singh and M. Gräfe (Eds.), *Developments in Soil Science.* Elsevier, pp. 289-312.

Li, B., Liu, S., Guo, J.,Zhang, L., 2018. Interaction between low rank coal and kaolinite particles: a DFT simulation. *Applied Surface Science 456*, 215-220.

Li, J., Li, Q., Xu, Z.,Yang, X., 2024. Molecular simulation of adsorption behavior for phenol aqueous solution into layered graphene oxides. *Separation and Purification Technology 335*, 126215.

Li, Q., Chang, J., Li, L., Lin, X.,Li, Y., 2023. Research progress of nano-scale secondary ion mass spectrometry (NanoSIMS) in soil science: evolution, applications, and challenges. *Science of The Total Environment 905*, 167257.

Liu, X., Barres, O., Pironon, J., Unger, M., Beck, P., Fan, J.,Ostadhassan, M., 2024. Molecular fractionation of ancient organic compounds in deeply buried Halite crystals. *Analytical Chemistry 96*(42), 16493-16498.

Lock, P.A.,Skipper, N.T., 2007. Computer simulation of the structure and dynamics of phenol in sodium montmorillonite hydrates. *European Journal of Soil Science 58*(4), 958-966.

Lv, J., Huang, Z., Luo, L., Zhang, S.,Wang, Y., 2022. Advances in molecular and microscale characterization of soil organic matter: current limitations and future prospects. *Environmental Science & Technology 56*(18), 12793-12810.

Mandelis, A., 1991. Photothermal applications to the thermal analysis of solids. *Journal of thermal analysis 37*(5), 1065-1101.

McBride, M.B., 1987. Adsorption and oxidation of phenolic compounds by iron and manganese oxides. *Soil Science Society of America Journal 51*(6), 1466-1472.

Mikutta, R., Mikutta, C., Kalbitz, K., Scheel, T., Kaiser, K.,Jahn, R., 2007. Biodegradation of forest floor organic matter bound to minerals via different binding mechanisms. *Geochimica et Cosmochimica Acta 71*(10), 2569-2590.

Millman, E., Chatterjee, A., Parker, K.M.,Catalano, J.G., 2024. Cation exchange to montmorillonite induces selective adsorption of amino acids. *Geochimica et Cosmochimica Acta 372*, 181-195.

Molina, C., Kim, D., Mehndiratta, L., Lee, J., Madawala, C.K., Slade, J.H., Tivanski, A.V.,Grassian, V.H., 2025. Comparison of different vibrational spectroscopic probes (ATR-FTIR, O-PTIR, Micro-Raman, and AFM-IR) of lipids and other compounds found in environmental samples: case study of substrate-deposited sea spray aerosols.

ACS Measurement Science Au 5(1), 74-86.

Newcomb, C.J., Qafoku, N.P., Grate, J.W., Bailey, V.L.,De Yoreo, J.J., 2017. Developing a molecular picture of soil organic matter–mineral interactions by quantifying organo–mineral binding. *Nature Communications 8*(1), 396.

Nikolova, V., Ilieva, S., Galabov, B.,Schaefer, H.F., III, 2014. Experimental measurement and theory of substituent effects in π-hydrogen bonding: complexes of substituted phenols with benzene. *The Journal of Organic Chemistry 79*(15), 6823-6831.

Norén, K., Loring, J.S.,Persson, P., 2008. Adsorption of alpha amino acids at the water/goethite interface. *Journal of Colloid and Interface Science 319*(2), 416-428.

Norén, K.,Persson, P., 2007. Adsorption of monocarboxylates at the water/goethite interface: the importance of hydrogen bonding. *Geochimica et Cosmochimica Acta 71*(23), 5717-5730.

Olson, N.E., Xiao, Y., Lei, Z.,Ault, A.P., 2020. Simultaneous optical photothermal infrared (O-PTIR) and raman spectroscopy of submicrometer atmospheric particles. *Analytical Chemistry 92*(14), 9932-9939.

Parikh, S.J., Goyne, K.W., Margenot, A.J., Mukome, F.N.D.,Calderón, F.J., 2014. Chapter one - Soil chemical insights provided through vibrational spectroscopy. In: D. L. Sparks (Ed.), *Advances in Agronomy.* Academic Press, pp. 1-148.

Pedersen, J.A., Simpson, M.A., Bockheim, J.G.,Kumar, K., 2011. Characterization of soil organic carbon in drained thaw-lake basins of Arctic Alaska using NMR and FTIR photoacoustic spectroscopy. *Organic Geochemistry 42*(8), 947-954.

Plekan, O., Feyer, V., Šutara, F., Skála, T., Švec, M., Cháb, V., Matolín, V.,Prince, K.C., 2007. The adsorption of adenine on mineral surfaces: iron pyrite and silicon dioxide. *Surface Science 601*(9), 1973-1980.

Possinger, A.R., Zachman, M.J., Enders, A., Levin, B.D.A., Muller, D.A., Kourkoutis, L.F.,Lehmann, J., 2020. Organo–organic and organo–mineral interfaces in soil at the nanometer scale. *Nature Communications 11*(1), 6103.

Prater, C.B., Kansiz, M.,Cheng, J.-X., 2024. A tutorial on optical photothermal infrared (O-PTIR) microscopy. *APL Photonics 9*(9), 091101.

Praus, P., Veteška, M.,Pospíšil, M., 2011. Adsorption of phenol and aniline on natural and organically modified montmorillonite: experiment and molecular modelling. *Molecular Simulation 37*(11), 964-974.

Rae Cho, K., Kim, Y.-Y., Yang, P., Cai, W., Pan, H., Kulak, A.N., Lau, J.L., Kulshreshtha, P., Armes, S.P., Meldrum, F.C.,De Yoreo, J.J., 2016. Direct observation of mineral–organic composite formation reveals occlusion mechanism. *Nature Communications 7*(1), 10187.

Ramos, M.E.,Huertas, F.J., 2014. Adsorption of lactate and citrate on montmorillonite in aqueous solutions. *Applied Clay Science 90*, 27-34.

Ryskin, Y.I., 1974. The vibrations of protons in minerals: hydroxyl, water and ammonium. In: *The Infrared Spectra of Minerals.* Mineralogical Society of Great Britain and Ireland, pp. 0.

Saidy, A.R., Smernik, R.J., Baldock, J.A., Kaiser, K.,Sanderman, J., 2013. The sorption of organic carbon onto differing clay minerals in the presence and absence of hydrous iron oxide. *Geoderma 209-210*, 15-21.

Schwertmann, U.,Cornell, R.M., 2000. Goethite. In: *Iron Oxides in the Laboratory.* Wiley, pp. 67-92.

Sollins, P., Swanston, C., Kleber, M., Filley, T., Kramer, M., Crow, S., Caldwell, B.A., Lajtha, K.,Bowden, R., 2006. Organic C and N stabilization in a forest soil: evidence from sequential density fractionation. *Soil Biology and Biochemistry 38*(11), 3313-3324.

Solomon, D., Lehmann, J., Harden, J., Wang, J., Kinyangi, J., Heymann, K., Karunakaran, C., Lu, Y., Wirick, S.,Jacobsen, C., 2012. Micro- and nano-environments of carbon sequestration: multi-element STXM–NEXAFS spectromicroscopy assessment of microbial carbon and mineral associations. *Chemical Geology 329*, 53-73.

Torn, M.S., Trumbore, S.E., Chadwick, O.A., Vitousek, P.M.,Hendricks, D.M., 1997. Mineral control of soil organic carbon storage and turnover. *Nature 389*(6647), 170-173.

Uchimiya, M.,Stone, A.T., 2006. Redox reactions between iron and quinones: Thermodynamic constraints. *Geochimica et Cosmochimica Acta 70*(6), 1388-1401.

Vogel, C., Mueller, C.W., Höschen, C., Buegger, F., Heister, K., Schulz, S., Schloter, M.,Kögel-Knabner, I., 2014. Submicron structures provide preferential spots for carbon and nitrogen sequestration in soils. *Nature Communications 5*(1), 2947.

Wan, J., Tyliszczak, T.,Tokunaga, T.K., 2007. Organic carbon distribution, speciation, and elemental correlations within soil microaggregates: applications of STXM and NEXAFS spectroscopy. *Geochimica et Cosmochimica Acta 71*(22), 5439-5449.

Wang, R., Zhu, X., Qian, W., Hong, Z., Tang, H., Xu, R.,Yu, Y., 2017. Pectin adsorption on amorphous Fe/Al hydroxides and its effect on surface charge properties and Cu(II) adsorption. *Journal of Soils and Sediments 17*(10), 2481-2489.

Weisseborn, P.K., Warren, L.J.,Dunn, J.G., 1995. Selective flocculation of ultrafine iron ore. 1. mechanism of adsorption of starch onto hematite. *Colloids and Surfaces A: Physicochemical and Engineering Aspects 99*(1), 11-27.

Weng, Z., Lehmann, J., Van Zwieten, L., Joseph, S., Archanjo, B.S., Cowie, B., Thomsen, L., Tobin, M.J., Vongsvivut, J., Klein, A., Doolette, C.L., Hou, H., Mueller, C.W., Lombi, E.,Kopittke, P.M., 2022. Probing the nature of soil organic matter. *Critical Reviews in Environmental Science and Technology 52*(22), 4072-4093.

Whalen, E.D., Grandy, A.S., Geyer, K.M., Morrison, E.W.,Frey, S.D., 2024. Microbial trait multifunctionality drives soil organic matter formation potential. *Nature Communications 15*(1), 10209.

Xiao, J., Wen, Y., Yu, G.,Dou, S., 2018. Strategy for microscale characterization of soil mineral-organic associations by synchrotron-radiation-based FTIR technology. *Soil Science Society of America Journal 82*(6), 1583-1591.

Yang, J.Q., Zhang, X., Bourg, I.C.,Stone, H.A., 2021. 4D imaging reveals mechanisms of clay-carbon protection and release. *Nature Communications 12*(1), 622.

Yeasmin, S., Singh, B., Johnston, C.T., Hua, Q.,Sparks, D.L., 2023. Changes in particulate and mineral-associated organic carbon with land use in contrasting soils. *Pedosphere 33*(3), 421-435.

Yeasmin, S., Singh, B., Kookana, R.S., Farrell, M., Sparks, D.L.,Johnston, C.T., 2014. Influence of mineral characteristics on the retention of low molecular weight organic compounds: a batch sorption–desorption and ATR-FTIR study. *Journal of Colloid and Interface Science 432*, 246-257.

Zhang, H., Rasamani, K.D., Zhong, S., Taujale, S., Baratta, L.R.,Yang, Z., 2019. Dissolution, adsorption, and redox reaction in ternary mixtures of goethite, aluminum oxides, and hydroquinone. *The Journal of Physical Chemistry C 123*(7), 4371-4379.

Chapter 6 Effect of land use change on molecular composition and concentration of organic matter in an Ferrasol

This chapter has been published on *Environmental Science & Technology* as:

Yang, Z., Ohno, T., Singh, B. (2024). Effect of land use change on molecular composition and concentration of organic matter in an Oxisol. *Environmental Science & Technology*. 58(23), 10095-10107.

Graphical abstract

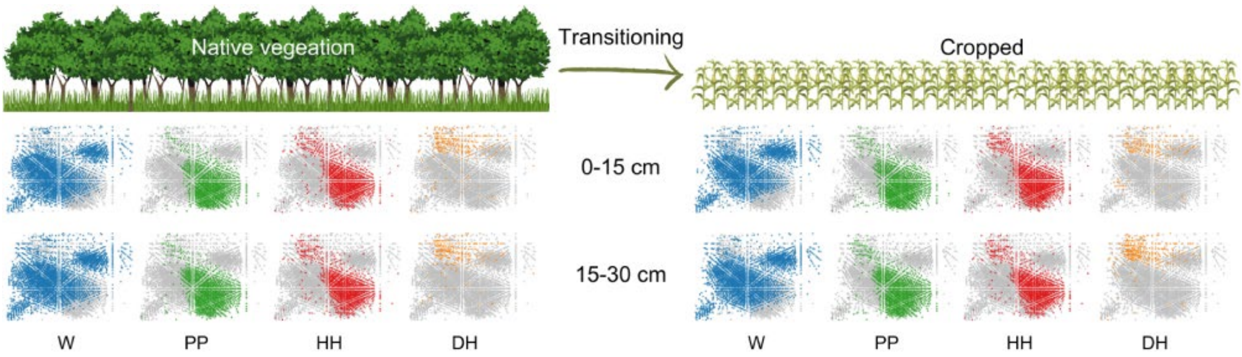

Abstract

Land use change from native vegetation to cropping can significantly affect the quantity and quality of soil organic matter (SOM). However, it remains unclear how the chemical composition of SOM is affected by such changes. This study employed a sequential chemical extraction to partition SOM from an Ferrasol into several distinct fractions: water-soluble fractions (W), organo-metal complexes (PP), short-range ordered (SRO) oxides (HH), and well-crystalline oxides (DH). Coupled with Fourier transform ion cyclotron resonance mass spectrometry (FT-ICR-MS), the impact of land use change on the molecular composition of different OM fractions was investigated. Greater amounts of OM were observed in the PP and HH fractions compared to other fractions, highlighting their importance in SOM stabilisation. The composition of different OM fractions varied based on extracted phases, with lignin-like and tannins-like compounds being prevalent in the PP and HH fractions, while aliphatic-like compounds dominated in the DH fraction. Despite changes in the concentration of each OM fraction from native vegetation to cropping, there was little influence of land use change on the molecular composition of OM associated with different mineral phases. No significant selective loss or preservation of organic carbon compounds was observed, indicating the composition of SOM remained unchanged.

Keywords

land use change, soil organic matter, mineral-associated organic matter, sequential extraction, FT-ICR-MS, organo-metal complexes, short-range ordered minerals, well-crystalline minerals

Synopsis

This study reveals that the concentration of soil organic matter associated different forms of Fe- and Al- bearing minerals can change when land use changing from native vegetation to a cropping, while their chemical composition remains unchanged.

6.1 Introduction

Soil organic matter (SOM) plays an important role in terrestrial ecosystems by maintaining soil fertility and contributing to the global carbon cycle (Lal et al., 2021). Land use change from native vegetation to arable cropping has been ongoing for decades and this has impacted the soil ecosystem, including SOM stocks and accumulation patterns (Chernyshova et al., 2011; Wei et al., 2014; Deng et al., 2016; Ramesh et al., 2019). The abundance of labile and stabilised components of SOM is expected to change with vegetation species (Guo et al., 2016). However, understanding of the drivers of SOM composition and stabilisation processes in response to land use change remains limited.

Among the diverse OM fractions, mineral associated organic matter (MAOM) plays an essential role in the stabilisation of OM in soils due to its chemical bonding with minerals and physical protection in small aggregates (Kögel-Knabner et al., 2008; Cotrufo et al., 2019). Iron- (Fe) or aluminium- (Al) bearing minerals are considered to dominate in mineral-organic interactions with the MAOM contributing up to 72% of the total organic carbon (OC) in soils and sediments (Kramer and Chadwick, 2018). Due to diverse physicochemical properties of the mineral adsorbent phases and SOM, OM components can undergo molecular fractionation in soils due to different mineral-organic interactions (Kleber et al., 2021; Chen et al., 2022). Previous research has demonstrated a preferential adsorption of lignin-like compounds onto short-range ordered (SRO) Fe and Al minerals, whereas lipid-like compounds tend to associate with well crystalline Fe and Al minerals (Kramer et al., 2012; Coward et al., 2018; Neurath et al., 2021; Lenhardt et al., 2022). During the process of mineral-organic associations, the saturation of mineral surfaces with organic compounds can lead to the formation of OM-OM multilayers with newly added OM compounds associating with adsorbed OM at the outer hydrophobic and kinetic zone (a zonal structure) (Gao et al., 2020; Zhao et al., 2020). The mineral-organic interactions are neither static nor irreversible, and multiple interactions, such as assembling, exchanging, competition and diffusion of OM compounds, can occur simultaneously at the mineral-organic interface (Kleber et al., 2021). Weakly bound or unprotected OM fragments can transit through the soil profile and may be stabilised by minerals in subsurface soil or utilised by microbes (Rumpel and Kögel-Knabner, 2011). These labile OM fractions are more vulnerable to change when exposed to altered environmental conditions including land use change. However, due to the similar processes involved in the SOM formation, the chemical composition of SOM may tend to converge, even with the diversity of OM sources (Bahadori et al., 2021; Yeasmin et al., 2023). This implies that the chemical composition of SOM may not change, or all OM components may change simultaneously under the land use change, resulting in their relative abundance remaining unchanged (Wang et al., 2023).

The chemical characterisation of OM composition has been recently advanced through the use of electrospray ionisation Fourier transform ion cyclotron resonance mass spectrometry (ESI FT-ICR-MS) (Huang et al., 2023; Ye et al., 2023). The technique, with its ultrahigh resolution capabilities, can identify OM compounds with precise molecular formulae. In this study, we employed FT-ICR-MS to determine changes in the molecular composition of OM in an Ferrasol following land use change from native vegetation to cropping systems. We used a sequential chemical extraction scheme to isolate OM fractions associated with different forms of metal oxide minerals. The sequential extraction procedure extracted OM present in water-soluble fraction, organo-metal complexes, SRO Fe/Al oxides and well crystalline Fe/Al oxides (Gabriel et al., 2018; Heckman et al., 2018). We hypothesised that the change in land use from native vegetation to cropping will not only influence the SOC concentration and stocks, but their chemical composition will also change. The objectives of this study were (1) to determine the relationship between Fe/Al phases and their associated OM, and (2) to explore the impact of land use change on the chemical composition of OM fractions. The results from this study will contribute to improved understanding of SOM stabilisation processes with land use change in an Ferrasol.

6.2 Materials and methods

6.2.1 *Soil sampling*

Soil samples were collected from paired native vegetation and cropped fields, near Robertson (34.6078339 S, 150.5393229 E) in New South Wales, Australia. The soil at the two sites is classified as an Ferrasol that is derived from Tertiary basalt. The climate at the site is temperate and warm, with an average yearly rainfall of approximately 850 mm and the mean annual temperature is 14.0 °C. The vegetation at the disturbed site consists with a mix of native plants in Australia including Eucalyptus species, Accacia species, kangaroo grass, tussock grass and weeping grass. The cropped field has been used for growing potatoes and other crop for over 20 years. Triplicate soil samples were taken from surface (0-15 cm) and subsurface (15-30 cm) layers within each field. Soil samples were air-dried and passed through a 2 mm sieve before laboratory analyses (Rayment and Lyons, 2010). General characteristics of the soil samples are presented in the Appendix (Table S 6.1 and Figure S 3.1). Briefly, the pH of the soil samples ranges from 5.0 to 5.6 and the clay content ranged from 28% to 45%. The clay fraction consisted of hematite, goethite, kaolinite, gibbsite, with minor amounts of hydroxy interlayered vermiculite, anatase and quartz.

6.2.2 *Selective dissolution extractions*

Finely ground soil samples (< 200 μm) were sequentially extracted to speciate metals and associated OM into different fractions following the procedure outlined by Heckman et al. (2018) The sequence of extraction was – (i) ultra-pure water (W); (ii) sodium pyrophosphate (PP); (iii) hydroxylamine-HCl (HH); and (iv) dithionite-HCl (DH). Detailed procedures are described in the SI (Section 2). The solutions after each extraction were analysed for Fe, Al, Mn and Si concentration by iCAP PRO Series inductively coupled plasma atomic emission spectrometer (ICP-AES). Original soil samples and residues after each extraction were analysed for total organic carbon (TOC) and total nitrogen (TN) using a vario MACRO cube CHNS analyser. The calculations for TOC and TN stocks, the concentration of extracted OC, and the molar ratio of OC to Fe and Al are provided in the Section 6.6.3.

6.2.3 *FT-ICR-MS analysis*

FT-ICR-MS analysis of the extracted solution was done to determine the molecular composition of OM associated with the different forms of metal oxides. The extracted solutions were desalinated and concentrated by solid phase extraction (SPE) following the procedure described by Dittmar et al. (2008) FT-ICR-MS analysis was carried out using negative ion mode electrospray ionisation with a 7 T Bruker SolariX 2xR FT-ICR-MS instrument. The detailed FT-ICR-MS procedure and formula assignments are supplied in the Section 6.6.4 and 6.6.5.

To characterise and compare the molecular composition of each OM fraction from FT-ICR-MS analysis, van Krevelen diagrams were used to visually observed changes in OM composition as a result of the land use change. In the presented van Krevelen diagrams, data points from all fractions are presented as the background, and data for each of extractants are overlayed in a unique colour. The molecular compounds extracted by each solvent were parsed into nine compound categories based on the stoichiometry of their molecular formulae (Ohno et al., 2010; Ohno and Ohno, 2013; Bianco et al., 2019; Li et al., 2019; McDonough et al., 2022; Sheng et al., 2023): (1) aliphatic-like compounds ($1.5 < H/C \leq 2.2$, $0.3 < O/C \leq 0.67$, $N = 0$); (2) lipids-like compounds ($1.5 < H/C \leq 2.0$, $O/C \leq 0.3$); (3) peptides-like compounds ($1.5 < H/C \leq 2.2$, $0.3 < O/C \leq 0.67$, $N > 0$); (4) unsaturated hydrocarbons-like compounds ($0.7 < H/C \leq 1.5$, $O/C \leq 0.1$); (5) carbohydrates-like compounds ($1.5 < H/C \leq 2.5$, $0.67 < O/C \leq 1.2$); (6) condensed aromatic-like compounds ($0.2 < H/C \leq 0.67$, $O/C \leq 0.67$); (7) lignin-like compounds ($0.67 < H/C \leq 1.5$, $0.1 < O/C \leq 0.67$); (8) tannins-like compounds ($0.67 < H/C \leq 1.5$, $0.67 < O/C \leq 1.2$); (9) others (unassigned unknown compounds). It should be noted that the molecular compound categories we have used are tentative classifications based on their H/C and O/C ratios, and not the actual molecular structure (Patel et al., 2021).

6.3 Results and discussion

6.3.1 *Impact of land use on bulk soil organic matter*

Total organic carbon (TOC) and total nitrogen (TN) concentrations varied significantly with the soil depth and land use ($p < 0.01$) (Figure 6.1). The TOC and TN concentrations were greater in the native surface soil (TOC: 83.7 ± 1.7 mg g^{-1} and TN: 6.6 ± 0.1 mg g^{-1}) than their concentrations in the cultivated surface soils (TOC: 66.4 ± 0.6 mg g^{-1} and TN: 5.5 ± 0.1 mg g^{-1}) (Figure 6.1). However, the TOC and TN concentrations in the subsoil were not significantly different for the native vegetation and cultivated sites. The decline in TOC and TN concentration in the subsurface soil compared to those in the surface is a result of the generally lower OM input and microbial biomass (Veldkamp et al., 2003). The main sources of subsoil OM are root biomass, dissolved organic matter (DOM) and particulate organic matter (POM) transported either physically or biologically, which is generally stabilised through organo-mineral associations between chemically labile organic matter and clay minerals, and/or metal oxides (e.g., Fe and Al) (Chabbi et al., 2009; Rumpel and Kögel-Knabner, 2011; Poeplau and Don, 2013). The conversion of native vegetation to cropland often results in the reduction of SOM due to changes in the quantity, quality, and pathways of OM input, as well as increased decomposition rate of OM, particularly in surface soils (Don et al., 2011; Rumpel and Kögel-Knabner, 2011; Paul, 2016). While we found that the concentration of TOC and TN in the subsurface soil remained similar with land use change, the TOC and TN stocks in both surface and subsurface soils decreased significantly, with reductions of 17-18% and 37-38%, respectively, after the conversion from native vegetation to a cropped system ($p < 0.01$) (Figure 6.1). The combined TOC stocks in the 0-30 cm soil layer were greater in the native vegetation site (189.2 t C ha^{-1} and 15.0 t N ha^{-1}) than the cropped site (155.9 t C ha^{-1} and 12.9 t N ha^{-1}). The TOC in soils from both sites are greater than the average stock in Australian soils (29.7 t C ha^{-1} in 0-30 cm) (Viscarra Rossel et al., 2014). With the assumption of a C:N ratio of 11.8 (Kirkby et al., 2011), the average TN stocks in the top 30 cm of all Australian soils are approximately 1.6 t N ha^{-1}. The TN stocks in the top 30 cm of studied native (15.0 t N ha^{-1}) and cropped sites (12.9 t N ha^{-1}) are also greater than the average total N stock in Australian soil. The decline in TOC and TN stocks observed in this study are relatively small compared to observed in other studies. From a global meta-analysis, Kopittke et al. (2017) reported median decrease of 43 % and 42 % in TOC and TN stocks, respectively, after land-use change from native vegetation to cropping. An earlier global meta-analysis study (Don et al., 2011), comprising of 385 studies, observed an average loss of 25% in the TOC stocks following the land use change from primary forest into cropland, which is slightly larger than the values observed in our study (17-18%).

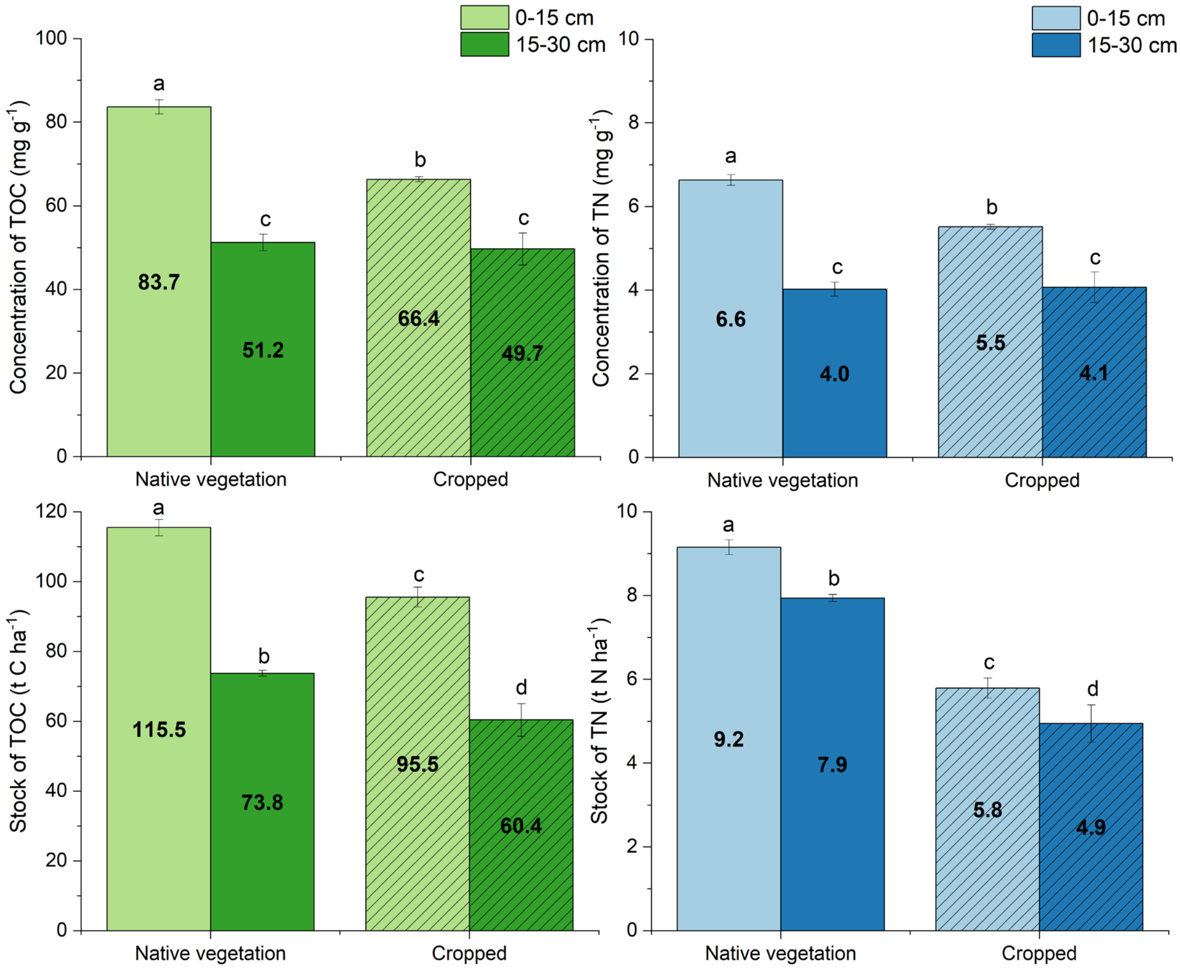

Figure 6.1 The concentration and stock of total organic carbon (TOC) and total nitrogen (TN) in the surface (0-15 cm) and subsurface (15-30 cm) soils from native vegetation and cropped field. Different letters indicate a significant difference between mean concentrations in two land uses and in two depths based on Tukey HSD test ($p < 0.05$). Error bars indicate one standard error ($n = 9$).

There was a linear relationship between TOC and TN (R^2=0.98, p<0.01), with carbon-to-nitrogen (C/N) ratio in soil remaining about 12.1 in all soil samples (Figure S 6.2). A similar C/N ratio suggests that the rates of C and N release, as well as their migration within soil, are similar (Ostrowska and Porębska, 2015). This is contrary to some studies where a decrease in C/N ratio has been reported from surface soil to subsurface soil (Rumpel and Kögel-Knabner, 2011). Some factors can explain the difference between previous studies and our results, for instance, the difference of climate (e.g., temperature and precipitation), management practices (e.g., input of organic and period of land use) and soil environmental conditions (e.g., humidity and mineralogy) (de Souza Medeiros et al., 2022). Generally, when fresh OM is transported within a soil profile, it is progressively adsorbed onto mineral surfaces that minimises its decomposition (Kleber et al., 2015). As OM content increases, additional OM can either weakly bind to mineral-OM associations in the surface soil, or migrate to the deeper layers as dissolved forms, where it becomes stabilised by minerals in subsurface soil or utilised by microbes (Rumpel and Kögel-Knabner, 2011). Compared to the OM fraction originating directly from plant or root litter in the surface soil, OM in the subsurface tends to be highly processed that has originated from plants or microbe exudates (Cotrufo et al., 2013; Córdova et al., 2018). However, based on the similar C/N ratio between the surface and subsurface soils in our study, we hypothesise that the capacity of the soil mineral fraction in the surface layer to stabilise OM may have reached its threshold point (i.e., the OC saturation limit) or its dynamic saturation point (Hassink, 1997; Ye et al., 2023; Yeasmin et al., 2023). Some studies suggested that a large OC concentration (approximately 25 % of OC) is required to approach the actual saturation limit in bulk soil (Cotrufo et al., 2019). However, soil aggregation or organo-mineral association may render some reactive sites remain inaccessible, potentially not requiring such high OC concentration (Stewart et al., 2007; Yeasmin et al., 2023). After saturation of all accessible reactive sites of mineral, additional OM is either weakly bound or remain dissolved that migrate to the subsurface. These labile OM fractions are more vulnerable to environmental conditions (e.g., climate condition and land use change). The study area receives approximately 850 mm of annual rainfall, which could cause the labile OM fraction, which would typically accumulate in the surface soil, to migrate to deeper layers (Zhang et al., 2019). On the other hand, sorption of OM to mineral phases is dynamic and reversible (Lilienfein et al., 2004; Kleber et al., 2021), adsorbed OM fractions on the minerals are also vulnerable to exchange and desorption. It has been reported that there may be competition between the adsorbed OM and newly introduced OM which may induce the release of previously adsorbed organic compounds (Lilienfein et al., 2004). The dynamic interface between mineral phase and OM continuously changes with variations in the chemistry of aqueous solution, OM and mineralogy, influencing the fate of organic compounds in the soil environment (Kleber et al., 2021). The C/N ratio in the native vegetation and cropped soils remained similar in our study, indicating a consistency in the bulk composition of C and N in SOM even after land use changes from native vegetation to cropping.

6.3.2 Extractable Fe- and Al- bearing phases

The concentration of OC associated with each extracted metal phase fraction in the whole soil followed the order: $C_{PP} > C_{HH} > C_{DH} > C_W$ (Figure 6.2a). There were no significant correlations between the concentration of each extracted OC fraction and their associated Fe, Al and (Fe+Al) ($p>0.05$) (Table S 6.2). In the water-soluble fraction, C_W ranged from 2.2-5.4 mg g^{-1} (Figure 6.2a), contributing the least amount to the TOC, with 5.1-6.4% in the native vegetation soil and 3.4-6.4% in the cropped soil (Figure 2b). In the surface soil, C_W decreased notably (59%) from native vegetation to cropping ($p < 0.01$), while subsurface C_W remained similar at 2.6-2.9 mg g^{-1} ($p = 0.99$) (Figure 6.2a). In the native vegetation soil, C_W decreased about 52% from surface to subsurface soil ($p < 0.01$), while it remained similar in cropped soil ($p = 0.88$) (Figure 2a). Low concentration of water-soluble Fe (Fe_W) and Al (Al_W) was observed (less than 0.10 mg g^{-1}) in all soils, which varied with the land use and soil depth (Table 6.1). The carbon to metal (C/M) molar ratio has been considered as an indicator of the formation of mineral-OM complexes in the soil solution (Wagai and Mayer, 2007). The molar ratio of C_W and $(Fe+Al)_W$ ranged from 74.7-373.0 (Figure 6.3), indicating substantial organic components in the water-soluble fraction. Some ionic OM-Fe/Al complexes may have been dissolved in this fraction, as the flocculation and precipitation of OM-Fe/Al complexes typically start at the high C/M ratios (about 33) (Kleber et al., 2015). However, considering the low concentration of water-soluble Fe and Al (Table 1) and higher C/(Fe+Al) ratio (over 70), the presence of OM-Fe/Al complexes in the water-soluble fraction would be minimal (Kleber et al., 2007; Gabriel et al., 2018). The labile and polar OM components in the water-soluble fraction are free or loosely bound to the mineral phases in the kinetic zone or the outer region, which are easily accessed by microbes (Kleber et al., 2007; Zhao et al., 2020). After land use change, the OC content in this fraction is easily altered due to shifts in organic matter input (Kleber et al., 2007).

The highest contribution to the TOC was found in the C_{PP} fraction, accounting for 54.7-60.4% in the native vegetation soil and 55.8-58.4% in the cropped soil (Figure 6.2b). The presence of most SOM as organo-metal complexes in this study is consistent with other studies, where the proportion of C_{PP} was the largest and accounted for up to 63% of the total SOC in the sequential extraction (Lopez-Sangil and Rovira, 2013; Gabriel et al., 2018). C_{PP} concentration was significantly decreased (16% reduction) in the surface soil after land use change from native vegetation to cropping, while it did not change in the subsurface soil (Figure 6.2a). The C_{PP} content decreased with depth in both native vegetation and cropped soils, decreasing by 32% and 23%, respectively. The C_{PP} fraction represents the OC co-precipitated with solid Fe and Al phases (Kaiser et al., 2012; Coward et al., 2017), which may consist of OM-cation-mineral, OM-cation-OM, or cation-OM associations, where polyvalent Fe and Al cations reacted are associated with negatively charged sites of organic (COO^-) and mineral phases (OH^-) via cation bridging (Kleber et al., 2021). Due to the pyrophosphate can act as a ligand, some OM that interacts with polyvalent cations that are part of amorphous Fe/Al oxides via ligand exchange, could also be extractable in the PP fraction (Kaiser et al., 2012). Some alkaline-soluble OC, which is not directly chelated with metal cations, could also be present in this fraction (Wagai et al., 2013). The concentrations of Fe and Al in the organo-metal complex fraction were not significantly affected at the two depths and under both land uses (Table 6.1). The Fe_{PP} and Al_{PP} fractions not only consist of dissolved Fe and Al from organo-metal complexes but may also include some amorphous Fe and Al (hydr)oxides (Schuppli et al., 1983; Kaiser and Zech, 1996). The dissolution of these amorphous Fe and Al colloidal particles could potentially release OC associated with these colloids (Lawrence et al., 2015). In our study, the molar ratio of C:(Fe+Al) in the PP fraction remained similar between the two land uses in the surface (3.9-4.5) and subsurface (2.3-3.0) soils (Figure 6.3). Relatively high C: (Fe+Al) ratio in the PP fraction indicates that the complexation and/or co-precipitation between OM and mineral phases may occur (Mikutta et al., 2011; Chen et al., 2014; Kleber et al., 2015). Although it is difficult to distinguish the complexation and co-precipitation of mineral-OM complexes just on the basis of the C/M molar ratio, higher C: (Fe+Al) ratio is consistent with higher OM mineralisation which is more susceptible to utilised by microbes and loss when land use change from native vegetation to cropping (Mikutta et al., 2011). As the C:(Fe+Al) ratio decreases, the contribution of Fe- and Al-bearing mineral species would increase, leading to a higher proportion of adsorption mineral-OM complexes (Chen et al., 2014), and the stabilities of these complexes also increase (Kleber et al., 2015).

In the short-range ordered Fe- and Al- bearing oxide fraction, C_{HH} contributed 13.5-14.5% of the TOC in our study (Figure 6.2b), which contrasts with previous sequential extraction studies where a small amount or even no OC was detected in their hydroxylamine extraction (Gabriel et al., 2018; Heckman et al., 2018). The difference may be due to difference in soil types and OC content. Compared to lower TOC concentration in other studies (Gabriel et al., 2018; Heckman et al., 2018), the large amounts of OC content in this study (49.7-83.7 mg g^{-1}) may have contributed to more to more OC associated the SRO fraction (Figure 6.2a). The concentration of C_{HH} remained stable with small variance in the surface soil (from 12.1 to 9.4 mg g^{-1}) and subsurface soil (6.7-7.0 mg g^{-1}) for both land uses (Figure 6.2a). It tended to decrease from surface soil to subsurface soil in native vegetation. The Fe_{HH} and Al_{HH} in SRO phases represent amorphous to poorly crystalline or SRO Al- or Fe-hydroxides (such as allophane or ferrihydrite), which have the potential to stabilise large amounts of OM via ligand exchange reaction, due to their highly reactive surfaces and large specific surface area (Duiker et al., 2003; Kleber et al., 2005). Al is the major metal species in the HH fraction with concentrations ranging from 35.3 to 53.1 mg g^{-1} and the concentration of Fe_{HH} was low (2.8-3.5 mg g^{-1}) (Table 6.1). The Al_{HH} increased significantly from native vegetation to cropping in both surface and subsurface soils, which indicates a greater content of SRO mineral phases in the cropped soil than the native vegetation soil. It may be due to changes in land management practices (e.g., physical disturbance) affecting soil conditions, such as pH, redox conditions, and soil solution composition (Sparks et al., 2024b). A low molar ratio of C: (Fe + Al) in the SRO fraction (0.28-0.75) was observed in our study (Figure 6.3), indicating that the surface adsorption may be the primary reaction between OM and SRO phases (Lawrence et al., 2015; Coward et al., 2017). The SRO-associated OM fractions tend to be more stable (more extraction-resistant or passive C pool) than the OM in organo-metal complex, but there is also a limit to the storage potential of this OM fraction due to the OC saturation (Hassink, 1997; Ye et al., 2023; Yeasmin et al., 2023). Based on the "layer-by-layer onion" theory, once the SRO phases reaches its OC saturation limit, any additional OM is unable to adsorb directly onto the surface (Ye et al., 2023). Instead, it may interact with adsorbed OM or free OM fragments via polyvalent cation bridges or hydrophobic interactions, forming weak OM-OM associations in the hydrophobic and kinetic zones (Kleber et al., 2007; Coward et al., 2019; Gao et al., 2020). The formation of these OM-OM associations may depend more on the OC content rather than the number of available binding sites (Gao et al., 2020).

The modified dithionite extraction was used as the final step in the extraction procedure to dissolve the secondary or well crystalline Fe and Al oxides and OM associated with these phases. A small concentration of C_{DH} was observed in all soil samples, representing only 8.1-9.9% of TOC in the native vegetation soil and 7.2-8.9% of TOC in the cropped soil (Figure 6.2b). The OC in the C_{DH} fraction can be considered to be more stable or passive OM pool, with a longer turnover time, compared to previous OM fraction (Gabriel et al., 2018; Heckman et al., 2018). From native vegetation soil to cropped soil, C_{DH} decreased in the surface soil ($p < 0.01$) but the change in magnitude was small (from 8.3 to 5.9 mg g^{-1}) and remained similar in the subsurface soil ($p = 0.77$) (Figure 2a). The distribution of Fe_{DH} was also affected by the land use change, with decreasing from native vegetation to cropping ($p < 0.01$) (Table 6.1). On the contrary, the concentration of Al_{HH} did not change at both soil depths of the native vegetation and cropped soils (32.8-35.1 mg g^{-1}) and accounted for 23.0-26.1% of the total Al (Table 6.1). The ligand exchange reaction is the dominant interaction between C_{DH} and well-crystalline Fe/Al phases (Coward et al., 2018), with a small C:(Fe+Al) ratio ranging from 0.21-0.44 (Figure 6.3). Surface hydroxyls (-OH) groups of crystalline Fe/Al phase can directly bound OM compounds through inner-sphere complexations via ligand exchange (Norén et al., 2008). This strong inner-sphere complexation contributes to the long-term OM preservation from microbial decomposition (Wagai and Mayer, 2007; Cloy et al., 2014).

Table 6.1 The concentration (mg g^{-1}) and proportion (expressed as % of their total content in brackets) of Fe and Al extracted by the four extractants in the surface soil (0-15 cm) and subsurface soil (15-30 cm) from native vegetation and cropped fields[a].

OM fractions		Native vegetation		Cropped	
		0-15 cm	15-30 cm	0-15 cm	15-30 cm
Extracted Fe (% of total Fe)	W	0.10±0.01^{a} (0.09)	0.07±0.01^{b} (0.06)	0.04±0.00^{c} (0.03)	0.01±0.01^{c} (0.01)
	PP	15.1±1.2^{ab} (12.5)	17.4±1.7^{a} (14.2)	11.5±0.2^{b} (9.5)	13.9±1.0^{ab} (11.4)
	HH	2.8±0.1^{b} (2.9)	3.2±0.1^{ab} (2.3)	3.2±0.2^{ab} (2.7)	3.5±0.2^{a} (2.9)
	DH	16.3±0.6^{ab} (13.5)	17.1±0.7^{a} (14.0)	14.0±0.4^{c} (11.5)	14.7±0.5^{bc} (12.0)
Extracted Al (% of total Al)	W	0.07±0.00^{a} (0.05)	0.03±0.01^{bc} (0.02)	0.05±0.00^{ab} (0.04)	0.03±0.01^{c} (0.02)
	PP	15.5±1.4^{a} (11.5)	13.7±0.7^{a} (9.7)	16.6±1.1^{a} (11.7)	16.4±1.3^{a} (11.4)
	HH	35.3±2.3^{c} (26.0)	42.2±1.9^{b} (29.8)	49.4±1.4a (34.7)	53.1±1.2^{a} (37.1)
	DH	35.1±2.1^{a} (26.1)	33.2±2.6^{a} (23.4)	32.8±0.5^{a} (23.0)	33.5±0.3^{a} (23.0)

[a] W: water-soluble fraction; PP: organo-metal complex fraction; HH: well-crystalline metal complex fraction; and DH: well-crystalline metal complex fraction. The concentration of Fe and Al in the residuals were not included. Different letters indicate a significant difference between mean concentrations in two land use and in two depths based on Tukey HSD test ($n = 9$, $p < 0.05$).

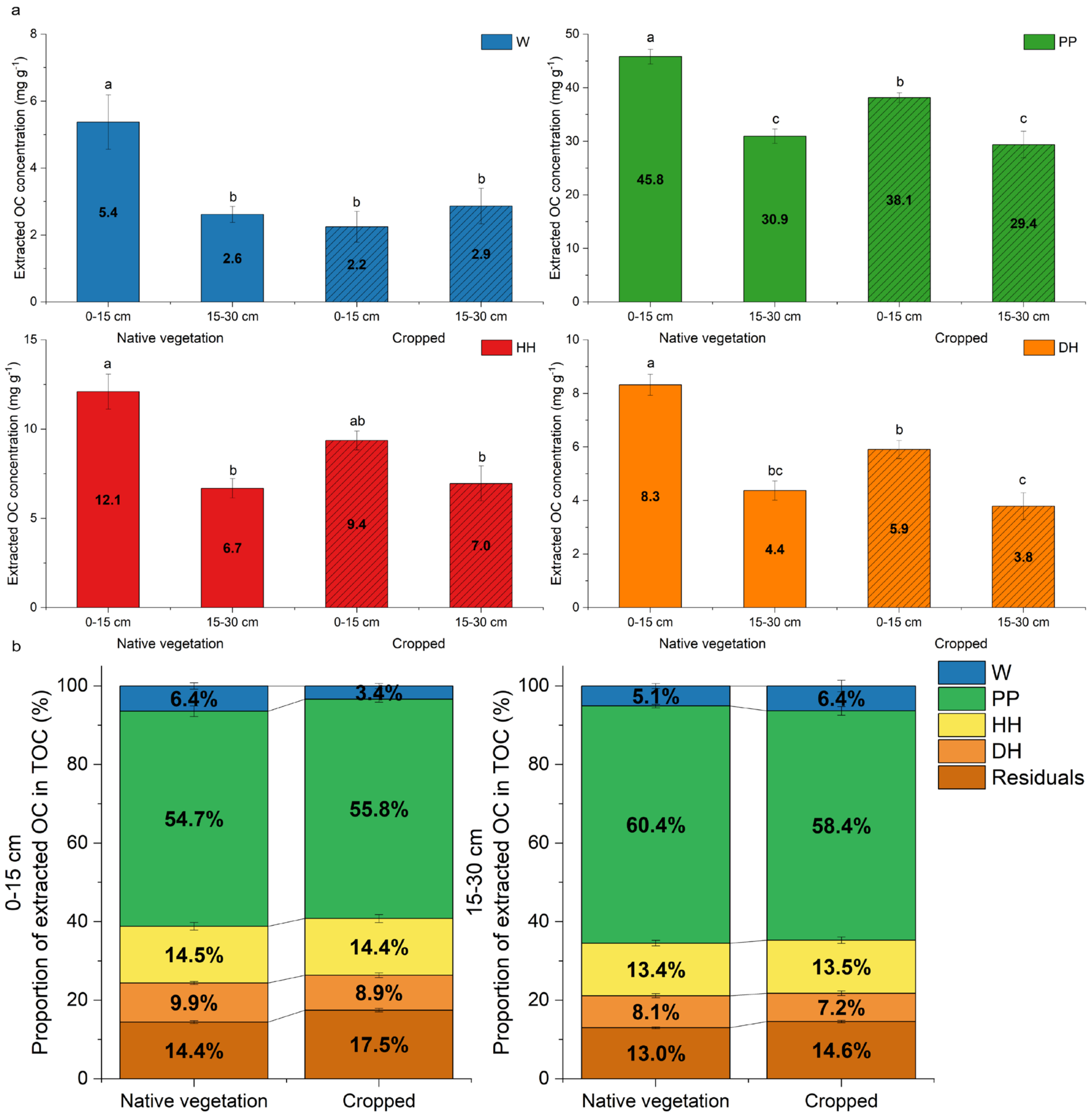

Figure 6.2 The concentration (a) and the proportion (b) of organic carbon (OC) (mg g^{-1}) in each extractable fraction (W: water-soluble fraction; PP: organo-metal complex fraction; HH: well-crystalline metal complex fraction; and DH: well-crystalline metal complex fraction) in the surface (0-15 cm) and subsurface (15-30 cm) soils from native vegetation and cropped fields. The proportion is expressed as percent of the total organic carbon (TOC). Different letters indicate a significant difference between mean concentrations in two land use and in two depths based on Tukey HSD test ($p < 0.05$). Error bars indicate one standard error ($n = 9$).

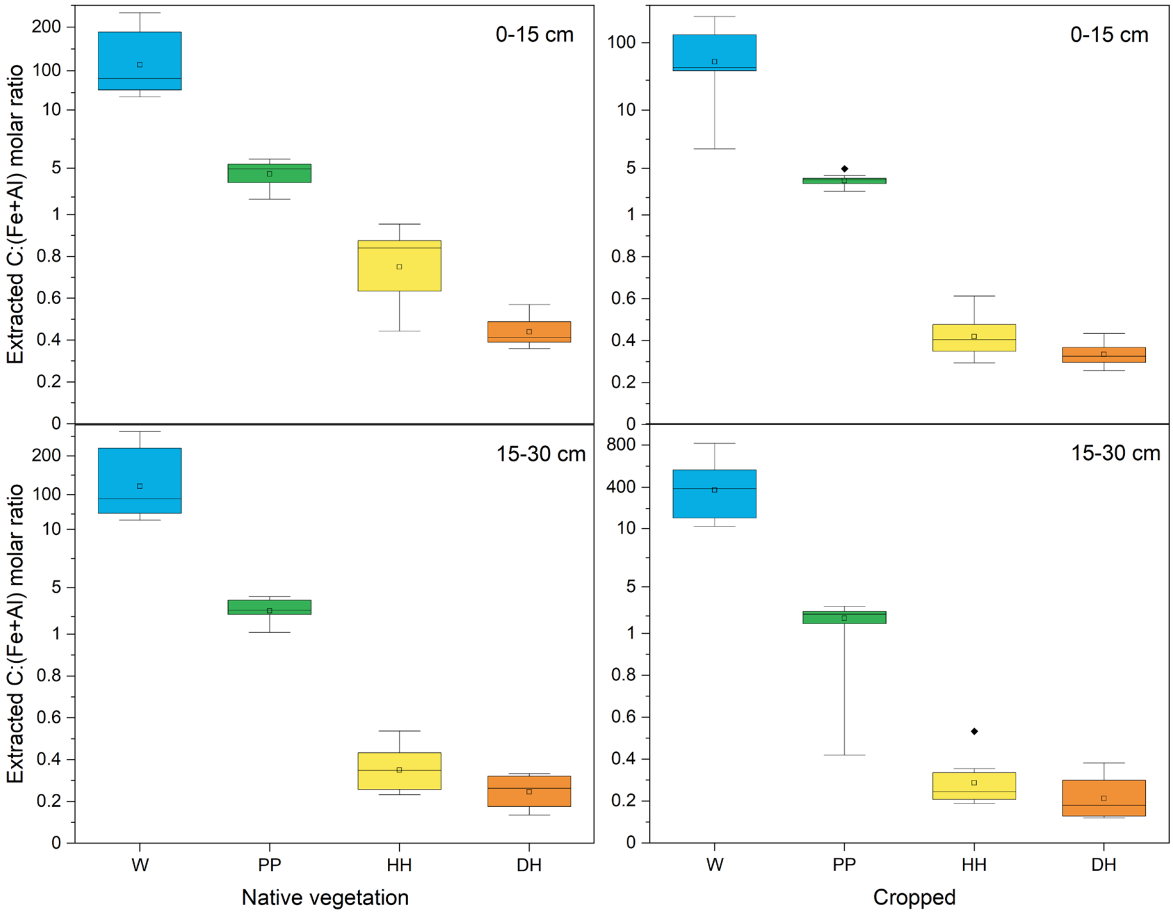

Figure 6.3 Box plots of the C:(Fe+ Al) molar ratios in each extractable (W: water-soluble fraction; PP: organo-metal complex fraction; HH: well-crystalline metal complex fraction; and DH: well-crystalline metal complex fraction) in the surface (0-15 cm) and subsurface (15-30 cm) soils from native vegetation and cropped fields.

6.3.3 Molecular composition of extractable OM fractions

The chemical characteristics of OM in water-soluble fraction was very diverse, with H/C ranging from 0.30 to 2.23 and O/C ranging from 0.02 to 1.18 (Figure 6.4). Although the water-soluble OM fraction constituted only 3.4-6.4% of the total SOC (Figure 6.2b), its composition may provide indication of the overall OM composition of the soil, as the soluble phase tends to reach equilibrium with the solid phase at the mineral-organic interface (Chantigny, 2003). The relative abundance of van Krevelen organic classification groups in the W fraction were similar across all soils and followed the order: lignin-like (58.2-62.8 %) > carbohydrates-like (12.3-17.2 %) > tannins-like (6.8-8.9 %) > condensed aromatic-like (6.1-8.1 %) > peptides-like (2.7-3.8 %) > aliphatic-like (2.7-3.5 %) > lipids-like (2.8-3.0 %) > unsaturated hydrocarbons-like (0.3-1.4 %) > others (0.1-0.4 %) (Figure 6.5). We also combined all molecules from all extracted fractions to present the entire pool of the extractable organic compounds (grey point in Figure 6.4). There were no significant differences in entire extractable pools observed soil depths and land use changes (Figure S 6.3). The relative abundance of each organic category in the entire pool was slightly different with the assigned molecules in the W fraction and followed the order: lignin-like (48.6-51.4 %) > tannins-like (16.5-17.8 %) > carbohydrates-like (7.2-9.7 %) > condensed aromatic-like (7.6-9.0 %) > aliphatic-like (5.1-6.4 %) > others (3.9-4.5 %) > lipids-like (2.7-3.3 %) > peptides-like (2%) > unsaturated hydrocarbons-like (0.2-0.8 %).

Despite the significant difference in their OC concentrations ($C_{PP} > C_{HH}$, Figure 6.2a), the distribution of assigned formulae of OM in the PP and HH fractions were visually similar in the van Kerevelen diagrams, with enrichment in low H/C and high O/C ratios (Figure 6.4). Lignin-like, tannnins-like and condensed aromatic-like compounds were the three dominant organic groups presenting in both the PP and HH fractions (Figure 6.5). The relative abundance of lignin-like compounds in the PP and HH fractions were similar, accounting for 39.7-43.6 % and 37.3-40.3 % of the total assigned formulae, respectively. The relative abundance of tannins-like and condensed aromatic-like compounds differed between the PP and HH fractions. Condensed aromatic-like compounds dominated in the PP fraction, while tannin-like compounds dominated in the HH fraction. Additionally, the proportion of aliphatic-like and lipids-like compounds showed an increasing trend from the PP fraction to the HH fraction. The assigned formulae in the DH fraction had high H/C and low O/C, and this fraction was dominated by aliphatic-like compounds (56.1-58.9 %), which was different from the PP and HH fractions (Figure 6.5). The relative abundacne of organic compounds with high aromaticity (e.g., condesed aromatic-like, lignin-like and tannins-like) in the DH fractions was low, followed by 6.2-11.7 % of lignin-like, 0.6-2.0 % of condensed aromatic-like, and 0.3-1.0% of tannins-like compounds. Some carbohydrates-like compounds can be dissoloved in the DH fraction and these compounds ranged from 9.3-12.2 % of the total assigned formulae. No peptides-like and unsaturated hydrocarbons-like compounds were catergorised in the DH fraction. Approximately 10.2-11.6%, 7.3-8.8%, and 4.4-7.1% of unknown formulae were not assigned to any categories in the PP, HH, and DH fractions, respectively. The unknown formulae in the PP fraction were CHO (average relative abundance 82.2 %) dominated, with smaller proportion of CHON (15.4 %) fromulae. Contrary to this, the unknown formulae in the HH and DH fractions were dominated by nitrogen-containing formulae (35.8% CHON in HH) and sulfur- and phosphorus-containing formulae (25.3% CHOS and 47.7% CHOP in DH), respectively. We suspect that the heteroatom-containing formulae in the PP and DH fractions might be from the organic compounds due to the contamination introduced by the extracting reagents (Lv et al., 2020).

The lignin-like compounds represent organic molecules derived from macromolecular lignin polymer (DiDonato et al., 2016), which present one or more aromatic rings and various functional groups (e.g., -OH and C=O) (Rivas-Ubach et al., 2018; Sparks et al., 2024a). It has undergone microbial degradation from plant residues to small molecules and has most likely been oxidised, as it needs to undergo depolymerisation before reacting with mineral phases (Thevenot et al., 2010). In our study, we observed a decreasing relative abundance of lignin-like compounds from water-soluble fraction (58.2-62.8 %) to organo-metal complex fraction (39.7-43.6 %), SRO fraction (6.2-11.7 %) and well-crystalline fraction (6.2-11.7 %) (Figure 6.5). This trend aligns well with previous studies, where the contribution of lignin-like compounds showed a decreasing trend from POM to mineral-associated fractions (Kleber et al., 2007; Angst et al., 2021). The condensed aromatic-like compounds can be termed as polycyclic aromatic compounds or black carbon, resulting from thermal alteration of natural OM and presenting a relatively stable pool of OM due to their recalcitrance (Czimczik and Masiello, 2007; Knicker, 2007). It has been reported that condensed aromatic compounds were more readily coagulated or flocculated with the presence of Fe and Al (Riedel et al., 2012), which is consistent with our findings, where a larger proportion of condensed aromatic-like compounds was observed in organo-metal complex fraction (13.9-15.8 %) than in other phases. The other aromatic biopolymers such as the tannins-like compounds are also resistant to microbial biodegradation due to their carboxyl-rich ring structures (Erktan et al., 2017). We observed that the proportion of tannins-like compounds in the HH fraction (34.8-37.6 %) was larger than in the PP fraction (27.6-28.9 %), suggesting that they may be preferentially bound to hydroxylated SRO oxide surface (Kramer et al., 2012).

It should be noted that the composition of assigned organic compounds in the crystalline fraction (also in the SRO fraction) may not represent its entire associated pool after the sequential extraction. However, it still comprises the most stable component groups remaining bound with crystalline phases. It is surprisingly to see the aliphatic-like compounds dominate in the crystalline fraction (56.1-58.9 %), which may originate from both plant and microbes (Clemente et al., 2011; Angst et al., 2021). Approximately 10% each of lipids-like, lignin-like, and carbohydrates-like compound also remained in the DH fraction. These findings support the view that Fe/Al phases, depending on their crystallinity, exhibit preferences for binding specific organic and preserving them in these organo-mineral associations for the long term. Both SRO phases tend to prefer lignin-like and tannins-like compounds while crystalline phases prefer aliphatic-like compounds (Kleber et al., 2007; Kramer et al., 2012; Coward et al., 2018; Neurath et al., 2021; Lenhardt et al., 2022). The aliphatic C compounds may be less susceptible to release form the mineral phases compared to aromatic C compounds (Adhikari and Yang, 2015; Coward et al., 2018; Zhao et al., 2020). This finding also indicates the potential of aliphatic C compounds in stabilising OM within mineral phases and suggests a possible important role in interactions within organo-mineral associations (Hernandez-Soriano et al., 2018). Although some laboratory simulation studies of mineral absorption or precipitation with OM have shown that Fe/Al phases preferentially adsorb aromatic compounds compared to aliphatic compounds regardless of their crystallinity (Hu et al., 2024), the term "preference" in our study refers to the stability or abundance of organic compound bonding with the mineral phases rather than the primary or strength of adsorption. And our understanding of MAOM is based on the operationally defined chemical pools, comparing discrepancies across studies becomes challenging (Zhao et al., 2020). According to the zonal model of the organo-mineral structure, additional organic components, such as aromatic and lignin compounds, are adsorbed by layer and layer in the dynamic zone through cations bridging, hydrogen bonding and other interactions (Zhao et al., 2020). Some studies have also emphasised the role of N-containing compounds in the hydrophobic zone (Kleber et al., 2007; Zhao et al., 2020). However, we observed a small proportion of these organic groups (i.e., peptides-like) in association with the Fe/Al phases in our study (Figure 5). The scale of further accumulation of organic molecular fragments in the hydrophobic zone may depend on the properties of the metal phases(Kleber et al., 2007).

Both the van Krevelen diagram and relative abundance histograms showed that land use and soil depth have little impact on the composition and the distribution of organic classification groups in each fraction (Figure 6.4 and Figure 6.5). Although the concentration of OC changed with the land use and soil depth (Figure 6.2a), the composition remained similar and is primarily related to the extracted fractions. The principal component analysis (PCA) (Figure S 6.4a) shows that PC1 (50.1%) and PC2 (29.4%) collectively explained 79.5% of the variation in the relative abundance. The OM in the PP fraction showed some overlaps and minor differences with the HH fraction in the PCA plots, mainly due to similar abundance of organic classification groups in the two fractions (Figure 6.5). From Figure S 6.4b, it can be observed that the native vegetation and cropped data largely overlapped, indicating a little impact of the land use change on the OM composition. However, the composition of the Fe/Al phases associated OM fraction under the land use change remains controversial (Clemente et al., 2011; Ding et al., 2017; Panettieri et al., 2017; Angst et al., 2021). The composition of OM fraction may depend on various environmental conditions such as soil pH, substrate quality, soil type, and soil mineralogy, which are particularly site-specific (Angst et al., 2021). Taking lignin-like compounds as an example, some studies have reported higher lignin-like content in the stable MAOM fraction in grassland compared to forest or arable land use (Panettieri et al., 2017). In contrast, other studies have found that decreased contents of lignin-like after conversion from forest to grassland, or that the lignin-like content in MAOM tends to be insensitive to land use change (Clemente et al., 2011; Angst et al., 2021). Similarly, the content of lipid and amino sugar in MAOM can either increase or decrease after the land use change (Ding et al., 2017). In our study, we found that land use and soil depth had little impact on the composition of each OM fraction. This observation is consistent with a study by Wissing et al. (2013), where after long-term cropping management on paddy soils, the OC content was changed, but the composition of SOM was not affected. Our results indicate that when the content of OM decreases, various organic groups decrease at the same rate and thus the relative abundance of each organic group in the OM fraction remains similar after the land use change.

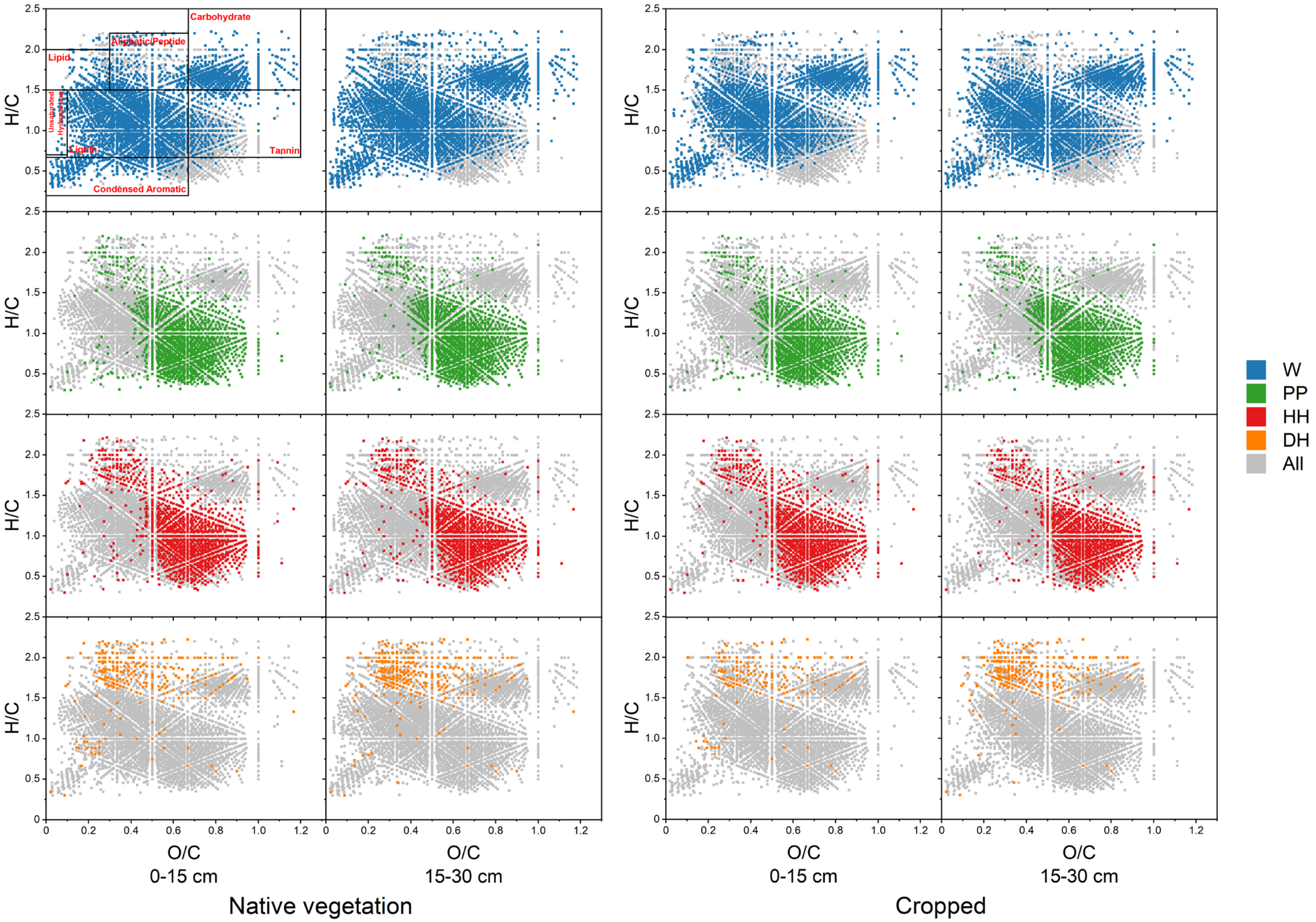

Figure 6.4 van Krevelen diagrams of assigned formulae of FT-ICR-MS data in each extractable fractions (W: water-soluble fraction; PP: organo-metal complex fraction; HH: well-crystalline metal complex fraction; and DH: well-crystalline metal complex fraction; All: all fractions) in the surface (0-15 cm) and subsurface (15-30 cm) soils from native vegetation and cropped fields.

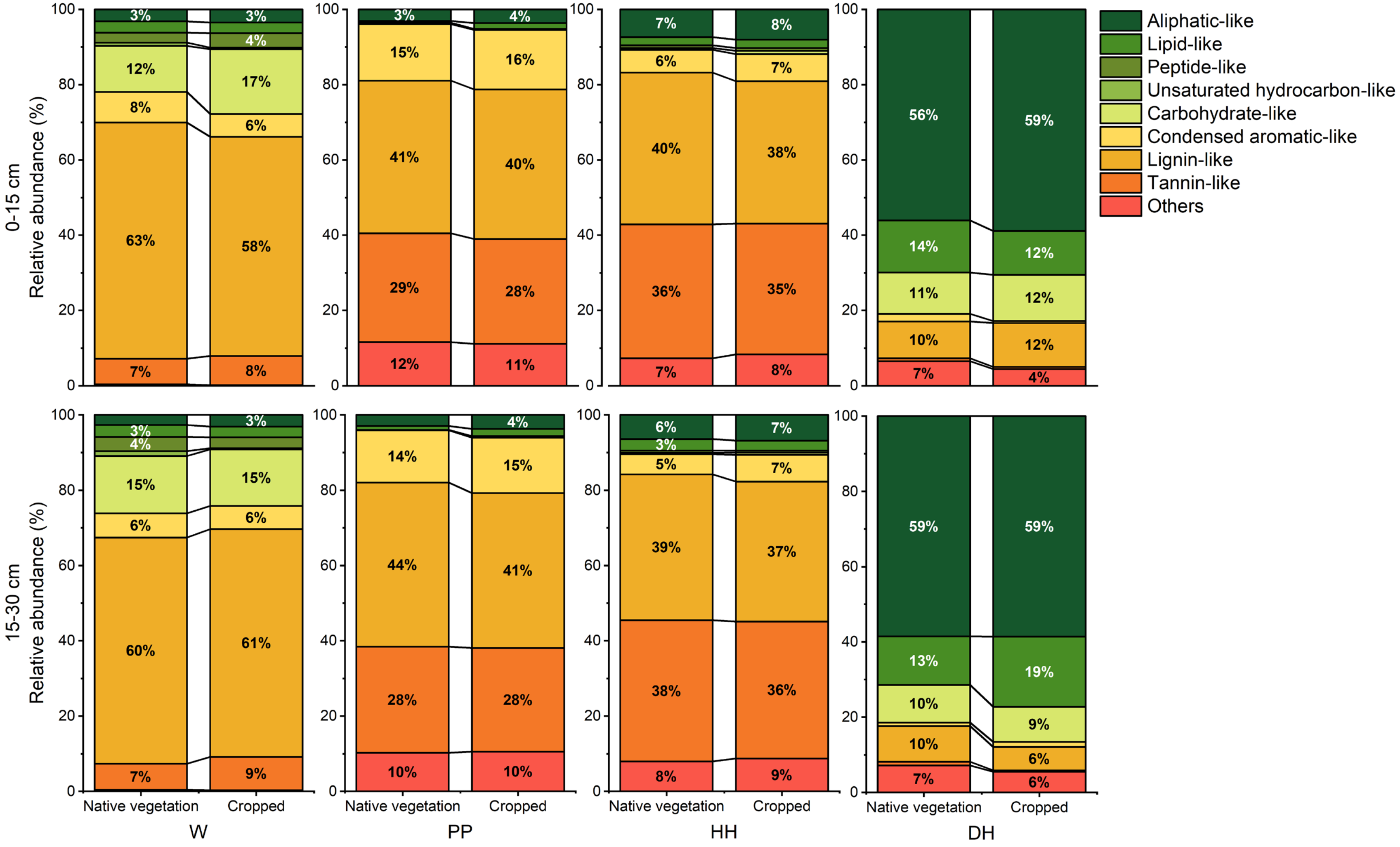

Figure 6.5 Histogram of the relative abundance of the major biochemical classes of assigned formulae in each extractable in each extractable fractions (W: water-soluble fraction; PP: organo-metal complex fraction; HH: well-crystalline metal complex fraction; and DH: well-crystalline metal complex fraction) in the surface (0-15 cm) and subsurface (15-30 cm) soils from native vegetation and cropped fields.

6.4 Environmental Implication

The response of different OM fractions to land use change may exhibit variations across different ecosystems. Generally, MAOM fractions remain more stable with a longer turnover time (Guo et al., 2016; Angst et al., 2023). However, we observed that the content of MAOM fractions (associated with Fe- and Al-bearing phases) also decreased with land use change from native vegetation to cropping, especially in the surface soil. Through the sequential extraction, we have provided experimental evidence to support the idea that the abundance of different organic compounds is related to different mineral phase. Aromatic compounds (such as lignin-like, tannins-like and condensed aromatic-like) play an important role in mineral-OM complexes and SRO oxides, while aliphatic-like compounds dominate in the well-crystalline oxide phases (Kramer et al., 2012; Coward et al., 2018; Neurath et al., 2021; Lenhardt et al., 2022). However, the procedure could not distinguish the interaction between organic compounds and mineral phases in their dynamic zones (hydrophobic and kinetic zone), which could be more susceptible to changes, especially in the presence of high OM content (Lv et al., 2022). Some studies have attempted to use organic solvents (e.g., MeOH and $CHCl_3$) to separate the OM fractions to study the dynamic zone (Tfaily et al., 2015; Tfaily et al., 2017), but their composition would vary significantly between different mineral phases (Zhao et al., 2020). Furthermore, the chemical reducing extractants (hydroxylamine and dithionite) can introduce molecular artifacts during extraction (Lv et al., 2020). We also identified some unknown heteroatom-containing organic compounds present in the HH and DH fractions. The separation of different pools of OM is very complex and an improved approach to separate and identify the different Fe- and Al-bearing phases associated with OM is urgently needed.

When SOC content decreases or increases due to the land use change, SOC compounds and their composition alter simultaneously (Wang et al., 2023). In our study, the relative abundance of organic van Krevelen classification groups in each extracted OM fraction remained similar across the two land uses and at both depths, although the OM content changed. This suggests that there is no selective preservation of specific organic compounds associated with Fe/Al phases, despite their differing affinities. All organic groups decrease or increase to similar extent when the SOM content change. This observation supports the view that the organo-mineral interface is dynamic and reversible (Kleber et al., 2021). The dynamic interactions, such as adsorption, desorption, competition and exchange reactions, present in the organo-mineral interface can affect the accumulation of any organic compounds involved, thereby maintaining their relative abundance uniformity (Bahadori et al., 2021; Yeasmin et al., 2023). The unchanged relative proportion or similar composition of organic compounds in OM fractions highlights the equal importance of any organic groups in influencing changes in environmental conditions, such as land use change. This finding provides a better understanding of SOM composition in response to diverse ecosystems coupled with anthropogenic activities.

Acknowledgement

This research was supported by the Australian Research Council (ARC) Discovery Project (DP220103026) and the University of Sydney. We are grateful to Edward Jones for his help in soil sample collection, Michael Turner for his assistance in the CHN analysis, Tom Savage for the ICP-AES analysis, and Nicholas Proschogo for his assistance with FT-ICR-MS data collection.

6.6 Appendix

6.6.1 Soil general characteristics

Table S 6.1 General characteristics of the soil samples (< 2 mm) used in this study*.

Land use	Native		Cropping	
Depth (cm)	0-15	15-30	0-15	15-30
pH (1:5 H_2O)	5.5±0.1	5.6±0.0	5.0±0.0	5.1±0.0
EC (mS cm^{-1})	10.3±0.7	6.3±0.0	17.5±2.2	13.1±1.5
CEC ($mmol_c$ kg^{-1})	103±0.5	40±0.3	102±0.7	43±0.8
Bulk density (g cm^{-3})	0.92	0.96	0.96	0.81
Clay (%)	31	43	28	45
Silt (%)	22	22	27	22
Sand (%)	47	36	45	33
Total Fe (mg g^{-1})	120.7 ± 0.8	122.7 ± 0.5	121.1 ± 0.6	122.4 ± 1.1
Total Al (mg g^{-1})	134.7 ± 2.0	141.7 ± 3.9	142.5 ± 1.5	143.1 ± 2.5
Minerals in the clay fraction	Hematite, goethite, kaolinite, vermiculite, gibbsite, anatase, quartz			

*Error bars indicate one standard error (n = 3).

Total concentration of Fe, Al, Mn, and Si of the soil samples were determined by a Niton XL3t portable X-Ray fluorescence analyser. The analysis was done in the Cu Mining Mode. The concentration of each metal was calibrated as Fe_2O_3, Al_2O_3, MnO_2, and SiO_2, respectively.

X-ray powder diffraction (XRPD) patterns were measured on a PANalytical X'Pert Pro diffractometer operating in Debye-Scherrer geometry with Cu Kα X-ray radiation and a PIXcel1D detector in continuous scanning mode over the 2θ angle range 5–65°. Samples were contained in flame-sealed thin-walled glass (WJM-Glas) capillaries that were rotated during the measurements.

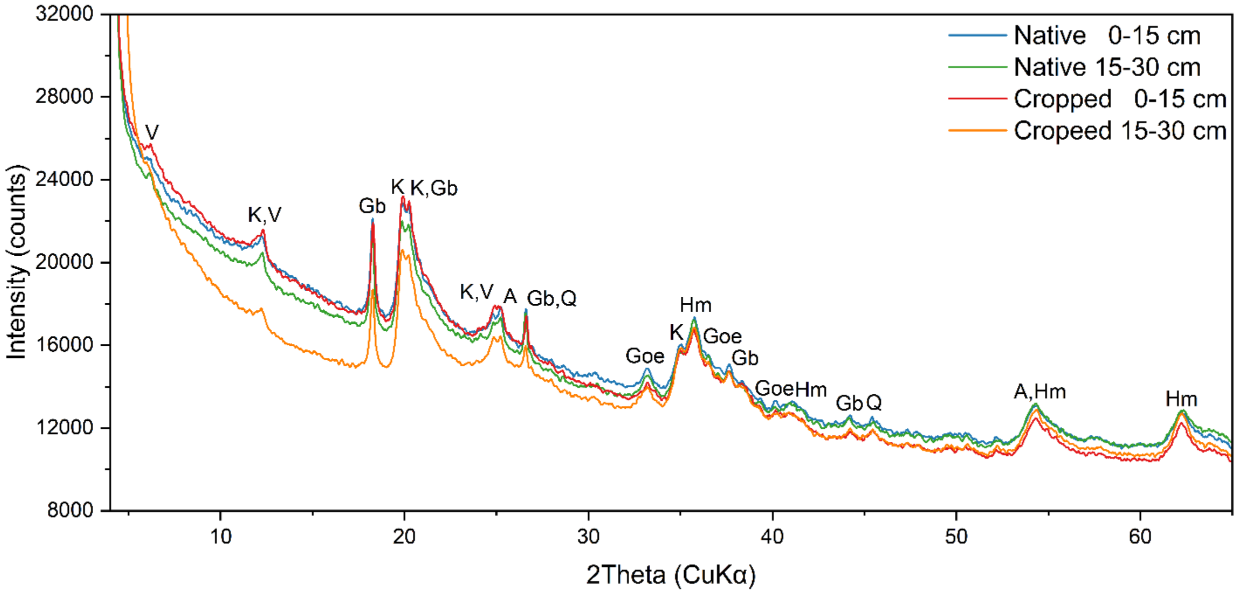

Figure S 6.1 X-ray powder diffraction (XRPD) pattern of soil samples from surface (0-15 cm) and subsurface (15-30 cm) at native vegetation and cropped field. V: vermiculite; K: kaolinite; Gb: gibbsite; A: anatase; Q: quartz; Goe: goethite; Hm: hematite.

6.6.2 Selective dissolution and post-extraction analyses

All soil samples for selective dissolution were air-dried, and finely ground (< 200 µm). The sequential selective dissolution procedure was followed by the methods described by Heckman et al. (2018) . For sequential extraction, 1.5 g of soil was weighed into a clean (pre-weighed) 50 ml centrifuge tube and the actual mass was recorded. For water-soluble fractions of carbon and mineral elements, 15 ml ultra-pure water (1:10 of soil: solution ratio) was added into each tube. Then the solutions were shaken overnight (approximately 16 h) on a rotary shaker at room temperature (23±1 °C) and then centrifuged at 3000 rpm for 60 mins. After centrifugation, the supernatants were decanted and syringe-filtered through a 0.2 µm non-pyrogenic hydrophilic syringe filter (Sartorious Stedium Biotech, Minisart High-flow, 26 mm diameter) into clean 50 mL sample tubes. 5 ml of ultra-pure H_2O was back-flushed through the filter to limit mass loss in the filter cartridge, which was added back to the original centrifuge tube. The extracted and filtered solutions were stored in the dark at 4 °C until further analyses. The residues were dried at 60 °C until all liquid had evaporated and dry weight was recorded. Before the next extraction step, the dried sample was pulverised using a clean glass rod to break up the pellet and homogenise the dried samples. A 300 mg sub-sample of the residue from each sample was removed from each replicate for total C analysis.

Next, the organically bound mineral complex fractions were extracted from the prior residues by shaking with 30 ml of 0.1 M sodium pyrophosphate. The procedure for steps including shaking, centrifugation, filtration, drying and subsampling was similar to water extraction. Short-ranged ordered mineral oxides were removed from the residual by extraction with acidified hydroxylamine (30 ml of 0.25 M NH_2OH 0.25 N HCl), using the identical steps as described earlier. But, A less sub-sample (150 mg) of residue from each sample was removed for total C analysis. Finally, remaining crystalline mineral oxides were extracted from the residues using inorganic dithionite (30 ml of 57.4 mM sodium dithionite). For the last extraction, before the filter back-flush procedure, we added 10 ml of 0.05 M HCl to the centrifuge tube and shaken with the residual soils for an additional one hour. The HCl rinse was centrifuged and filtered into the sample tube already containing the dithionite extract. Then we back-flushed the filters with 5 ml ultra-pure H_2O into the sample tube already containing the combined dithionite and HCl extracts. Same procedure was repeated again to possibly extract all of remaining minerals. The residual samples were finally analysed for the total C after drying.

Table S 6.2 The sequential extractable phases and conditions (Coward et al., 2017; Heckman et al., 2018).

Dissolution solvent	Solvent molarity	Solvent pH	Target phases	Dissolution mechanism
Ultra-pure water	H_2O	7	Water-soluble OC fractions	Dispersion
Sodium pyrophosphate	0.1 M $Na_4P_2O_7$	10	Colloidal or OM-chelated metal complex	Dispersion and chelation
Hydroxylamine-HCl	0.25 M NH_2OH 0.25 M HCl	2	OC fractions associated with Short-range ordered metal oxides	Reduction
Dithionite-HCl	57.4 mM $Na_2S_2O_4$ 0.05 M HCl	4	OC fractions associated well-crystalline metal oxides	Reduction

6.6.3 Calculations

The stocks of total organic carbon (TOC) and total nitrogen (TN) were calculated by the following equation:

$$C\ or\ N\ stock\ (t\ C\ ha^{-1}\ or\ t\ N\ ha^{-1}) = \frac{C_{conc} or\ N_{conc} \times BD \times D \times 1000}{100}$$

Where C_{conc} and N_{conc} are the concentration of total SOC and TN (mg g^{-1}), respectively; BD is the bulk density (g cm^{-3}), and D is the soil depth (m).

The C content extracted by each extractant was calculated by the difference C content in soil before and after the extractions:

$$C_{extracted}(mg\ C\ g^{-1}\ soil) = \frac{C_{conc_{Initial}} \times Soil\ mass_{Initial} - C_{conc_{after}} \times Residual\ mass_{after}}{Soil\ mass_{Initial}}$$

Where $\mathrm{C}_{\mathrm{conc}_{\mathrm{Initial}}}$ is the TOC in the soil used for a particular extraction step, $\mathrm{C}_{\mathrm{conc}_{\mathrm{after}}}$ is the TOC in the soil after the particular extraction step, $\mathrm{Soil\ mass}_{\mathrm{Initial}}$ is the original soil mass (oven-dried) used for the extraction procedure, and $\mathrm{Residual\ mass}_{\mathrm{after}}$ is the dried mass (oven-dried) after the extraction step.

The molar ratio of extracted OC and associated Fe and Al in each fraction was calculated by the following equation:

$$Molar\ ratio\ of\ C{:}\,(Fe + Al) = \frac{{OC_{Extracted}}/{M_C}}{{Fe_{Extracted}}/{M_{Fe}} + {Al_{Extracted}}/{M_{Al}}}$$

Where $OC_{Extracted}$, $Fe_{Extracted}$, and $Al_{Extracted}$ are the OC, Fe, and Al concentration in each extracted fraction (mg g^{-1}), M_C, M_{Fe}, and M_{Al} are the molar mass of each element (g mol^{-1}).

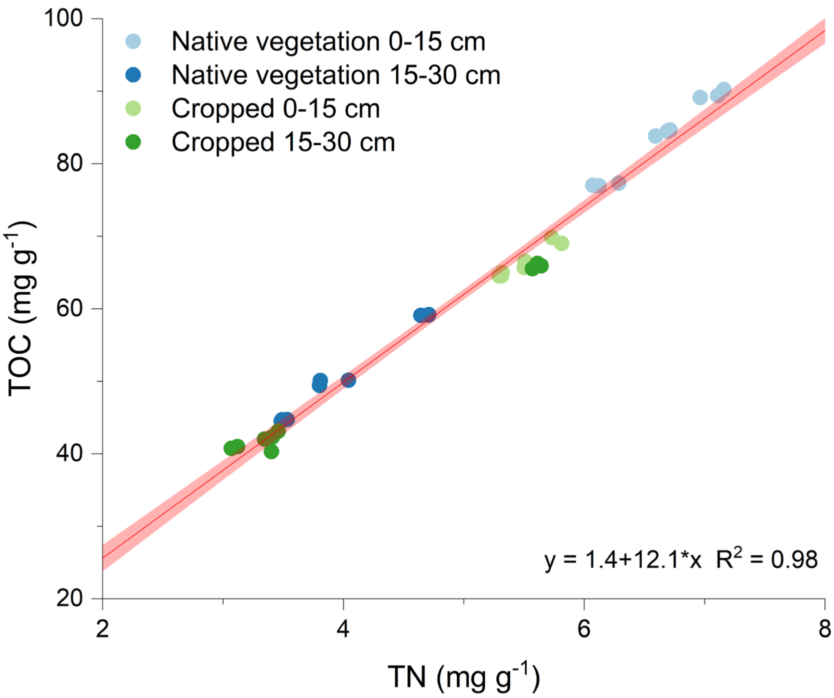

Figure S 6.2 Relationship between the concentration of total organic carbon (TOC) and total nitrogen (TN) in the surface (0-15 cm) and subsurface (15-30 cm) soils from native vegetation and cropped field.

Table S 6.3 Correlation between extracted organic carbon (OC) and Fe, Al, and Fe+Al in each extractable fraction*.

OC: Metals	Fractions	Correlation			R^2
		Coefficient	Std. Error	p-value	
OC:Fe	W	9.69	8.21	0.25	0.04
	PP	-0.22	0.58	0.71	0.005
	HH	-4.85	2.41	0.06	0.11
	DH	-0.24	0.77	0.76	0.003
OC:Al	W	8.89	12.00	0.46	0.02
	PP	0.51	0.54	0.36	0.03
	HH	-0.26	0.14	0.06	0.10
	DH	0.03	0.24	0.90	0.001
OC:(Fe+Al)	W	5.72	5.27	0.29	0.04
	PP	0.13	0.48	0.79	0.003
	HH	-0.25	0.13	0.06	0.10
	DH	0.01	0.27	0.98	0.00004

*W: water-soluble fraction; PP: organo-metal complex fraction; HH: well-crystalline metal complex fraction; and DH: well-crystalline metal complex fraction; $p<0.05$.

6.6.4 FT-ICR-MS data collection

Prior FT-ICR-MS analysis for the entrants, the suspensions were desalinated and concentrated through solid phase extraction (SPE) (Dittmar et al., 2008; Coward et al., 2018). Agilent PPL cartridges (200 mg, 3 ml) were rinsed with 1 cartridge volume (3 ml) with methanol (HPLC grade), and 2 cartridge volumes (6 ml) of 0.01 M HCl before use. The pH of extracted solutions was adjusted to 2 using HCl to increase the extraction efficiency for the DOC. Six cartridge volumes (18 ml) of extracted solution were passed through the cartridge under gravity. The cartridges were then acidified again with 6 ml of HCl to remove the salts and dried with clean air for 10 mins before the elution process. One cartridge volume (3 ml) of methanol was passed through the cartridge obtain the final elutes. The elutes were stored at -20 °C for further FT-ICR-MS analysis.

After SPE, extracted solution phases were characterized by FT-ICR-MS analysis using a 7 T Bruker SolariX 2xR FT-ICR-MS instrument with negative ion mode electrospray ionization. At the beginning of the analysis, an Agilent tunemix solution was used to externally calibrate the instrument. Extracts were diluted with LCMS grade methanol to final composition of 50:50 (v:v), and were introduced by a syringe pump providing an infusion rate of 120 μL h^{-1} and analysed with electrospray voltages of 4500 V with end plate offset of -800 V for each samples. Nebulizer gas was at 1.0-1.5 bar, and dry gas flow rate was set at 4 L min^{-1} with the dry temperature of 200 °C. Collision cell accumulation time was set 1.0s. The mass range of 150-3000 m/z were acquired with 4MWord time domains with 300 scans co-added. Co-added free induction decay signals were fast Fourier Transformed in Magnitude mode after 1 zero fill and Full-Sine apodization within ftmsControl software. At the beginning of FT-ICR-MS analysis, the instrument was externally calibrated with an Agilent tunemix solution, and all spectra were ultimately internally calibrated with a natural organic matter list before data analysis (Tolić et al., 2017). After post-spectral processing to identify and collect the peaks presented in at least four times out of nine replicates, 4025-180 mass spectral peaks were found in the extractants, and elemental compositions were assigned in the range of $150 < m/z < 850$ with signal-to-noise (S/N) ratio ≥ 10.

6.6.5 Molecular formula assignment

The molecular formula calculation aimed to generate empirical formula matches for the FT-ICR-MS peaks, following the procedure described by Ohno et al.(Ohno and Ohno, 2013) .The combination of atomic values was set as C (8–50 atoms), H (8–100 atoms), O (1-30 atoms), N (0–5 atoms), S (0–3 atoms), and P (0–2 atoms). The formulae of chemically feasible organic matter were followed by the below criteria: O/C≤ 1.2, H/C≤ 2.25, H/C≥ 0.3, N/C≤ 0.5, S/C≤ 0.2, P/C≤ 0.1, (S + P)/ C≤ 0.2, double-bond equivalence (DBE) ≥ 0, and must be a whole number(Koch and Dittmar, 2006).

The equation of DBE calculation was:

$$DBE = 1 + 1/2(C - H + N + P)$$

The organic compound classification was used to identify different groups OM compounds based on their H/C, O/C(Ohno et al., 2010; Ohno and Ohno, 2013; Bianco et al., 2019; Li et al., 2019; McDonough et al., 2022; Sheng et al., 2023), with six categories: aliphatic-like, lipids-like, peptides-like, unsaturated hydrocarbons-like, carbohydrates-like, condensed aromatic-like, lignin-like, tannins-like compounds, and others (unassigned compound formulae).

Table S 6.4 Classification of organic compound groups.

Category	H/C	O/C	N
Aliphatic-like	$1.5<H/C\leq2.2$	$0.3<O/C\leq0.67$	N=0
Lipids-like	$1.5<H/C\leq2.0$	$O/C\leq0.3$	
Peptides-like	$1.5<H/C\leq2.2$	$0.3<O/C\leq0.67$	N>0
Unsaturated Hydrocarbons-like	$0.7<H/C\leq1.5$	$O/C\leq0.1$	
Carbohydrates-like	$1.5<H/C\leq2.5$	$0.67<O/C\leq1.2$	
Condensed Aromatic-like	$0.2<H/C\leq0.67$	$O/C\leq0.67$	
Lignin-like	$0.67<H/C\leq1.5$	$0.1<O/C\leq0.67$	
Tannins-like	$0.67<H/C\leq1.5$	$0.67<O/C\leq1.2$	
Others	Unassigned formulae		

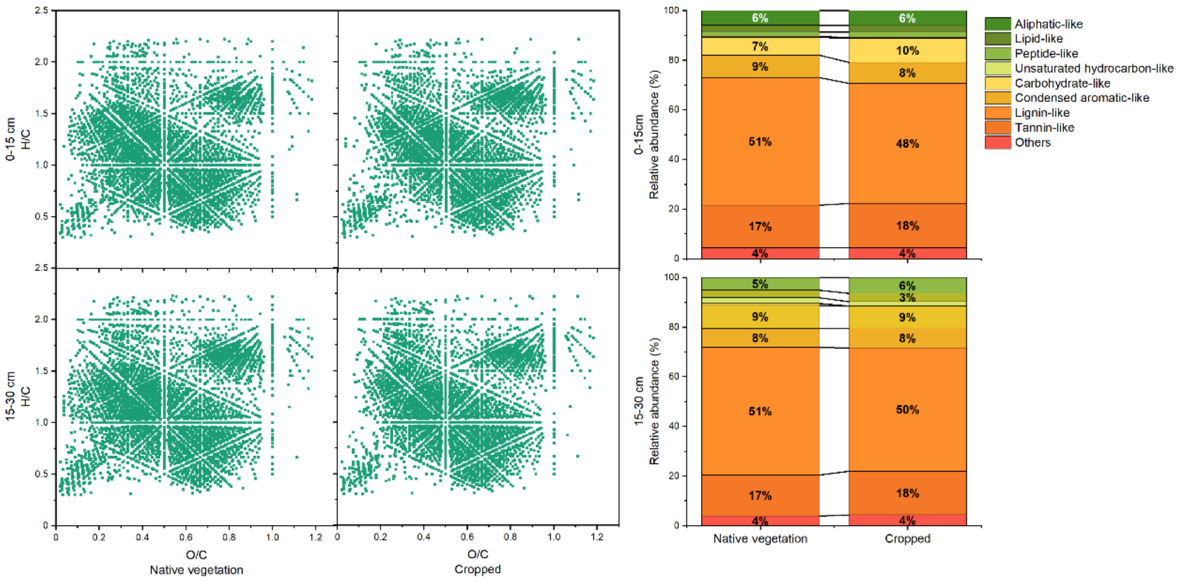

Figure S 6.3 van Krevelen diagrams and histograms of the relative abundance of entire assigned formulae of FT-ICR-MS data from all extractable fractions in the surface (0-15 cm) and subsurface (15-30 cm) soil from native vegetation and cropped fields.

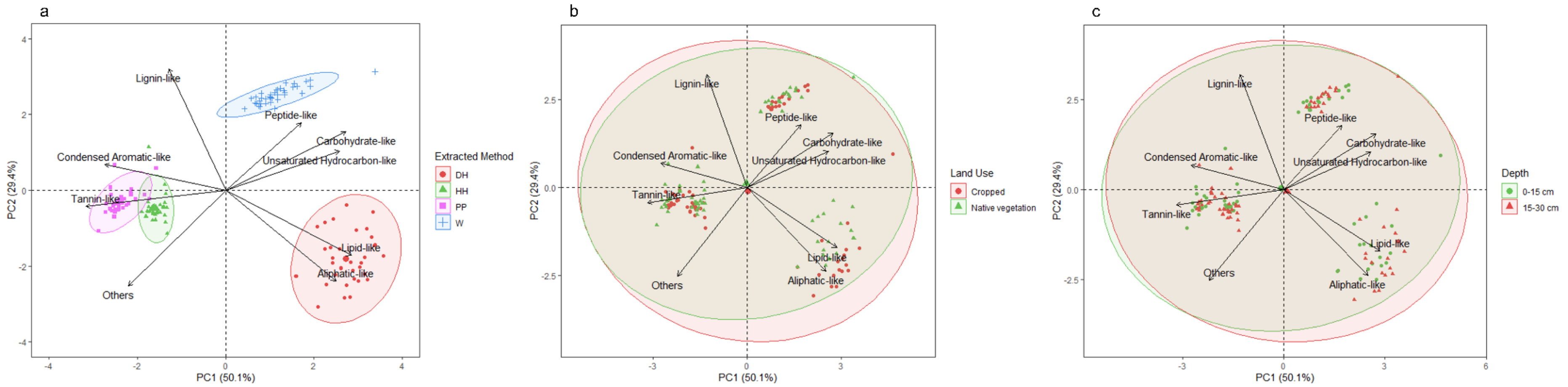

Figure S 6.4 Biplots of class groups of assigned formulae in each extractable fraction (W: water-soluble fraction; PP: organo-metal complex fraction; HH: well-crystalline metal complex fraction; and DH: well-crystalline metal complex fraction) (a), and for native vegetation and cropped land use (b).

References

Adhikari, D.,Yang, Y., 2015. Selective stabilization of aliphatic organic carbon by iron oxide. *Scientific Reports 5*(1), 11214.

Angst, G., Mueller, K.E., Castellano, M.J., Vogel, C., Wiesmeier, M.,Mueller, C.W., 2023. Unlocking complex soil systems as carbon sinks: multi-pool management as the key. *Nature Communications 14*(1), 2967.

Angst, G., Mueller, K.E., Nierop, K.G.J.,Simpson, M.J., 2021. Plant- or microbial-derived? A review on the molecular composition of stabilized soil organic matter. *Soil Biology and Biochemistry 156*, 108189.

Bahadori, M., Chen, C., Lewis, S., Boyd, S., Rashti, M.R., Esfandbod, M., Garzon-Garcia, A., Van Zwieten, L.,Kuzyakov, Y., 2021. Soil organic matter formation is controlled by the chemistry and bioavailability of organic carbon inputs across different land uses. *Science of The Total Environment 770*, 145307.

Bianco, A., Deguillaume, L., Chaumerliac, N., Vaïtilingom, M., Wang, M., Delort, A.-M.,Bridoux, M.C., 2019. Effect of endogenous microbiota on the molecular composition of cloud water: a study by Fourier-transform ion cyclotron resonance mass spectrometry (FT-ICR MS). *Scientific Reports 9*(1), 7663.

Chabbi, A., Kögel-Knabner, I.,Rumpel, C., 2009. Stabilised carbon in subsoil horizons is located in spatially distinct parts of the soil profile. *Soil Biology and Biochemistry 41*(2), 256-261.

Chantigny, M.H., 2003. Dissolved and water-extractable organic matter in soils: a review on the influence of land use and management practices. *Geoderma 113*(3), 357-380.

Chen, C., Dynes, J.J., Wang, J.,Sparks, D.L., 2014. Properties of Fe-organic matter associations via coprecipitation versus adsorption. *Environmental Science & Technology 48*(23), 13751-13759.

Chen, S., Klotzbücher, T., Lechtenfeld, O.J., Hong, H., Liu, C., Kaiser, K., Mikutta, C.,Mikutta, R., 2022. Legacy effects of sorption determine the formation efficiency of mineral-associated soil organic matter. *Environmental Science & Technology 56*(3), 2044-2053.

Chernyshova, I.V., Ponnurangam, S.,Somasundaran, P., 2011. Adsorption of fatty acids on iron (hydr)oxides from aqueous solutions. *Langmuir 27*(16), 10007-10018.

Clemente, J.S., Simpson, A.J.,Simpson, M.J., 2011. Association of specific organic matter compounds in size fractions of soils under different environmental controls. *Organic Geochemistry 42*(10), 1169-1180.

Cloy, J.M., Wilson, C.A.,Graham, M.C., 2014. Stabilization of organic carbon via chemical interactions with Fe and Al oxides in gley soils. *Soil Science 179*(12), 547-560.

Córdova, S.C., Olk, D.C., Dietzel, R.N., Mueller, K.E., Archontouilis, S.V.,Castellano, M.J., 2018. Plant litter quality affects the accumulation rate, composition, and stability of mineral-associated soil organic matter. *Soil Biology and Biochemistry 125*, 115-124.

Cotrufo, M.F., Ranalli, M.G., Haddix, M.L., Six, J.,Lugato, E., 2019. Soil carbon storage informed by particulate and mineral-associated organic matter. *Nature Geoscience 12*(12), 989-994.

Cotrufo, M.F., Wallenstein, M.D., Boot, C.M., Denef, K.,Paul, E., 2013. The microbial efficiency-matrix stabilization (MEMS) framework integrates plant litter decomposition with soil organic matter stabilization: do labile plant inputs form stable soil organic matter? *Global Change Biology 19*(4), 988-995.

Coward, E.K., Ohno, T.,Plante, A.F., 2018. Adsorption and molecular fractionation of dissolved organic matter on iron-bearing mineral matrices of varying crystallinity. *Environmental Science & Technology 52*(3), 1036-1044.

Coward, E.K., Ohno, T.,Sparks, D.L., 2019. Direct evidence for temporal molecular fractionation of dissolved organic matter at the iron oxyhydroxide interface. *Environmental Science & Technology 53*(2), 642-650.

Coward, E.K., Thompson, A.T.,Plante, A.F., 2017. Iron-mediated mineralogical control of organic matter accumulation in tropical soils. *Geoderma 306*, 206-216.

Czimczik, C.I.,Masiello, C.A., 2007. Controls on black carbon storage in soils. *Global Biogeochemical Cycles 21*(3).

de Souza Medeiros, A., dos Santos, T.C.,Maia, S.M.F., 2022. Effect of long-term and soil depth on soil organic carbon stocks after conversion from native vegetation to conventional tillage systems in Brazil. *Soil and Tillage Research 219*, 105336.

Deng, L., Zhu, G.-y., Tang, Z.-s.,Shangguan, Z.-p., 2016. Global patterns of the effects of land-use changes on soil carbon stocks. *Global Ecology and Conservation 5*, 127-138.

DiDonato, N., Chen, H., Waggoner, D.,Hatcher, P.G., 2016. Potential origin and formation for molecular components of humic acids in soils. *Geochimica et Cosmochimica Acta 178*, 210-222.

Ding, X., Qiao, Y., Filley, T., Wang, H., Lü, X., Zhang, B.,Wang, J., 2017. Long-term changes in land use impact the accumulation of microbial residues in the particle-size fractions of a Mollisol. *Biology and Fertility of Soils 53*(3), 281-286.

Dittmar, T., Koch, B., Hertkorn, N.,Kattner, G., 2008. A simple and efficient method for the solid-phase extraction of dissolved organic matter (SPE-DOM) from seawater. *Limnology and Oceanography: Methods 6*(6), 230-235.

Don, A., Schumacher, J.,Freibauer, A., 2011. Impact of tropical land-use change on soil organic carbon stocks – a meta-analysis. *Global Change Biology 17*(4), 1658-1670.

Duiker, S.W., Rhoton, F.E., Torrent, J., Smeck, N.E.,Lal, R., 2003. Iron (hydr)oxide crystallinity effects on soil aggregation. *Soil Science Society of America Journal 67*(2), 606-611.

Erktan, A., Balmot, J., Merino-Martín, L., Monnier, Y., Pailler, F., Coq, S., Abiven, S., Stokes, A.,Le Bissonnais, Y., 2017. Immediate and long-term effect of tannins on the stabilization of soil aggregates. *Soil Biology and Biochemistry 105*, 197-205.

Gabriel, C.E., Kellman, L.,Prest, D., 2018. Examining mineral-associated soil organic matter pools through depth in harvested forest soil profiles. *PLOS ONE 13*(11), e0206847.

Gao, J., Mikutta, R., Jansen, B., Guggenberger, G., Vogel, C.,Kalbitz, K., 2020. The multilayer model of soil mineral–organic interfaces—a review. *Journal of Plant Nutrition and Soil Science 183*(1), 27-41.

Guo, X., Meng, M., Zhang, J.,Chen, H.Y.H., 2016. Vegetation change impacts on soil organic carbon chemical composition in subtropical forests. *Scientific Reports 6*(1), 29607.

Hassink, J., 1997. The capacity of soils to preserve organic C and N by their association with clay and silt particles. *Plant and Soil 191*(1), 77-87.

Heckman, K., Lawrence, C.R.,Harden, J.W., 2018. A sequential selective dissolution method to quantify storage and stability of organic carbon associated with Al and Fe hydroxide phases. *Geoderma 312*, 24-35.

Hernandez-Soriano, M.C., Dalal, R.C., Warren, F.J., Wang, P., Green, K., Tobin, M.J., Menzies, N.W.,Kopittke, P.M., 2018. Soil organic carbon stabilization: mapping carbon speciation from intact microaggregates. *Environmental Science & Technology 52*(21), 12275-12284.

Hu, Z., McKenna, A.M., Wen, K., Zhang, B., Mao, H., Goual, L., Feng, X.,Zhu, M., 2024. Controls of mineral solubility on adsorption-induced molecular fractionation of dissolved organic matter revealed by 21 T FT-ICR MS. *Environmental Science & Technology 58*(5), 2313-2322.

Huang, X., Liang, Y., Ye, Q., Ding, Z., Liu, F.,Shi, Z., 2023. Theoretical modeling of molecular fractionation of dissolved organic matter on ferrihydrite and its impact on proton and metal binding properties. *Science of The Total Environment 888*, 164276.

Kaiser, K.,Zech, W., 1996. Defects in estimation of aluminum in humus complexes of podzolic soils by pyrophosphate extraction. *Soil Science 161*(7), 452-458.

Kaiser, M., Ellerbrock, R.H., Wulf, M., Dultz, S., Hierath, C.,Sommer, M., 2012. The influence of mineral characteristics on organic matter content, composition, and stability of topsoils under long-term arable and forest land use. *Journal of Geophysical Research: Biogeosciences 117*(G2).

Kirkby, C.A., Kirkegaard, J.A., Richardson, A.E., Wade, L.J., Blanchard, C.,Batten, G., 2011. Stable soil organic matter: a comparison of C:N:P:S ratios in Australian and other world soils. *Geoderma 163*(3), 197-208.

Kleber, M., Bourg, I.C., Coward, E.K., Hansel, C.M., Myneni, S.C.B.,Nunan, N., 2021. Dynamic interactions at the mineral–organic matter interface. *Nature Reviews Earth & Environment 2*(6), 402-421.

Kleber, M., Eusterhues, K., Keiluweit, M., Mikutta, C., Mikutta, R.,Nico, P.S., 2015. Chapter one - Mineral–organic associations: formation, properties, and relevance in soil environments. In: D. L. Sparks (Ed.), *Advances in Agronomy.* Academic Press, pp. 1-140.

Kleber, M., Mikutta, R., Torn, M.S.,Jahn, R., 2005. Poorly crystalline mineral phases protect organic matter in acid subsoil horizons. *European Journal of Soil Science 56*(6), 717-725.

Kleber, M., Sollins, P.,Sutton, R., 2007. A conceptual model of organo-mineral interactions in soils: self-assembly of organic molecular fragments into zonal structures on mineral surfaces. *Biogeochemistry 85*(1), 9-24.

Knicker, H., 2007. How does fire affect the nature and stability of soil organic nitrogen and carbon? A review. *Biogeochemistry 85*(1), 91-118.

Koch, B.P.,Dittmar, T., 2006. From mass to structure: an aromaticity index for high-resolution mass data of natural organic matter. *Rapid Communications in Mass Spectrometry 20*(5), 926-932.

Kögel-Knabner, I., Guggenberger, G., Kleber, M., Kandeler, E., Kalbitz, K., Scheu, S., Eusterhues, K.,Leinweber, P., 2008. Organo-mineral associations in temperate soils:

integrating biology, mineralogy, and organic matter chemistry. *Journal of Plant Nutrition and Soil Science 171*(1), 61-82.

Kopittke, P.M., Dalal, R.C., Finn, D.,Menzies, N.W., 2017. Global changes in soil stocks of carbon, nitrogen, phosphorus, and sulphur as influenced by long-term agricultural production. *Global Change Biology 23*(6), 2509-2519.

Kramer, M.G.,Chadwick, O.A., 2018. Climate-driven thresholds in reactive mineral retention of soil carbon at the global scale. *Nature Climate Change 8*(12), 1104-1108.

Kramer, M.G., Sanderman, J., Chadwick, O.A., Chorover, J.,Vitousek, P.M., 2012. Long-term carbon storage through retention of dissolved aromatic acids by reactive particles in soil. *Global Change Biology 18*(8), 2594-2605.

Lal, R., Monger, C., Nave, L.,Smith, P., 2021. The role of soil in regulation of climate. *Philosophical Transactions of the Royal Society B: Biological Sciences 376*(1834), 20210084.

Lawrence, C.R., Harden, J.W., Xu, X., Schulz, M.S.,Trumbore, S.E., 2015. Long-term controls on soil organic carbon with depth and time: a case study from the Cowlitz River Chronosequence, WA USA. *Geoderma 247-248*, 73-87.

Lenhardt, K.R., Breitzke, H., Buntkowsky, G., Mikutta, C.,Rennert, T., 2022. Interactions of dissolved organic matter with short-range ordered aluminosilicates by adsorption and co-precipitation. *Geoderma 423*, 115960.

Li, L., Fang, Z., He, C.,Shi, Q., 2019. Separation and characterization of marine dissolved organic matter (DOM) by combination of Fe(OH)3 co-precipitation and solid phase extraction followed by ESI FT-ICR MS. *Analytical and Bioanalytical Chemistry 411*(10), 2201-2208.

Lilienfein, J., Qualls, R.G., Uselman, S.M.,Bridgham, S.D., 2004. Adsorption of dissolved organic carbon and nitrogen in soils of a weathering chronosequence. *Soil Science Society of America Journal 68*(1), 292-305.

Lopez-Sangil, L.,Rovira, P., 2013. Sequential chemical extractions of the mineral-associated soil organic matter: an integrated approach for the fractionation of organo-mineral complexes. *Soil Biology and Biochemistry 62*, 57-67.

Lv, J., Huang, Z., Christie, P.,Zhang, S., 2020. Reducing reagents induce molecular artifacts in the extraction of soil organic matter. *ACS Earth and Space Chemistry 4*(11), 1913-1919.

Lv, J., Huang, Z., Luo, L., Zhang, S.,Wang, Y., 2022. Advances in molecular and microscale characterization of soil organic matter: current limitations and future prospects. *Environmental Science & Technology 56*(18), 12793-12810.

McDonough, L.K., Andersen, M.S., Behnke, M.I., Rutlidge, H., Oudone, P., Meredith, K., O'Carroll, D.M., Santos, I.R., Marjo, C.E., Spencer, R.G.M., McKenna, A.M.,Baker, A., 2022. A new conceptual framework for the transformation of groundwater dissolved organic matter. *Nature Communications 13*(1), 2153.

Mikutta, R., Zang, U., Chorover, J., Haumaier, L.,Kalbitz, K., 2011. Stabilization of extracellular polymeric substances (Bacillus subtilis) by adsorption to and coprecipitation with Al forms. *Geochimica et Cosmochimica Acta 75*(11), 3135-3154.

Neurath, R.A., Pett-Ridge, J., Chu-Jacoby, I., Herman, D., Whitman, T., Nico, P.S., Lipton, A.S., Kyle, J., Tfaily, M.M., Thompson, A.,Firestone, M.K., 2021. Root carbon interaction with soil minerals is dynamic, leaving a legacy of microbially derived residues. *Environmental Science & Technology 55*(19), 13345-13355.

Norén, K., Loring, J.S.,Persson, P., 2008. Adsorption of alpha amino acids at the water/goethite interface. *Journal of Colloid and Interface Science 319*(2), 416-428.

Ohno, T., He, Z., Sleighter, R.L., Honeycutt, C.W.,Hatcher, P.G., 2010. Ultrahigh resolution mass spectrometry and indicator species analysis to identify marker components of soil- and plant biomass-derived organic matter fractions. *Environmental Science & Technology 44*(22), 8594-8600.

Ohno, T.,Ohno, P.E., 2013. Influence of heteroatom pre-selection on the molecular formula assignment of soil organic matter components determined by ultrahigh resolution mass spectrometry. *Analytical and Bioanalytical Chemistry 405*(10), 3299-3306.

Ostrowska, A.,Porębska, G., 2015. Assessment of the C/N ratio as an indicator of the decomposability of organic matter in forest soils. *Ecological Indicators 49*, 104-109.

Panettieri, M., Rumpel, C., Dignac, M.F.,Chabbi, A., 2017. Does grassland introduction into cropping cycles affect carbon dynamics through changes of allocation of soil organic matter within aggregate fractions? *Science of The Total Environment 576*, 251-263.

Patel, K.F., Tejnecký, V., Ohno, T., Bailey, V.L., Sleighter, R.L.,Hatcher, P.G., 2021. Reactive oxygen species alter chemical composition and adsorptive fractionation of soil-derived organic matter. *Geoderma 384*, 114805.

Paul, E.A., 2016. The nature and dynamics of soil organic matter: plant inputs, microbial transformations, and organic matter stabilization. *Soil Biology and Biochemistry 98*, 109-126.

Poeplau, C.,Don, A., 2013. Sensitivity of soil organic carbon stocks and fractions to different land-use changes across Europe. *Geoderma 192*, 189-201.

Ramesh, T., Bolan, N.S., Kirkham, M.B., Wijesekara, H., Kanchikerimath, M., Srinivasa Rao, C., Sandeep, S., Rinklebe, J., Ok, Y.S., Choudhury, B.U., Wang, H., Tang, C., Wang, X., Song, Z.,Freeman Ii, O.W., 2019. Chapter one - Soil organic carbon dynamics: impact of land use changes and management practices: a review. In: D. L. Sparks (Ed.), *Advances in Agronomy.* Academic Press, pp. 1-107.

Rayment, G.E.,Lyons, D.J. (2010). *Soil chemical methods - Australasia*: CSIRO Publishing.

Riedel, T., Biester, H.,Dittmar, T., 2012. Molecular fractionation of dissolved organic matter with metal salts. *Environmental Science & Technology 46*(8), 4419-4426.

Rivas-Ubach, A., Liu, Y., Bianchi, T.S., Tolić, N., Jansson, C.,Paša-Tolić, L., 2018. Moving beyond the van Krevelen diagram: a new stoichiometric approach for compound classification in organisms. *Analytical Chemistry 90*(10), 6152-6160.

Rumpel, C.,Kögel-Knabner, I., 2011. Deep soil organic matter-a key but poorly understood component of terrestrial C cycle. *Plant and Soil 338*(1), 143-158.

Schuppli, P.A., Ross, G.J.,McKeague, J.A., 1983. The effective removal of suspended materials from pyrophosphate extracts of soils from tropical and temperate regions. *Soil Science Society of America Journal 47*(5), 1026-1032.

Sheng, M., Chen, S., Liu, C.-Q., Fu, Q., Zhang, D., Hu, W., Deng, J., Wu, L., Li, P., Yan, Z., Zhu, Y.-G.,Fu, P., 2023. Spatial and molecular variations in forest topsoil dissolved organic matter as revealed by FT-ICR mass spectrometry. *Science of The Total Environment 895*, 165099.

Sparks, D.L., Singh, B.,Siebecker, M.G., 2024a. Chapter 3 - Chemistry of soil organic matter. In: D. L. Sparks, B. Singh, and M. G. Siebecker (Eds.), *Environmental Soil Chemistry (Third Edition).* Academic Press, pp. 105-167.

Sparks, D.L., Singh, B.,Siebecker, M.G., 2024b. Chapter 9 - The chemistry of soil acidity. In: D. L. Sparks, B. Singh, and M. G. Siebecker (Eds.), *Environmental Soil Chemistry (Third Edition).* Academic Press, pp. 381-410.

Stewart, C.E., Paustian, K., Conant, R.T., Plante, A.F.,Six, J., 2007. Soil carbon saturation: concept, evidence and evaluation. *Biogeochemistry 86*(1), 19-31.

Tfaily, M.M., Chu, R.K., Tolić, N., Roscioli, K.M., Anderton, C.R., Paša-Tolić, L., Robinson, E.W.,Hess, N.J., 2015. Advanced solvent based methods for molecular characterization of soil organic matter by high-resolution mass spectrometry. *Analytical Chemistry 87*(10), 5206-5215.

Tfaily, M.M., Chu, R.K., Toyoda, J., Tolić, N., Robinson, E.W., Paša-Tolić, L.,Hess, N.J., 2017. Sequential extraction protocol for organic matter from soils and sediments using high resolution mass spectrometry. *Analytica Chimica Acta 972*, 54-61.

Thevenot, M., Dignac, M.-F.,Rumpel, C., 2010. Fate of lignins in soils: a review. *Soil Biology and Biochemistry 42*(8), 1200-1211.

Tolić, N., Liu, Y., Liyu, A., Shen, Y., Tfaily, M.M., Kujawinski, E.B., Longnecker, K., Kuo, L.-J., Robinson, E.W., Paša-Tolić, L.,Hess, N.J., 2017. Formularity: software for automated formula assignment of natural and other organic matter from ultrahigh-resolution mass spectra. *Analytical Chemistry 89*(23), 12659-12665.

Veldkamp, E., Becker, A., Schwendenmann, L., Clark, D.A.,Schulte-Bisping, H., 2003. Substantial labile carbon stocks and microbial activity in deeply weathered soils below a tropical wet forest. *Global Change Biology 9*(8), 1171-1184.

Viscarra Rossel, R.A., Webster, R., Bui, E.N.,Baldock, J.A., 2014. Baseline map of organic carbon in Australian soil to support national carbon accounting and monitoring under climate change. *Global Change Biology 20*(9), 2953-2970.

Wagai, R.,Mayer, L.M., 2007. Sorptive stabilization of organic matter in soils by hydrous iron oxides. *Geochimica et Cosmochimica Acta 71*(1), 25-35.

Wagai, R., Mayer, L.M., Kitayama, K.,Shirato, Y., 2013. Association of organic matter with iron and aluminum across a range of soils determined via selective dissolution techniques coupled with dissolved nitrogen analysis. *Biogeochemistry 112*(1), 95-109.

Wang, H., Ding, Y., Zhang, Y., Wang, J., Freedman, Z.B., Liu, P., Cong, W., Wang, J., Zang, R.,Liu, S., 2023. Evenness of soil organic carbon chemical components changes with tree species richness, composition and functional diversity across forests in China. *Global Change Biology 29*(10), 2852-2864.

Wei, X., Shao, M., Gale, W.,Li, L., 2014. Global pattern of soil carbon losses due to the conversion of forests to agricultural land. *Scientific Reports 4*(1), 4062.

Wissing, L., Kölbl, A., Häusler, W., Schad, P., Cao, Z.-H.,Kögel-Knabner, I., 2013. Management-induced organic carbon accumulation in paddy soils: the role of organo-mineral associations. *Soil and Tillage Research 126*, 60-71.

Ye, Y., Wang, Z., Liu, L., Qi, K.,Xie, X., 2023. Novel insights into the temporal molecular fractionation of dissolved black carbon at the iron oxyhydroxide - water interface. *Water Research 229*, 119410.

Yeasmin, S., Singh, B., Johnston, C.T., Hua, Q.,Sparks, D.L., 2023. Changes in particulate and mineral-associated organic carbon with land use in contrasting soils. *Pedosphere 33*(3), 421-435.

Zhang, X., Li, Z., Nie, X., Huang, M., Wang, D., Xiao, H., Liu, C., Peng, H., Jiang, J.,Zeng, G., 2019. The role of dissolved organic matter in soil organic carbon stability under water erosion. *Ecological Indicators 102*, 724-733.

Zhao, Q., Callister, S.J., Thompson, A.M., Kukkadapu, R.K., Tfaily, M.M., Bramer, L.M., Qafoku, N.P., Bell, S.L., Hobbie, S.E., Seabloom, E.W., Borer, E.T.,Hofmockel, K.S., 2020. Strong mineralogic control of soil organic matter composition in response to nutrient addition across diverse grassland sites. *Science of The Total Environment 736*, 137839.

Chapter 7 Conclusion and outlook

7.1 The heterogeneity and chemical convergence of DOM fraction composition

DOM is inherently heterogeneous. It originates from many sources, including the decomposition of above-ground litter (stems and leaves), below-ground root exudates and secondary metabolites, and microbial metabolites and necromass (Kalbitz et al., 2000; Cleveland et al., 2004). Distinct chemical signatures of plant residues can be reflected in DOM composition (Kalbitz et al., 2000; Kögel-Knabner, 2002). In Chapter 3, apart from the differences in their DOC quantity (pine > eucalyptus > wheat > pasture), source-specific differences among plant residues were evident in the relative abundances of DOM compound characteristics. Pine DOM retained its inherent plant-derived signatures, with large contributions from lignin, aromatic and carboxylic compounds. DOM derived from eucalyptus residues exhibited unsaturated signatures, with large contributions from unsaturated hydrocarbon and ketone compounds. Wheat DOM undergone through intensively microbial processes, with large proportion of aliphatic, lipid, alkyl and O-alkyl compounds. Pasture DOM showed large contributions from condensed aromatic, phenolic, peptide, and O-alkyl compounds. However, once DOM is released, a chain of similar degradation steps including physical, chemical and biological transformation processes can rapidly alter the initial compositional and spatial heterogenous signature (Harfmann et al., 2019; Davenport et al., 2023). Continuous transformation and remineralisation of DOM tend to produce a progressively more chemically homogeneous pool of DOM compounds (An et al., 2024; Freeman et al., 2024). In Chapter 3, none of the DOM fractions displayed a unique characteristic of molecular structures that could fully distinguish them apart. Similar spectroscopic patterns and chemical compositions were observed among different DOM fractions, supporting the hypothesis that microbial processing influences chemical convergence in DOM composition (Davenport et al., 2023; Freeman et al., 2024). These microbial processes can be seen as a funnel to break down large plant-derived macromolecules into smaller molecules, which can be further transformed into larger microbially-derived products (Roth et al., 2019).

In Chapter 3, different techniques reveal complementary aspects of DOM compositions, including molecular composition, bonding environment and compound structure (Minor et al., 2014; Lv et al., 2022). Each method required specific sample preparation and offered different sensitivity. No single technique can fully capture the complexity of DOM compositions. The integration of multiple techniques for DOM characterisations is therefore essential. Regardless of some consistent information aligned with biochemical expectations, the multivariate analysis also revealed contrasting results across analytical techniques. For example, the abundance of O-alkyl C and aromatic C estimated by XPS, NMR, and NEXAFS showed negative correlations. Such discrepancies should be interpreted cautiously and verified using additional methods to eliminate potential artifacts arising from sample preparation, calibration, and peak assignment. A reliable and comprehensive understanding of DOM composition requires integrating multiple techniques. Same approach can also be applied to other critical fractions in soil chemistry and will increase our understanding of complexity of the “black box” of SOM.

7.2 Both DOM composition and mineral surface chemistry modulate the mineral-organic interaction

Mineral-organic interactions are governed by the match between adsorbent (mineral) and adsorbate (DOM). At the mineral-organic interfaces, mineral surface chemistry controls the initial adsorption capacity and binding mechanism for the DOM adsorption, whereas DOM functionality controls the sequential assembly as multilayer architectures on mineral-organic complexes (Eusterhues et al., 2011; Chen et al., 2014; Hong et al., 2020; Liu et al., 2023). In Chapter 4, under acidic conditions, DOM adsorption capacity of minerals for DOM in acidic condition followed the order: ferrihydrite > allophane > goethite > kaolinite > birnessite > montmorillonite. Different reaction mechanisms including ligand exchange, electrostatic attraction, H-bonding, π-π EDA interaction, and hydrophobic attractions occurred at mineral-organic interfaces. However, surface sites can become saturated or occluded by preferentially reactive functional groups in DOM (Kleber et al., 2007; Azimzadeh and Martínez, 2025). Control of the interactions then gradually shifted from mineral selectivity to the chemistry of the adsorbed molecules as increasing loading (Kleber et al., 2021; Chen et al., 2022). In Chapter 4, the sequential reaction order of organic functional groups varied across mineral surfaces. However, conjugated C=C/C=O, C-O-C and C-O moieties consistently dominated at each mineral-organic interface, indicating that subsequent uptake proceeded via organic-organic interactions and the assembly of multiplayer structures. These subsequently assembled associations may be generally weaker and more reversible than primary mineral-organic bonds, making the resulting complexes more sensitive to microbial accessibility and to shifts in soil conditions (Zhao et al., 2020).

Overall, mineral-organic and organic-organic interactions cooperatively contributed the selective retention of DOM on minerals surfaces. Variable charged minerals (ferrihydrite, allophane, goethite, kaolinite) preferentially accumulated DOM rich in carboxylic, aromatic, aliphatic moieties, whereas negatively charged minerals (birnessite and montmorillonite) accumulated more quinone and phenolic C components. The quality of DOM from different sources also matters. The more functionally diverse eucalypt DOM was adsorbed more strongly than wheat DOM, which contained fewer reactive carboxyl groups. Mineral surface chemistry determines the principles for which bonds can be formed and how strong they are, while DOM composition supplies the functional groups that follows those principles. Therefore, predicting the persistence of SOM in natural environments and designing strategies to enhance its formation and stabilisation require attention to both mineral and DOM chemistry.

7.3 OPTIR technique can be used as a powerful analytical approach to directly characterise OM within MAOM fractions

In Chapter 5, compared to traditional FTIR spectroscopy, the OPTIR spectroscopy provides submicron chemical maps and directly resolves organic functional groups on mineral-organic complexes with minimal sample preparation (Prater et al., 2024; Molina et al., 2025). Whether characterising synthesised mineral-organic complexes or POM and MAOM fractions isolated from soils, ATR spectra were largely dominated by lattice vibrations from Si-O, Al-O and Fe-O bonds and revealed only weak organic bands. In contrast, OPTIR can detect the key moieties that anchor OM to mineral surfaces. It identified carboxylic C=O groups engaging in ligand exchange with surface Fe/Al-OH groups, alcoholic C-O groups sharing H-bonds with edge hydroxyl groups on octahedral sheets, aromatic and phenolic C=C groups associating with siloxane sheets through hydrophobic partitioning and π-π EDA interactions, as well as the participation of N functional groups in binding. By localising where specific organic moieties reside and distinguishing organic layers from adjacent mineral surface, OPTIR can identify the chemistry at interfaces, including organic coatings and multilayer assemblies at mineral surfaces, which is essential for understanding SOM stabilisation. Compared to ATR which can scarcely distinguish POM and MAOM fractions in a soil, OPTIR detected OM from both POM and MAOM fractions in the Ferrasol showed a distinct and patchy distribution, while in the Vertisol, they appeared uniformly distributed. In addition, OPTIR resolved sharp aliphatic C-

H bands and clearer organic bands in the region of 1800-1500 cm^{-1} across OM fractions. Therefore, given its high spatial resolution, flexibility and sensitivity to OM fractions, OPTIR is well suited to analyse complex mineral-organic interactions at the microscale and to track their interactions over time.

7.4 Molecular composition of OM fractions does not change with land use change

Land use change can alter soil carbon concentration and stocks, but it does not always change the relative composition of OM fractions within mineral associated pools (Dalal et al., 2021; Hondroudakis et al., 2024). In Chapter 6, land use changing from native vegetation to cropping reduced carbon content in OM fractions, particularly in the surface soils. However, these sequentially extracted mineral associated fractions exhibited consistent similar compositions across land uses and depths. The OM within organo-metal complexes and short-ranged ordered Fe/Al oxides was enriched in lignin-like and condensed aromatic-like compounds, while aliphatic-like compounds dominated within the crystalline Fe/Al oxides. Although the possibly change within molecular class cannot be ruled out, this pattern of changing concentration of OM fractions while maintaining their relative composition can be explained by the kinetic nature of mineral-organic interfaces (Kleber et al., 2021). OM retained on mineral phases may be less stable than often expected, due to the dynamic adsorption, desorption, competition, exchange and diffusion occurring continuously at interfaces. When the supply of OM matter changes, the entire OM pools simultaneously change to maintain the dynamic equilibrium at mineral-organic interfaces, rather than selectively favouring any single organic group. This further emphasises the importance role of soil mineralogy in controlling the selective preservation of OM fractions, while changes in environmental conditions, such as land use change, primarily change their content rath than their relative composition. However, this does not imply the land management is irrelevant. Instead, practices that increase organic inputs, reduce disturbance, and maintain favourable moisture and redox regimes can still enhance the preservation of OM as MAOM fractions, supporting long-term SOM sequestration.

7.5 Environmental implication

The persistence of SOM is primary controlled by physical protection within soil aggregates and by chemical interactions with reactive mineral surfaces (Kleber et al., 2015). Conventionally, most of previous laboratory studies have focused on a single predictor in examining carbon sequestration, such as the abundance of specific organic input, mineral species, clay content and their specific surface area (Feng et al., 2005; Mikutta et al., 2014; Zhang et al., 2021; Lenhardt et al., 2022). In the contrary, this thesis takes a more systematic approach by considering the complexity of DOM composition, the diversity of mineral and metal oxide surface chemistries, the complementary use of traditional and advanced analytical techniques, and the effects of land use conversion from molecular scales to larger spatial scales. The heterogeneity and chemical convergence observed in DOM derived from different plant residues suggest that the influence of land use on the fate of DOM in terrestrial environments may be overestimated. Land use can still affect the quantity of DOM, but its chemical composition may be only shifted in the relative abundance of certain organic compounds. When DOM interact with soil minerals, selective retention of certain organic compounds can occur at mineral-organic interfaces, depending on both DOM composition and the surface chemistry of mineral phases. The protection by minerals can buffer MAOM against external environmental changes such as land use conversion (Bahadori et al., 2021; Yang et al., 2024). This thesis shows that land use can alter SOC stocks without necessarily having significant effect on selective preservation or loss of certain organic compounds within mineral associated pools. Therefore, future predictive SOC models for soil and climate management should explicitly represent adsorption, desorption, exchange and completion processes at mineral-organic interfaces and also integrate mineral surface properties, including surface charge, specific surface area, reactive site density, and crystal structure, along with the abundance and characteristics of functional groups and compound families within DOM pool. Models used to understand the fate of SOC typically represent SOM as a set of conceptual pools. For example, the traditional Century and RothC models treat SOM as a continuum of pools with different turnover rates, while the more recent Millennial model expands the number of OM pools based on residence time (Johnston and Poulton, 2018; Nicoloso et al., 2020; Abramoff et al., 2022). However, these conceptual models still tend to underrepresent the role of mineral phases and the diversity of mineral-organic interactions that strongly influence SOC dynamics. The future predictive SOC models should provide a more accurate and mechanistically grounded framework for estimating the dynamic of SOC and their implications for soil functions and climate regulations.

7.6 Limitation and outlook

Overall, the central conclusion is that the formation of MAOM fractions depends on the composition of DOM input, the surface chemistry of minerals, and environmental conditions related to land use. Mineral surfaces provide reactive sites and govern which reactions are thermodynamically and kinetically favoured. DOM fractions supply the functional groups that can bind to, exchange with, and assemble on mineral surfaces. Land use and management modulate the quantity, quality and timing of organic inputs, influencing the amount and extent of SOM preservation. However, the experiments in these studies focused on abiotic processes, and the role of the microbes in the SOM stabilisation was not considered.

In Chapter 3, DOM characterisation inferred the decomposition state of plant residues from resulting DOM composition rather than directly tracking DOM releasing from fresh to decomposed residues. It was difficult to clearly distinguish plant-derived inputs from microbial-derived inputs. There was also large uncertainty regarding the representativeness of DOM composition for the corresponding plant residues with only four samples characterised. Therefore, future studies should focus on using isotopic or molecular tracer for source attribution and include controlled decomposition stages to determine when and how plant signatures are lost or preserved. In addition, characterising DOM from a broader range of plant types across diverse locations and climate conditions would help develop more robust structural models of DOM composition.

In Chapter 4, mineral-organic interactions and the stabilisation of MAOM can also be affected by microbial processes through exudation production, extracellular enzyme activity, biofilm formation, and microbial-derived redox reactions (Kleber et al., 2015; Bailey et al., 2019; Angst et al., 2021). The desorption kinetics, enzymatic accessibility and priming responses of the synthesised MAOM fractions were not measured, thus their biological resistance remains unclear. Therefore, future studies should integrate microbial communities into mineral-organic interactions and ageing experiments to establish a comprehensive model of mineral-organic-microbial interfaces, predicting the formation and stabilisation of MAOM fractions. In addition, mineral-organic interactions are influenced by solution conditions, including pH, ionic strength and composition, moisture condition, and redox potential, which would vary widely across field soils (Allard et al., 2017; Mayer et al., 2019; Millman et al., 2024). Therefore, careful attention to the solution chemistry at mineral-organic interfaces is also essential for understanding the formation of MAOM.

In Chapters 5 and 6, the isolation approaches of the POM and MAOM fractions, as well as the OM fractions associated with specific mineral phases from soils, remained imperfect. Whether using physical separation by density or size, or chemical extraction involving dispersion, chelation and reduction, there is still a significant overlap among the target fractions (Heckman et al., 2018; Lavallee et al., 2020). Some artifacts can also be produced during the chemical extraction (Lv et al., 2020). These would complicate distinguishing among OM fractions and obscure their true compositions during characterisation. An improved extraction approach to clearly sperate different OM fractions is urgently needed. The OPTIR tool used in Chapter 5 relies on photothermal expansion following IR adsorption by molecular bonds, thus, the possibility of thermal damage from samples cannot be neglected (Jamoteau et al., 2025). In Chapter 6, only one group of weathered soil type was evaluated for the effect of land use change, which can provide a controlled comparison but limit to generalisability to other soils. Because mineralogy varies across soil orders, it is necessary to systematically study soils with different mineralogies, depths, and management histories to determine whether the relative composition of OM associated with mineral phases is consistent.

In the end, the next phase of research should integrate organic inputs, microbial activity, and mineralogy, and controlled environmental conditions that encompass both biotic and abiotic factors. Employing a suite of complementary molecular and imaging methods will facilitate the development of a comprehensive and reliable mechanism to predict the fate and dynamic of SOM. This approach will close key knowledge gaps in SOM stabilisation and provide a robust foundation for designing land management practises that enhancing long-term SOC storage for climate mitigation.

References

Abramoff, R.Z., Guenet, B., Zhang, H., Georgiou, K., Xu, X., Viscarra Rossel, R.A., Yuan, W.,Ciais, P., 2022. Improved global-scale predictions of soil carbon stocks with Millennial Version 2. *Soil Biology and Biochemistry 164*, 108466.

Allard, S., Gutierrez, L., Fontaine, C., Croué, J.-P.,Gallard, H., 2017. Organic matter interactions with natural manganese oxide and synthetic birnessite. *Science of The Total Environment 583*, 487-495.

An, S., Du, Y., Huang, X., Lu, Y., Mao, Z., Shi, L., Cotner, J.B., Xing, P.,Zhang, Y., 2024. Long-term photochemical and microbial alterations lead to the compositional convergence of algal and terrestrial dissolved organic matter. *Environmental Science & Technology 58*(42), 18765-18776.

Angst, G., Mueller, K.E., Nierop, K.G.J.,Simpson, M.J., 2021. Plant- or microbial-derived? A review on the molecular composition of stabilized soil organic matter. *Soil Biology and Biochemistry 156*, 108189.

Azimzadeh, B.,Martínez, C.E., 2025. Dynamic sorption and interfacial assembly of polysaccharide on hydrophobic vs hydrophilic surfaces. *ACS Earth and Space Chemistry 9*(5), 1030-1042.

Bahadori, M., Chen, C., Lewis, S., Boyd, S., Rashti, M.R., Esfandbod, M., Garzon-Garcia, A., Van Zwieten, L.,Kuzyakov, Y., 2021. Soil organic matter formation is controlled by the chemistry and bioavailability of organic carbon inputs across different land uses. *Science of The Total Environment 770*, 145307.

Bailey, V.L., Pries, C.H.,Lajtha, K., 2019. What do we know about soil carbon destabilization? *Environmental Research Letters 14*(8), 083004.

Chen, C., Dynes, J.J., Wang, J.,Sparks, D.L., 2014. Properties of Fe-organic matter associations via coprecipitation versus adsorption. *Environmental Science & Technology 48*(23), 13751-13759.

Chen, S., Klotzbücher, T., Lechtenfeld, O.J., Hong, H., Liu, C., Kaiser, K., Mikutta, C.,Mikutta, R., 2022. Legacy effects of sorption determine the formation efficiency of mineral-associated soil organic matter. *Environmental Science & Technology 56*(3), 2044-2053.

Cleveland, C.C., Neff, J.C., Townsend, A.R.,Hood, E., 2004. Composition, dynamics, and fate of leached dissolved organic matter in terrestrial ecosystems: results from a decomposition experiment. *Ecosystems 7*(3), 175-285.

Dalal, R.C., Thornton, C.M., Allen, D.E., Owens, J.S.,Kopittke, P.M., 2021. Long-term land use change in Australia from native forest decreases all fractions of soil organic carbon, including resistant organic carbon, for cropping but not sown pasture. *Agriculture, Ecosystems & Environment 311*, 107326.

Davenport, R., Bowen, B.P., Lynch, L.M., Kosina, S.M., Shabtai, I., Northen, T.R.,Lehmann, J., 2023. Decomposition decreases molecular diversity and ecosystem similarity of soil organic matter. *Proceedings of the National Academy of Sciences 120*(25), e2303335120.

Eusterhues, K., Rennert, T., Knicker, H., Kögel-Knabner, I., Totsche, K.U.,Schwertmann, U., 2011. Fractionation of organic matter due to reaction with ferrihydrite: coprecipitation versus adsorption. *Environmental Science & Technology 45*(2), 527-533.

Feng, X., Simpson, A.J.,Simpson, M.J., 2005. Chemical and mineralogical controls on humic acid sorption to clay mineral surfaces. *Organic Geochemistry 36*(11), 1553-1566.

Freeman, E.C., Emilson, E.J.S., Dittmar, T., Braga, L.P.P., Emilson, C.E., Goldhammer, T., Martineau, C., Singer, G.,Tanentzap, A.J., 2024. Universal microbial reworking of dissolved organic matter along environmental gradients. *Nature Communications 15*(1), 187.

Harfmann, J.L., Guillemette, F., Kaiser, K., Spencer, R.G.M., Chuang, C.-Y.,Hernes, P.J., 2019. Convergence of Terrestrial Dissolved Organic Matter Composition and the Role of Microbial Buffering in Aquatic Ecosystems. *Journal of Geophysical Research: Biogeosciences 124*(10), 3125-3142.

Heckman, K., Lawrence, C.R.,Harden, J.W., 2018. A sequential selective dissolution method to quantify storage and stability of organic carbon associated with Al and Fe hydroxide phases. *Geoderma 312*, 24-35.

Hondroudakis, L., Kopittke, P.M., Dalal, R.C., Barnard, M.,Weng, Z.H., 2024. The influence of land use and management on the behaviour and persistence of soil organic carbon in a subtropical Ferralsol. *SOIL 10*(2), 451-465.

Hong, H., Fang, Q., Churchman, G.J., Zhao, L., Ji, K., Jin, X., Yin, K., Wang, C.,Liu, C., 2020. Study of organic-matter intercalated vermiculitic phases in the hydromorphic red earth sediments. *Applied Clay Science 196*, 105744.

Jamoteau, F., Kansiz, M., Unger, M.,Keiluweit, M., 2025. Probing mineral-organic interfaces in soils and sediments using optical photothermal infrared microscopy. *Environmental Science & Technology 59*(1), 501-512.

Johnston, A.E.,Poulton, P.R., 2018. The importance of long-term experiments in agriculture: their management to ensure continued crop production and soil fertility; the Rothamsted experience. *European Journal of Soil Science 69*(1), 113-125.

Kalbitz, K., Solinger, S., Park, J.H., Michalzik, B.,Matzner, E., 2000. Controls on the dynamics of dissolved organic matter in soils: a review. *Soil Science 165*(4).

Kleber, M., Bourg, I.C., Coward, E.K., Hansel, C.M., Myneni, S.C.B.,Nunan, N., 2021. Dynamic interactions at the mineral–organic matter interface. *Nature Reviews Earth & Environment 2*(6), 402-421.

Kleber, M., Eusterhues, K., Keiluweit, M., Mikutta, C., Mikutta, R.,Nico, P.S., 2015. Chapter one - Mineral–organic associations: formation, properties, and relevance in soil environments. In: D. L. Sparks (Ed.), *Advances in Agronomy.* Academic Press, pp. 1-140.

Kleber, M., Sollins, P.,Sutton, R., 2007. A conceptual model of organo-mineral interactions in soils: self-assembly of organic molecular fragments into zonal structures on mineral surfaces. *Biogeochemistry 85*(1), 9-24.

Kögel-Knabner, I., 2002. The macromolecular organic composition of plant and microbial residues as inputs to soil organic matter. *Soil Biology and Biochemistry 34*(2), 139-162.

Lavallee, J.M., Soong, J.L.,Cotrufo, M.F., 2020. Conceptualizing soil organic matter into particulate and mineral-associated forms to address global change in the 21st century. *Global Change Biology 26*(1), 261-273.

Lenhardt, K.R., Breitzke, H., Buntkowsky, G., Mikutta, C.,Rennert, T., 2022. Interactions of dissolved organic matter with short-range ordered aluminosilicates by adsorption and co-precipitation. *Geoderma 423*, 115960.

Liu, D., Li, M., Yu, R., Li, H., Shen, Y., Tian, Q., Bu, H., Huang, C.,Tan, W., 2023. Interlayer organic matter within hydroxy-interlayered clay minerals enhances soil organic carbon stability under long-term organic fertilization. *Applied Clay Science 239*, 106963.

Lv, J., Huang, Z., Christie, P.,Zhang, S., 2020. Reducing reagents induce molecular artifacts in the extraction of soil organic matter. *ACS Earth and Space Chemistry 4*(11), 1913-1919.

Lv, J., Huang, Z., Luo, L., Zhang, S.,Wang, Y., 2022. Advances in molecular and microscale characterization of soil organic matter: current limitations and future prospects. *Environmental Science & Technology 56*(18), 12793-12810.

Mayer, S., Kühnel, A., Burmeister, J., Kögel-Knabner, I.,Wiesmeier, M., 2019. Controlling factors of organic carbon stocks in agricultural topsoils and subsoils of Bavaria. *Soil and Tillage Research 192*, 22-32.

Mikutta, R., Lorenz, D., Guggenberger, G., Haumaier, L.,Freund, A., 2014. Properties and reactivity of Fe-organic matter associations formed by coprecipitation versus adsorption: clues from arsenate batch adsorption. *Geochimica et Cosmochimica Acta 144*, 258-276.

Millman, E., Chatterjee, A., Parker, K.M.,Catalano, J.G., 2024. Cation exchange to montmorillonite induces selective adsorption of amino acids. *Geochimica et Cosmochimica Acta 372*, 181-195.

Minor, E.C., Swenson, M.M., Mattson, B.M.,Oyler, A.R., 2014. Structural characterization of dissolved organic matter: a review of current techniques for isolation and analysis. *Environmental Science: Processes & Impacts 16*(9), 2064-2079.

Molina, C., Kim, D., Mehndiratta, L., Lee, J., Madawala, C.K., Slade, J.H., Tivanski, A.V.,Grassian, V.H., 2025. Comparison of different vibrational spectroscopic probes (ATR-FTIR, O-PTIR, Micro-Raman, and AFM-IR) of lipids and other compounds found in environmental samples: case study of substrate-deposited sea spray aerosols. *ACS Measurement Science Au 5*(1), 74-86.

Nicoloso, R.S., Amado, T.J.C.,Rice, C.W., 2020. Assessing strategies to enhance soil carbon sequestration with the DSSAT-CENTURY model. *European Journal of Soil Science 71*(6), 1034-1049.

Prater, C.B., Kansiz, M.,Cheng, J.-X., 2024. A tutorial on optical photothermal infrared (O-PTIR) microscopy. *APL Photonics 9*(9), 091101.

Roth, V.-N., Lange, M., Simon, C., Hertkorn, N., Bucher, S., Goodall, T., Griffiths, R.I., Mellado-Vázquez, P.G., Mommer, L., Oram, N.J., Weigelt, A., Dittmar, T.,Gleixner, G., 2019. Persistence of dissolved organic matter explained by molecular changes during its passage through soil. *Nature Geoscience 12*(9), 755-761.

Yang, Z., Ohno, T.,Singh, B., 2024. Effect of land use change on molecular composition and concentration of organic matter in an Oxisol. *Environmental Science & Technology 58*(23), 10095-10107.

Zhang, M., Peacock, C.L., Cai, P., Xiao, K.-Q., Qu, C., Wu, Y.,Huang, Q., 2021. Selective retention of extracellular polymeric substances induced by adsorption to and coprecipitation with ferrihydrite. *Geochimica et Cosmochimica Acta 299*, 15-34.

Zhao, Q., Callister, S.J., Thompson, A.M., Kukkadapu, R.K., Tfaily, M.M., Bramer, L.M., Qafoku, N.P., Bell, S.L., Hobbie, S.E., Seabloom, E.W., Borer, E.T.,Hofmockel, K.S.,

2020. Strong mineralogic control of soil organic matter composition in response to nutrient addition across diverse grassland sites. *Science of The Total Environment 736*, 137839.